論文 / 著書情報
Article / Book Information

題目(和文)	Nbシリサイドを基盤とした超高温構造用合金の設計
Title(English)	Design of ultra-high temperature structural alloys based on Niobium silicides
著者(和文)	関戸信彰
Author(English)	
出典(和文)	学位:博士(工学), 学位授与機関:東京工業大学, 報告番号:甲第5127号, 授与年月日:2002年3月26日, 学位の種別:課程博士, 審査員:
Citation(English)	Degree:Doctor (Engineering), Conferring organization: Tokyo Institute of Technology, Report number:甲第5127号, Conferred date:2002/3/26, Degree Type:Course doctor, Examiner:
学位種別(和文)	博士論文
Type(English)	Doctoral Thesis

Design of Ultra-High Temperature Structural Alloys Based on Niobium Silicides

Nobuaki Sekido

Department of Materials Science and Engineering
Tokyo Institute of Technology
2002

Design of Ultra-High Temperature Structural Alloys Based on Niobium Silicides

A Dissertation for the Degree

Doctor of Engineering

Field of Materials Science and Engineering

by

Nobuaki Sekido

Tokyo Institute of Technology

2002

INDEX

CHAPTER 3

EFFECT OF ANNEALING TEMPERATURE ON MICROSTRUCTURES AND MECHANICAL PROPERTIES

CHAPTER 4

COMPARISON OF MICROSTRUCTURE AND MECHANICAL PROPERTIES OF THE ALLOYS FABRICATED BY INGOT AND POWDER METALLUGY

CHAPTER 5

MICROSTRUCTURAL CONTROL BY DIRECTIONAL SOLIDIFICATION

CHAPTER 6

CHAPTER 1

GENERAL INTRODUCTION

1. BACKGROUND

From the standpoint of energy conservation and environment protection, a need for the development of new materials has grown rapidly having superior potential as structural materials at ultra-high temperatures to any other present commercial alloys. Nickel-base superalloys, being currently the champion material among heat resistant alloys, are used as jet engine parts exposed to slightly over 1373 K. The operating temperature, however, obviously reached the limit to be used for structural applications since it is over 80% of their melting temperatures.

In the current electric power generation systems using fossil fuels, typically an ultra-super critical steam plant, the average thermal efficiency is as high as 40% with the inlet steam temperature of about 873 K. If such a system were replaced by an advanced power generating system, e.g. a combined cycle gas turbine engine plant using coal and natural gas or a hydrogen combustion system, the efficiency is believed to jump up with a tremendous reduction in harmful CO_2 exhaust. For example in a combined cycle gas turbine engine, thermal efficiency will be as high as 53% if the inlet temperature is 1773 K, and 65% if it is 1973 K. If the latter system comes true, considering the fraction of CO_2 exhaust by electric power generation system being about one third of the total, both fuel and the CO_2 exhaust will cut down to a quarter as a result. The development of materials to endure as structural components in such advanced power generation systems is obviously a desire to sustain our modern life while keeping the global environment.

Candidate materials for applications mentioned above should be based on such as refractory metal elements Nb, Mo, W and Ta having a sufficiently high melting point over 2700 K with respect to the service temperatures. However, there is a major drawback of the extremely

poor oxidation resistance at elevated temperatures in the alloys based on such refractory metal elements. This is the reason why their intermetallics, particularly aluminides and silicides, have attracted the interest. They have much better properties as compared to the alloys based the major constituent in respect to high stiffness, lower density, better high temperature strength as well as excellent creep resistance and good oxidation resistance. Many of refractory metal aluminides and silicides in monolithic form, however, exhibit extremely low damage tolerance and fracture toughness at room temperature. It is therefore crucial to provide some ductility or toughness at ambient temperature by alloy design involving optimization in composition of the compound and/or controlling the microstructure of the alloy having ductile phase with proper morphology. The latter technique on alloy design is based on the concept called ductile phase toughening.

One of the alloy system for such interest is the binary Nb-Si, which phase diagram is shown in Fig. 1-1 [1], where the two-phase of niobium silicide phase, α-Nb_5Si_3, and Nb primary solid solution, (Nb), is stable up to 2043 K. From the published information on its ordered crystal structure [2], the Nb_5Si_3 phase is expected to exhibit high strength at elevated temperatures but to be intrinsically brittle at room temperature. Therefore the introduction of ductile (Nb) phase into the microstructure would be appropriate to expect the ductile phase toughening. In order to develop alloys consisting of Nb_5Si_3 and (Nb) according to the binary Nb-Si phase diagram, it should be noted that the (Nb)/Nb_5Si_3 two-phase lamellar structure can be obtained through the eutectoid decomposition of the high temperature intermetallic phase Nb_3Si. Therefore, the major interest in the present work is placed on a controlling of the lamellar microstructure resulted from the eutectoid reaction of high-temperature phase Nb_3Si.

2. PROPERTIES OF Nb_5Si_3 PHASE

Refractory metal silicides are potential candidates for an application to ultra-high temperature structural materials. In particular, the transition metal silicides with 5:3 stoichiometry are shown to lay on the envelope occupying the highest melting temperature and lowest densities of intermetallics formed from over 20 crystal structure types [2]. Figure 1-2 shows the relation between density and melting temperature for 5:3 transition metal silicides [3]. Among the silicides shown in Fig. 1-2, Nb_5Si_3 has the highest melting temperature (2757 K) of those with densities below that of the nickel-base superalloy.

The α-Nb_5Si_3 phase has the $D8_l$ crystal structure shown in Figure 1-3. The $D8_l$ crystal

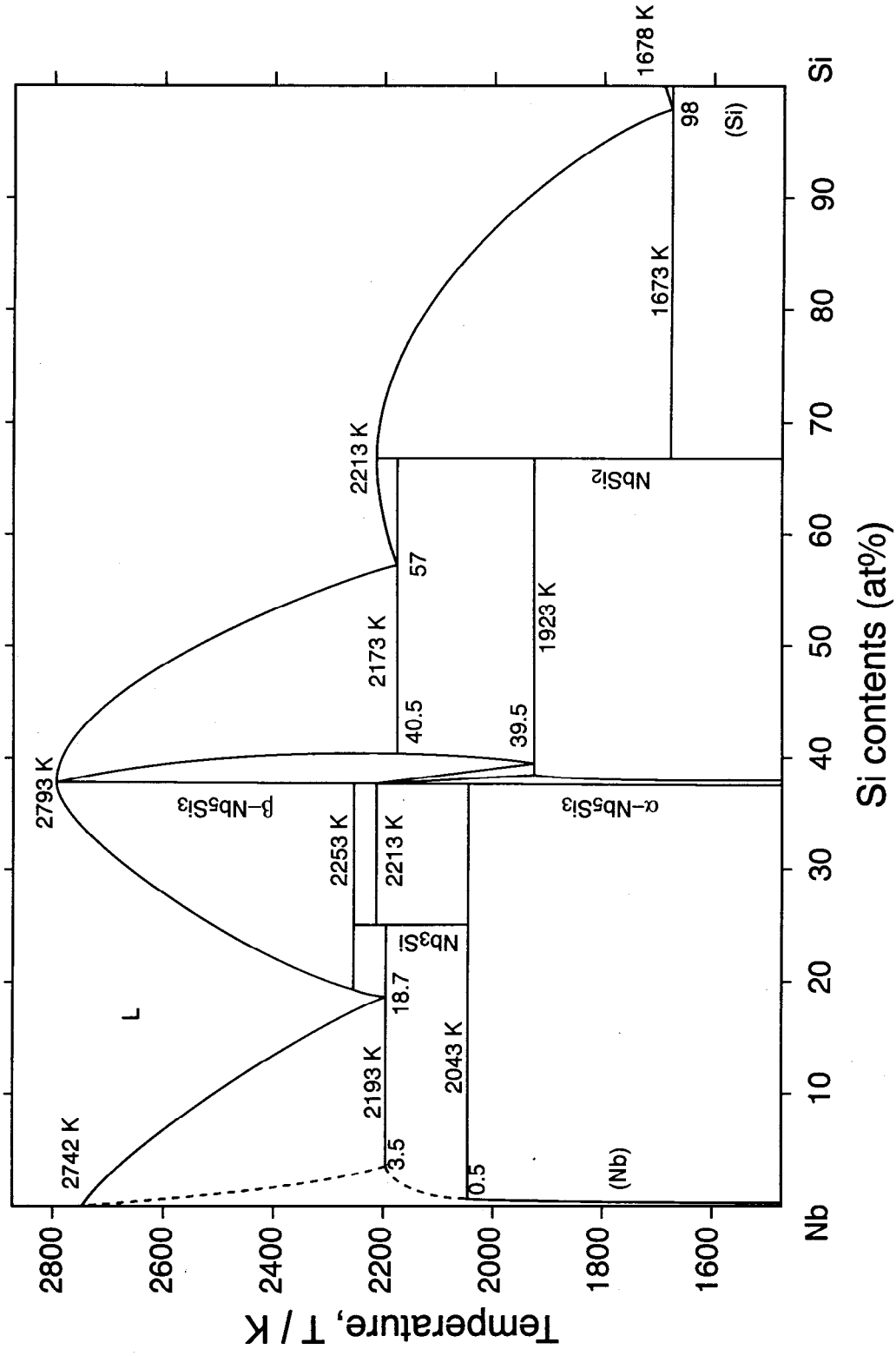

Fig. 1-1 The Nb-Si binary phase diagram [1].

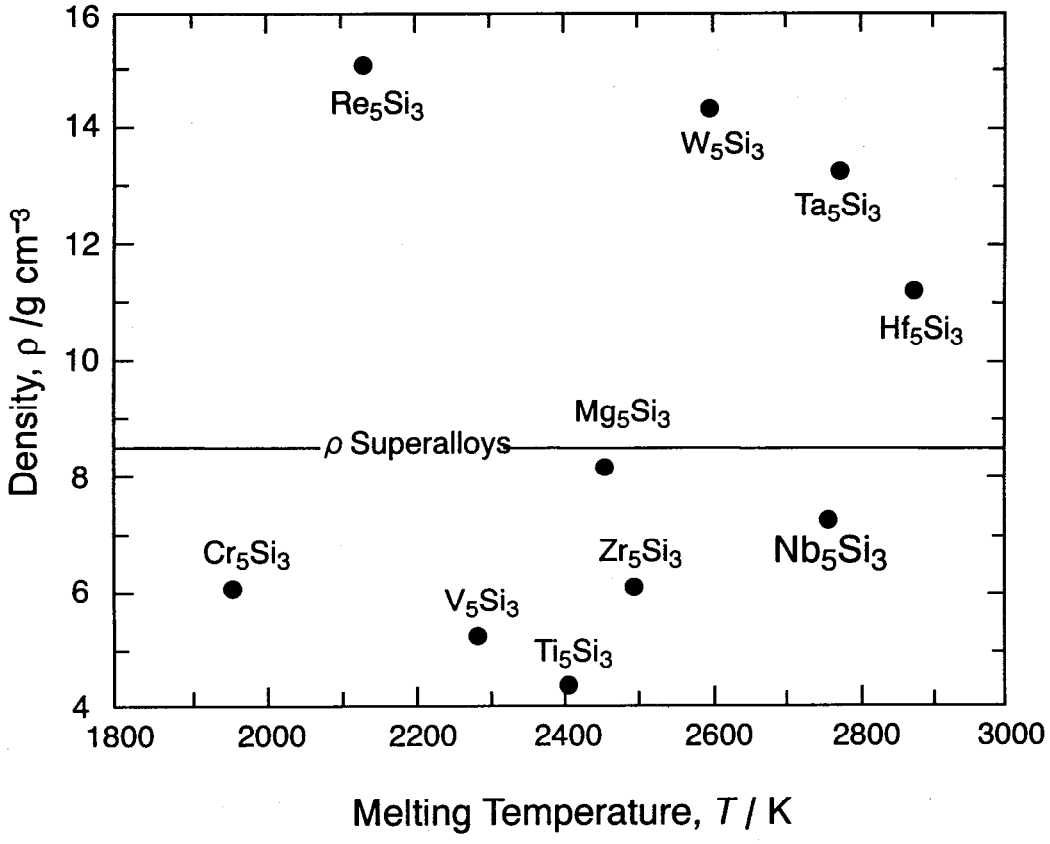

Fig. 1-2 Relation between density and melting temperature for 5:3 transition-metal silicides [4].

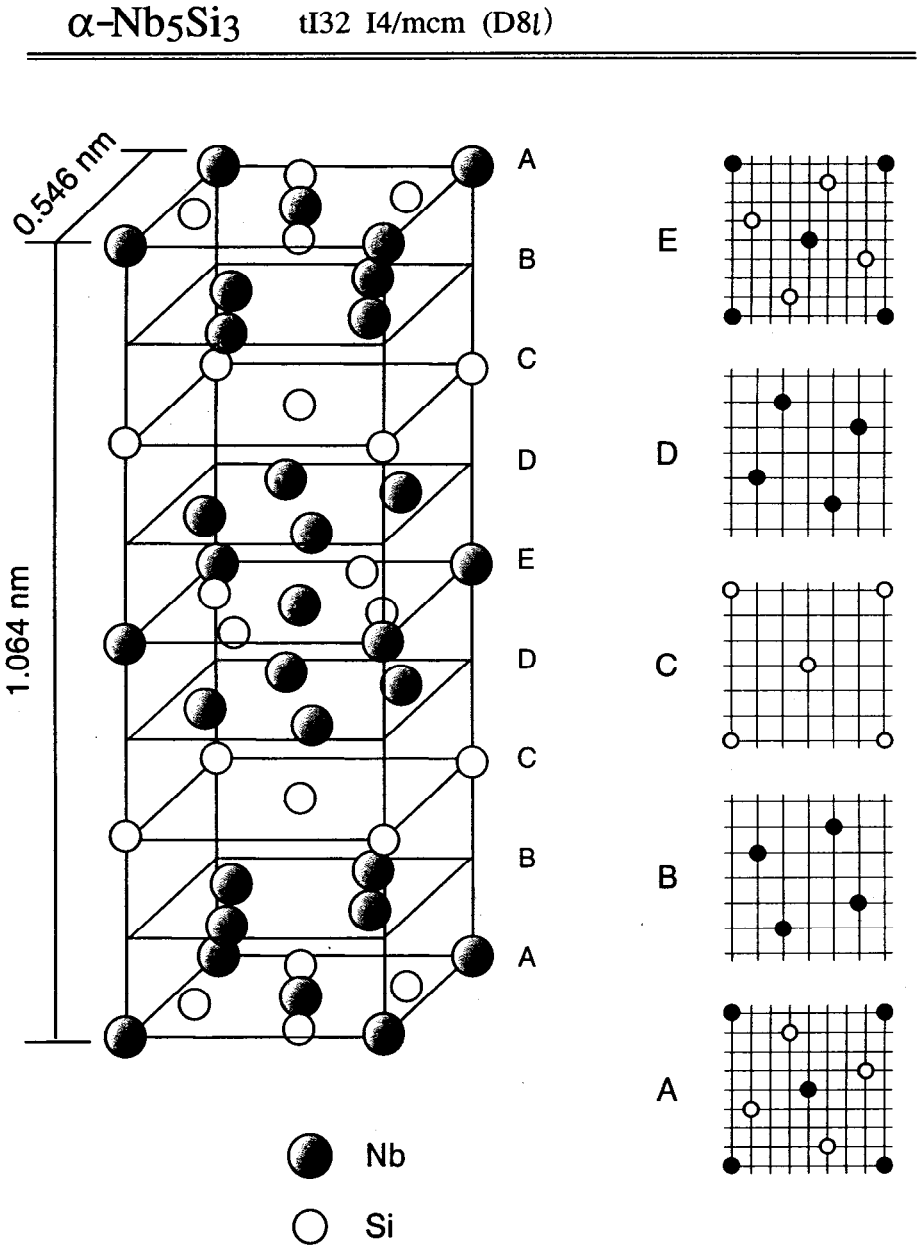

Fig. 1-3 Crystal structure of the α-Nb5Si3 (D8l).

structure consists of five different planes stacking regularly toward [001] direction following the order of "...BABCDEDCBABC...". This quite complex crystal structure would provide a excellent strength up to elevated temperature but a poor fracture toughness. In practice, Nb_5Si_3 is reported to show high strength at elevated temperature [4,5]. Compressive fracture strength of the Nb_5Si_3 single phase alloy is reported to be ~670 MPa at 1773 K [4]. And single phase Nb_5Si_3 alloy shows excellent creep resistance at least up to 1673 K [5]. On the other hand, it has been reported that fracture toughness of single phase Nb_5Si_3 alloy in polycrystalline is about 1~3 MPa $m^{1/2}$ [4,6], which means it is totally brittle by itself.

Considering the circumstances mentioned above, Nb_5Si_3 could be a candidate for ultra-high temperature structural materials if its intrinsic brittleness is improved to some extent. To establish a strategy to accomplish this by having a ductile phase in the compound and controlling the microstructure is the purpose of the present work.

3. PHASE EQUILIBRIA IN THE Nb-Si BINARY AND Nb-Ti-Si TERNARY SYSTEM

Information on phase equilibria is required to determine the optimum compositions and microstructures for property improvements and high temperature stability. Though much efforts have been made to investigate the phase equilibria in the Nb-Si binary system, the latest Nb-Si phase diagram compiled in the Binary Alloy Phase Diagrams published by ASM [7] is mainly based on the data reported by Kochherzhinskiy et al. [8]. The eutectic composition of " $L \rightarrow (Nb) + Nb_3Si$ " has been revised from 18.7 at% Si [1] to 17.5 at% [7,8]. Another report has been made by Mendiratta et al. that the eutectic point is 18.2 at%Si [9].

Schlesinger et al. have also revised the Nb_3Si transus temperature to be 2043 K from 2038 K, by considering experimental error [10], but Mendiratta et al. have reported between 1933 and 1953 K [11]. The former is determined by DTA and the latter is determined basically by microstructural observation. The large difference between the two reports on Nb_3Si transus temperature indicates that measuring such high temperature is difficult, and that decomposition kinetics is extremely slow [11]. In addition, it has been pointed out that the effect of oxidation on phase equilibria should be considered at such high temperature because oxygen is known to lower the stability of Nb_3Si [12].

The (Nb)/Nb_5Si_3 two phase microstructure is formed basically by the eutectic reaction of (Nb) and Nb_3Si from liquid phase and the subsequent eutectoid reaction of Nb_3Si decomposing into (Nb)/Nb_5Si_3. Certainly there is difference in primary solidification phase of (Nb), Nb_3Si, or

β-Nb_5Si_3 depending on alloy compositions for the eutectic decomposition, " L → (Nb) + Nb_3Si ", and that for the eutectoid decomposition, " Nb_3Si → (Nb) + α-Nb_5Si_3 ". When alloy composition is hypereutectic, peritectic reaction occurs in the form of " L + β-Nb_5Si_3 → Nb_3Si " prior to the two invariant reactions. The two-phase microstructure with (Nb)/Nb_5Si_3 lamellar morphology, which is of interest in the present work, can basically be obtained through the decomposition of high-temperature phase Nb_3Si.

Subramanian et al. have shown that the Ti addition stabilizes the Nb_3Si in the ternary Nb-Si-Ti system toward lower temperatures [13]. Liquidus surface and reaction scheme in the ternary system experimentally determined by Bewlay et al. are shown in Fig. 1-4 [14]. Ti_3Si forms by a peritectoid reaction between Ti_5Si_3 and Ti. The Nb_5Si_3 and Ti_5Si_3 are not isomorphous and have tI32 and hP16 crystal structures, respectively. Although Ti_3Si and Nb_3Si are isomorphous, Nb_3Si is stable at the temperature range over 2043 K, and Ti_3Si is stable below 1443 K. Thus, the Nb_3Si and Ti_3Si should form continuous solid solution as shown in Fig. 1-5 [15]. This figure indicates that the Nb_3Si transus temperature can be lowered by the Ti addition, which means that the eutectoid temperature and kinetics for the decomposition of the high temperature Nb_3Si can be controlled by the Ti addition. Therefore, detailed investigation of the phase equilibria in the Nb-Ti-Si ternary system, especially for the Nb_3Si phase, is of great importance in the present study.

4. PREVIOUS EFFORTS ON DESIGNING THE ALLOYS BASED ON NIOBIUM SILICIDES

Over the last decade, alloys based on niobium silicide have been widely investigated in the Nb-Si binary and Nb-Ti-Si ternary systems. In most of such works, the alloys are designed to have a large amount of ductile (Nb) phase in order to assure some room temperature ductility and toughness. The alloy compositions are therefore mostly hypo-eutectic with respect to the reaction of " L → (Nb) + Nb_3Si ". Mendiratta et al. have shown that alloys consisting of the Nb_5Si_3 matrix and ductile (Nb) particle dispersion exhibit a good balance of room temperature toughness and high temperature strength up to 1673 K [16]. They have also shown that room temperature toughness can be greatly improved by hot extrusion in the Nb-10Si alloy by which ductility of the (Nb) phase would be improved [16,17]. Bewlay et al. have investigated the relationship between room temperature toughness and alloy composition in directionally solidified alloys [18]. At around the eutectic composition, the minimum appears in the Si

(a)

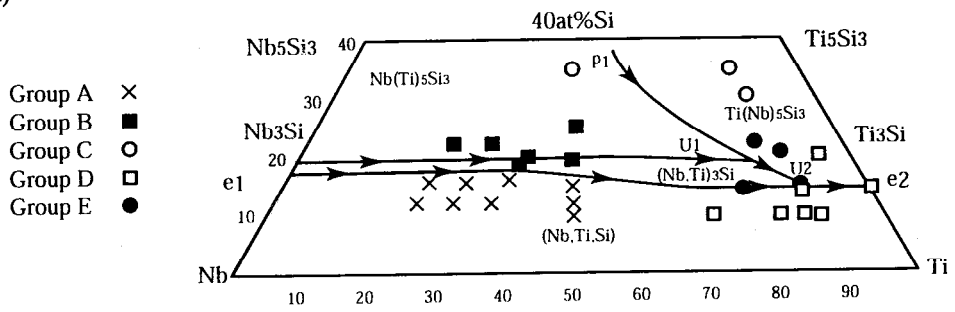

(b)

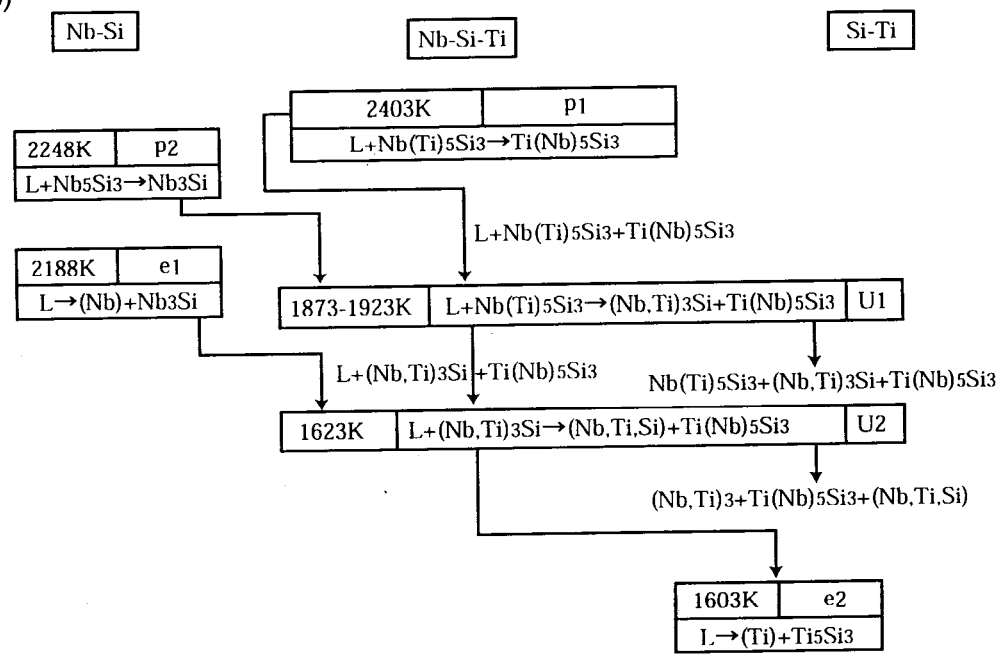

Fig. 1-4 The liquids surface projection (a), and partial reaction scheme for the Si-lean region of the Nb-Ti-Si ternary system (b) proposed by Bewlay et al. [12]. Eutectic and peritectic reactions are indicated by *e* and *p*, respectively. The transitions are represented by *U*.

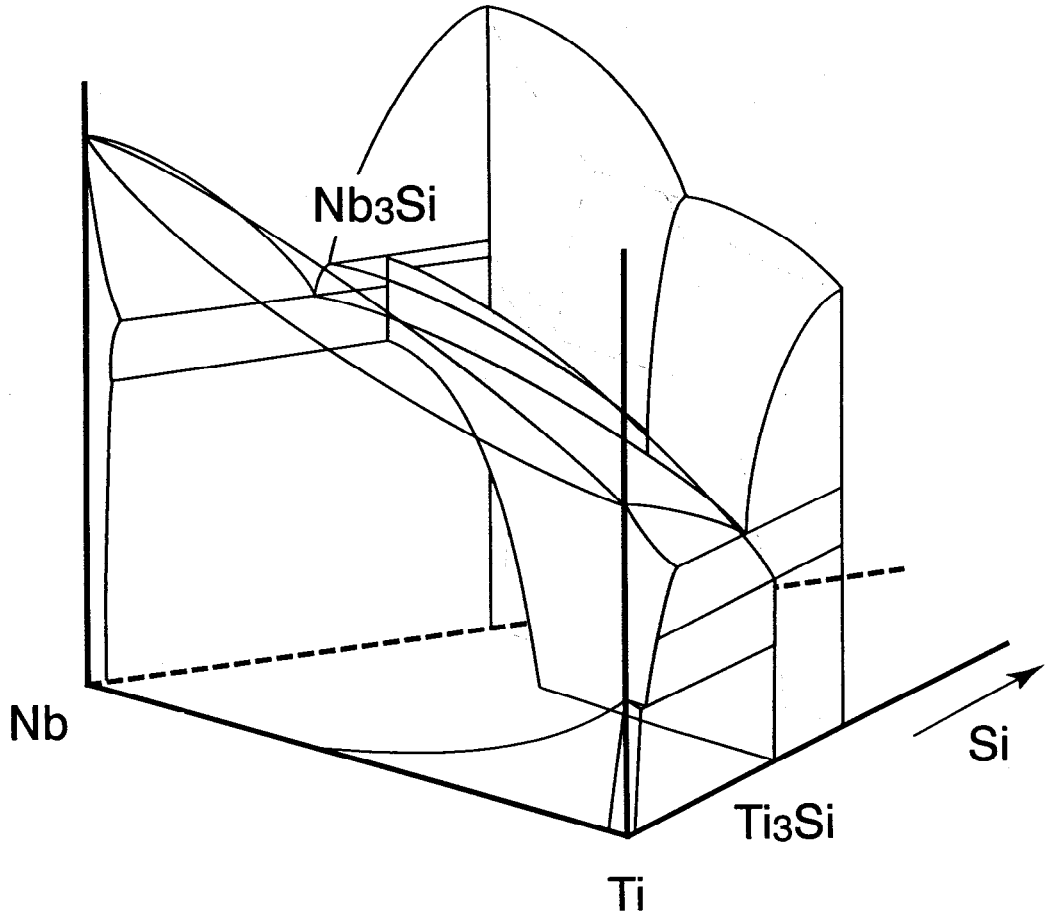

Fig. 1-5 A three-dimensional illustration of the Nb-Ti-Si ternary diagram proposed by Subramanian et al. [15].

composition dependence of toughness of the Nb-Si binary alloys. It is well known that size and morphology of ductile phase play a major role for toughening in ductile phase toughening mechanism [19]. Larger size of ductile phase provides a higher toughness wherein crack bridging mechanism operates. Above all, the room temperature toughness can be assured by a certain degree by increasing the volume fraction of (Nb) phase and by controlling its morphology.

Mendiratta et al. have reported that the binary Nb-Si alloys with Si contents higher than 10 at% contain numerous micro-cracks which are introduced during cooling from the melt [16]. Formation of micro-cracks during the alloy preparation is one of the major problems against a practical application in this alloy system. A strategy to avoid micro-cracking is to apply the alloy processing based on powder metallurgy. Kajuch et al. have succeeded in preparation of Nb_5Si_3 single phase alloy by both mechanical alloying and reactive sintering [6]. However it have been shown that pure niobium and silicon elemental powders are hard to be mechanically alloyed by a conventional ball milling, and an amorphous phase is formed when the volume fraction of niobium is high [20,21]. Fukui et al. have reported that fine microstructure consisting of equiaxed (Nb) and Nb_5Si_3 grains can be obtained by the reactive sintering using high-energy ball milled powder, though the severe adhesion of niobium powder to metallic vial is a problem of ball milling [22]. They have also shown that the high temperature strength of the alloy with equiaxed grains can be improved by the microstructural control to form the (Nb)/Nb_5Si_3 lamellar by utilizing the decomposition of Nb_3Si into the two phases.

Though (Nb)/Nb_5Si_3 alloy shows an acceptable balance of room temperature toughness and high temperature strength including creep resistance, catastrophic oxidation and embrittlement of these materials limit their usefulness in structural application. Subramanian et al. have shown that marked improvements in oxidation resistance could be obtained through the Ti and Al addition [13]. In such alloy systems, room temperature toughness can be improved by the well-aligned ductile phase by using directional solidification but strength, especially at elevated temperature, is lower than that of Nb-Si binary alloys.

These observations lead us to select a strategy for the purpose to choose alloys based on niobium silicide which composition is toward hypereutectic compositions in the binary Nb-Si system for higher volume fraction of Nb_5Si_3 and for high elevated temperature strength. The morphology of the ductile (Nb) in the Nb_5Si_3 matrix should be optimized for room temperature ductility in their lamellar structure as a result of the eutectoid decomposition of the Nb_3Si phase.

This basic strategy should be extended to the ternary Nb-Si-Ti system since the Ti addition seems to have some beneficial effect.

5. OBJECTIVE AND OUTLINE OF THIS THESIS

The objective of the present work is to develop a new class of heat resistant alloy based on niobium silicide that exhibits superior elevated temperature strength to the commercial nickel base superalloy aiming for an application as structural materials in a new energy conversion systems operative at over 1773 K. For an excellent elevated temperature strength at such high temperatures, the alloy should be based on refractory metal elements and the alloy should be based on a silicide or aluminide of the element for oxidation resistance. In the present work, niobium silicide is chosen as a candidate material. Since the intermetallic compound is generally brittle at ambient temperature, introduction of ductile phase into the strong but brittle compound is attempted. By the careful examinations on the Nb-Si binary and the Nb-Si-Ti ternary systems, alloys with lamellar microstructure consisting of the (Nb)/Nb_5Si_3 are designed. Microstructural control is pursued to optimize the elevated temperature strength and room temperature toughness.

This thesis is composed of six chapters.

Chapter 1 is "GENERAL INTRODUCTION", where a necessity is firstly described to develop ultra-high temperature materials for a new energy conversion system for effective use of fossil fuels while maintaining the global environment. Then the background, the motivation and the objective of the present work on the development of alloys based on niobium silicides are stated.

Chapter 2 is "PHASE EQUILIBRIA AND EFFCET OF ALLOY COMPOSITION ON MICROSTRUCTURE AND MECHANICAL PROPERTIES", where microstructure and phase equilibria are investigated in the Nb-Si binary and the Nb-Si-Ti ternary systems. The relationship between microstructure and mechanical properties are extensively investigated.

Chapter 3 is "EFFECT OF ANNEALING TEMPERATURE ON MICROSTRUCTURE AND MECHANICAL PROPERTIES", where the TTT-diagram for the decomposition of $(Nb,Ti)_3Si$ phase in the Nb-Si-Ti ternary alloys was evaluated. The correlations of inter-lamellar spacing and lamellar colony size with annealing temperatures are discussed using theoretical models. The effects of inter-lamellar spacing and lamellar colony size on mechanical properties are investigated. The deformation mechanisms and the toughening mechanisms are discussed.

Chapter 4 is "COMPARISON OF MICROSTRUCTURE AND MECHANICAL PROPERTIES OF THE ALLOYS FABRICATED BY INGOT AND POWDER METALLUGY", where the alloys based on niobium silicides are prepared by powder metallurgy and the effect of the processing condition on the microstructure and mechanical properties are investigated. The mechanical properties are compared in respect of microstructural features between the alloys prepared by the proposed powder metallurgy and ingot metallurgy using arc-melting. The strengthening mechanisms as well as the toughening mechanisms operating in these alloys are discussed.

Chapter 5 is "MICROSTRUCTURAL CONTROL BY DIRECTIONAL SOLIDIFICATION", where directional solidification technique is conducted in order to control microstructure of the (Nb)/Nb_3Si eutectic alloy in the Nb-Si binary and Nb-Si-Ti ternary systems. The relationship between microstructures and directional solidification conditions was investigated. The toughening mechanisms of the directionally solidified alloys are discussed focusing on the distinctive microstructural features comparing with that of arc-cast alloys.

Chapter 6 is "SUMMARY AND CONCLUSION", where the results obtained in each chapter are summarized and concluding remarks are presented.

REFERENCES

[1] H. Okamoto, A.B. Gokhale and G.J. Abbaschian, in "Binary Alloy Phase Diagrams, Second Edition", Ed T.B. Massalski et al., ASM Intnl., 1990.

[2] R.L. Fleisher, Mater, Sci. 22 (1987), p. 2281

[3] J.D. Rigney, P.M. Singh, and J.J. Lewandowski, JOM, August 1992, pp. 36-41.

[4] R. Nekkanti and D.M. Dimiduk, MRS Symp. Proc., vol. 194 (1990), p.175.

[5] P.R. Subramanian, T.A. Parthasarathy, M.G. Mendiratta, and D.M. Dimiduk, Scripta Met. Mater., vol. 32 (1995), pp. 1227-1232.

[6] J. Kajuch, J.D. Rigney and J.J. Lewandowski, Mater. Sci. Eng. A, vol. 155 (1992), pp. 59-65.

[7] H. Okamoto, in "Phase Diagrams for Binary Alloys", ASM Intnl., 2000.

[8] Yu.A. Kocherzhinskiy, L.M. Yupko, and E.A. Shishkin, Ross. Metall., No. 1 (1980), pp. 184-188.

[9] B.P. Bewlay, H.A. Lipsitt, M.R. Jackson, W.J. Reeder and J.A. Sutliff, Mater. Sci. Eng. A, vol. 192/193 (1995), pp. 534-543.

[10] M.E. Schlesinger, H. Okamoto, A.B. Gokhale and R. Abbaschian, Journal of Phase Equilibria, vol. 14 (1993), No. 4, pp. 502-509.

[11] M.G. Mendiratta and D.M. Dimiduk, Scripta Met. Mat., vol. 25 (1991), pp. 237-242.

[12] Seiji Miura, Hokkaido University, private communication.

[13] P.R. Subramanian, M.G. Mendiratta, and D.M. Dimiduk, MRS Symp. Proc., vol. 322 (1994), pp. 491-502.

[14] B.P. Bewlay and M.R. Jackson, Journal of Phase Equilibria, Vol. 18, No. 3 (1997), pp. 264-278.

[15] B.P. Bewlay, M.R. Jackson, W.J. Reeder and H.A. Lipsitt, MRS Symp. Proc., vol. 364 (1995), pp. 943-948.

[16] M.G. Mendiratta, J.J. Lewandowski and D.M. Dimiduk, Metall. Trans. A, vol. 22A (1991), pp. 1573-1583.

[17] M.G. Mendiratta and D.M. Dimiduk, Metall. Trans. A, vol. 24A (1993), pp. 501-504.

[18] B.P. Bewlay, H.A. Lipsitt, M.R. Jackson, W.J. Reeder and J.A. Sutliff, Mater. Sci. Eng. A, vol. 192/193 (1995), pp. 534-543.

[19] M.F. Ashby, F.J. Blunt and M. Bannister, Acta Metall. Mater., 37 (1989), pp.

1847-1857.

[20] K. S. Kumar and S. K. Mannan, MRS Symp. proc., vol. 133 (1989), pp. 415-420.

[21] M. Nazareth R. V. Perdigao, Jose A.R. Jordao, Claudi S. Kiminami, and Walter J. Botta F., Journal of Non-Crystalline Solid, vol. 219 (1997), pp. 170-175.

[22] Fukui et al., "Summary of R&D Report for FY1999 Proposal-Based R&D Program of NEDO" (in Japanese), No.98Ec07-004-3, New Energy and Industrial Technology Development Organization, 1999.

CHAPTER 2

PHASE EQUIRIBRIA AND EFFECT OF ALLOY COMPOSITION ON MICROSTRUCTURE AND MECHANICAL PROPERTIES

1. INTRODUCTION

The interests of the present work are placed on establishing the basis of microstructural control of the (Nb)/Nb_5Si_3 lamellar structure in the Nb-Si system, because it has a potential to provide a good balance of room temperature toughness and high temperature strength. The (Nb)/Nb_5Si_3 lamellar microstructure is formed by the eutectoid decomposition of the high temperature phase Nb_3Si, where the eutectoid temperature is reported as 2043 K [1]. Also it has been shown that the eutectoid decomposition is sluggish [2]. Therefore, the lamellar microstructure control requires the specific heat treatment at very high temperatures for a long period of time. It was reported that the addition of Ti improves the toughness of both the (Nb) solid solution phase and Nb_5Si_3 phase [3], as well as the oxidation resistance of the alloys at elevated temperatures [4,5]. It indicates that the Ti addition is advantageous to pursue the good balance of ambient temperature toughness and elevated temperature strength in the present alloy system. It was also reported that the Ti addition stabilizes the Nb_3Si phase towards lower temperatures since there exists the Ti_3Si phase, having the same ordered crystal structure with the Nb_3Si, staying stable from room temperature to 1443 K in the Ti-Si binary system [6]. While the Nb_3Si phase exists in the temperature range between 2043 and 2193 K in the Nb-Si binary system. The continuous solid solution (Nb, $Ti)_3Si$ phase is supposed to be formed in the Nb-Si-Ti ternary system, though it is impossible to utilize the eutectoid decomposition for the lamellar formation in the ternary alloys having higher Ti contents because the (Nb, $Ti)_3Si$ phase is stable down to ambient temperatures. Investigations for the phase equilibria in the Nb-Si-Ti ternary system are important, especially with respect to the stability of the (Nb,$Ti)_3Si$ phase and

the eutectoid temperature.

The objective in this chapter is to investigate the phase equilibria in the Nb-Si binary and Nb-Si-Ti ternary systems. The relationship between microstructure and mechanical properties were extensively investigated as well, in order to establish the optimum alloy compositions and microstructures for the ultra-high temperature structural application. Ambient temperature fracture toughness measurement is conducted using the chevron-notched specimen which is especially useful for measuring the fracture toughness of brittle materials. Effect of the Ti addition on the fracture toughness improvement could be explained by changes in microstructural characteristics and hardness of the ductile (Nb) phase.

2. EXPERIMENTAL

Alloys were prepared by arc-melting using high purity raw materials (Nb, Ti > 99.5%, Si > 99.9%) under an argon atmosphere. Nominal compositions of the alloys investigated in this work are listed in Table 2-1. Alloy preparation was carefully controlled so that the weight loss after the melting was less than 0.2% of total weight. Three alloy compositions were selected as the base alloys, the eutectic Nb-18.7at%Si, hereafter denoted as Nb-18.7Si, and the hypereutectic Nb-20Si and Nb-25Si alloys. The Ti addition was made on the base alloys in a compositional range up to 40at% assuming that Ti atoms substitute for Nb sites.

After melting, annealing was conducted on alloys at various temperatures between 1373 and 1773 K for 100 h under an Ar atmosphere. Microstructural observation was performed by means of scanning electron microscope (SEM) using back-scattered electron image (BEI). Constituent phases in the alloys were identified by X-ray diffractometry (XRD), energy dispersive X-ray spectroscopy (EDS), and electron prove X-ray micro analysis (EPMA). Some alloys were solution-treated in the (Nb)/Nb_3Si two-phase region at 2073 K for 24 h in a vacuum or at 2023 K for 100 h in an argon gas atmosphere to reduce the volume fraction of primary Nb_5Si_3 phase. The subsequent heat treatments for the decomposition of Nb_3Si phase into (Nb) and Nb_5Si_3 via the eutectoid reaction were conducted at 1673 K.

Transmission electron microscopy (TEM) observations were performed using a JEOL JEM-2011 (200 kV) microscope. TEM foils were ground to 150 μm thickness, mechanically dimpled to 80 μm and then perforated using the ion milling apparatus. Electron micro-diffraction was used to determine the crystal orientation relationship between the (Nb) and silicide phases.

Table 2-1 Nominal alloy compositions prepared in the present work.

Nb	Si	Ti (at%)	Nb	Si	Ti (at%)
bal.	0	3	bal.	20	0
		6			5
		9			10
	1	0			15
		2.5			20
		5			25
		7.5			30
	4	0		25	0
		5			5
		10			10
	18.7	0			15
		10			20
	37.5	0			25
		5			30
					35
					40

Four-point bending tests were carried out to evaluate the fracture toughness using chevron-notched specimens. Test specimens, of which dimension is shown in Fig. 2-1, were prepared by electro-discharge machining (EDM), and were mechanically polished to remove the damaged surface layer prior to testing. Tests were carried out using an Instron type testing machine with the cross-head speed of 5×10^{-2} mm/min. The bending test specimen was supported by free rollers with the outer and inner spans being 21 mm and 7 mm, respectively. The chevron-notch fracture toughness, K_Q, is calculated using the Bluhm's slice model [7]. The test was conducted once on each alloy because it was very difficult to obtain sound test specimens.

Compression tests were conducted at nominal strain rate of 1.0×10^{-4} s^{-1} in air at room temperature, and in vacuum ($1\sim3\times10^{-4}$ Torr) at elevated temperatures. Test specimens, $2\times2\times5$ mm^3 rectangular pillar, were prepared by EDM and were mechanically polished to remove the damaged surface layer prior to testing.

Vickers hardness measurement was conducted with a load of 0.2 and 10 kgf for 30 s. The hardness number stands for the average value of overall microstructure.

3. RESULTS

3-1. Microstructures and Phase Equilibria

3-1-1. Microstructures of As-Cast Alloys

Typical microstructures of the as-cast Nb-Si binary alloys, the eutectic Nb-18.7Si, and the hypereutectic Nb-20Si and Nb-25Si, are shown in Fig. 2-2. Bright phase in these micrographs is (Nb), gray phase, the Nb_3Si, and dark phase, the Nb_5Si_3, respectively. The eutectic Nb-18.7Si alloy exhibits a typical eutectic microstructure consisting of the (Nb) solid solution phase with rod-like or spheroidal morphology and the Nb_3Si matrix, as shown in Fig. 2-2a. A rod-like morphology indicates that the volume fraction of (Nb) is relatively small and that the (Nb) phase may have a certain preference in the growth direction. The primary solidification phase in the hypereutectic alloys is the dendritic Nb_5Si_3. The inter-dendrite region is filled by the fine eutectic product of (Nb)/Nb_3Si, that is observed in the Nb-20Si and Nb-25Si alloys in common. The peritectic Nb_3Si is formed surrounding the primary Nb_5Si_3 in the Nb-20Si alloy. In the case of Nb-25Si alloy, the primary Nb_5Si_3 is surrounded by thin films of (Nb) phase. It is explained by so-called *halo effect* [8] that Nb atoms are rejected into the liquid phase and enriched enough to form (Nb) phase in front of the solid/liquid interface during the solidification of the primary

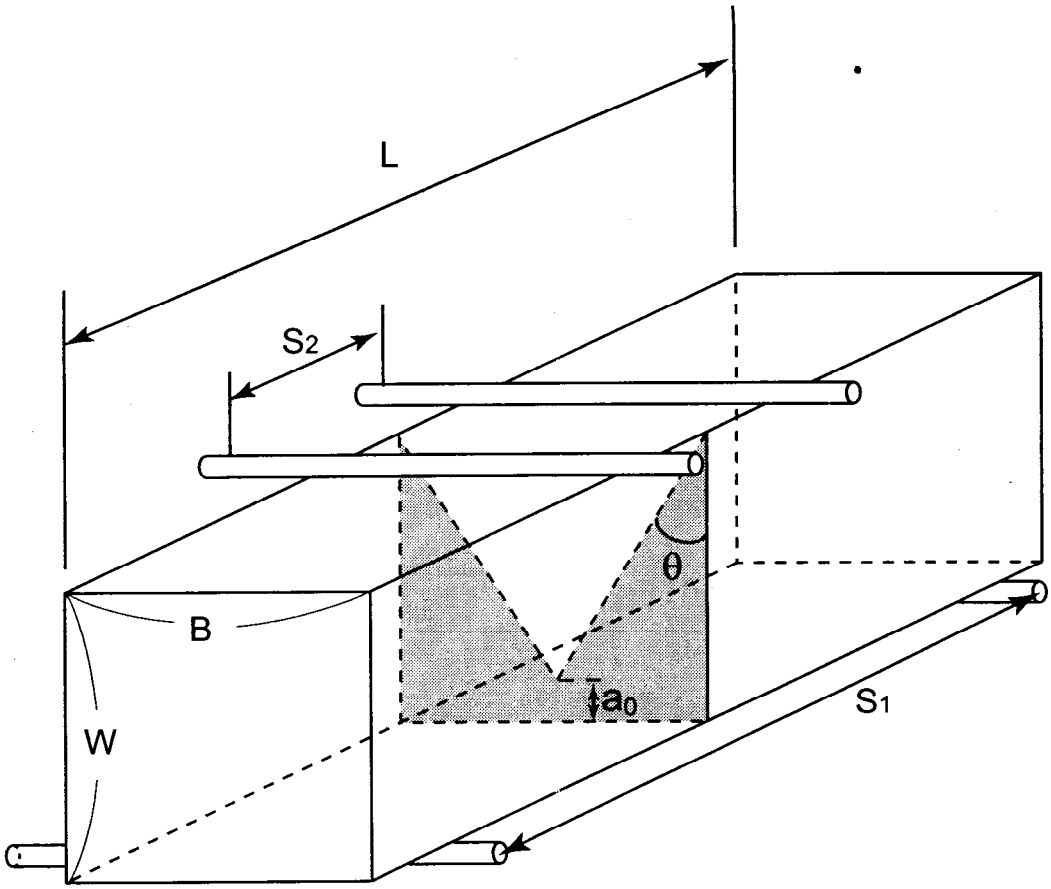

W = B = 5 mm	S_1= 21 mm
L = 30 mm	S_2= 7 mm
θ = 32°	a_0 / W = 0.2

Fig. 2-1 Dimensions of a four-point bending test specimen having a chevron-notch to evaluate the fracture toughness.

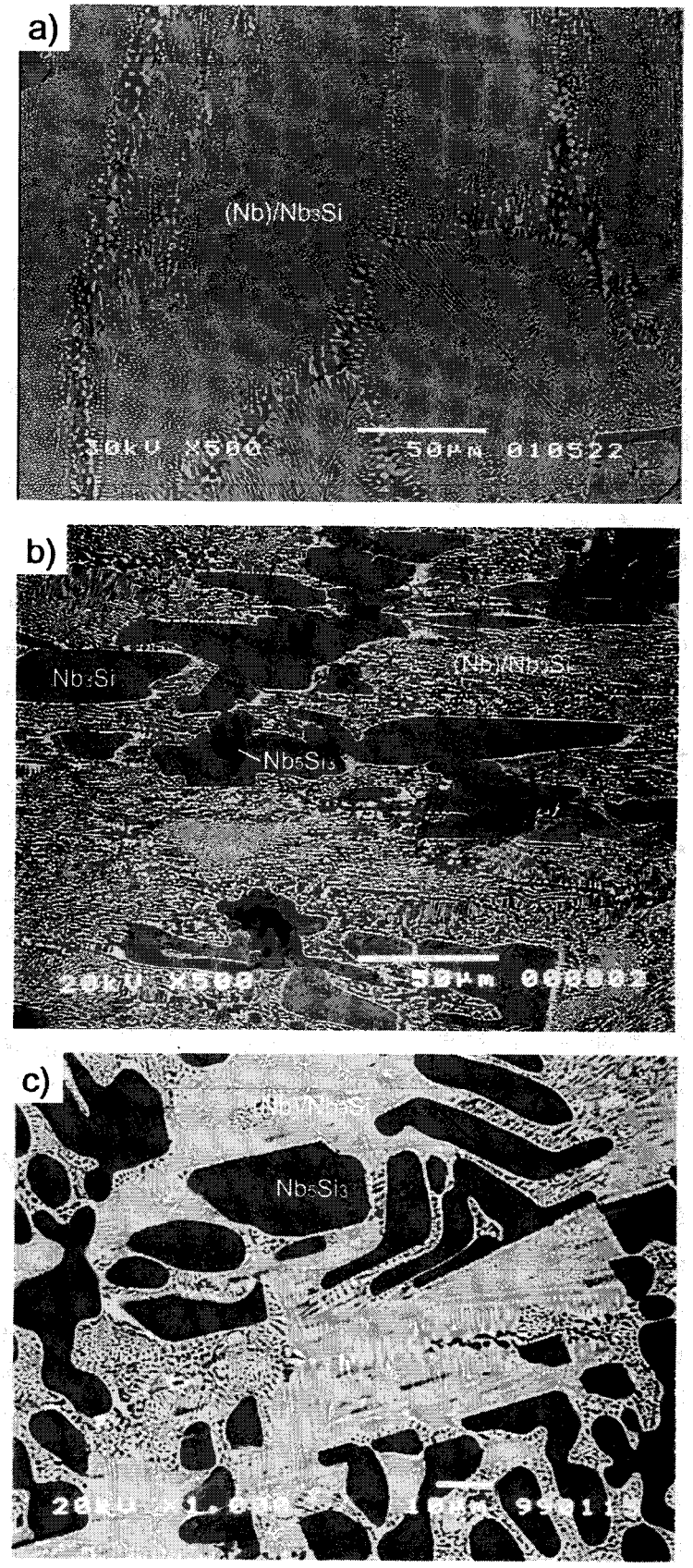

Fig. 2-2 Microstructures of as-cast Nb-Si binary alloys, a) eutectic Nb-18.7Si, b) hypereutectic Nb-20Si, and c) Nb-25Si.

Nb_5Si_3. Subsequently, the eutectic reaction of (Nb)/Nb_5Si_3 takes place skipping a formation of peritectic Nb_3Si phase.

Micrographs of Nb-Si-Ti ternary as-cast alloys with 10 and 20at% Ti are shown in Fig. 2-3. Generally in a ternary system, a competitive growth of two phases from liquid hardly takes place as a eutectic reaction since it is no longer an invariant reaction. Therefore the fine (Nb)/Nb_3Si eutectic product which is observed in the binary alloys are not formed in the ternary alloys. Microstructure of the Nb-18.7Si-10Ti alloy is dominated by fine (Nb) particles in the Nb_3Si matrix. In the hypereutectic alloys, the primary solidification phase is dendritic Nb_5Si_3, and it is surrounded by the peritectic Nb_3Si being subsequently formed. The (Nb)/Nb_3Si two-phase microstructure fills up the inter-dendrite region of the primary Nb_5Si_3 phase surrounded by the peritectic Nb_3Si. There exists no significant difference in as-cast microstructures with Ti contents, between the alloys with 10% and 20%Ti.

3-1-2. Microstructures of Annealed Alloys

Figure 2-4 shows typical microstructures of the alloys after annealing at 1673 K for 100h. High-temperature phase Nb_3Si completely decomposes into (Nb) and Nb_5Si_3 in all the binary alloys and the ternary alloys with 10at% Ti, which has been also confirmed by XRD and EDS. Mendiratta et al. [2] have reported that decomposition of the Nb_3Si requires a long-term annealing at high temperatures in the Nb-19Si binary alloy: for 100 h at 1773 K and for 500 h at 1673 K. Contrary to this, the decomposition of Nb_3Si completes at 1673 K for 100 h in the present work. Although the exact reason of this faster decomposition rate than that reported is not understood, the penetration of impurity atoms such as oxygen is possibly involved which might affect the kinetics of the decomposition [9,10]. It is found that the Ti addition also increases the eutectoid decomposition kinetics, yet this mechanism has not been fully clarified either. Further discussion is given in Chapter 3, where the TTT diagram is determined.

In the Nb-20Si binary alloy, the eutectoid (Nb)/Nb_5Si_3 microstructure provides two distinctive features depending on the morphology of the Nb_3Si phase in as-cast state. As mentioned in the previous section, there exist two regions where Nb_3Si phase is found to have different morphology: one is as the matrix containing fine rods of (Nb) phase in the (Nb)/Nb_3Si eutectic product and the other is formed by the peritectic reaction surrounding the primary Nb_5Si_3. After the eutectoid decomposition of the Nb_3Si phase during annealing, the irregular (Nb)/Nb_5Si_3 eutectoid type microstructure affected by the as-cast (Nb)/Nb_3Si eutectic product is

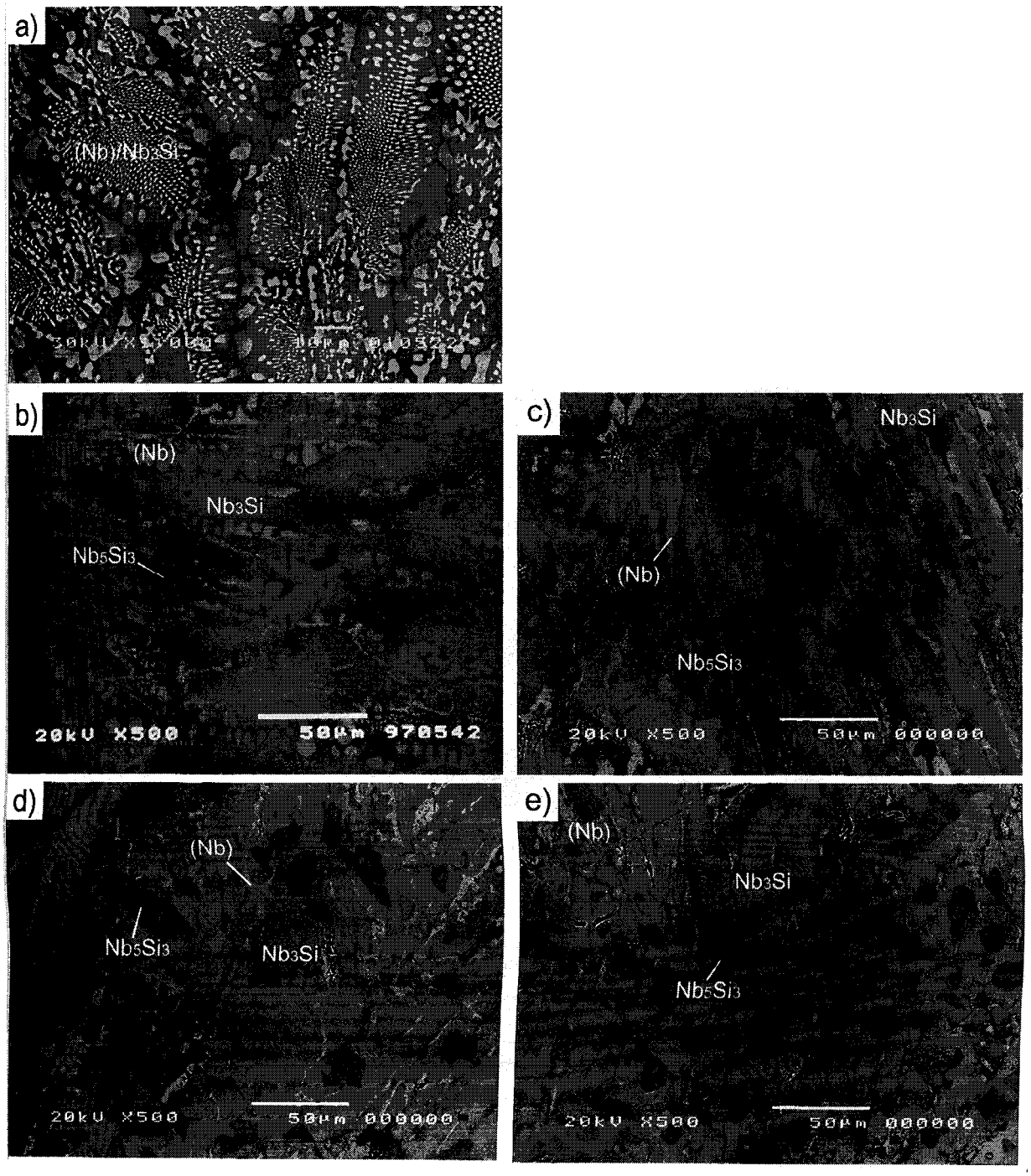

Fig.2-3 Microstructures of as-cast Nb-Si-Ti ternary alloys, a) Nb-10Ti-18.7Si, b) Nb-10Ti-20Si, c) Nb-20Ti-20Si, d) Nb-10Ti-25Si, and e) Nb-20Ti-25Si.

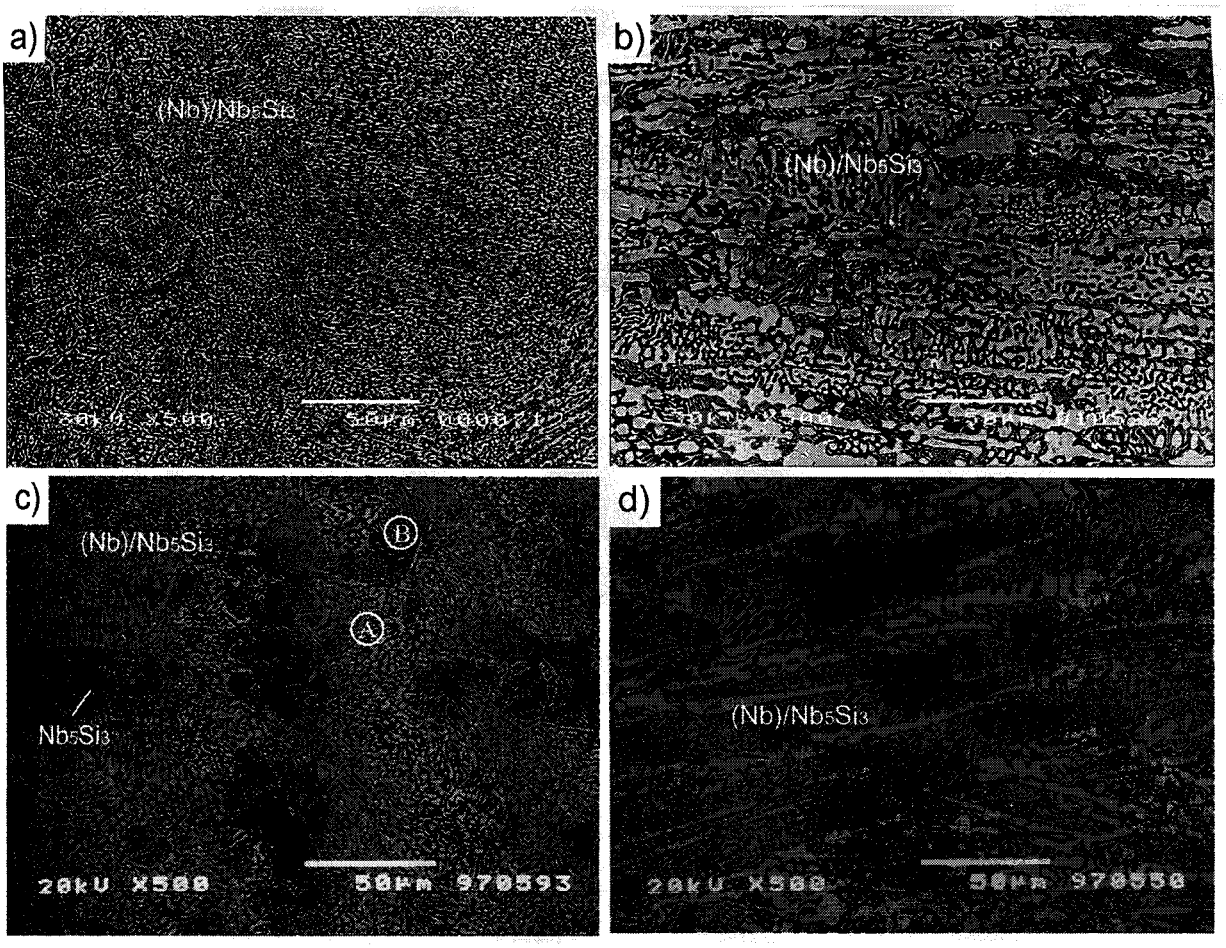

Fig. 2-4 Microstructures of annealed alloys, a) Nb-18.7Si, b)Nb-10Ti-18.7Si, c) Nb-20Si, d) Nb-10Ti-20Si, e) Nb-20Ti-20Si, f)Nb-25Si, g) Nb-10Ti-25Si, and h) Nb-20Ti-25Si.

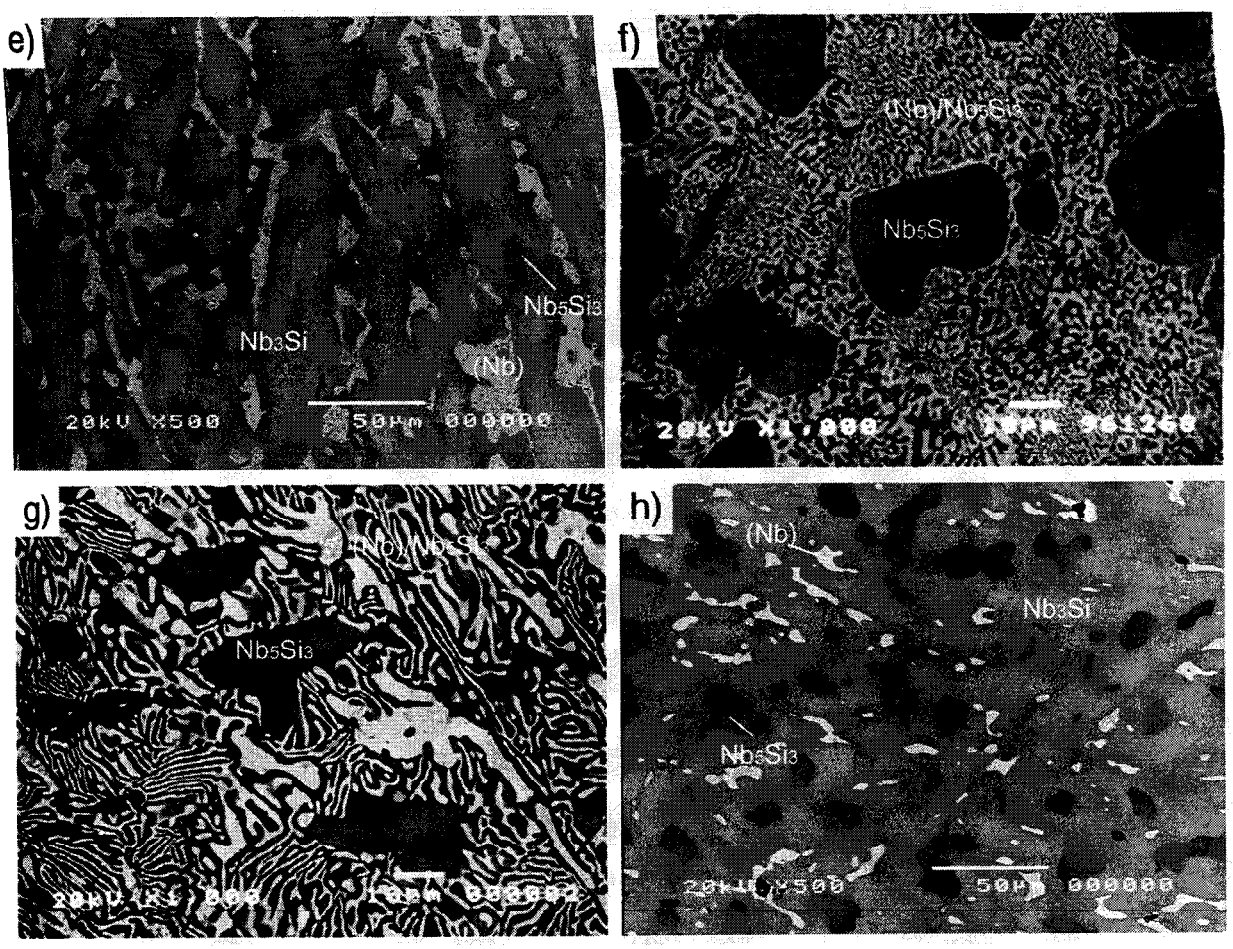

Fig.2-4 Continued.

formed at the former region, denoted *A* in Fig. 2-4c, while rather regular (Nb)/Nb_5Si_3 eutectoid lamellar microstructure is formed at the latter region, *B*. Note that the spheroidizing seems to take place on the (Nb) phase in the former (Nb)/Nb_3Si eutectic region during annealing.

In the ternary alloys with 10at% Ti, the Nb_3Si phase decomposes into the regular (Nb)/Nb_5Si_3 lamellar microstructure since the fine eutectic product is not formed. On the other hand in the alloys with 20at% Ti, the eutectoid decomposition of the Nb_3Si phase is never completed under the present annealing condition. It is observed that Nb_3Si phase remains not to decompose in alloys with Ti exceeding 20at% even after annealing, though microstructures are not shown here. It suggests that the Nb_3Si phase is stable at 1673 K in alloys with more than 20 at% Ti, which is consistent with the results reported by Subramanian et al. [4].

3-1-3. Phase Diagram Determination in the Nb-Si-Ti Ternary System

Further microstructural observations and XRD analyses were performed on the Nb-Si-Ti ternary alloys to reveal whether the eutectoid decomposition of the Nb_3Si phase is completed or not during annealing at various temperatures.

Figure 2-5 shows the isothermal section of the Nb-Ti-Si ternary phase diagram at 1673 K for the (Nb+Ti)-rich portion. Solid symbols show nominal compositions of alloys and open symbols represent the equilibrium concentration of each element in each constituent phase measured by EPMA. The (Nb)/Nb_5Si_3 two-phase region is extended up to about 10% Ti, which is in a good agreement with the results of microstructural observation. However, the (Nb)/Nb_3Si/Nb_5Si_3 three-phase region adjacent to the (Nb)/Nb_5Si_3 two-phase region is relatively small as compared with the result reported by Bewlay et al. [11]. The scattering in Ti concentration analyzed in the Nb_3Si phase is considerably large even after annealing, especially in alloys with higher Ti contents, although the results of EPMA are not shown in detail here. This indicates that the annealing condition of 100 h at 1673 K is insufficient to attain an equilibrium state at least in the Nb_3Si phase.

The vertical section at a constant 25at%Si, along the line from Nb_3Si to Ti_3Si, in the Nb-Si-Ti ternary system is shown in Fig. 2-6. Open circles represent that the Nb_3Si decomposes fully into the (Nb)/Nb_5Si_3 two-phase, while solid circles show that the Nb_3Si phase remains undecomposed. Squares indicate the data from the literature [1,6]. The boundary between the Nb_3Si single-phase region and the (Nb)/Nb_3Si/Nb_5Si_3 three-phase region is predicted from microstructural observation and the results of EPMA shown in Fig. 2-5, and it is indicated by a

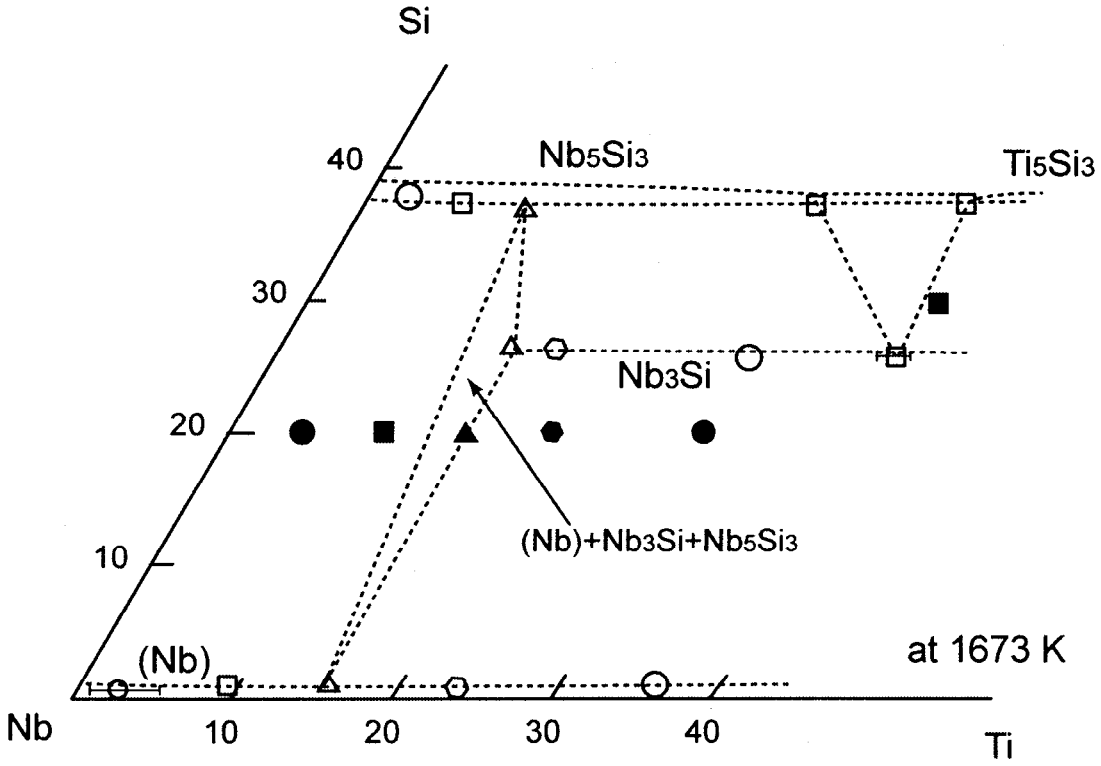

Fig. 2-5 The isothermal section of Nb-rich portion of the Nb-Si-Ti ternary phase diagram at 1673 K .

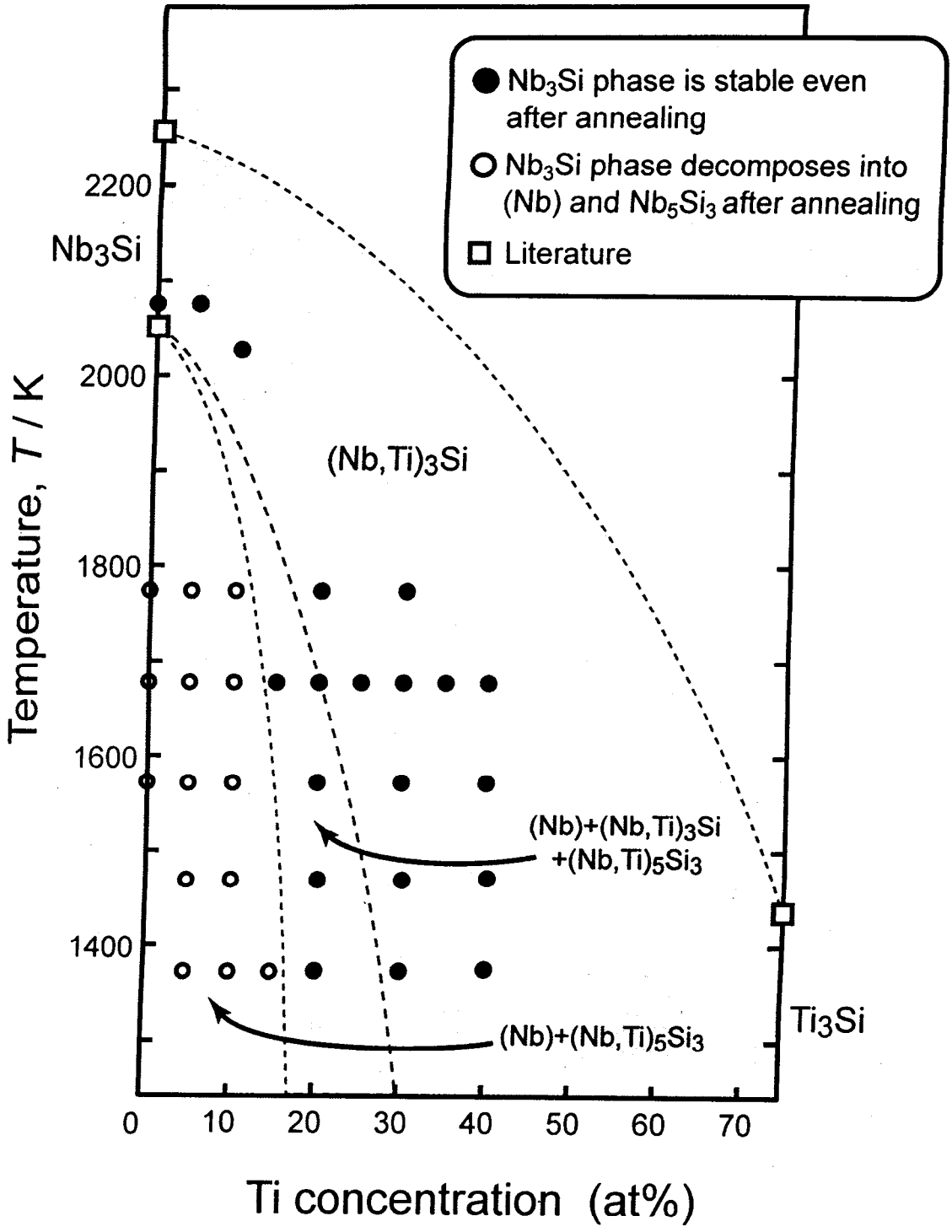

Fig. 2-6 The vertical section at a constant 25 at%Si, along the line from Nb_3Si to Ti_3Si, in the Nb-Si-Ti ternary system.

broken line in the figure.

3-2. Microstructure Control for the Lamellar Formation

3-2-1. Solution Treatment

One of the characteristic of microstructures is the eutectoid (Nb)/Nb_5Si_3 lamellar that would effectively control the mechanical properties of the alloy. To maximize the volume fraction of the lamellar and to control the morphology, it is important to increase the volume of Nb_3Si phase as much as possible via the heat treatment since the (Nb)/Nb_5Si_3 lamellar is formed by the eutectoid decomposition of the Nb_3Si. On the other hand, the coarse primary Nb_5Si_3 causes the extremely low toughness of the alloy, which will be discussed later in the section 3-3. Consulting with the phase diagram shown in Figs. 1-1 and 2-6, the primary Nb_5Si_3 phase can be eliminated by heat treatments at temperatures in the Nb_3Si single-phase region or the (Nb)/Nb_3Si two-phase region. Hereafter, the heat treatments for the elimination of primary Nb_5Si_3 phase is called as the "*solution-treatment*" in the present work regardless of phase constitutions at the heat-treating temperatures.

Comparisons of microstructures between the as-cast and solution-treated alloys are shown in Fig. 2-7 for the Nb-20Si, Nb-20Si-10Ti, Nb-25Si, and Nb-25Si-10Ti alloys. It is clearly seen that the volume fraction of the primary Nb_5Si_3 phase is drastically reduced by the solution-treatment in all the alloys. But a small amount of the primary Nb_5Si_3 phase remains in both the Nb-25Si alloy and Nb-25Si-10Ti alloy.

3-2-2. Eutectoid Decomposition and Lamellar Formation

Annealing for the eutectoid decomposition was subsequently conducted on the alloys at 1673 K for 100 h after the solution-treatment. Typical microstructures of the annealed alloys are shown in Fig. 2-8 for the Nb-20Si, Nb-20Si-10Ti, Nb-25Si, and Nb-25Si-10Ti alloys. The (Nb)/Nb_5Si_3 lamellar microstructure formation by the eutectoid decomposition of the Nb_3Si phase is observed in all the alloys. It is noteworthy that rather regular eutectoid lamellar is formed even in the binary alloys because the fine eutectic product is eliminated or thoroughly coarsened during the solution-treatment. In Chapter 3, the basis of lamellar microstructure control is precisely described focusing on the heat treatment conditions for the inter-lamellar spacing and lamellar colony size control.

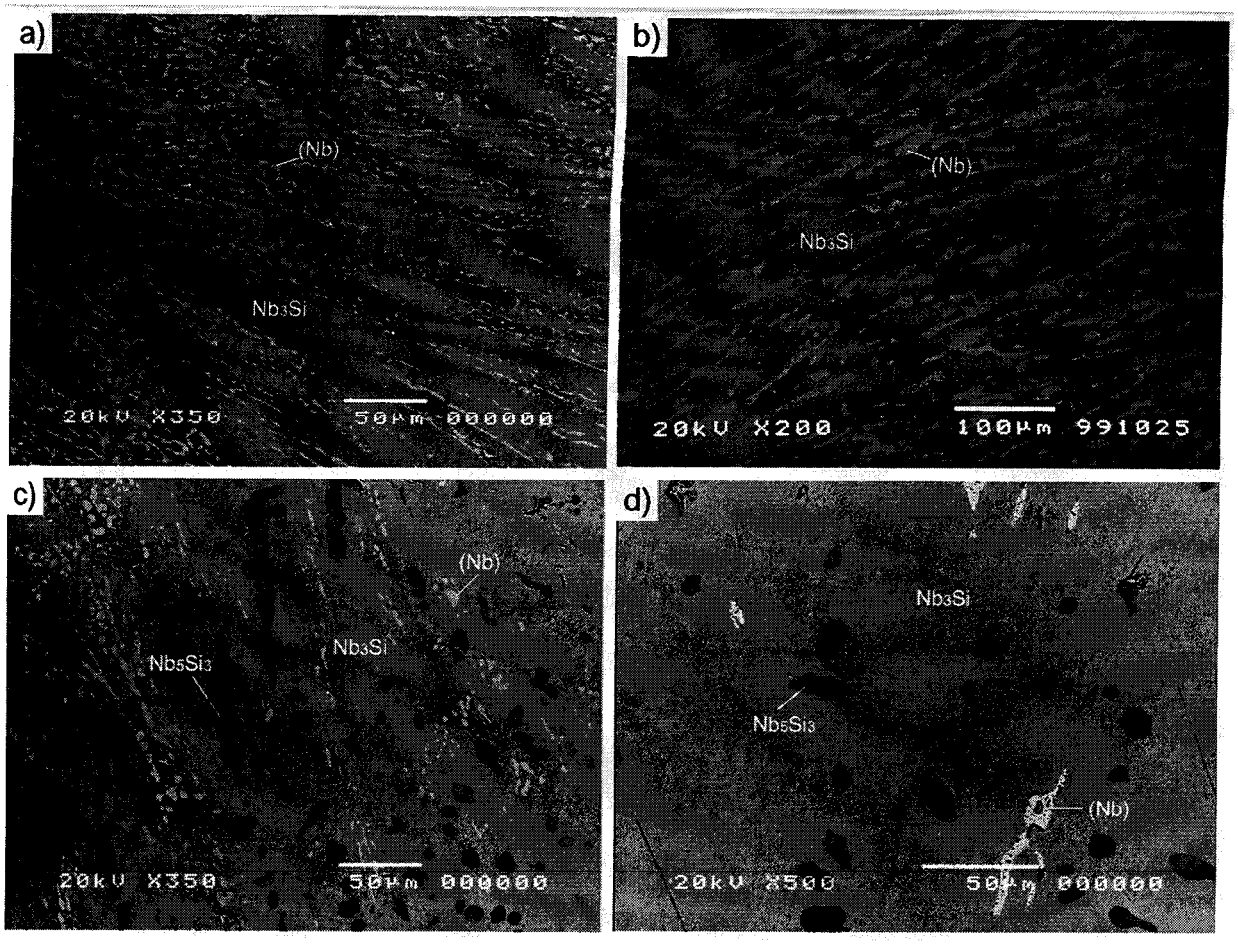

Fig. 2-7 Microstructures of solution-treated alloys, a) Nb-20Si, b) Nb-20Si-10Ti, c) Nb-25Si, and d) Nb-25Si-10Ti.

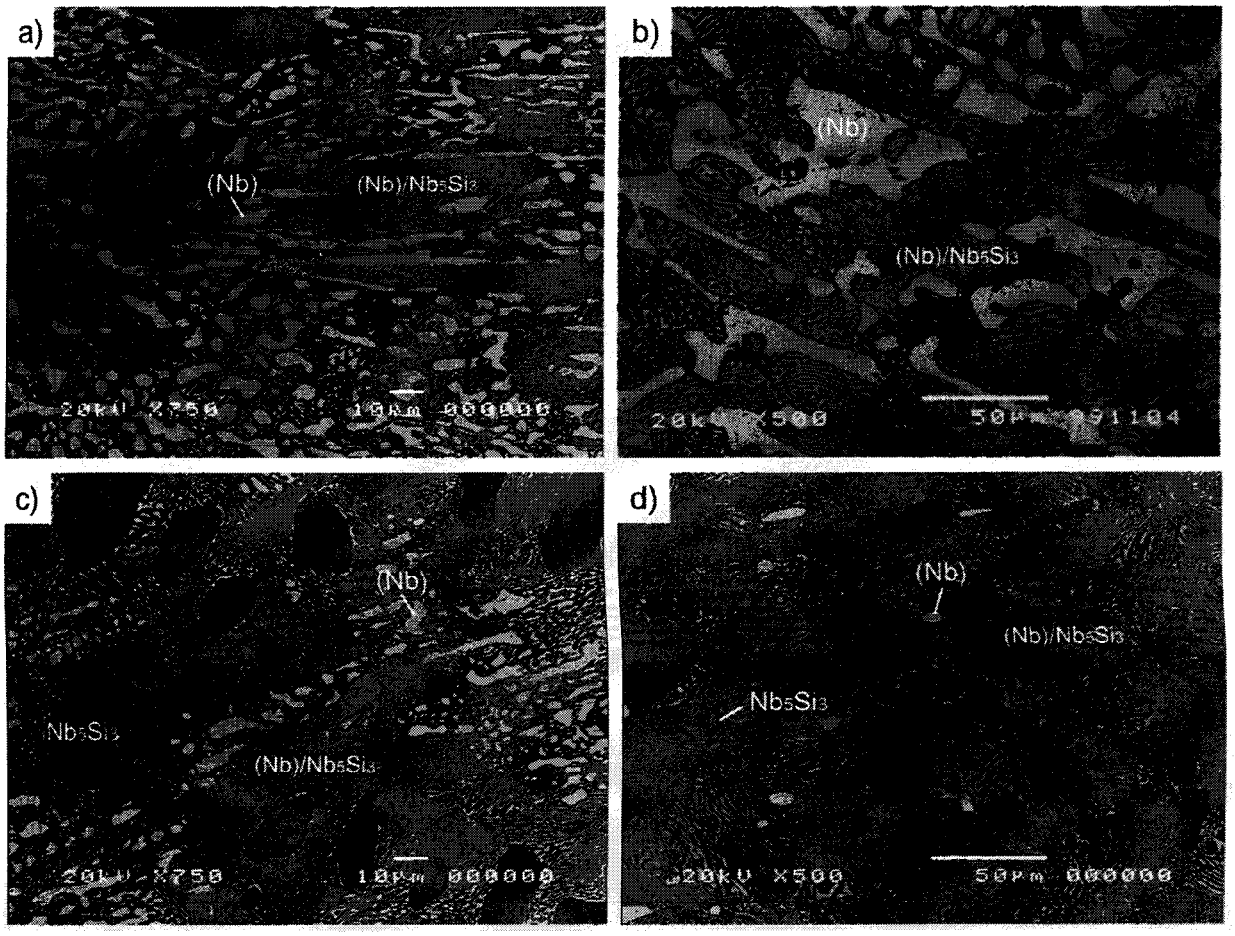

Fig. 2-8 Microstructures of annealed alloys after solution-treatment, a) Nb-20Si, b) Nb-20Si-10Ti, c) Nb-25Si, and d) Nb-25Si-10Ti.

3-3. Orientation Relationship Between (Nb) and Nb_5Si_3 in the Eutectoid Lamellar Microstructure

Figure 2-9 shows a bright field image and the corresponding selected area diffraction (SAD) pattern taken from the (Nb)/ Nb_5Si_3 lamellar boundaries in the Nb-20Si-10Ti alloy annealed at 1673 K for 100 h. The lamellar microstructure is formed by the eutectoid decomposition of Nb_3Si during annealing. It is found that the most parts of the (Nb)/Nb_5Si_3 lamellar boundaries shown in Fig. 2-9a are nearly edged-on. As can be seen from the SAD pattern shown in Fig. 2-9c that (Nb) and Nb_5Si_3 phases obey an orientation relationship (OR):

$$(1\bar{1}0)_{Nb} // (12\bar{3})_{Nb5Si3}$$
$$[331]_{Nb} // [111]_{Nb5Si3}$$

The OR was also confirmed by observations of diffraction patterns along different zone axes. It is found that most of the (Nb)/Nb_5Si_3 lamellar interfaces like the one marked by "A" in Fig. 2-9a, are oriented parallel to the $(0\bar{1}1)_{Nb5Si3}$, which is nearly parallel to the $(-11,9,6)_{Nb}$. Another typical interface marked by "B" is parallel to the $(1\bar{1}0)_{Nb}$ plane and $(12\bar{3})_{Nb5Si3}$ plane.

The stereographic projection of $[331]_{Nb}$ and $[111]_{Nb5Si}$ shown in Figure 2-10 expresses the OR between (Nb) and Nb_5Si_3 obtained above.

The atomic matching of $(12\bar{3})$ plane of Nb_5Si_3 phase and $(1\bar{1}0)$ plane of Nb phase which obey the OR mentioned above is shown in Fig. 2-11. The middle sized solid circle indicates Nb atom on $(1\bar{1}0)_{Nb}$, large sized solid circle Nb atom on $(12\bar{3})_{Nb5Si3}$, and open circle Si atom on $(12\bar{3})_{Nb5Si3}$. The $(12\bar{3})$ atomic plane illustrated in Fig. 2-11 is the most densely packed atomic plane for Nb_5Si_3 phase. Here, Nb atoms from both phases are fixed at the origin marked by "O". It can be seen that all of the Nb atoms in the $(12\bar{3})_{Nb5Si3}$ plane are located close to those in the $(1\bar{1}0)_{Nb}$ plane around the origin. But deviation increases gradually along $[111]_{Nb5Si3}$ direction and larger deviation arises along $[2\bar{1}0]_{Nb5Si3}$ when the distance exceeds 14.7Å. There is 4.5 % mismatch in the directions of $[331]_{Nb}$ and $[111]_{Nb5Si3}$ between the two phases. It is supposed that deviations along $[111]_{Nb5Si3}$ and $[2\bar{1}0]_{Nb5Si3}$ directions may be accommodated by arrays of interfacial dislocations. For example, a dislocation with a Burgers vector indicated by arrows in Fig.2-11 along $[111]_{Nb5Si3}$ and $[2\bar{1}0]_{Nb5Si3}$ directions may satisfy this requirement. Such an operation will minimize the long-range elastic strain. The good coincidence of Nb atoms

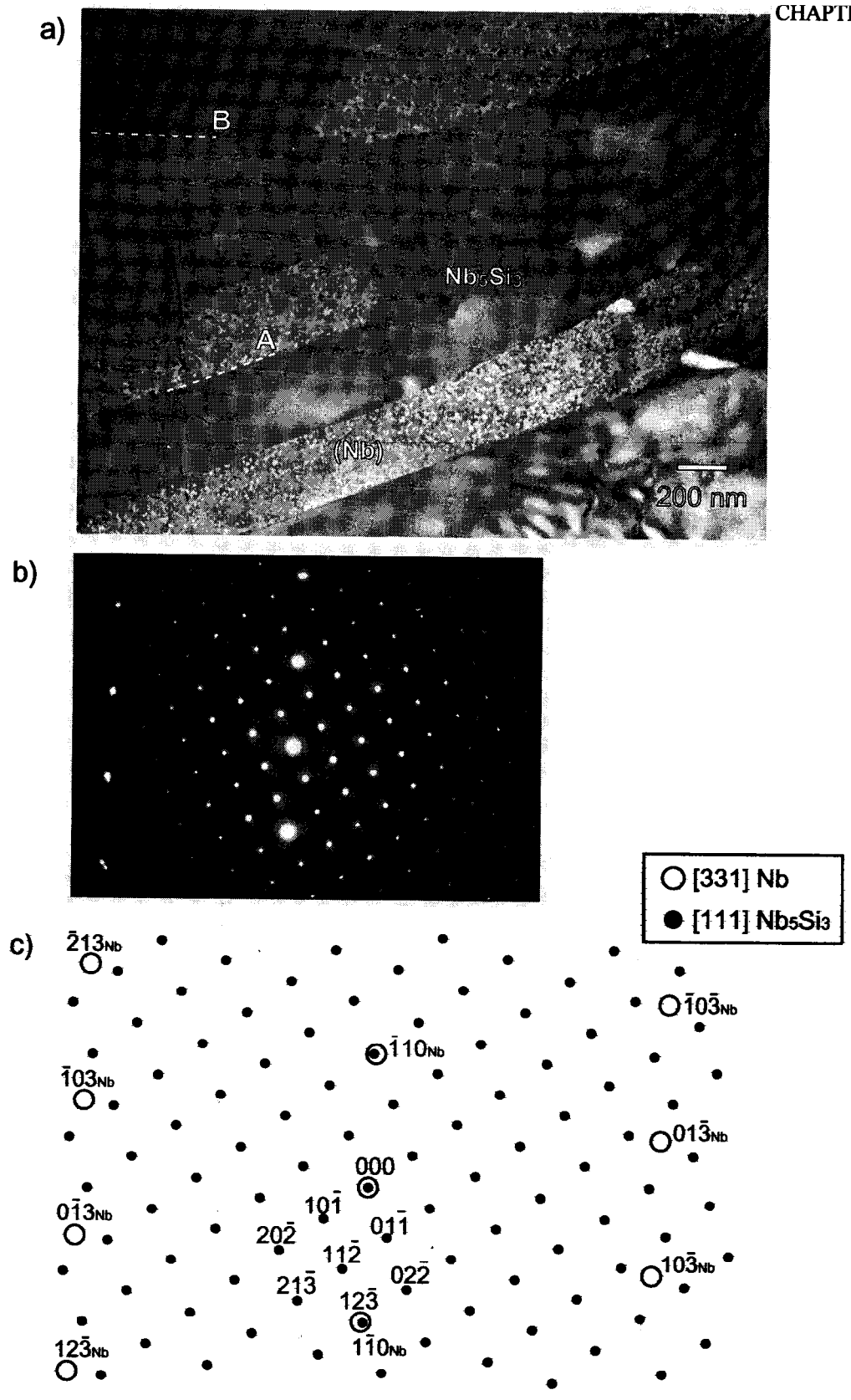

Fig. 2-9 TEM micrographs for the (Nb)/Nb_5Si_3 lamellar microstructure in Nb-20Si-10Ti alloy; a) BF, b) SAD pattern, and c) its indexing.

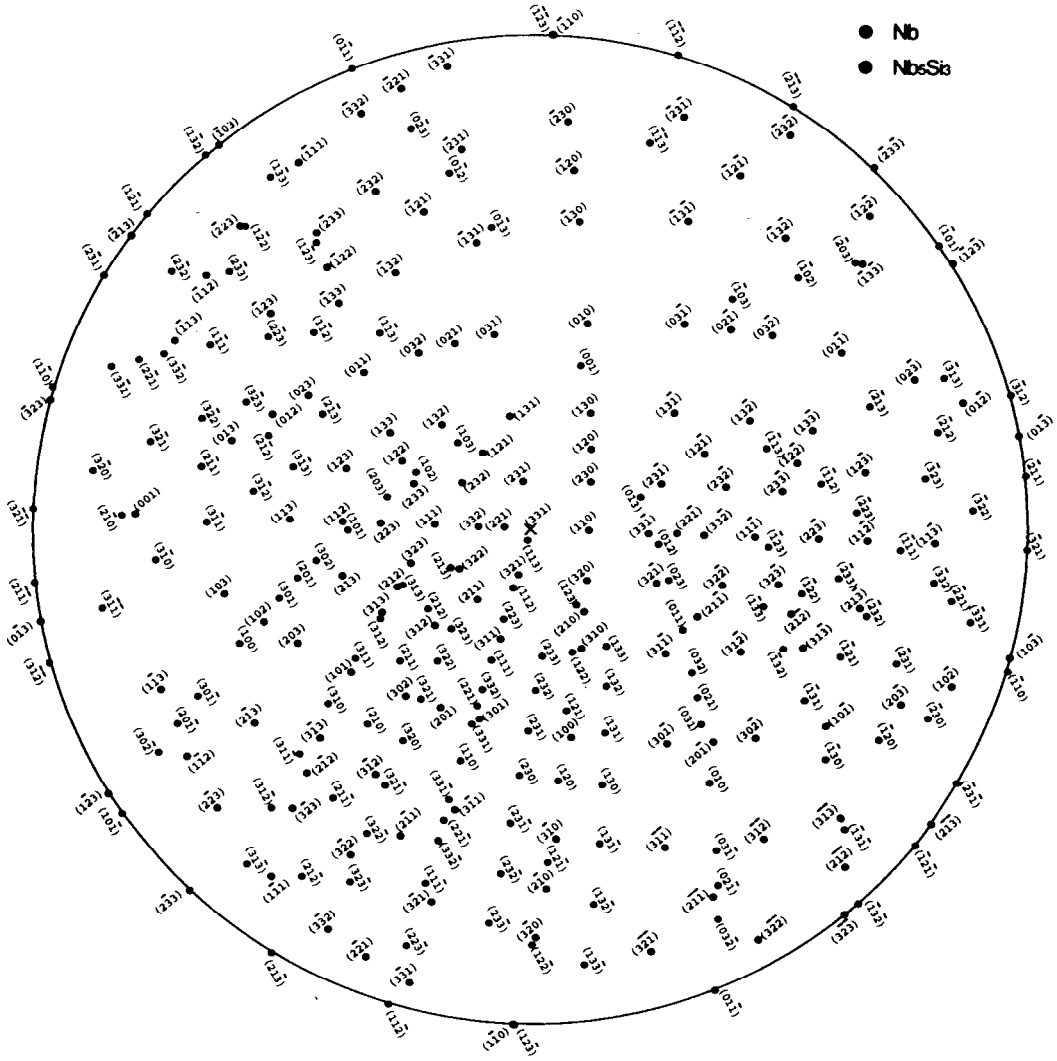

Fig. 2-10 Stereographic projection along $[331]_{Nb}$ (or $[111]_{Nb5Si3}$) representing the orientation relationship between (Nb) and Nb_5Si_3 shown in Fig. 2-9.

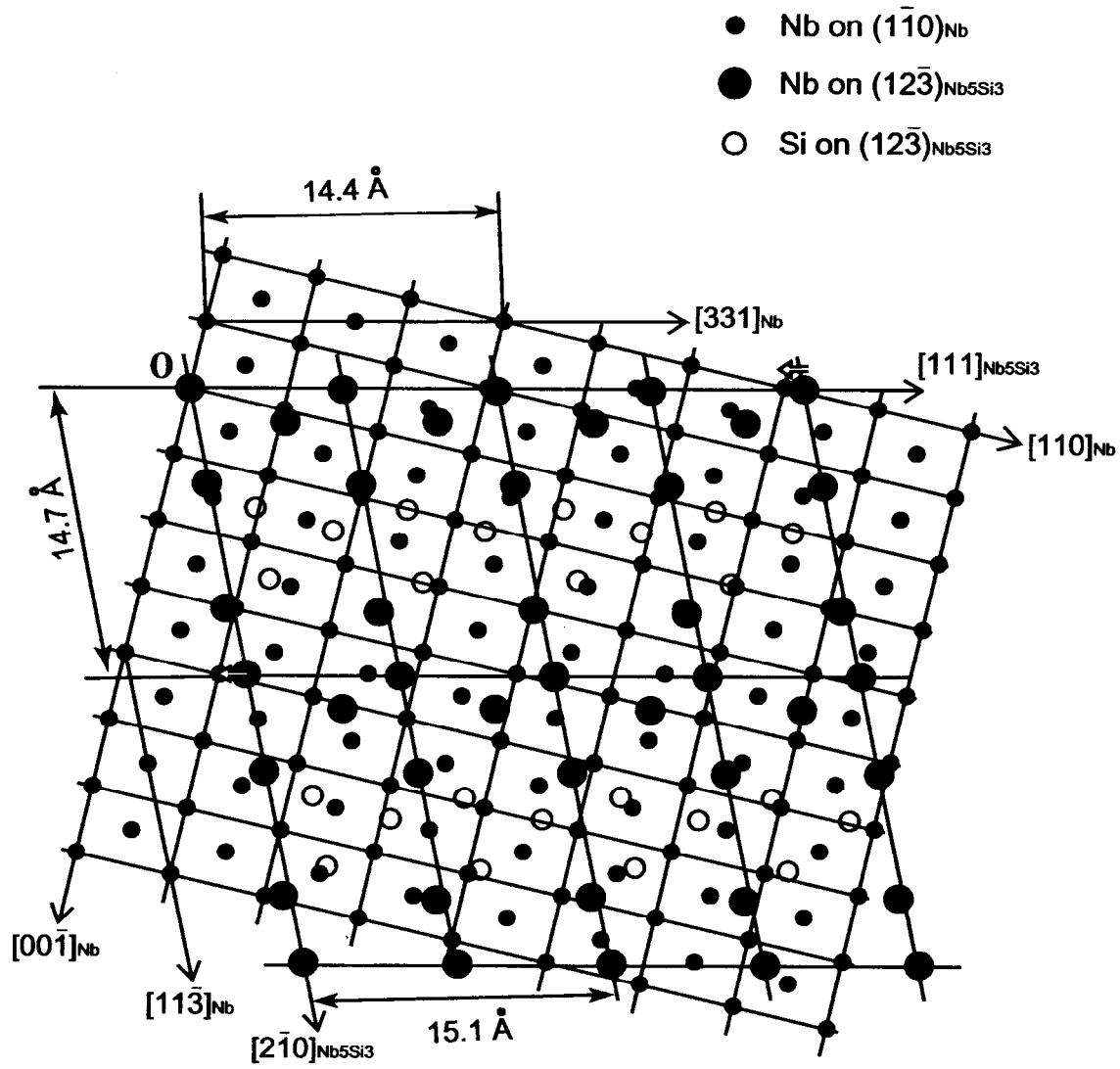

Fig. 2-11 Atomic matching of $(1\bar{1}0)_{Nb}$ and $(12\bar{3})_{Nb5Si3}$ according to the orientation relationship shown in Fig. 2-10.

between $(1\bar{1}0)_{Nb}$ and $(12\bar{3})_{Nb5Si3}$ indicates that the orientation relationship determined in the present work is reasonable.

3-4. Mechanical Properties

3-4-1. Toughness Evaluation by Bending Test with the Chevron-Notched Specimen

One of the easiest method to roughly estimate the toughness of the alloy is to observe the initiation and propagation of micro-cracks introduced by using the micro-Vickers indentation. Figure 2-12 shows an example of the micro-cracks propagating from the corner of the micro-Vickers indent, which is observed in the as-cast Nb-25Si alloy. It is found that many cracks are generated at the primary Nb_5Si_3 phase, but almost no crack is observed in the region of eutectic microstructure. While the Nb_3Si phase, even it is as brittle as the Nb_5Si_3, has a contribution to toughening cooperative with ductile (Nb) phase. Consequently, the large and blocky primary Nb_5Si_3 phase is a preferable site for micro-crack generation. It indicates that the elimination of large blocky primary phase would be favorable for improving room temperature toughness.

In a conventional toughness measurement by using bending test, the straight-notch specimen is used. Chevron-notched specimen (see Fig. 2-1 for the dimensions) is especially useful for measuring the plane-strain fracture toughness of brittle materials, because an adequately sharp micro-crack is naturally produced during the early stage of loading so that no pre-crack is required [7]. Regulations and requirements for chevron-notched specimens, measurements, analytical methods and so forth are available in the ASTM standard [12]. The plane-strain (chevron-notch) fracture toughness, K_{IC} (or K_{IV}), is calculated using the following formula:

$$K_{IC} = \frac{P_{max}}{B\sqrt{W}} Y^* \tag{1}$$

$$Y^* = \left(3.08 + 5.00x + 8.33x^2\right)\frac{S_1 - S_2}{W}\left[1 + 0.007\left(\frac{S_1 \cdot S_2}{W^2}\right)^{1/2}\right] \tag{2}$$

where P_{max} is the maximum load in the load-deflection curve, B the specimen thickness, W the specimen height, S_1 and S_2 the length of outer and inner span at four point bending, x the relative

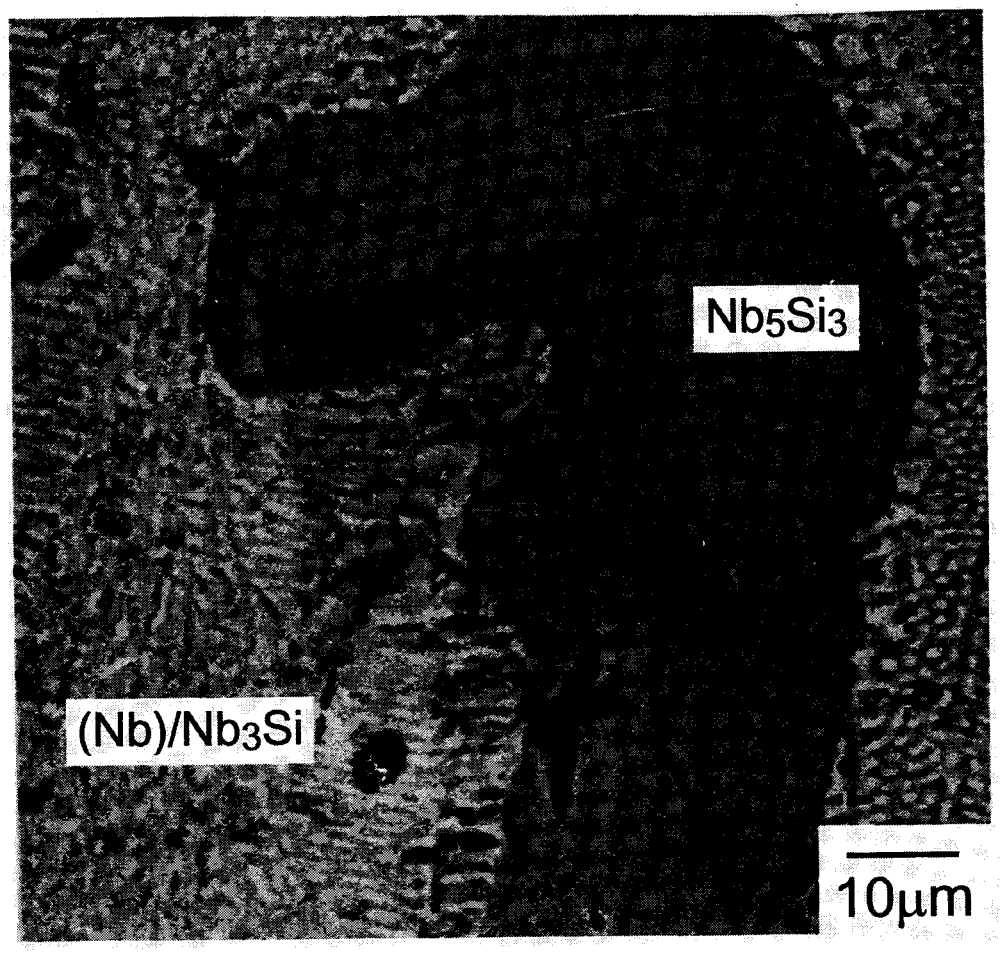

Fig. 2-12 Example of micro-cracks propagating from the corner of a micro-Vickers indent observed inas-cast Nb-25Si alloy.

crack length (= a_0/W), and Y^* the geometry function based on the Bluhm's slice model [7]. The values of K_Q obtained for some selected alloys in the present study are summarized in Table 2-2. Fracture toughness K_Q of the binary eutectic alloy, Nb-18.7Si, evaluated in the present study is 3.4 MPa $m^{1/2}$ relatively lower than 5.5 MPa $m^{1/2}$ reported by Bewlay et al. [13]. The Nb-18.7Si-10Ti and Nb-20Si-10Ti ternary alloys show moderate fracture toughness as high as 10.3 and 11.8 MPa $m^{1/2}$. These results indicate that the Ti addition is effective in improving room temperature toughness. Regarding the effect of difference in microstructure, the alloy annealed after solution-treatment shows higher toughness than the as-annealed alloy. Judging from microstructural observations, the regular lamellar microstructure with relatively thick (Nb) phase is advantageous for enhancing ambient temperature toughness due to the ductile phase toughening mechanism. The detail will be discussed in Chapter 3.

3-4-2. Compressive Mechanical Behavior

To investigate the mechanical behavior of the Nb-Si-Ti ternary two-phase alloys having the (Nb)/Nb_5Si_3 lamellar and primary (Nb), compression tests were conducted at room temperature and at elevated temperatures higher than 1273 K. The present alloys are so brittle that a considerable amount of cracks are formed by thermal stress during cooling after the arc-melting. So the compression test specimens were carefully prepared from an ingot to avoid any micro-cracks visible on its surface as possible. The stress-strain curves obtained from compression tests at room temperature are shown in Fig. 2-13. The Nb-18.7Si-10Ti and Nb-20Si-10Ti alloys show a few percent of compressive plastic strain before fracture, while the binary alloys and the Nb-25Si-10Ti alloy fails in the elastic region showing no compressive plastic deformation. The Nb-20Si-10Ti and Nb-18.7Si-10Ti alloys annealed after solution-treatment exhibit better compressive plastic deformability than as-annealed counterparts.

Compression tests were also conducted on the Nb-Si-Ti ternary alloys at high temperatures ranging from 1273 K up to 1673K. Figure 2-14 shows the compressive stress-plastic strain curves tested at 1273 K, 1473 K, and 1673 K. The Nb-18.7Si-10Ti and Nb-20Si-10Ti alloys exhibit good compressive plastic deformability at 1473 K showing plastic strain over 10 %. At 1673 K, these alloys show even better deformability exceeding 20 % without any cracking on the surface of specimens. The Nb-25Si-10Ti alloy fractures in the elastic region below 1473 K, however it shows fairly good deformability of as much as 10 % at 1673 K. Any significant

Table 2-2 Summary of the chevron-notch fracture toughness, K_Q, for selected alloys.

Alloy Composition	Process / annealing	K_Q (MPa$\sqrt{m}$)
Nb-18.7Si	HT	3.4
Nb-20Si	HT	—
Nb-25Si	HT	6.4
Nb-18.7Si-10Ti	HT	11.8
Nb-20Si-10Ti	HT	10.3
Nb-20Si-10Ti	ST+HT	13.4
Nb-25Si-10Ti	HT	—
Nb-25Si-10Ti	ST+HT	—

HT : 1673 K /100 h ST : 2023 K /100 h — : not measured

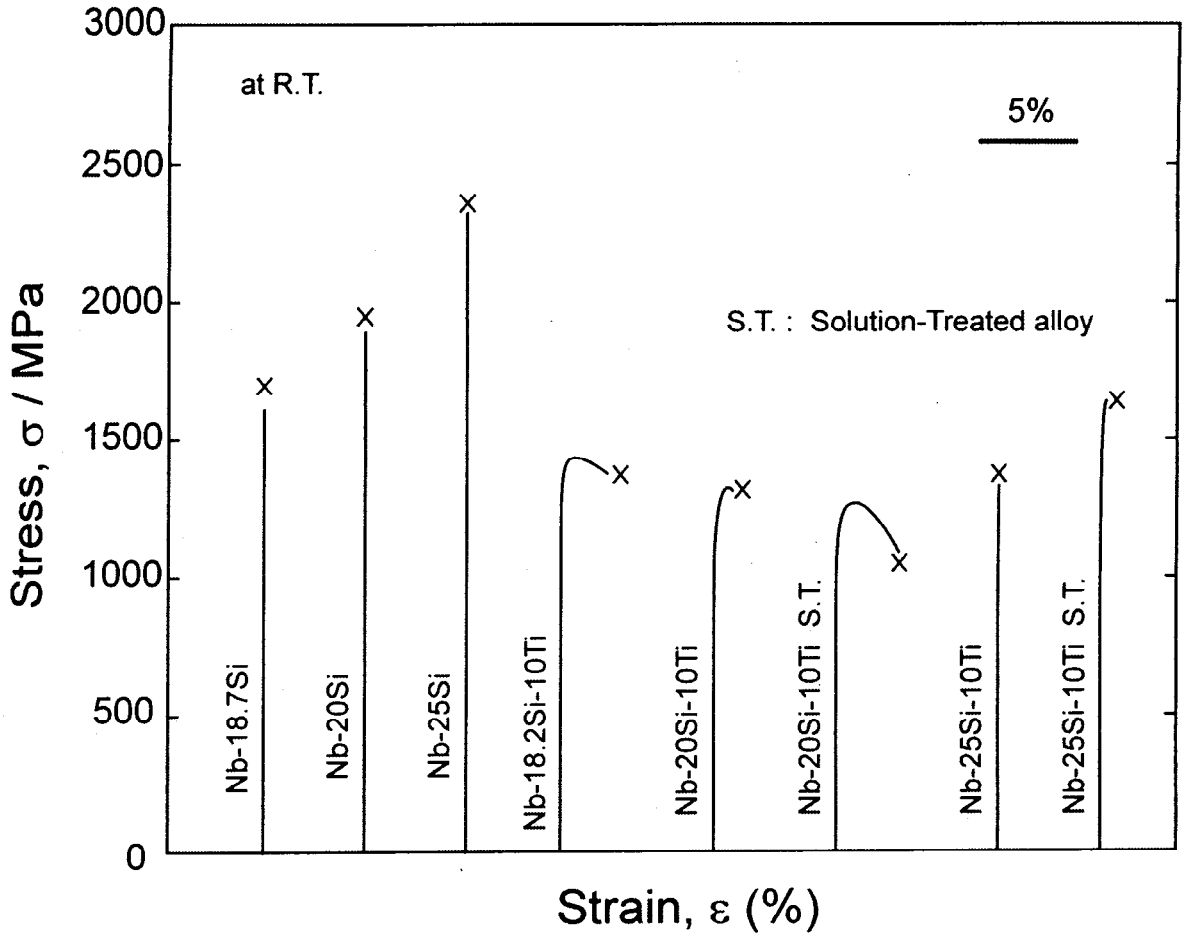

Fig. 2-13 Compressive stress-strain curves of binary Nb-Si-Ti alloys tested at room temperature.

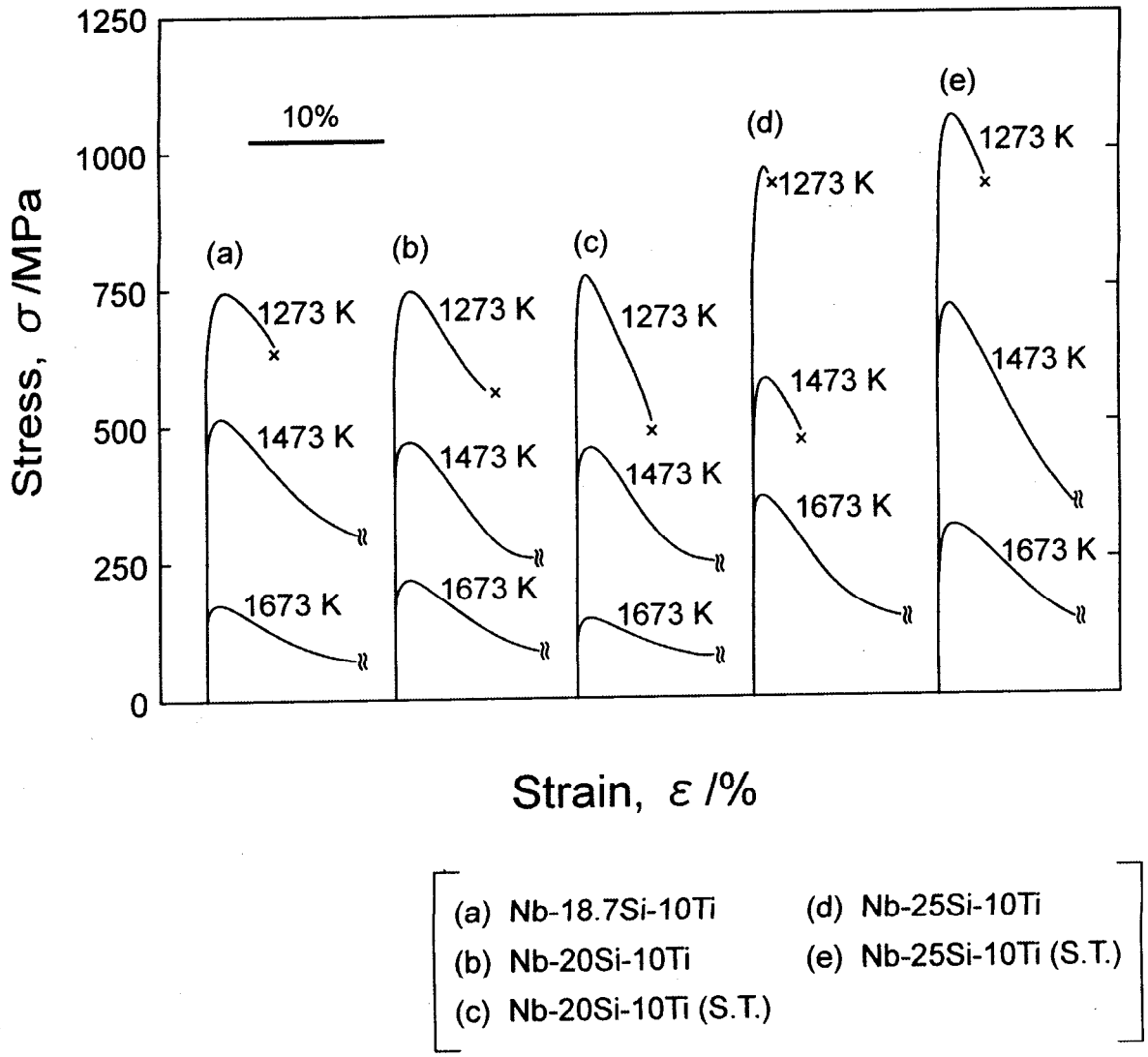

Fig. 2-14 Compressive stress-plastic strain curves tested at 1273 K, 1473 K, and 1673 K for the Nb-Si-Ti ternary alloys.

difference in compressive deformability between the alloys, annealed after solution-treatment and as-annealed, is not observed at high temperatures. Temperature dependence of the 0.2 % compressive flow stress investigated in this study is shown in Fig. 2-15. Strength of the commercial Ni-base superalloys, Inconel-713C and CMSX-10 [14], is also shown for a comparison. The Nb-25Si-10Ti alloy exhibits the highest strength in the present alloys because of the highest volume fraction of the Nb_5Si_3 phase. The Nb-18.7Si-10Ti andNb-20Si-10Ti alloys show comparable strength at overall temperatures. There is no significant difference in the 0.2 % compressive flow stress between the alloys, annealed after solution-treatment and as-annealed. The present alloys show superior strength to Ni-base superalloys at high temperatures over 1273 K, indicating that the (Nb)/Nb_5Si_3 two-phase alloy is a promising candidate as a next generation ultra-high temperature structural material.

3-4-3. Effect of Ti Addition on the Hardness and Toughness

The present results of fracture toughness measurements and compression tests indicate that the Ti addition is effective to improve room temperature toughness. The Ti content dependence of micro-Vickers hardness is shown in Fig. 2-16 for the Nb-Si-Ti ternary alloys annealed at 1673 K for 100 h after solution treatment. The hardness number stands for the average value of overall microstructure regardless of a local morphology. The alloys with 25 at% Si show higher hardness than the alloys with 20 at% Si, because the former alloys have larger volume fraction of the Nb_5Si_3 phase than the latter alloys. The propensity that hardness of the alloys decreases with the amount of Ti addition agrees with the results of compression tests where 0.2% flow-stress decreases with the Ti addition. These results should be explained by two factors: 1) solution softening of (Nb) phase and 2) microstructural change.

Figure 2-17 shows the dependence of micro-Vickers hardness as a function of the Ti content for the Nb-xTi, Nb-1Si-xTi, Nb-4Si-xTi, and Nb-37.5Si-xTi alloys (x = 0 to 10). Note that the solubility limit of Si in (Nb) is less than 1 at%, i.e., the Nb-1Si-xTi and Nb-4Si-xTi alloys are the (Nb)/Nb_5Si_3 two-phase at room temperature [1]. In the Nb-xTi binary alloys, hardness slightly increases with the amount of Ti addition, which is due to the solution hardening by Ti substitution for Nb in the (Nb) phase. Hardness of the Nb-37.5Si-xTi alloy, the Nb_5Si_3 single-phase, increases with Ti addition. As is also mentioned in Fig. 2-12 that the micro-cracks are generated at the corner of the micro-Vickers indentation in Nb_5Si_3 phase. Therefore this could be explained by toughness improvement rather than solution hardening, i.e.,

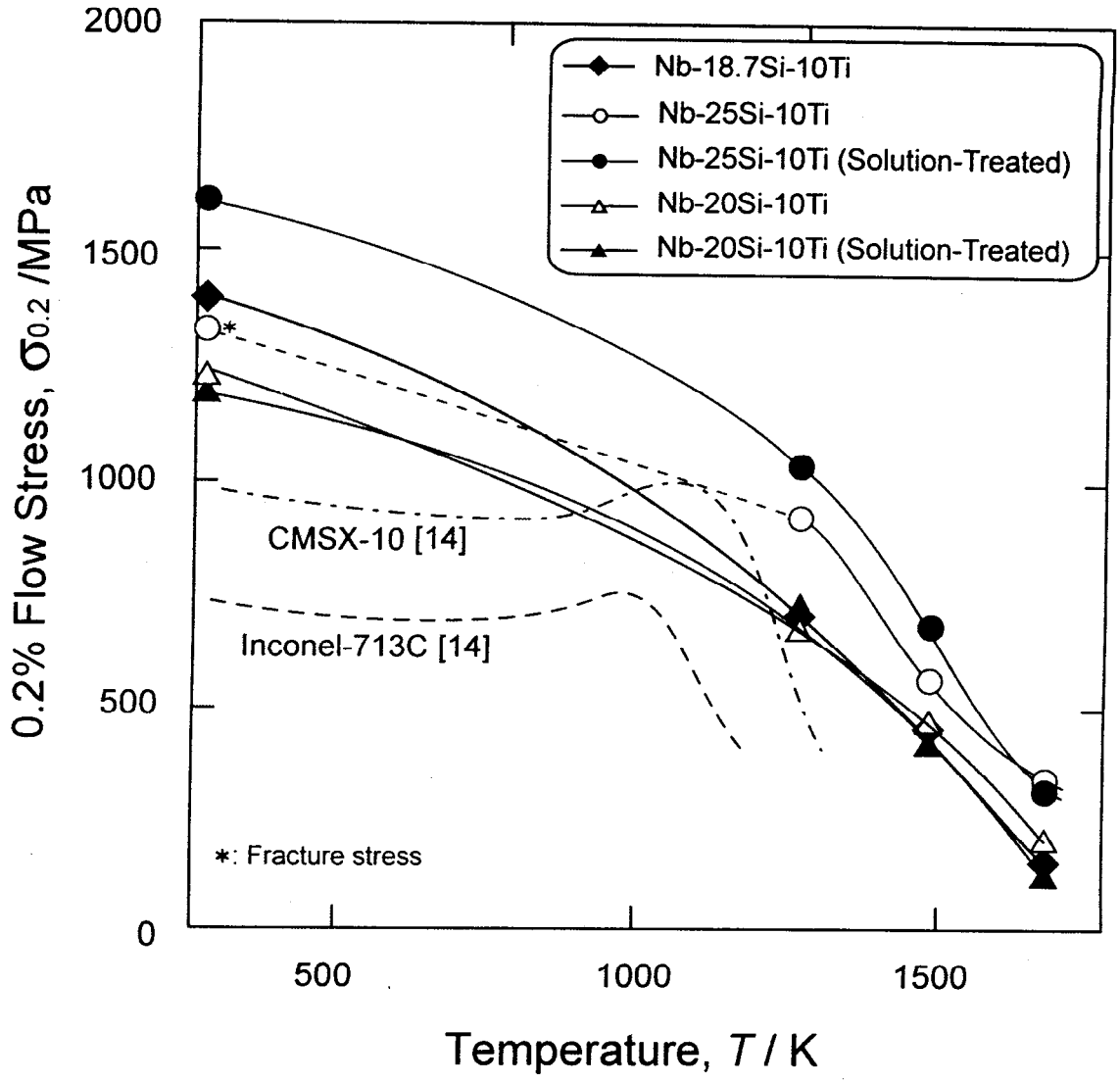

Fig. 2-15 Temperature dependence of the 0.2% compressive flow stress of ternary Nb-Si-Ti alloys. Strength of commercial Ni-base superalloys, Inconel-713C and CMSX-10, is also shown for comparison.

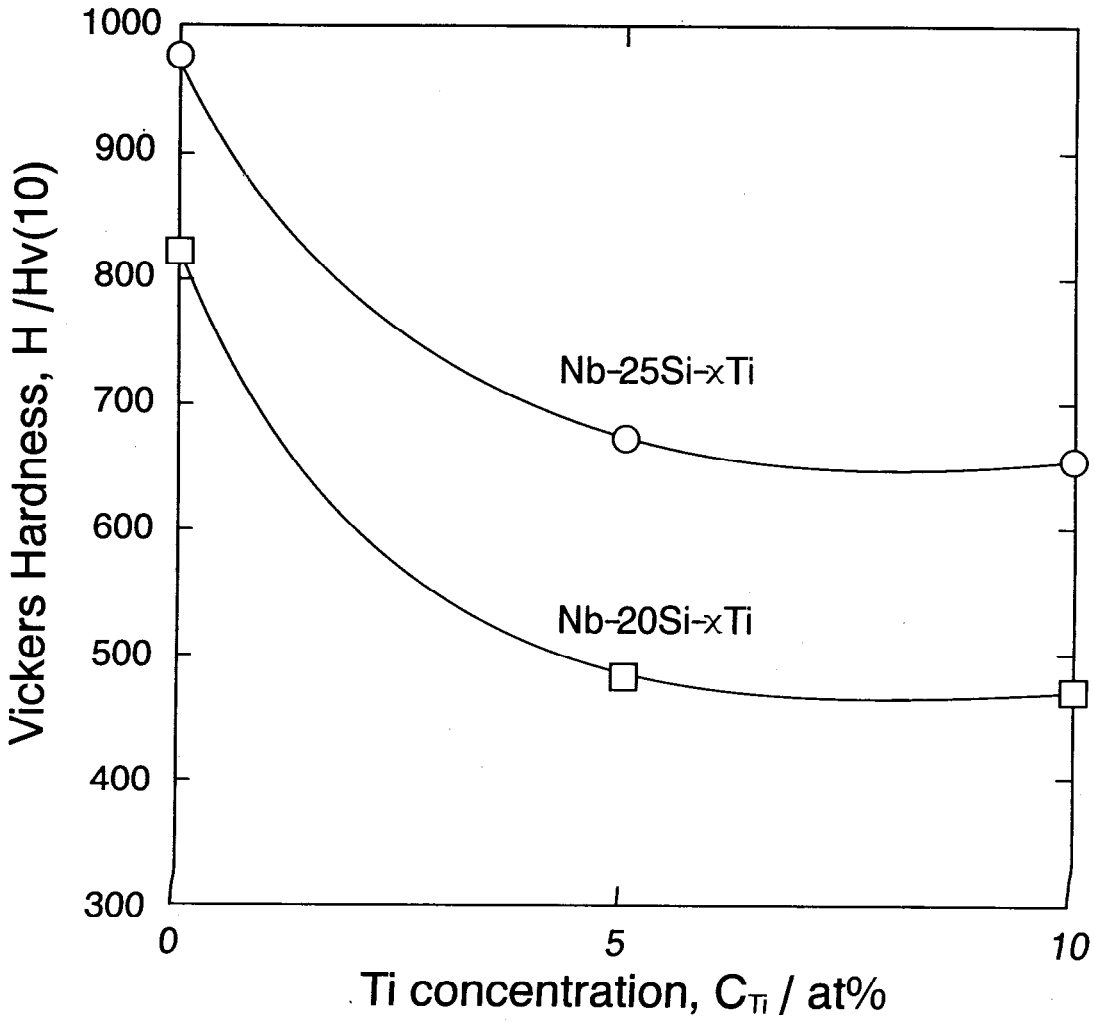

Fig. 2-16 Ti content dependence of micro-Vickers hardness for the alloys annealed at 1673 K for 100 h after solution treatment.

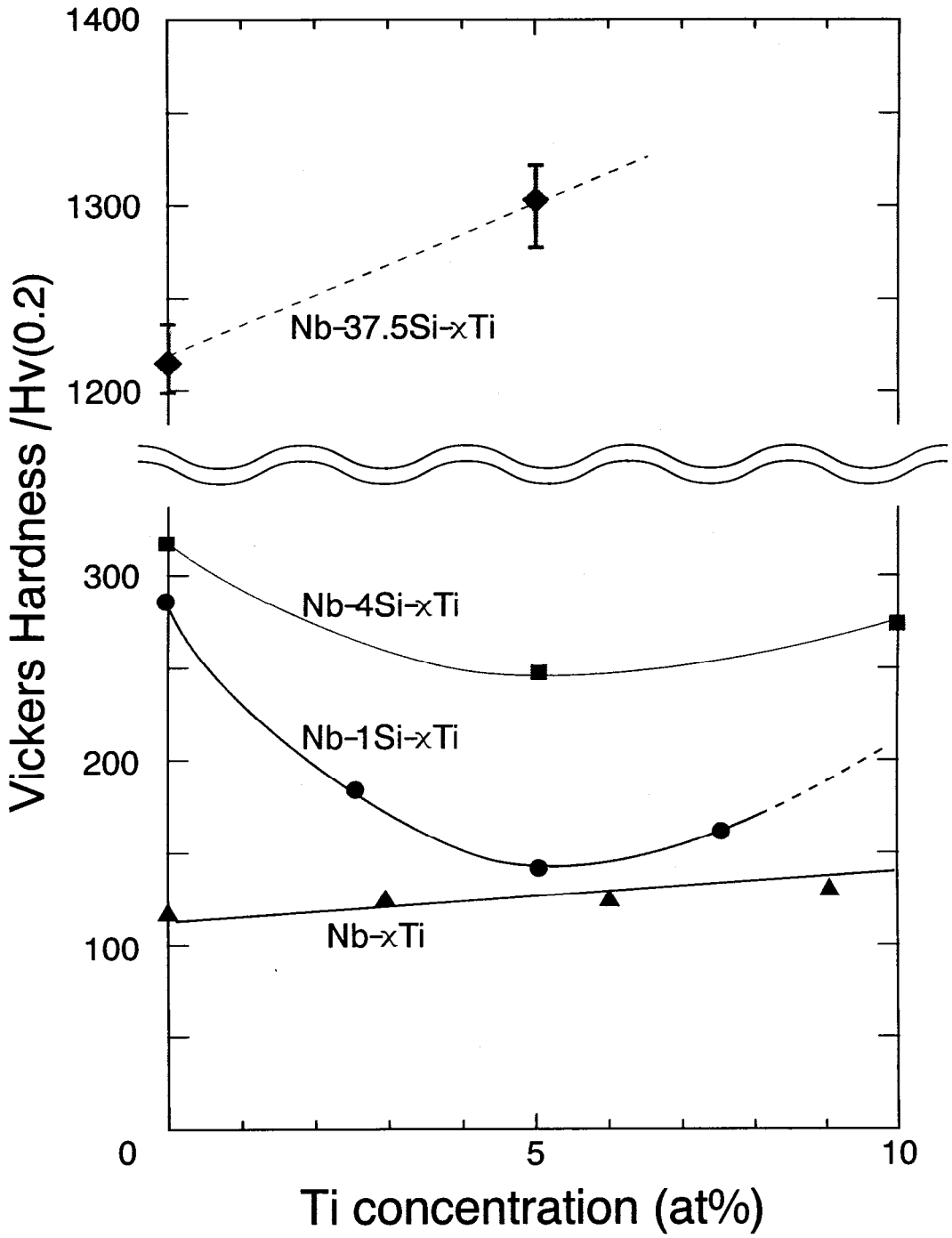

Fig. 2-17 Variation in micro-Vickers hardness as a function of the Ti content for Nb-xTi, Nb-1Si-xTi, Nb-4Si-xTi, and Nb-37.5Si-xTi alloys (x = 0 to 10).

hardness number is underestimated because of the stress relief due to micro-cracking introduced during indentation, and micro-cracking is effectively reduced by Ti addition. Comparing the Nb-1Si-xTi and Nb-4Si-xTi alloys at Ti-free (0at%Ti) in Fig. 2-17, a drastic solution hardening effect can be expected for Si, e.g., the hardness increases by about triple at the first 1at% Si addition in (Nb) phase. A small increase in hardness for another 3at% Si addition should be attributed to the precipitation hardening by the Nb_5Si_3 precipitates. The hardness of these alloys decreases with increasing the amount of Ti addition, and the minimum peak appears at around 5 at% Ti addition. This decrease in hardness with Ti addition is assumed to be the solution softening of the (Nb,Si) phase. For the further discussion in detail, the size and morphology of the Nb_5Si_3 precipitates must be taken into account. It is confirmed by EPMA of which results are shown in Fig. 2-5 that the solubility of Si in Nb solid solution is hardly changed by the addition of Ti. The same results are reported in the literature [4,11]. Therefore, it at least assures that the volume fraction of the Nb_5Si_3 is constant. It should be noted that almost the same propensity of solution softening is observed in the Nb-xTi-20Si and Nb-xTi-25Si alloys (see Fig. 2-16). As a consequent, toughness improvement due to the solution softening of (Nb) solid solution phase by the Ti addition must be one of major factors to affect the mechanical properties of the present alloys.

The second reason is the change of microstructural morphology, especially the primary (Nb) phase, by Ti addition. Based on the ductile-phase-toughening mechanism, the toughness increases with the size of ductile phase [15]. Titanium addition prevents a formation of fine eutectic product and promotes the formation of large (Nb) phase (see Fig. 2-4). The thicker the primary (Nb) phase becomes the larger the ability to prevent micro-crack propagation during the bending and compression tests. These microstructural changes would be an additional effect on improving room temperature toughness.

4. CONCLUSIONS

In order to design a new class of heat resistant alloy based on niobium silicides for ultra-high temperature structural applications, phase equilibria and microstructures were investigated for the two-phase (Nb)/Nb_5Si_3 alloys in the Nb-Si binary and Nb-Ti-Si ternary systems. Special interest in microstructure control was placed on the lamellar formation by the eutectoid decomposition of the Nb_3Si into (Nb) and Nb_5Si_3. Toughness measurements using chevron-notched specimen and compression tests at wide temperature range were conducted to

understand the relationship between microstructures and mechanical properties of the alloys. Conclusions drawn in this chapter are the following.

1. Phase equilibria involving major reactions were experimentally confirmed with the microstructure formation for the related phases, (Nb), Nb_3Si and Nb_5Si_3, in the Nb-Si binary and Nb-Ti-Si ternary systems. Annealing conditions were determined for the eutectoid decomposition of Nb_3Si phase into the (Nb) and Nb_5Si_3 two-phase. The vertical section of the Nb-Si-Ti ternary system was evaluated at a constant 25 at%Si, along the line from Nb_3Si to Ti_3Si.

2. The solution treatment, as defined in the present work, is effective to improve the room temperature fracture toughness through the microstructure modification with two-fold purpose; to eliminate the coarse primary solidification Nb_5Si_3 phase and to form the lamellar microstructure in a subsequent annealing.

3. The crystallographic orientation relationship between (Nb) and Nb_5Si_3 phases was determined in lamellar microstructure formed by the eutectoid decomposition as follows;

$$(1\bar{1}0)_{Nb} // (12\bar{3})_{Nb5Si3}$$

$$[331]_{Nb} // [111]_{Nb5Si3}.$$

4. The uniform lamellar microstructure with large (Nb) phase is advantageous for pursuing a good balance of ambient temperature fracture toughness and high temperature strength. The Ti addition is effective to improve the fracture toughness by the effects of coarsening microstructure and solid solution softening of the (Nb) phase.

REFERENCES

[1] H. Okamoto, A.B. Gokhale and G.J. Abbaschian, in "*Binary Alloy Phase Diagrams, Second Edition*", Ed T.B. Massalski et al., ASM Intnl., 1990.

[2] M.G Mendiratta and D.M. Dimiduk, Scripta Met. Mat., vol. 25 (1991), pp. 237-242.

[3] M.R. Jackson and K.D. Jones, Refractory Metals Extraction Processing and Application, Ed K.C. Liddell et al. TMS Publication (1991), pp. 310-320.

[4] P.R. Subramanian, M.G Mendiratta, and D.M. Dimiduk, MRS Symp. Proc., vol. 322 (1994), pp. 491-502.

[5] B.P. Bewlay, M.R. Jackson, W.J. Reeder and H.A. Lipsitt, MRS Symp. Proc., Vol. 364 (1995), pp. 943-948.

[6] J.L. Murray, in "*Binary Alloy Phase Diagrams Second Edition*", Ed T.B. Massalski et al, ASM Intnl., 1990.

[7] Dietrich G Munz, Int. Journal of Fracture 16 (1980), p.p. 137-140.

[8] Paul Gordon, "Principles of Phase Diagrams in Materials Systems", McGraw-Hill inc. (1968).

[9] *Summary of R&D Report for FY1999 Proposal-Based R&D Program of NEDO* (in Japanese), No.98Ec07-004-2, New Energy and Industrial Technology Development Organization, 1999.

[10] S. Miura, Hokkaido University, private communication.

[11] B.P. Bewlay, M.R. Jackson, and R.P. Bishop, Journal of Phase Equilibria, vol.19 (1998), No. 6, pp.577-586.

[12] "Standard Test Method for Plane-Strain (Chevron-Notch) Fracture Toughness of Metallic Materials", Annual Book of ASTM Standards, E1304-89.

[13] B.P. Bewlay, H.A. Lipsitt, M.R. Jackson, W.J. Reeder and J.A. Sutliff, Mater. Sci. Eng. A, vol. 192/193 (1995), pp. 534-543.

[14] G L. Elickson, Superalloys 1996, TMS Publish (1996), p. 35.

[15] M.F. Ashby, F.J. Blunt and M. Bannister, Acta Metall. Mater., 37 (1989), pp. 1847-1857.

CHAPTER 3

EFFECT OF ANNEALING TEMPERATURE ON MICROSTRUCTURE AND MECHANICAL PROPERTIES

1. INTRODUCTION

Special interest in the present chapter is focused on optimization of the morphology, especially the inter-lamellar spacing, of the (Nb)/Nb_5Si_3 lamellar microstructure. Microstructural observations have revealed that inter-lamellar spacing and colony size of the (Nb)/Nb_5Si_3 lamellar microstructure are controllable by selecting annealing temperatures for the decomposition of Nb_3Si without changing the volume fraction of each phase. To systematically control the lamellar microstructure, the determination of the TTT-diagram (time-temperature-transformation diagram) is necessary for the eutectoid decomposition of high-temperature phase Nb_3Si to (Nb)/Nb_5Si_3 two-phase. The TTT-diagram of the Nb_3Si decomposition has been reported by Mendiratta et al. for the Nb-Si binary alloy [1]. In the present chapter, the TTT-diagram for the Nb-Si-Ti ternary alloys is evaluated mainly by microstructural observation. It is important to recognize that the TTT-diagram is composed with the superimposition of two terms; the rate of nucleation and the rate of growth [2]. The former term is related to chemical driving force and the latter to atomic diffusivity. From the viewpoint of thermodynamics, the average inter-lamellar spacing, λ, is generally proportional to the reciprocal of the degree of super-cooling, $1/\Delta T$ [2]. The correlations of inter-lamellar spacing and lamellar colony size with annealing temperatures are discussed using theoretical models.

In the present chapter, the Nb-20Si-10Ti alloy is selected for further investigation since the alloy exhibits some compressive ductility after solution treatment followed by the isothermal decomposition into the lamellar microstructure, as shown in Chapter 2. The effects of inter-lamellar spacing and lamellar colony size on the 0.2% flow stress at temperatures ranging

from room temperature to 1673 K and on the room temperature ductility are investigated by compression tests. The deformation mechanisms, micro-crack propagation paths, and the toughening mechanisms are discussed in detail for ambient temperature and elevated temperature.

2. EXPERIMENTAL

Alloys were prepared by arc-melting using high purity raw materials (Nb, Si > 99.9%, Ti > 99.5%) under an argon atmosphere. Nominal composition of the alloy prepared for the investigations in this chapter is the Nb-20Si-10Ti, which is accepted if the weight loss after the melting is less than 0.1 %. To eliminate the primary solidification phase, Nb_5Si_3, alloys were solution-treated in the (Nb)/Nb_3Si two-phase field at 2023 K for 90 h under a flowing argon gas atmosphere. To minimize the oxidation during solution treatment, alloys were wrapped with a Nb-foil. Note that the temperature for the eutectoid decomposition of Nb_3Si in the Nb-Si binary system is 2043 K at 20at%Si [3,4], however, it has been found from Fig. 2-6 that the addition of 10 at% Ti lowers the eutectoid temperature down to about 1873 K [5]. Subsequent heat treatments for the eutectoid decomposition of Nb_3Si phase into (Nb) and Nb_5Si_3 phases were conducted at various temperatures between 1373 and 1773 K.

Microstructural observations were performed by using a scanning electron microscope (SEM). Measurement of the average interlamellar spacing was carried out by the linear intercept method. Accurate measurement of the interlamellar spacing requires the condition that lamellar plates must be edge-on. As it is conducted in other researches for pearlitic steels as well [6-8], it is assumed that the edge-on lamellar plates should give the smallest spacing in a lamellar colony. The interlamellar spacing is evaluated as to take the average of the smallest spacing measured in every lamellar colony.

Mechanical properties of the alloy were investigated by compression tests at the temperature range between room temperature and 1673 K. Compression tests were conducted in air at room temperature, and in a vacuum ·($1\sim3\times10^{-4}$ Torr) at elevated temperatures. Compression test specimens, $2\times2\times5$ mm^3, were prepared by electro-discharge machining (EDM) and mechanically polished to remove the damaged surface layer prior to testing. A nominal strain rate is basically 1.0×10^{-4} s^{-1}, and it is varied in the range between 1.6×10^{-5} and 1.0×10^{-1} to investigate the dependence of strain rate on the 0.2 % flow stress at 1673 K. To visualize the relative displacement of lamellar and/or colony boundaries before and after the test,

some compression test specimens were scratched by a polishing paper, and wrapped with a Ta-foil to prevent from oxidation damage on the surface during the tests.

Four-point bending tests were conducted using straight-notch specimens to observe a crack propagation. Test specimens were prepared by EDM, and mechanically polished to remove the damaged surface layer prior to testing. Tests were carried out using an Instron type testing machine with the cross-head speed of 5×10^{-2} mm/min. The bending test specimen was supported by free roller with the outer and inner spans being 21 mm and 7 mm.

3. RESULT AND DISCUSSION

3-1. Microstructural Observation and Metallographic Analysis

3-1-1. The TTT-diagram evaluation of the Nb_3Si decomposition

In order to control lamellar microstructures by selecting annealing temperatures, it is necessary to determine the TTT-diagram (time-temperature-transformation diagram) for the eutectoid decomposition of high-temperature phase Nb_3Si to (Nb)/Nb_5Si_3 two-phase. The TTT-diagram has been determined by Mendiratta et al. for the Nb_3Si decomposition in the Nb-19Si binary alloy [1], however it can not be applied to the Nb-Si-Ti ternary alloys in the present work without any modification because the kinetics of the decomposition must be affected by the Ti addition. Therefore it is necessary to determine the TTT-diagram in the Nb-Si-Ti ternary system. A Nb-25Si-10Ti ternary alloy is then selected for this purpose. Alloys were furnace-cooled after annealing for various periods of time at various temperatures. Figure 3-1 shows the TTT-diagram evaluated mainly by microstructural observation. The temperature for the eutectoid decomposition of the Nb_3Si, T_e, is approximately determined as 1873 K from the vertical section at constant 25at% Si of the Nb-Si-Ti ternary system shown in Fig. 2-6 of the previous chapter. Definition of T_e will be discussed in detail later in the section 3-1-3. The TTT diagram reported by Mendiratta et al. for the binary alloy [1] and the other reports on the eutectoid temperature [3,4] are also shown by dotted lines for a comparison. Both the binary and ternary alloys exhibit so-called C-curve which is basically described by a classical nucleation and growth behavior. The C-curves of the ternary alloy shift towards lower in temperature and shorter in time from those of the binary alloy.

A general concept of C-curve type behavior of a transformation is well recognized that it is determined by the *superimposition* of the rate of nucleation, *chemical driving force*, and the rate

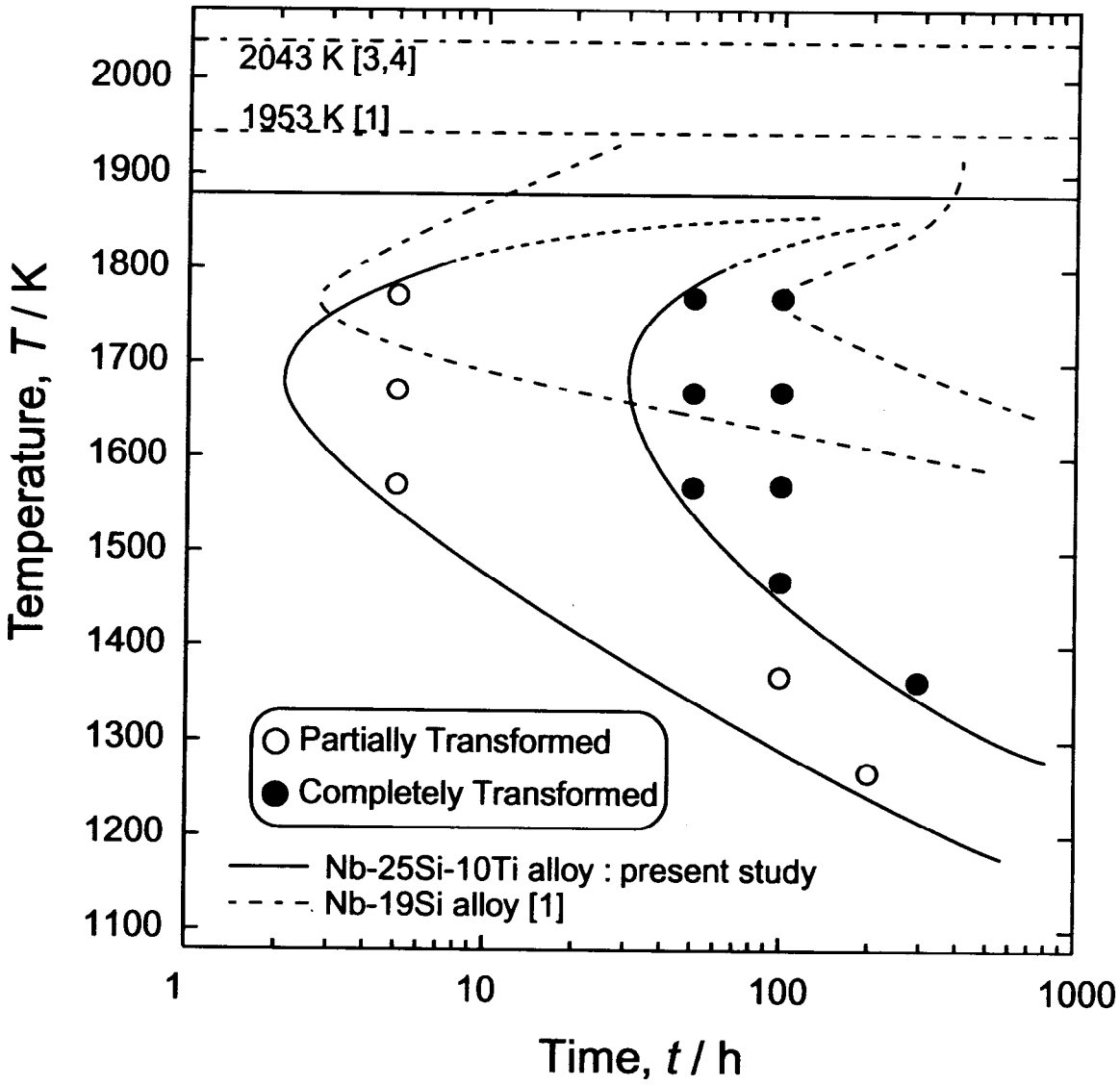

Fig. 3-1 The TTT-diagram for Nb_3Si decomposition determined for a Nb-25Si-10Ti alloy.

of growth, *atomic diffusivity* [2]. The *chemical driving force* of a transformation increases with a degree of super-cooling, i.e. the larger super-cooling requires the shorter duration for a transformation. While the *atomic diffusivity* increases with annealing temperature, i.e. the solute diffusion required for a transformation is enhanced at higher temperature. A C-curve has the so-called nose temperature as a result of superimposition of these two propensities, meaning that a transformation is controlled by the *chemical driving force* at higher temperatures and by the *atomic diffusivity* at lower temperatures than the nose.

The shift of C-curves towards lower temperature seems to be attributed to that the eutectoid temperature is decreased by the Ti addition. However, the tendency of C-curves shifting toward shorter time can not be explained by that. Titanium is the element to stabilize the Nb_3Si, therefore an addition of Ti must delay the transformation kinetics. It is not clarified that why the Nb_3Si decomposition is faster in the Nb-Si-Ti ternary than in the Nb-Si binary, but it is presumably true that the decomposing reaction rate and/or atomic diffusivity are somehow enhanced by the Ti addition, for Ti addition lowers the melting point of the alloy. On the other hand, decomposition of the Nb_3Si still requires a long-term annealing at high temperatures; for the shortest, 50 h at 1673 K. This result indicates that atomic diffusion could be very slow at temperatures below 1773 K in the Nb-Si-Ti ternary system, and that the resistance against coarsening of microstructure, namely the stability of microstructure is expected to be high even at such high-temperature.

The eutectoid decomposition rate should strongly depend on the grain size of the parent Nb_3Si phase, since the eutectoid decomposition of the Nb_3Si is a grain boundary reaction type. It is intuitively predicted that the smaller the grain size becomes the faster the decomposition finishes with increasing in the total area of grain boundaries. It is noteworthy that the TTT-diagram determination is easily affected by the condition of alloy preparations as well. In the present alloy systems, Nb-Si and Nb-Si-Ti, it has been revealed that the eutectoid decomposition rate may be enhanced by impurities such as oxygen and chlorine [9]. The mechanism to rationally describe this phenomenon has not yet been clarified, though, there exists the experimental fact that the decomposition progresses faster in the outer portion of an ingot than in the center of it. The decomposition could be enhanced by, for instance, the inward diffusion of oxygen during annealing. Another interesting experimental fact is that the decomposition rate differs in alloys prepared by arc-melting and by directionally solidification using floating zone melting, as will be shown in Chapter 5, where the eutectoid decomposition

rate is faster in the alloy prepared by the former method than in the latter. This tendency should be attributed to the mixed contribution of grain size and impurities effects.

3-1-2. Microstructures

Alloys were solution-treated, as defined in the previous chapter in the (Nb)/Nb_3Si two-phase field at 2023 K for 90 h to eliminate the primary solidification phase, Nb_5Si_3. As mentioned in the previous chapter, the coarse primary Nb_5Si_3 reduces room temperature toughness of the alloy. Figure 3-2 shows microstructures of the as-cast and as-solution-treated Nb-20Si-10Ti alloys. Bright phase in these micrographs is (Nb), gray phase the Nb_3Si, and dark phase the Nb_5Si_3, respectively. Dendritic primary solidification phase, Nb_5Si_3, observed in the as-cast alloy can be completely eliminated by solution treatment. Since the alloy composition is not stoichiometric of the Nb_3Si (i.e. Nb-25Si), microstructure consists of (Nb) and Nb_3Si two-phase after solution treatment. The (Nb) phase is much coarsened during solution treatment. The (Nb)/Nb_5Si_3 lamellar microstructure can be obtained by the subsequent heat treatment via the eutectoid decomposition of the high-temperature phase Nb_3Si.

Figure 3-3 shows the typical microstructures of the Nb-20Si-10Ti alloys annealed at various temperatures between 1373 K and 1773 K after the solution treatment. Note that annealing was conducted for sufficient time to complete the eutectoid decomposition at each temperature by consulting with the TTT-diagram shown in Fig. 3-1. Lamellar spacing becomes larger with increasing annealing temperature. Lamellar colony size (or nodule size) also increases with annealing temperature, however colony boundaries tend to become unclear as annealing temperature increases. No other remarkable microstructural change except the lamellar spacing and colony size is observed among the alloys annealed at various temperatures.

3-1-3. Quantitative Metallographic Analyses

Quantitative metallographic analyses were performed to characterize the microstructure. As shown in Fig. 3-3, lamellar spacing and lamellar colony size increase with annealing temperature. Zener has pointed out that the average lamellar spacing, λ, is proportional to the reciprocal of the degree of super-cooling, $1/\Delta T$, in pearlitic steels [2]. According to his analysis, the minimum interlamellar spacing, λ_0, of the isothermally formed eutectoid pearlite is computed on the assumption that the growth of a pearlite nodule lowers the total Gibbs free energy of the whole system. Figure 3-4 shows a schematic of a pearlite nodule, with the depth

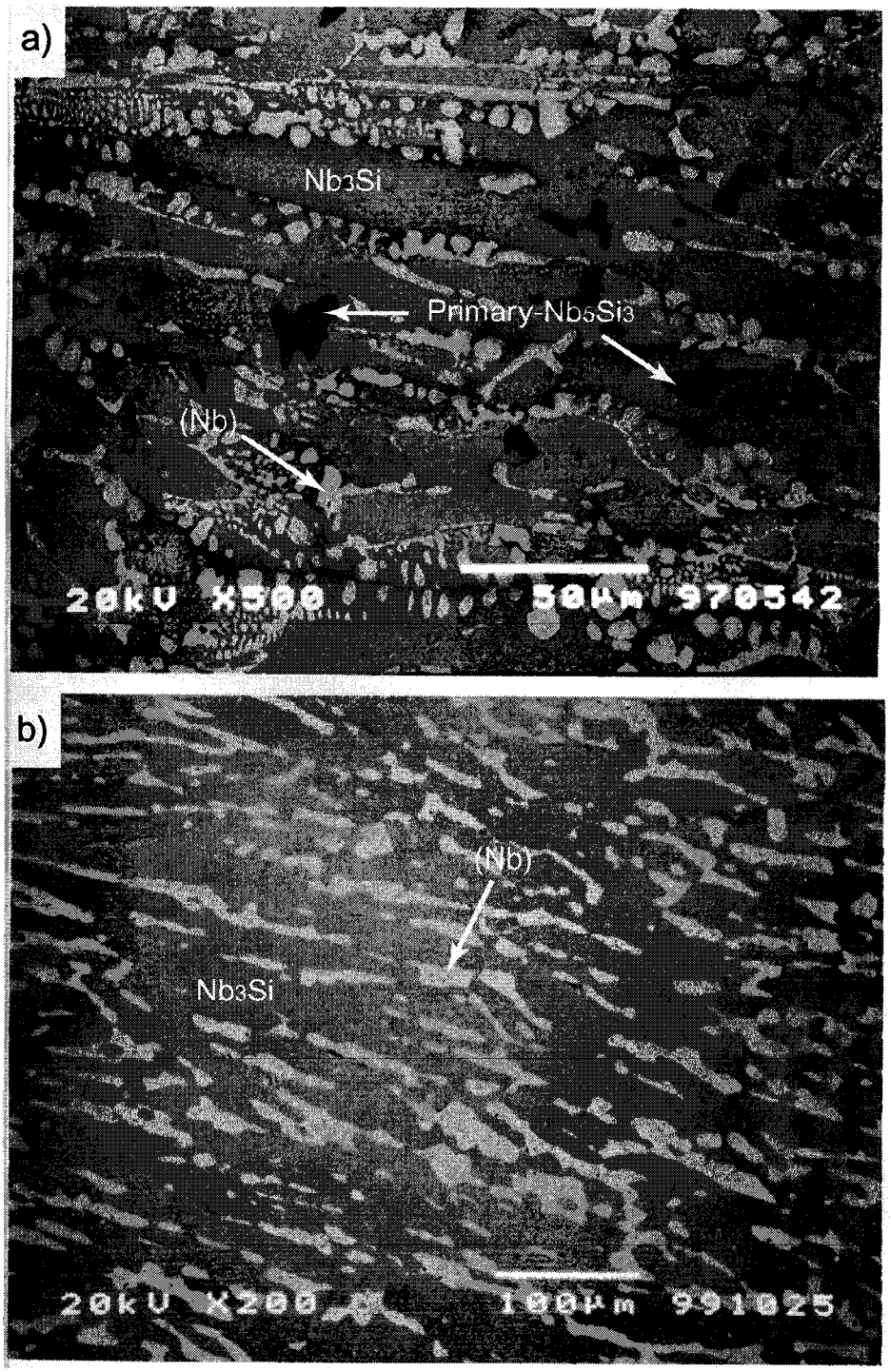

Fig. 3-2 Microstructure of the Nb-20Si-10Ti alloy, a) as-cast, and b) solution-treated at 2023 K for 90 h.

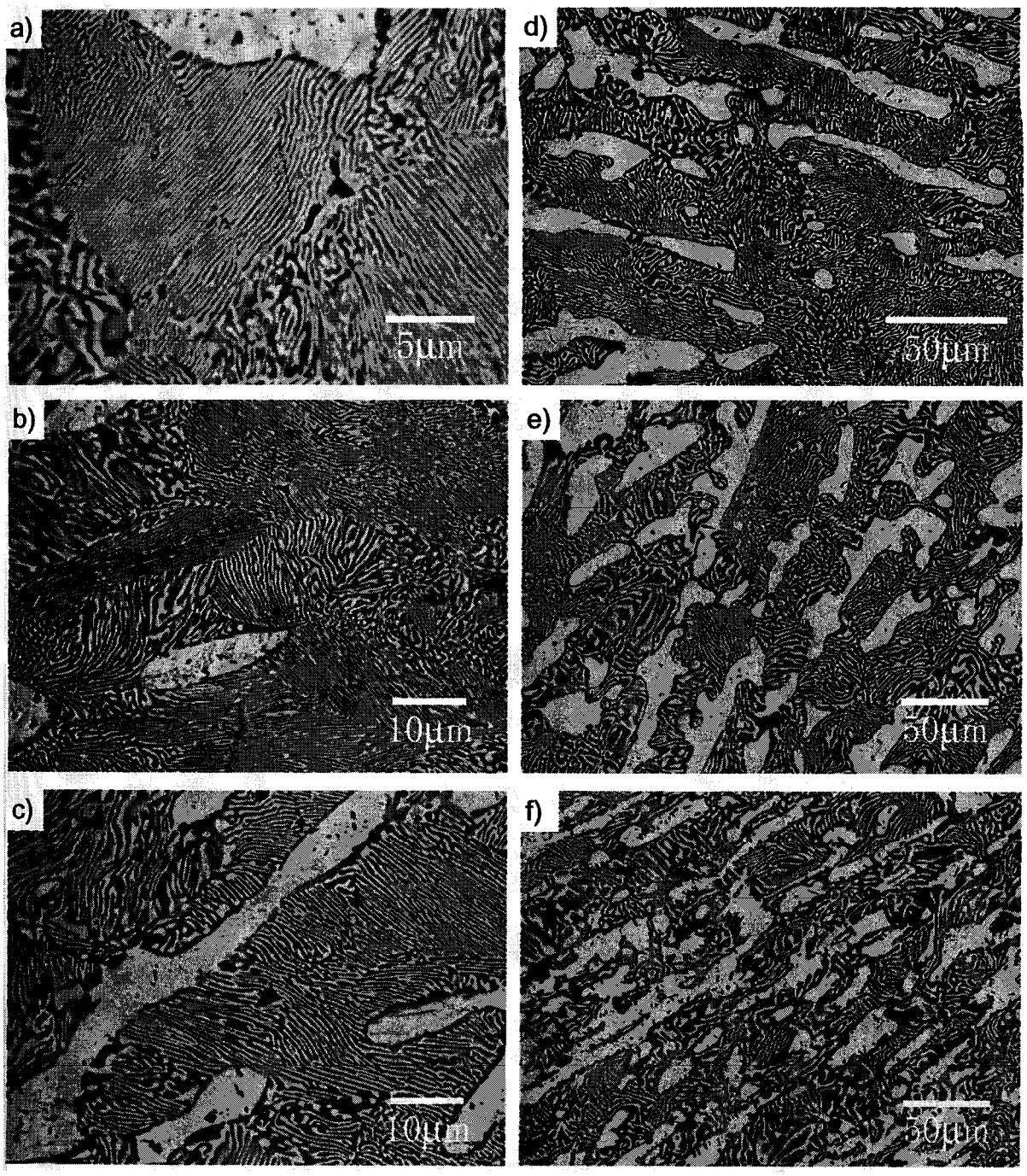

Fig. 3-3 Microstructure of the alloy sebsequently annealed after the solution treatment at a) 1373 K, b) 1473 K, c) 1573 K, d) 1673 K, e) 1723 K, and f) 1773 K.

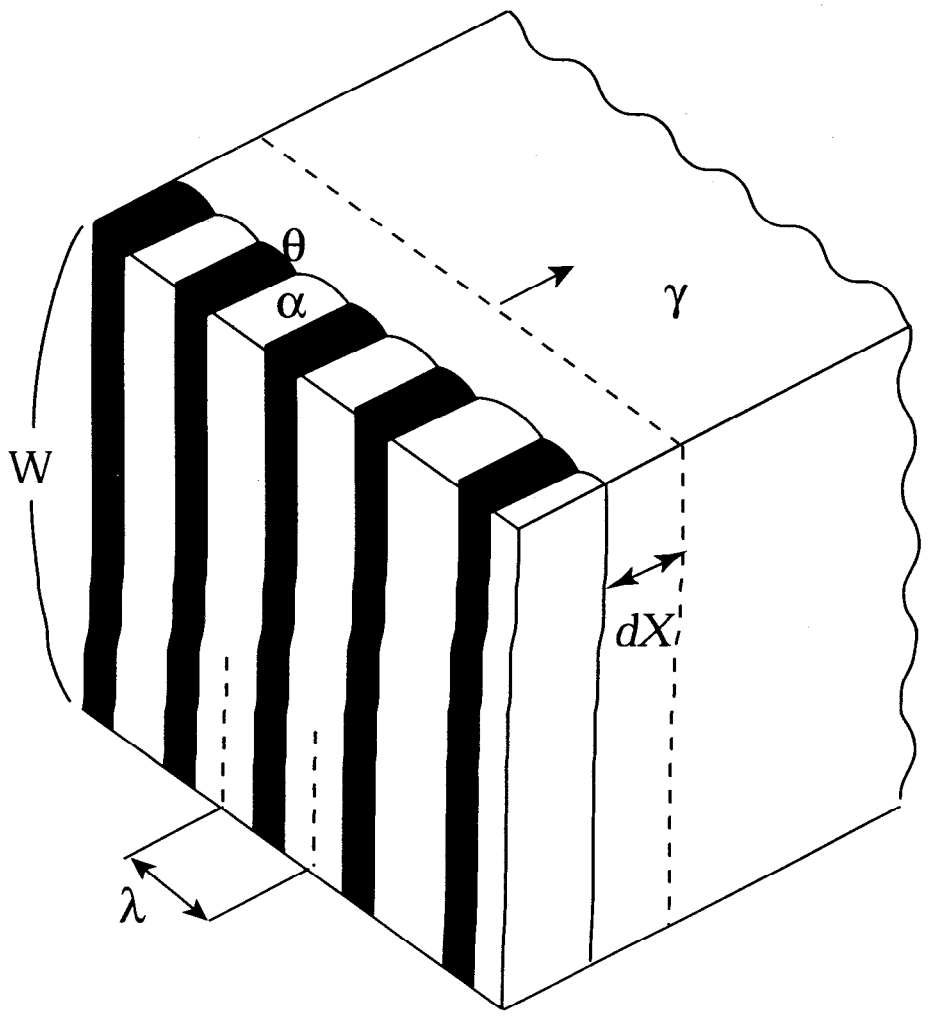

Fig. 3-4 A schematic of a pearlite nodule, with the depth W, growing in the parent austenite.

W, growing in the parent austenite. When the nodule advances a distance *dX*, the volume of pearlite nodule transformed from austenite is given by $\lambda_0 WdX$. The free energy change, ΔG_V, associated with the formation of new interfaces at temperature *T* is

$$\Delta G_V = \Delta H \frac{T_e - T}{T_e} \lambda_0 WdX \qquad (1)$$

where ΔH is the latent heat of transformation per unit volume, and *Te* is the eutectoid temperature. Increase in the total interfacial area is *2WdX*. Taking γ as the surface energy per unit area, increase in interfacial energy, ΔG_S, is given by

$$\Delta G_S = 2\gamma WdX \qquad (2)$$

The free energy change due to pearlite nodule formation is equal to the excessive interfacial energy;

$$\Delta H \frac{T_e - T}{T_e} \lambda_0 WdX = 2\gamma WdX \qquad (3)$$

Therefore, the interlamellar spacing is given by

$$\lambda_0 = \frac{2\gamma T_e}{\Delta H(T_e - T)} \qquad (4)$$

According to Eq. (4), the minimum interlamellar spacing is inversely proportional to the degree of super-cooling. This explanation might as well be valid for lamellar microstructures formed by the eutectoid reaction in other alloy systems. In the present alloys, however, further consideration is necessary to apply this explanation especially for the definition of the eutectoid temperature, T_e.

Figure 3-5 shows a schematic illustration of the vertical section at constant 10at% Ti in the Nb-Si-Ti ternary phase diagram. The three-phase region of (Nb), Nb_3Si, and Nb_5Si_3 exists below the Nb_3Si single-phase region. Therefore, a schematic drawing of Gibbs free energy

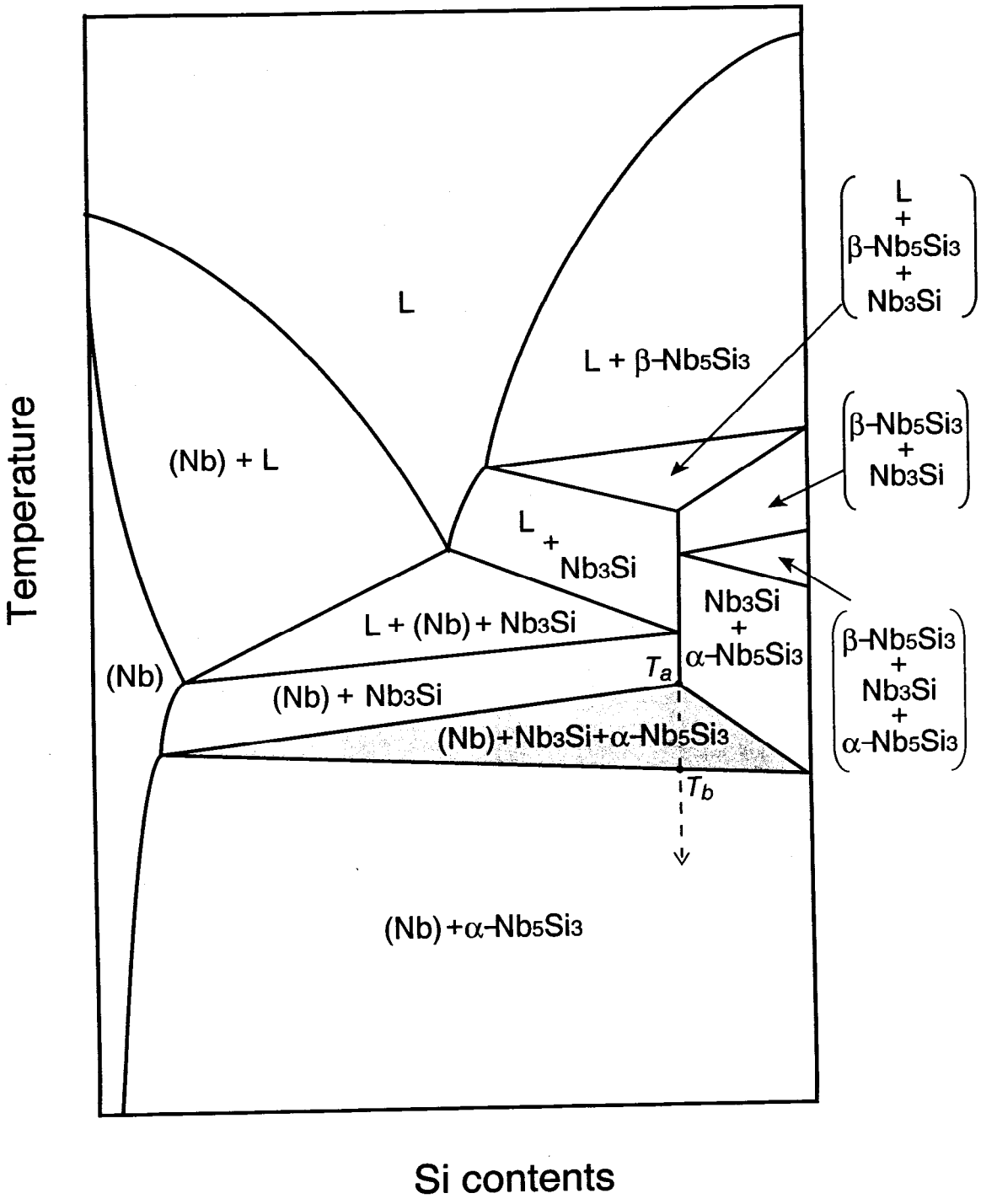

Fig. 3-5 A schematic of vertical section at constant titanium of 10at% in the Nb-Si-Ti ternary phase diagram.

versus temperature for the Nb-25Si-10Ti alloy is given as shown in Fig. 3-6. Here after, Gibbs free energy curves representing the Nb_3Si single-phase equilibrium is denoted as G_1, {(Nb)+Nb_5Si_3} two-phase equilibrium as G_2, and {(Nb)+Nb_3Si+Nb_5Si_3} three-phase equilibrium as G_3, respectively. Assume that G_1 and G_3 are equal at temperature T_A, G_2 and G_3 at T_B, and G_1 and G_2 at T_C. Annealing at temperature T, the Gibbs energy change, ΔG_V, due to decomposition of the Nb_3Si is given as the difference between G_1 and G_2. When the {(Nb)+Nb_5Si_3} nodule having the depth W advances a distance dX in the parent Nb_3Si, the volume of decomposed Nb_3Si is $\lambda_0 W dX$, which is the same procedure as shown in Fig. 3-4 for a pearlite nodule. Since a tangent of the free energy curve gives entropy, i.e. $(\partial G/\partial T)_P=-S$, ΔG_V can be approximately calculated as follows;

$$\Delta G_V = \Delta S(T_c - T)\lambda_0 W dX \qquad (5)$$

where ΔS is the change in the entropy per unit volume on the transformation. Taking γ as the surface energy per unit area, the increase in interfacial energy, ΔG_S, is given by Eq. (2). The Gibbs free energy change is equal to the increase in interfacial energy;

$$\Delta S(T_c - T)\lambda_0 W dX = 2\gamma W dX \qquad (6)$$

Finally, the interlamellar spacing is given as;

$$\lambda_0 = \frac{2\gamma}{\Delta S(T_c - T)} \qquad (7)$$

Equations (4) and (7) are essentially the same because $\Delta H/T_e$ is regarded as ΔS. Accordingly, the determination of T_c is important to evaluate the interlamellar spacing as a function of a degree of super-cooling in the ternary alloy system. However, it is very difficult to determine T_c by experiments. The simplest approximation to evaluate T_c is to take the average of T_a and T_b, because it is possible to experimentally determine these temperatures. Still, it is very hard to precisely evaluate T_a and T_b in the present study since the complete decomposition of Nb_3Si requires an enormous time at such high temperatures close to the eutectoid temperature. Fortunately, temperature difference between T_a and T_b is supposed to be very small, so that T_c is

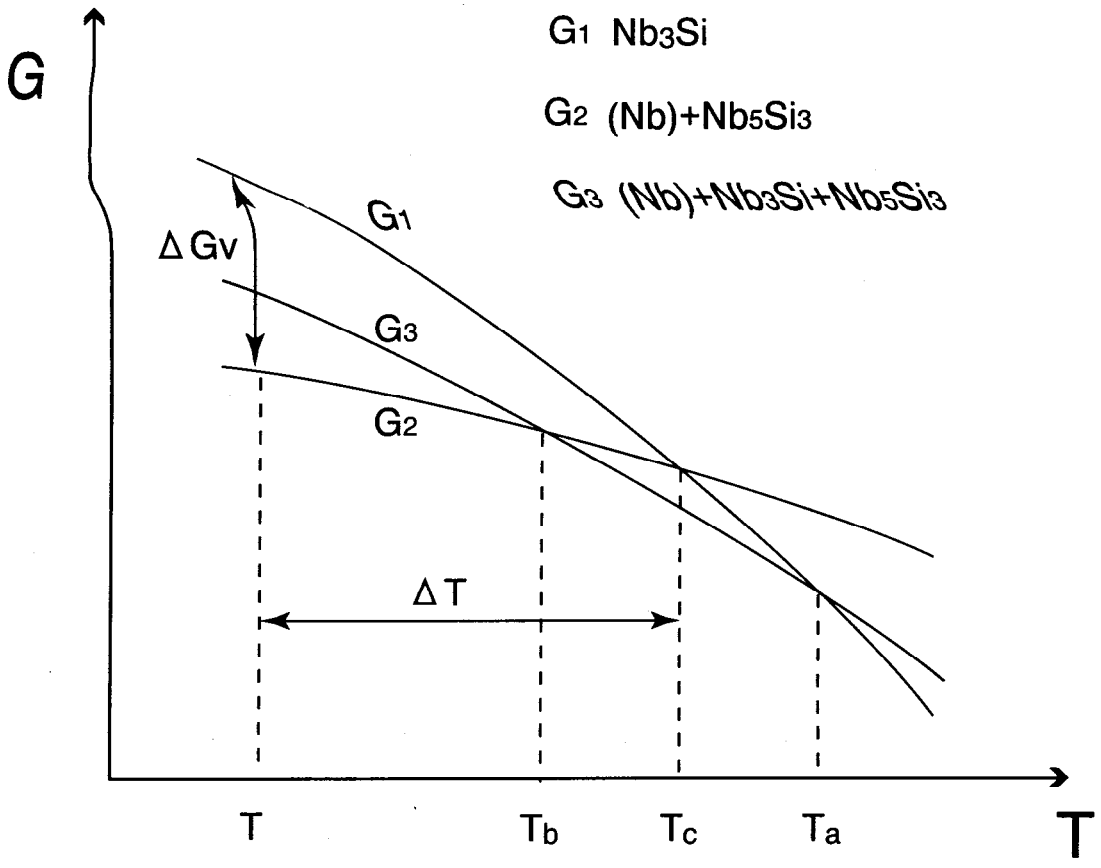

Fig. 3-6 A schematic arrangement of Gibbs free energy versus temperature curves for {Nb_3Si}, {(Nb)+Nb_5Si_3}, and {(Nb)+Nb_3Si+Nb_5Si_3} in Nb-20Si-10Ti alloy.

roughly estimated as 1873 K (1600 ℃) [5]. The correlation is shown in Fig. 3-7 between the average inter-lamellar spacing, λ, and the degree of super-cooling, $\Delta T(=T_e-T)$. In this figure, scattering of error bars depends on the method of measuring the inter-lamellar spacing. The linear relation is obviously seen between λ and $1/\Delta T$, which is consistent with the prediction. This indicates that the lamellar spacing of the alloy can be controlled to some extent by heat treatment temperatures.

Microstructural observation revealed that lamellar colony size becomes larger as heat treatment temperature increases. However, in the present study, it was not able to measure the colony size for the whole heat treatment temperatures range because the colony boundaries tend to be unclear at high temperatures. Since many of the eutectoid reactions are categorized in a type of grain boundary reaction, the eutectoid decomposition would not start from inside of the parent Nb_3Si grains but from the Nb_3Si grain boundaries. The lamellar colony boundaries are formed where advancing fronts of nodules meet with each other. Furthermore, interfacial advancing front of nodule itself can be nucleation sites for another nodules. It can be qualitatively understood that the colony size gets smaller as annealing temperature becomes lower, because the frequency of nucleation increases with a degree of supercooling. However, the colony size itself is greatly influenced by the size of parent Nb_3Si grain or the curvature of its grain boundary, in addition to annealing temperature. This fact makes it difficult to evaluate the colony size only as a function of the heat treatment temperature, which is contrary to the case of inter-lamellar spacing.

3-2. Mechanical Properties

3-2-1. Compression Test

Compression tests were conducted at temperatures between room temperature and 1673 K to examine effects of microstructural factors controlled by annealing temperatures on mechanical properties of alloys. Figure 3-8 shows the summary of compression tests. The 0.2% flow stress is shown as a function of the average lamellar spacing at each test temperature. Note that the test temperature of 1673 K is higher than the annealing temperature in some alloys, however, it is assured that the microstructure stays thermally stable without coarsening during the test.

There are two important features in the results of compression tests that must be emphasized. First, at room temperature, the alloys fracture in a very brittle manner showing only

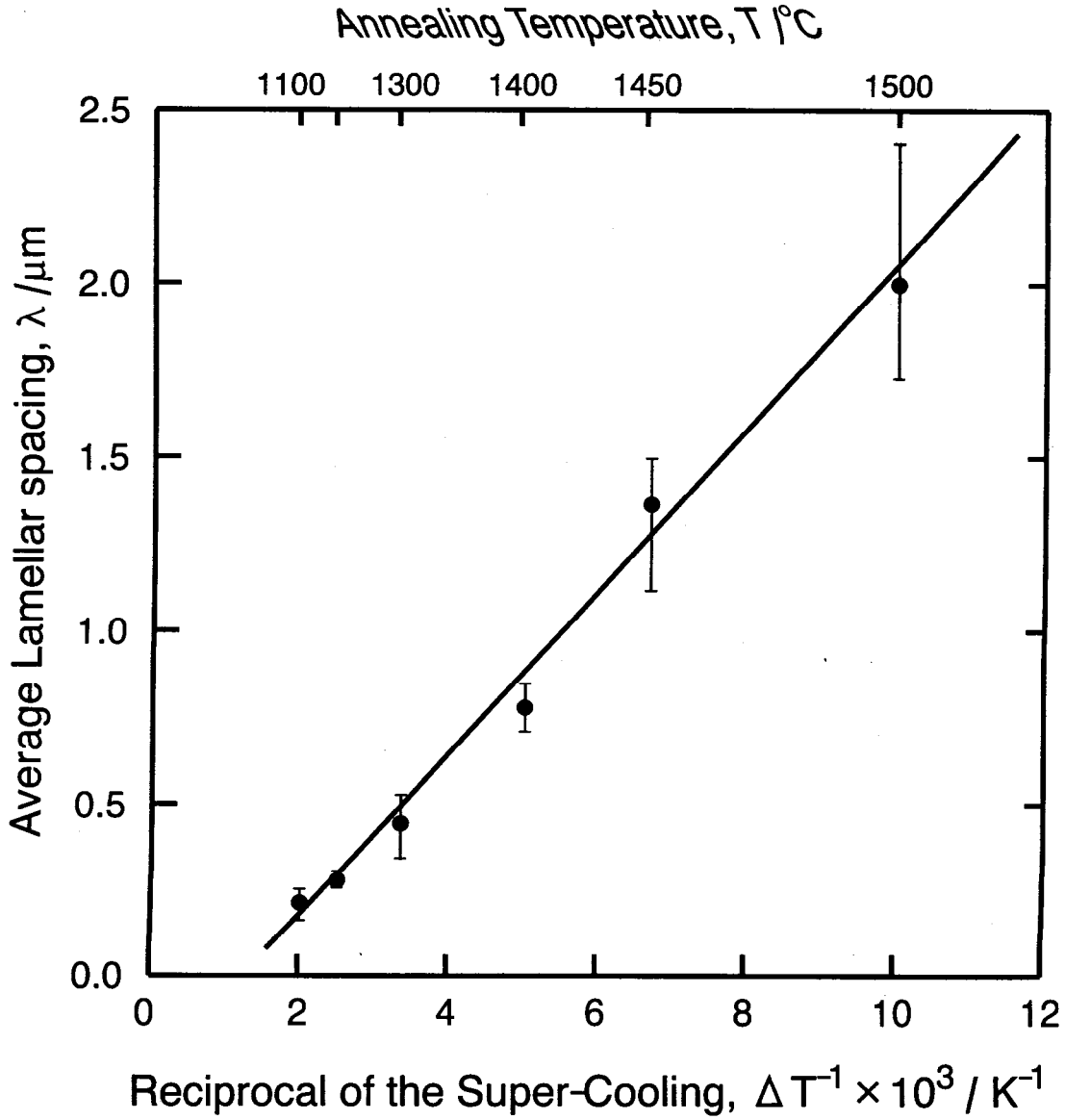

Fig. 3-7 Relation between reciprocal of the degree of supercooling and average lamellar spacing.

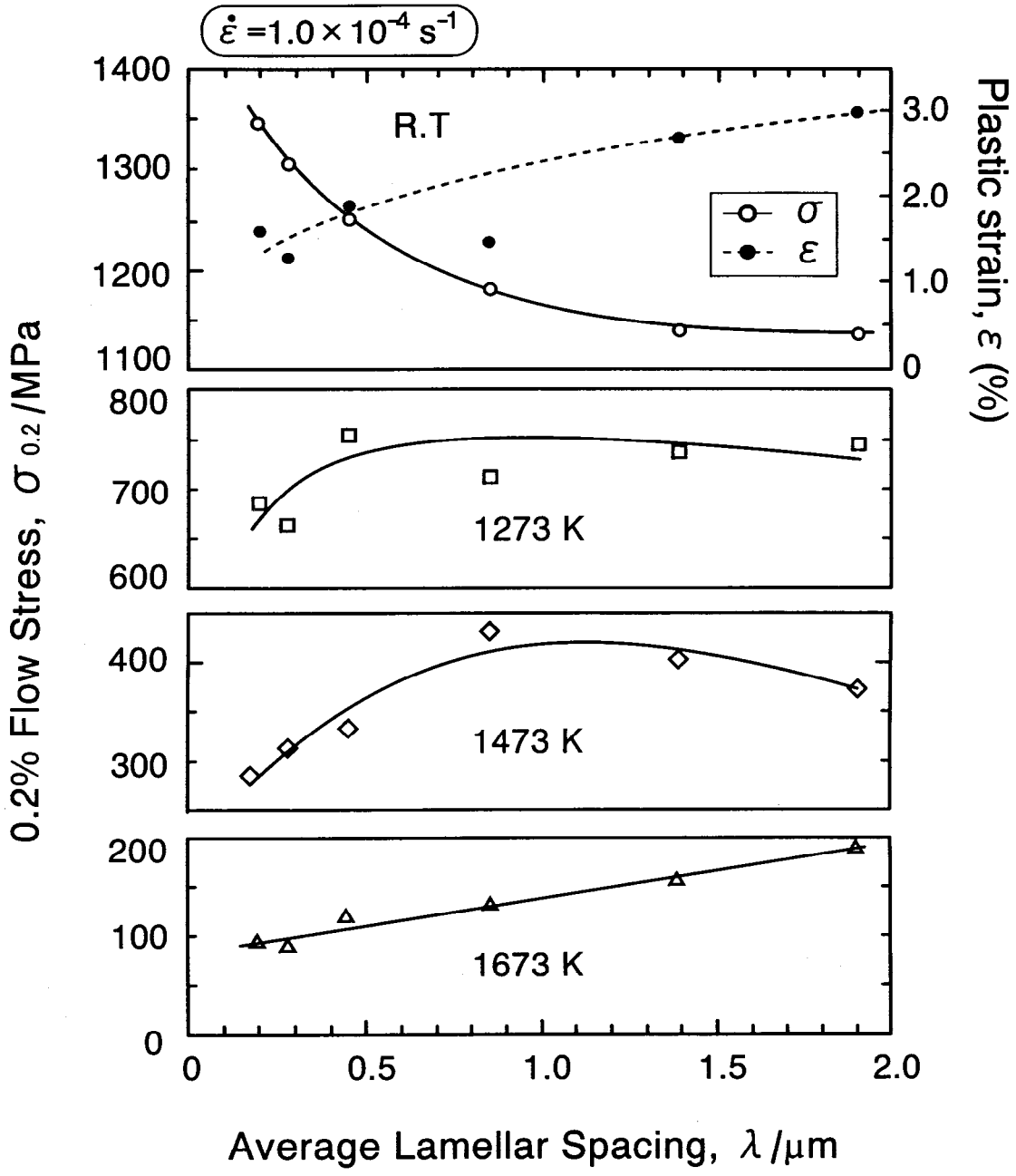

Fig. 3-8 Summary of the results of compression tests. The 0.2% flow stress is shown as a function of average lamellar spacing at each test temperature.

a few percent of macroscopic plastic strain. It is clear in Fig. 3-8 that room temperature compressive plastic strain to failure increases with increasing interlamellar spacing. The reason will be discussed in the next section. Second, strength at room temperature decreases with increasing inter-lamellar spacing, but on the contrary strength at 1673 K increases with increasing inter-lamellar spacing. The dependence of inter-lamellar spacing on strength at room temperature and at 1673 K shows inverse tendency with each other. At room temperature, 0.2% flow stress increases with decreasing length for dislocation pile-up as the interlamellar spacing is smaller. On the other hand, strength at elevated temperatures is lowered by increasing in total area of interfaces that are controlled by the inter-lamellar spacing as well as the lamellar colony size. The reason of this inversed tendency of strength at room temperature and at 1673 K will be discussed in the section 3-2-3.

The temperature dependence of the compressive 0.2% flow stress of the present alloys is summarized in Fig. 3-9. The hatched area shows the range of strength among the alloys with different heat treatment conditions at each test temperature. The strengths of commercial Ni-base superalloys [10] and the directionally solidified Nb-Ti-Hf-Cr-Al-Si alloy [11] are also shown for a comparison. The present alloys show superior strength to Ni-base superalloys at temperatures over 1273 K, indicating that the niobium silicide based composite would be a promising candidate as a ultra-high temperature structural material for the next generation.

3-2-2. Deformation and Crack Propagation Behavior at Room Temperature

Figure 3-10 shows stress-strain curves obtained from compression tests at room temperature conducted on alloys annealed at various temperatures. The 0.2% flow stress is indicated by a triangle, and the average interlamellar spacing λ is represented together with annealing temperature. As described in the previous section, alloys with larger interlamellar spacing, i.e. annealed at higher temperature, show lower 0.2% flow stress and larger plastic strain to failure than the alloys with smaller interlamellar spacing. Compressive mechanical behavior observed in the stress-strain curves is that the flow stress rapidly decreases showing the maximum peak on the flow stress. This rapid drop of the flow stress is most likely due to the micro-crack generation and propagation. On this deformation stage, ductile (Nb) phase plays a role of preventing the micro-crack propagation. It is possible to roughly evaluate the resistance to a crack propagation, such as toughness, of alloys using the value of macroscopic plastic strain.

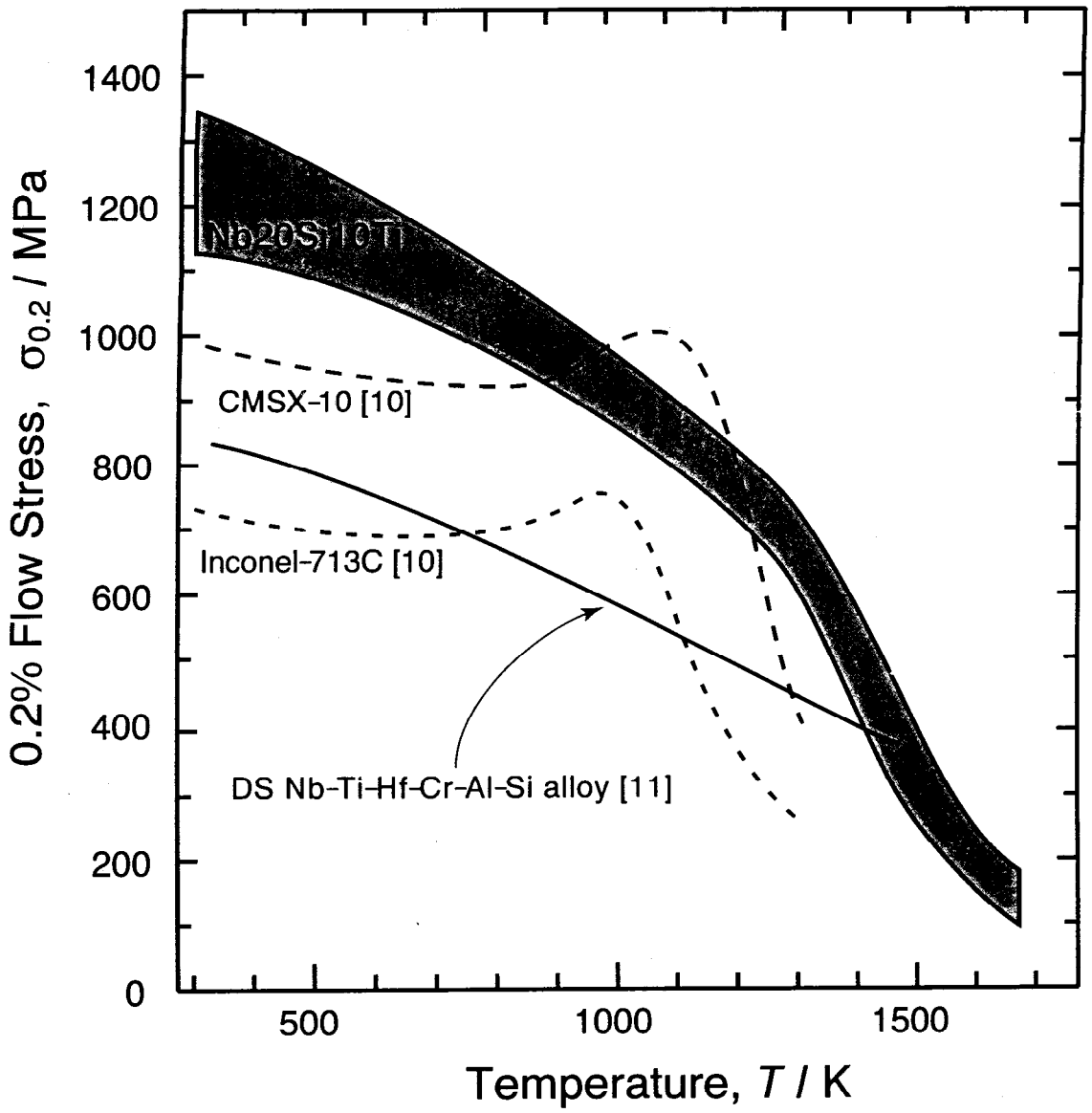

Fig. 3-9 Temperature dependence of 0.2 % compressive flow stress in the Nb-20Si-10Ti alloys.

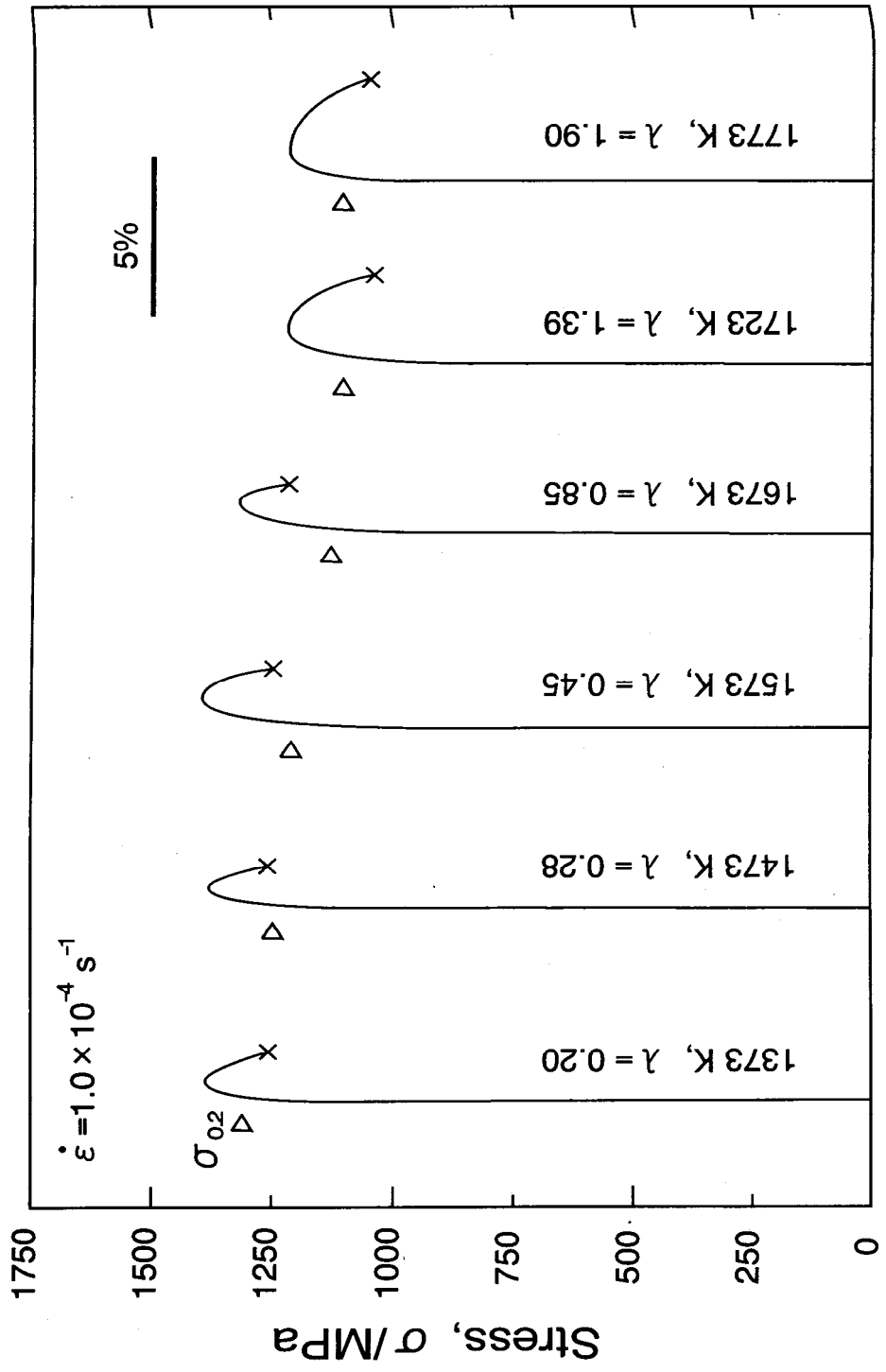

Fig. 3-10 Room temperature compressive stress-strain curves of the Nb-20Si-10Ti alloys annealed at various temperatures and having different interlamellar spacing.

A compressive plastic strain to failure at room temperature is shown as a function of interlamellar spacing in Fig. 3-8. The colony size is simultaneously changed with interlamellar spacing by the annealing temperature for the eutectoid decomposition of Nb_3Si. Figure 3-11 shows a schematic to describe the relationship among the lamellar spacing, colony size, and annealing temperature. Annealing at high temperatures increase interlamellar spacing and lamellar colony size at the same time. It was reported in TiAl alloy that the toughness increases as the lamellar colony size increases [14-18], therefore, the effect of colony size on toughness increment must be taken into account. A crack propagation behavior observed in bending test at room temperature is shown in Fig. 3-12. The test was conducted on the straight notched specimen by four-point bending under a crosshead speed of 5.0×10^{-2} mm/min. It is found that cracks are mainly deflected at coarse primary (Nb) while cracks propagate straightly in the Nb_5Si_3/(Nb) lamellar region. There exists few cracks propagating along the lamellar interfaces or lamellar colony boundaries. If the colony size plays a major role on toughening the alloy, cracks should be observed deflecting at colony boundaries. Consequently, the effect of colony size on room temperature toughness can be regarded as small.

It is well-known that toughness of the alloy increases with increasing a size or thickness of ductile phase in the ductile-phase-toughening (DPT) mechanism [12]. From this point of view, the contribution for toughening by the coarse primary (Nb) phase must be much larger than that by the fine lamellar (Nb) plates when the crack bridging by ductile (Nb) takes place. However, a crack should mainly propagate through the lamellar regions, because the primary (Nb) phase is discontinuous and inhomogeneous in nature, so that a crack can be easily deflected by the primary (Nb) phase. Therefore lamellar microstructural control is a key to enhance room temperature toughness of the alloys. On the other hand, it has been reported that the DPT mechanism works effectively when the thickness of ductile phase is large enough for the large-scale yielding because the size of plastic zone formed at a crack-tip in ductile phase becomes larger proportionally to the size of ductile phase [13]. In the present study, interlamellar spacing can be controlled ranging from 0.2 to 2 μm. Then the (Nb) lamellae may be small to impart a sufficient toughness to the alloy. However, it is found that (Nb) lamellae plays a important role to enhance a compressive plastic strain to failure by the observation of the crack propagation behavior during the compression tests. The BEI in Fig. 3-13 shows the sub-cracking behavior around the main crack which was formed at the final catastrophic failure in compression test. It can be speculated from the observation of sub-cracks that how the

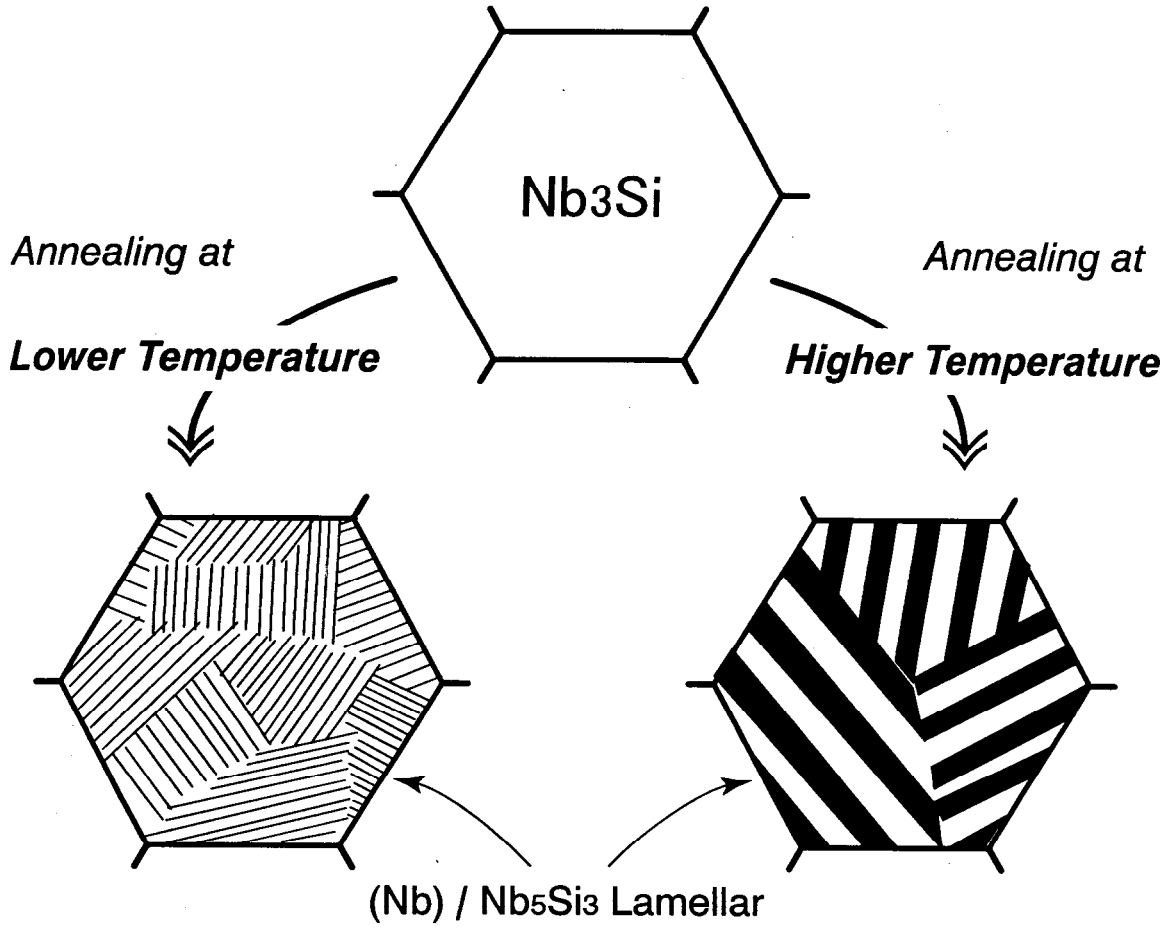

Fig. 3-11 A schematic explaining the relationship among lamellar spacing, colony size, and annealing temperature.

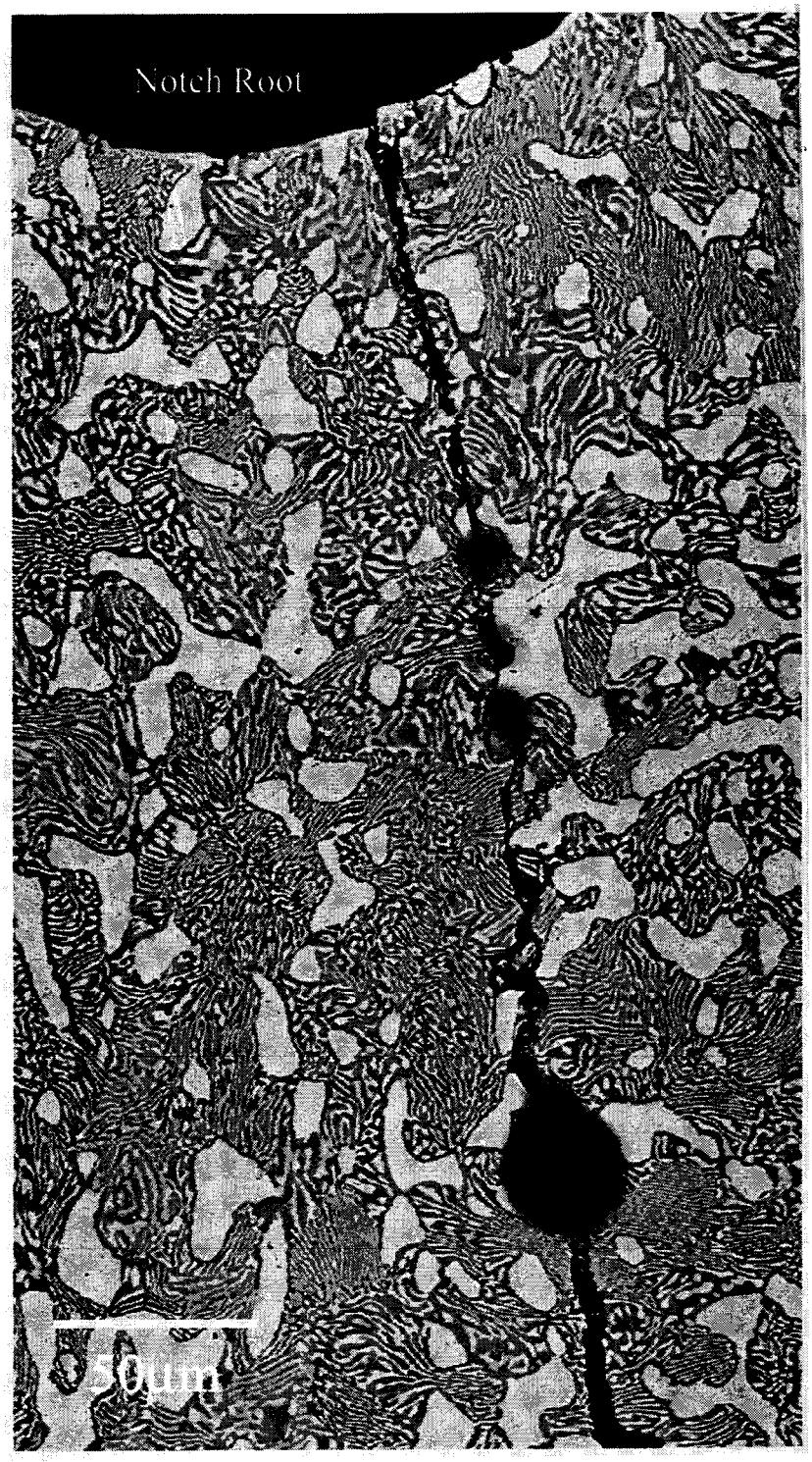

Fig. 3-12 Crack propagation behavior in four point bending test with the straight-notched specimen.

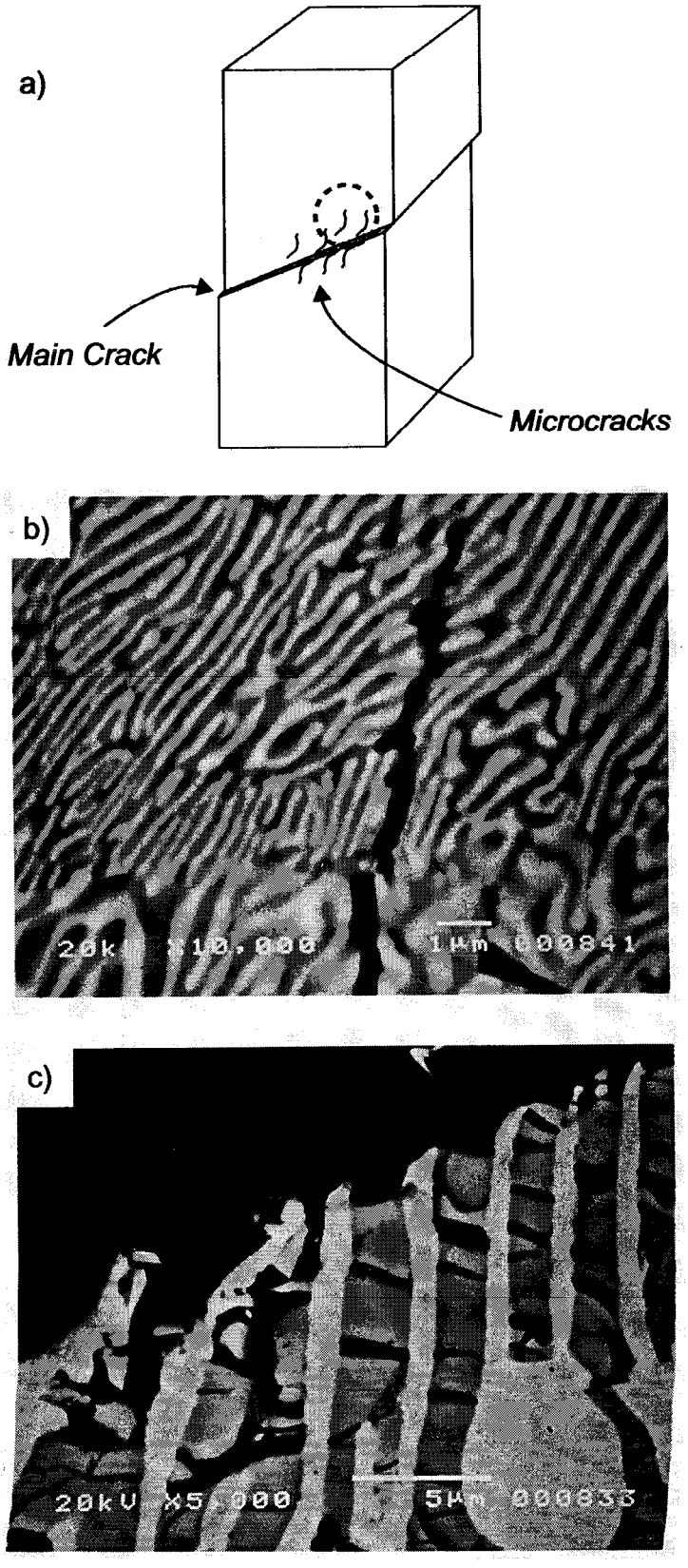

Fig. 3-13 Micro-cracking behavior around the main crack formed at final catastrophic failure, a) a schematicexplanation, b) the alloy annealed at 1373 K, and c) the alloy annealed at 1773 K.

micro-cracks initiate and propagate during deformation. In the alloy with small lamellar spacing, micro-cracks are hardly observed around the main crack. It suggests that no sooner micro-crack was generated than propagates the entire cross section of the specimen, leading to the final catastrophic failure without being deflected nor blunted. As an evidence to support this explanation, there seldom exists very straight micro-cracks as shown in Fig. 3-13b. In the case of alloy with large lamellar spacing, a considerable amount of micro-cracks are found to be generated not only around the main crack as shown in Fig. 3-13c. Consequently, thick (Nb) lamellar plates are supposed to effectively prevent the propagation of micro-cracks generated during compression test.

Hsia et al. have shown that a number of equilibrium dislocations emitted from a crack tip decreases with a thickness of ductile phase in the laminates consisting of alternating ductile and brittle layers in sub-micron order [19]. Dislocations emitted from the crack tip have two effects; one is to blunt the crack tip and thereby reducing the tensile stress at the crack tip, and the other is to send the back stress to the crack tip to hinder further dislocations emission. The crack tip is no longer blunted by this effect once the number of pile-up dislocations reaches equilibrium. Therefore decreasing in the thickness of a ductile phase would lead to a high stress concentration at a crack tip, which results in the reduction in the toughness of a laminate. Nino et al. have numerically estimated for the Mo_3Al-Mo_3Al_8 two-phase lamellar microstructure that the net value of tensile stress starts drastically increasing at the crack tip while the interlamellar spacing decreases in the range less than about 1 μm [20]. They have interpreted this propensity using the above model proposed by Hsia et al. An extensive tensile stress is anticipated at the crack tip in the present alloy since the average interlamellar spacing is evaluated in the range between 0.2 to 2 μm.

It can be concluded that the (Nb) lamellae should play a important role to prevent a propagation of micro-crack formed during the compression tests. Apparent compressive plastic strain to failure would be increased in alloys with large lamellar spacing, because micro-crack blunting and bridging at the thick (Nb) plates make the coalescence and growth of micro-cracks be delayed to form the main crack.

3-2-3. Deformation Behavior at High Temperatures

The correlation between the average inter-lamellar spacing and the degree of super-cooling is shown in Fig. 3-7. Temperature dependence of the compressive strength of the present alloy

shown in Fig. 3-8 tells that alloys annealed at lower temperatures, i.e. having narrower interspacing of lamellar, show higher 0.2% flow stress at room temperature while alloys annealed at elevated temperatures, having wide lamellar spacing, exhibit high strength at 1673 K. The explanation was presented in the previous section for ambient temperature strengthening: the shorter a dislocations pile up distance becomes with decreasing in the lamellar spacing, the higher the flow stress becomes since the deformation resistance is raised by a large back stress from dislocations pile-up. It is obvious that another mechanism must be responsible for the strengthening at 1673 K.

It is pointed out that the interfacial slip is a major mode of plastic deformation at high temperatures. The interfacial slip would possibly take place at the lamellar interface, lamellar colony boundary and grain boundary. If the interfacial slip is the deformation mechanism dominant at elevated temperatures in the present alloys, deformation behavior especially the flow stress should be greatly influenced by strain rates. Figure 3-14 shows the dependence of strain rate on the 0.2 % compressive flow stress at 1673 K of the alloy annealed at 1773 K for 100 h. The transition in deformation mechanism can be predicted at a strain rate between 10^{-3} s^{-1} and 10^{-4} s^{-1}, judging from the stress exponent, n. In the lower stress region, stress exponent n is equal to 2.0, which is consistent with the value for the super-plasticity or viscous creep. It indicates that interfacial slips are responsible for the deformation at 1673 K. On the other hand, stress exponent n is equal to 21.7 in higher stress region. Subramanian et al. have shown that the high stress creep data in Nb_5Si_3 single phase alloy at 1673 K showing a stress exponent of $n>2$ should be due to localized crack generation and propagation [21,22]. The very high stress exponent in higher stress region may be explained by such reason.

As mentioned before, there exist three types of interfaces in the present alloys on which interfacial slips could operate; lamellar interfaces, lamellar colony boundaries, and original grain boundaries. To investigate which type of interface is responsible for the interfacial slip, the surface of a specimen was observed after compression tests. Scratched marking was made on the surface of specimens using a polishing paper, in order to visualize the deformation mode by measuring a relative displacement of an interface before and after the test. Samples were wrapped with a Ta-foil to prevent from oxidation damage on the surface during the tests. Figure 3-15 shows scanning electron micrographs of the surface of compression test specimen after 15 % plastic deformation at 1673 K under a strain rate of 1.0×10^{-4} S^{-1}. Scratched lines were found to jog at grain boundaries and at lamellar colony boundaries. Additionally, it is clearly

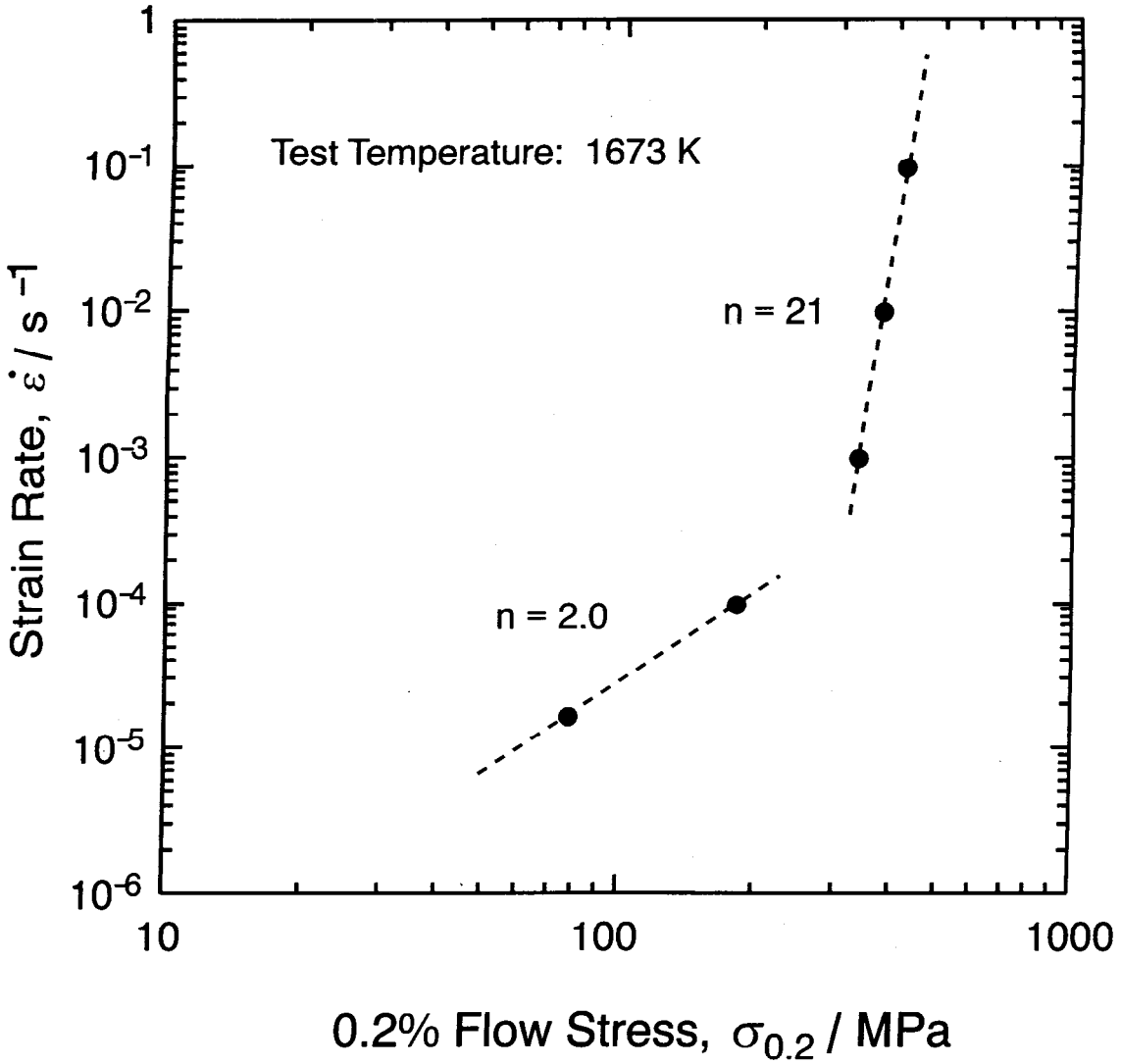

Fig. 3-14 Strain rate dependence of 0.2 % flow stress at 1673 K in the alloy annealed at 1773 K.

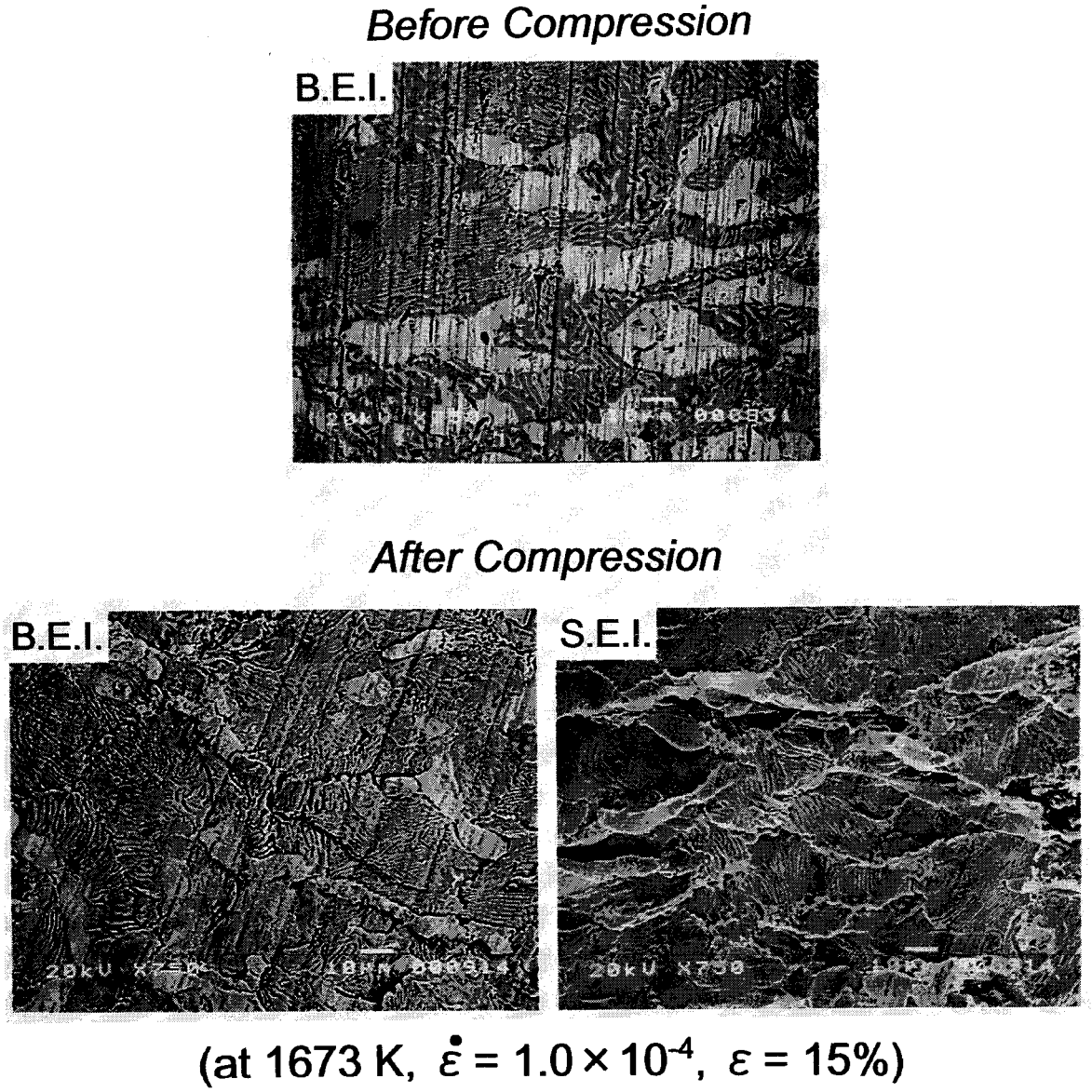

Fig. 3-15 Scanning electron micrograph of the surface of the compression test specimen after the 15 % plastic deformation at 1673 K under a strain rate of 1.0×10^{-4} s^{-1}.

seen in the secondary-electron image that some lamellar colonies are up-heaved during deformation. These results suggest that interfacial slips take place at the lamellar colony and grain boundaries, and that they are supposed to be weaker than the lamellar interface.

The relationship between the compressive 0.2% flow stress at 1673 K and the lamellar spacing is explained as follows. The interlamellar spacing and lamellar colony size are reduced at the same time by annealing at low temperatures as shown in Fig. 3-11. In the high temperature range where interfacial slips operate as a deformation mode, strength of the alloy is lowered as the lamellar colony size getting smaller, since the total area of colony boundaries increases with decreasing in the lamellar colony size. It is contrary to that the small inter-lamellar spacing brings about high strength at room temperature.

4. CONCLUSIONS

In order to control the inter-lamellar spacing and colony size of the (Nb)/Nb_5Si_3 lamellar microstructure, heat treatment conditions are determined for the eutectoid decomposition of the Nb_3Si phase. The TTT-diagram evaluation was conducted for the eutectoid decomposition of the Nb_3Si phase in the Nb-Si-Ti ternary system chiefly by microstructural observation. The relationship between microstructures and mechanical properties were investigated for the (Nb)/Nb_5Si_3 two-phase lamellar alloys in the Nb-Si binary and Nb-Si-Ti ternary systems. The correlations of inter-lamellar spacing and colony size with annealing temperatures are theoretically discussed considering the degree of super-cooling. The following conclusions are drawn in this chapter.

1. The TTT-diagram was evaluated for the eutectoid decomposition of Nb_3Si in the Nb-Si-Ti ternary system. The C-curve shifts towards lower in temperature and shorter in time from those of the Nb-Si binary alloys. The shift toward lower temperature is in association with lowering the eutectoid temperature while toward shorter time is presumably due to decomposition rate and/or atomic diffusivity being enhanced by the Ti addition.

2. Lamellar microstructure is successfully controlled for the (Nb)/Nb_5Si_3 two-phase alloys by utilizing the eutectoid decomposition of Nb_3Si phase. The average inter-lamellar spacing is evaluated ranging from 0.2 to 2 μm in the Nb-20Si-10Ti alloy. It is confirmed that the average inter-lamellar spacing, λ, is proportional to reciprocal of the degree of super-cooling,

$1/\Delta T$, where ΔT is defined as the difference between annealing temperature and the eutectoid temperature.

3. Compression tests revealed that the alloys with (Nb)/Nb_5Si_3 lamellar microstructure are brittle showing only a few percent of plastic strain at room temperature. Compressive deformability can be improved by increasing inter-lamellar spacing.

4. The dependence on compressive strength for inter-lamellar spacing at room temperature and 1673 K shows inversed tendency. This is due to that the deformation mechanism at elevated temperatures is the interfacial slip mainly at the lamellar colony boundaries. Strength decreases with increase in total area of interfaces as the lamellar colony size is reduced with the inter-lamellar spacing.

REFERENCES

[1] M.G. Mendiratta and D.M. Dimiduk, Scripta Met. Mat., vol. 25 (1991), pp. 237-242.

[2] C. Zener, Trans. AIME, 167 (1946), pp. 550-595.

[3] Yu. A. Kocherzhinskiy, L.M. Yupko, and E.A. Shishkin, Ross. Metall., No. 1 (1980), pp. 184-188.

[4] H. Okamoto, A.B. Gokhale and G.J. Abbaschian, in "*Binary Alloy Phase Diagrams, Second Edition*", Ed T.B. Massalski et al., ASM Intnl., 1990.

[5] N. Sekido, F. G. Wei, Y. Kimura, S. Miura and Y. Mishima, J. Japan Inst. Metals, vol. 41 (2000), No. 11, pp. 1056-1061.

[6] A. R. Marder and B. L. Bramfitt, Metall. Trans. A, vol. 6A (1975), pp. 2009-2014.

[7] J.M. Hyzak and I.M. Bernstein, Metall. Trans. A, vol. 7A (1976), pp. 1217-1224.

[8] H. Sunwoo, M.E. Fine, M. Meshi, and D.H. Stone, Metall. Trans. A, vol. 13A (1982), pp. 2035-2046.

[9] Seiji Miura, Hokkaido University, private communication.

[10] G. L. Elickson, Superalloys 1996, TMS Publish (1996), p. 35.

[11] M.F. Ashby, F.J. Blunt and M. Bannister, Acta Metall. Mater., 37 (1989), pp. 1847-1857.

[12] B.P. Bewlay, M.R. Jackson, and H.A. Lipsitt, Metall. Trans. A, 1996, vol.27A, pp. 3801-3808.

[13] M.C. Shaw, D.B. Marshall, M.S. Dadkhah, and A.G. Evans, Acta Metall. Mater., 41 (1989), pp. 3311-3322.

[14] D. M. Dimiduk, Intermetallics, 6 (1998), pp. 613-621.

[15] Y-W. Kim, Acta metall. mater., Vol. 40, No. 6 (1992), pp. 1121-1134.

[16] D. M. Dimiduk, Gamma Titanium Aluminides, Ed Y-W. Kim, R. Wagner, and M. Yamaguchi, TMS Publish (1995), pp. 2-20.

[17] Y-W. Kim and F. H. Froes, High Temperature Aluminides and Intermetallics, Ed S. H. Whang, C. T. Liu, D. P. Pope and J. O. Stiegler, TMS Publish (1990), pp. 465-492.

[18] Y-W. Kim, Gamma Titanium Aluminides, Ed Y-W. Kim, R. Wagner, and M. Yamaguchi, TMS Publish (1995), pp. 637-654.

[19] K. J. Hsia, Z. Suo, and W. Yang, Acta metall. mater., vol. 42 (1996), pp. 877-896.

[20] R. Nino, S. Miura, and T. Mohri, Intermetallics, 9 (2001), pp. 113-118.

[21] P.R. Subramanian, T.A. Parthasarathy, M.G. Mendiratta, and D.M. Dimiduk, Scripta Met. Mater., vol. 32, No. 8 (1995), pp. 1227-1232.

[22] A. Crosby and P.E. Evans, J. Mater. Sci., 8 (1973), P. 1759.

CHAPTER 4

COMPARISON OF MICROSTRUCTURE AND MECHANICAL PROPERTIES OF THE ALLOYS FABRICATED BY INGOT AND POWDER METALLUGY

1. INTRODUCTION

As mentioned in Chapter 2, the (Nb)/Nb_3Si eutectic and hyper-eutectic alloys are so brittle that a considerable amount of micro-cracks are induced by thermal stress during cooling after the arc-melting, especially in the Nb-25Si and Nb-25Si-10Ti alloys. Mendiratta et al. have reported that the binary Nb-Si alloys with Si contents higher than 10 at% contain numerous micro-cracks which are introduced during cooling from the melt [1]. The problem of micro-cracking in the alloy preparation due to thermal stress must be overcome in order to develop the present alloys as candidate materials for structural application at ultra-high temperature.

A strategy to avoid micro-cracking is to apply the alloy processing based on powder metallurgy since a large thermal stress raised in casting from the melt is regarded as a sort of inevitable problem. As described in Chapter 1, there are some reports on the fabrication of Nb-Si binary alloys by the reactive sintering and mechanical alloying [2-5]. The process of reactive sintering includes a formation of transient liquid phase, that provides a problem in controlling the grain size of alloys. It is reported that pure niobium and silicon elemental powders are hard to be mechanically alloyed by a conventional ball milling. Kumar et al. have shown that an amorphous phase is formed when the volume fraction of niobium is high [2,3], and Fukui et al. have reported that the severe adhesion of niobium powder to metallic vial is a problem of ball milling [5]. The most commonly anticipated disadvantage in the powder metallurgy is a contamination, especially oxidation, caused from a considerably large total area

of active surface of the powder. It is known that the contamination of Nb leads to room temperature embrittlement and that formation of SiO_2 could be fatal problems reducing mechanical properties of alloys.

Based on these reports, a new route to alloy fabrication based on powder metallurgy is proposed: the pure niobium elemental powder and the pulverized Nb_5Si_3 alloy powder are used for solid-state sintering by means of hot pressing. Preparation of the pulverized Nb_5Si_3 powder is a key of the proposed alloy processing method, that is targeting on three effects. First, it is expected that avoiding pure Si powder results in suppressing the SiO_2 formation. It is possible that large amount of SiO_2 are formed when the liquid phase of Si is involved during reactive sintering due to the relatively low melting point of Si. Second, the solid-state sintering becomes available at much higher temperatures than the melting point of Si, though it is impossible to utilize the reactive sintering involving liquid/solid reaction. Third, a prevention of micro-cracking is expected in the Nb_5Si_3 phase since the thermal stress induced from the volume change, other than a thermal shrinkage on cooling, is avoidable in the proposed process. As long as the melting and reactive sintering involve the liquid phase, the formation of high temperature phase β-Nb_5Si_3 is inevitable which consequently transforms to the lower temperature phase α-Nb_5Si_3. For this β to α transformation on cooling, about 0.6% expansion is estimated from a change in the volume per atom calculated by using each lattice parameter and the number of atoms per unit cell. Even a slight expansion would cause a thermal stress on cooling to trigger a sever cracking in extremely brittle materials.

The objective in the present chapter is to investigate the effect of the newly proposed alloy processing on the microstructure, compressive mechanical properties and fracture toughness. The mechanical properties are compared in respect of microstructural features between the alloys prepared by the present powder metallurgy and ingot metallurgy using arc-melting. The strengthening mechanisms as well as the toughening mechanisms operating in these alloys are discussed using the rule of mixture of strength.

2. EXPERIMENTAL

2-1. Nb_5Si_3 Powder Fabrication

The Nb_5Si_3 powder was prepared by pulverizing the poly-crystalline Nb_5Si_3 single-phase alloy having the stoichiometric Nb_5Si_3, Nb-37.5at%Si, composition. The alloy ingot was first prepared by arc-melting using high purity raw materials (Nb, Si > 99.9%) under an argon

atmosphere. Nominal composition of the alloy was accepted when the weight loss after the melting was less than 0.2%. Ingots were then preliminarily crashed in an alumina mortar, and subsequently pulverized by ball milling. The container and balls used in this milling process are made of alumina. After the ball milling, pulverized powder were sieved by #325-mesh to control the size of Nb_5Si_3 powder under 45 μm.

2-2. Alloy Preparation

Alloys prepared for the experiments in the present chapter are with the eutectic composition Nb-18.7Si and the eutectoid composition Nb-25Si at the stoichiometric Nb_3Si. The pulverized Nb_5Si_3 powder and the commercial pure Nb powder (#325-mesh under) were mixed to the alloy composition by using a roller mixer under the condition of 72rpm for 24h with alumina ball. The plastic container was used for mixing the powder. The mixed powders were consolidated by hot pressing. The scheme of hot pressing performed in the present study is shown in Fig. 4-1. Degassing stage was provided at 873 K for 1 h under a vacuum since it is reported that degassing is effective to form sound compacts [4]. After the degassing stage, the chamber was filled with Ar gas. The sample was heated up to 1923 K at 7 K/min and the sintered for 4 h under a pressure of 50 MPa. Since the carbon push-rods and dies were used, pieces of Ta-foil were placed between the sample and dies to avoid carbon contamination. In this chapter, the alloy fabricated by powder metallurgy using hot pressing is denoted as the "PM-alloy".

The cast alloys having the same chemical compositions of the PM-alloys were fabricated by arc-melting to investigate the effects of processing on the microstructures and mechanical properties. Hereafter, the alloy prepared by arc-melting is denoted as the "AM-alloy". The AM-alloys were annealed at 1673 K for 100 h targeting for the eutectoid decomposition of the high temperature phase Nb_3Si into the (Nb) and Nb_5Si_3.

2-3. Microstructure Characterization and Mechanical Tests

Microstructural observation was done by the scanning electron microscope (SEM) using back-scattered electron (BEI) mode. Constituent phases of the alloys were identified by X-ray Diffractometry (XRD), and Energy Dispersive X-ray Spectroscopy (EDS). Density measurements are conducted on the PM-alloys. Archimedes method by immersing the sample into pure-water is employed for the purpose.

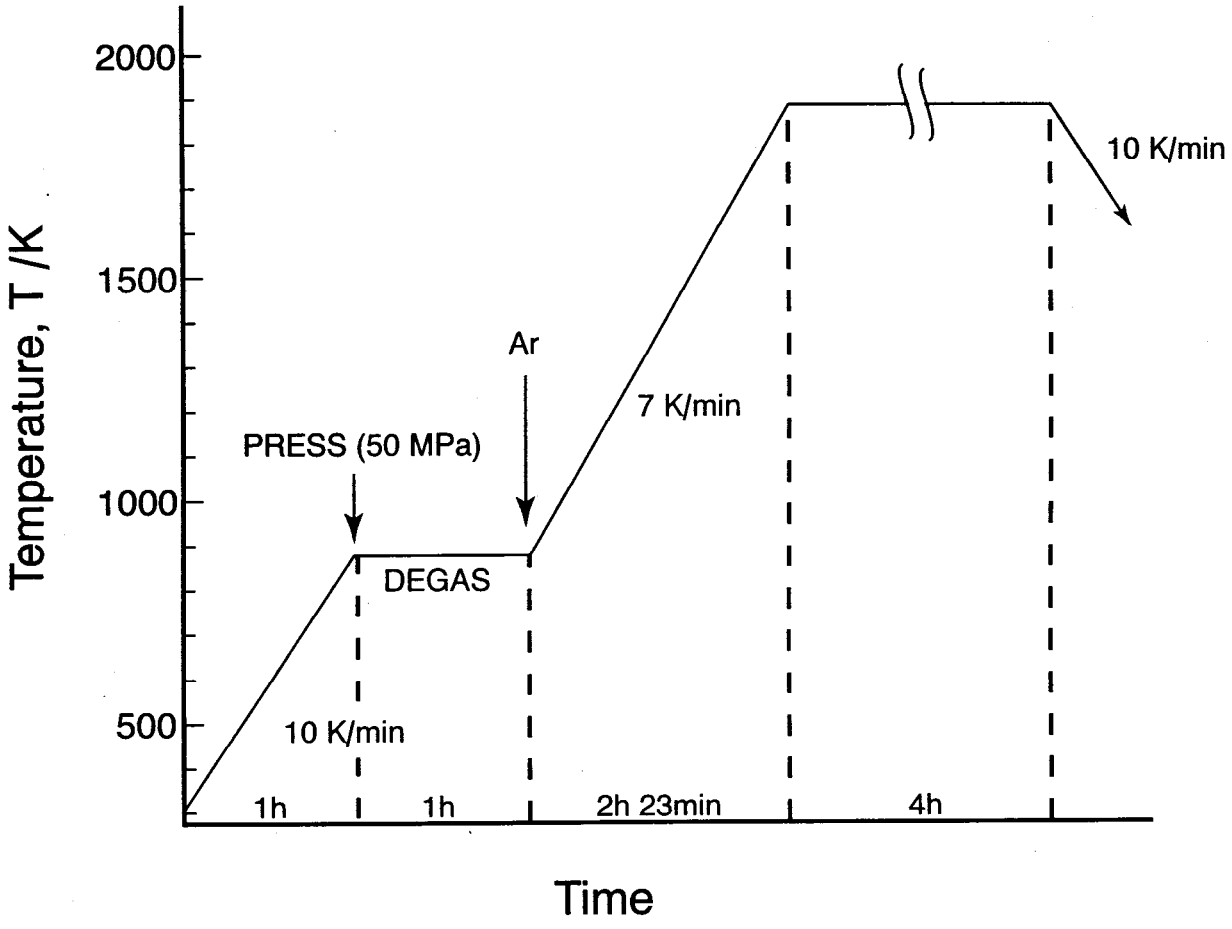

Fig. 4-1 General hot-pressing scheme in the present study.

Four-point bending tests were carried out to determine the fracture toughness using Chevron-notched specimens. The method of the test and the geometry of the test piece have already been explained in Chapter 2. Compression tests were conducted at a nominal strain rate of 1.0×10^{-4} s^{-1} in air at room temperature, and in a vacuum ($1\sim3\times10^{-4}$ Torr) at elevated temperatures ranging from 1273 to 1673 K. Test specimens, $2\times2\times5$ mm^3, were prepared by EDM and were mechanically polished to remove the damaged surface layer prior to testing. Vickers Hardness measurement was conducted with the load between 0.2 and 10 kgf for 30 s to give a large enough indentation to evaluate the overall hardness of the alloy.

3. RESULTS AND DISCUSSION

3-1. Materials Characterization

3-1-1. Identification of the constituent phase

Figure 4-2 shows X-ray diffraction profiles of the pulverized Nb_5Si_3 powder and the PM-alloys. The peaks in the profile of Nb_5Si_3 powder correspond to the mixture of low-temperature phase α-Nb_5Si_3 and high-temperature phase β-Nb_5Si_3. It is reported that accumulation of cold works promotes the formation of β phase [2], though it is not sure that β phase has formed during fabrication of Nb_5Si_3 ingot or on subsequent pulverization. After consolidation by hot pressing, the peaks in the XRD profile of PM-alloys correspond to the mixture of bcc-(Nb) phase and α-Nb_5Si_3 phase. The peaks of β-Nb_5Si_3 are not observed in the PM-alloys, indicating that the β phase completely transforms to the α phase during hot pressing. Oxidation and impurity contamination are serious problems in the powder metallurgy. In the present study, neither any oxides nor the γ-Nb_5Si_3 phase, being stabilized by carbon contamination [6], is detected by the XRD after the hot pressing.

3-1-2. Density Measurement

Results of density measurements are shown in Table 4-1. Here the packing factor is defined as the relative density with respect to the value calculated from the volume fraction of each phase using the reported value for densities of Nb and Nb_5Si_3 [7]. The packing factors are very high; 99.8% in the Nb-18.7Si alloy and 98.9% in the Nb-25Si alloy. This indicates that the hot pressing scheme conducted in the present study is appropriate to obtain dense compacts. The packing factor is greater in the Nb-18.7Si alloy since the volume fraction of niobium is larger

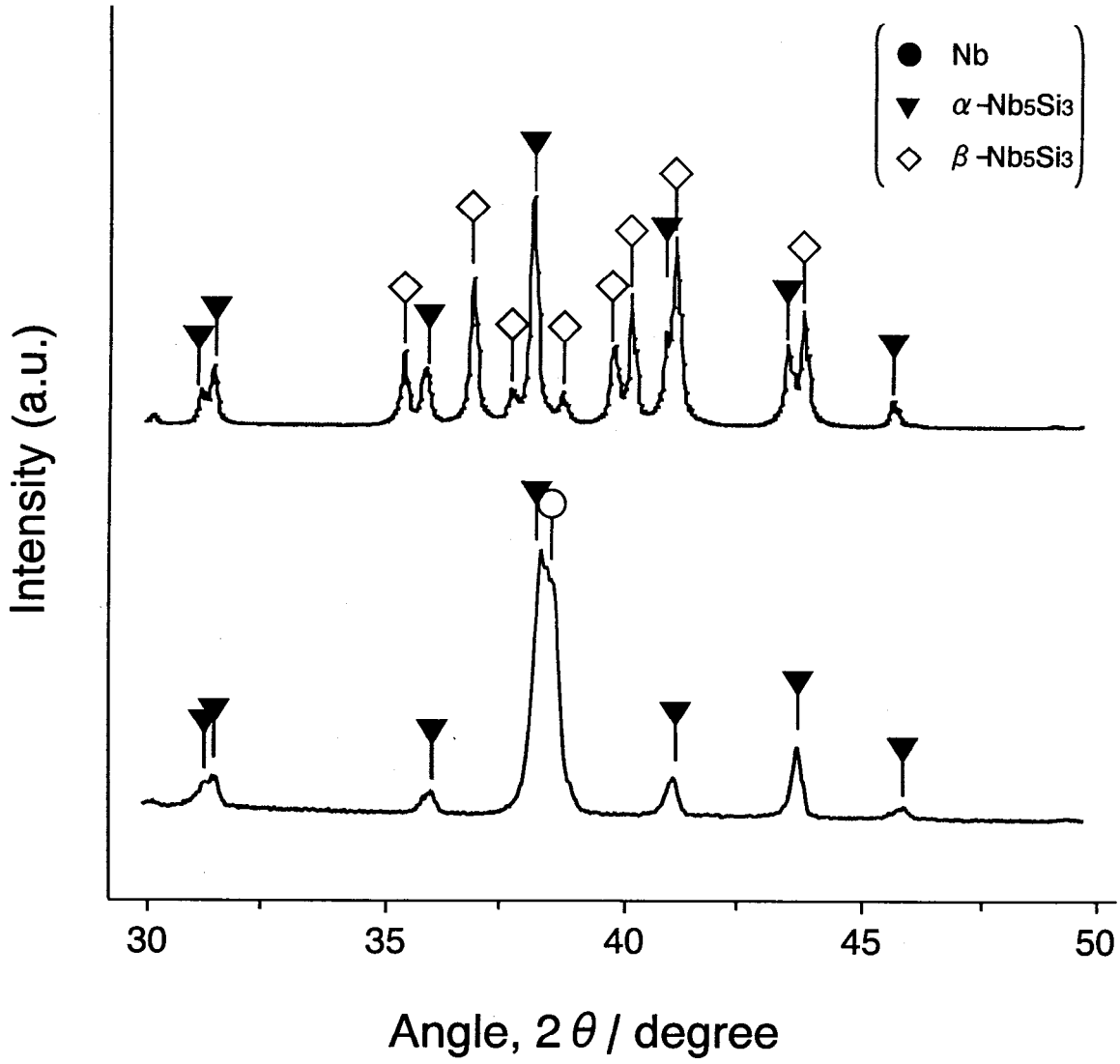

Fig. 4-2 X-ray diffraction profiles of the Nb_5Si_3 powder and the PM-Nb-18.7Si alloys.

Table 4-1 Results of density measurement.

Alloy Composition	Measured Density, d_m (g/cm^3)	Theoretical Density, d_t (g/cm^3)	Packing Factor, P (%)
Nb-18.7Si	7.85	7.87	99.8
Nb-25Si	7.61	7.70	98.8
Pure-Nb	8.56 [6]	—	—
Nb_5Si_3	7.14 [6]	—	—

$$dt = 8.56\ V_{Nb} + 7.14\ V_{Nb5Si3}$$

$$P = dm / dt$$

than in the Nb-25Si alloy. The ductile (Nb) powder particles plastically deforms to effectively fill the spaces amongst the Nb_5Si_3 powder particles. The detail will be discussed in the next section on microstructural observation. It must be noted that impurity contamination during hot pressing would result in the overestimation of measured densities in the PM-alloys.

3-1-3. Microstructure of PM-Alloy

Figure 4-3 shows scanning electron micrographs of the powders used in the present study. The appearance of the Nb_5Si_3 powder particles is characterized by the cleavage facets and river-patterns on the surface. It indicates that the pulverization of the Nb_5Si_3 is progressed by repeats of cleavage fracture. On the other hand, the Nb powder particles show the form of irregular polygon which is typical for the commercially available Nb powder particles. The particle size is distributed in a wide range from about sub-microns to several ten micrometers, which is the tendency both the Nb_5Si_3 and (Nb) powders have in common. In the case of pulverized Nb_5Si_3 powder, relatively large particles seem to be covered with fine particles.

Microstructures of the PM-alloys are shown in Fig. 4-4. No significant difference is observed in the microstructural feature between the Nb-18.7Si and Nb-25Si alloys except the volume fractions of constituent phases, (Nb) and Nb_5Si_3. The average grain size of both the (Nb) and Nb_5Si_3 phases roughly equals to the initial powder particle size of about 45 μm. A small amount of voids or cavities are formed inside the Nb_5Si_3 phase, but they are seldom observed on the (Nb)/Nb_5Si_3 interfaces. A schematic explaining the hot pressing process is shown in Fig. 4-5. Ductile niobium particles plastically deform extensively to fill up the spaces among the Nb_5Si_3 particles, while the Nb_5Si_3 particles have insufficient plastic deformability even at the hot-pressing temperature. As a consequent, the (Nb)/Nb_5Si_3 interface would be firmly bonded by ductile (Nb) particles deforming to fit their shapes to the adjacent Nb_5Si_3 particles. In between the Nb_5Si_3 particles themselves, spaces would never be filled and should remain as voids or cavities. From this speculation, the matrix of the PM-alloys should be the (Nb) phase regardless of the volume fraction of each phase. In fact, the distinctive microstructural feature of the alloys is regarded as the Nb_5Si_3 phase is dispersed in the (Nb) phase.

In addition to the problem of the void or cavity formation, another problem is that some Nb_5Si_3 have a coarse grain size with hundreds micrometers. These problems can presumably be eliminated by optimizing the powder mixing condition. Since the plastic container was used in the present study, powder mixing was performed at low rotational speed of 72 rpm. It is to avoid

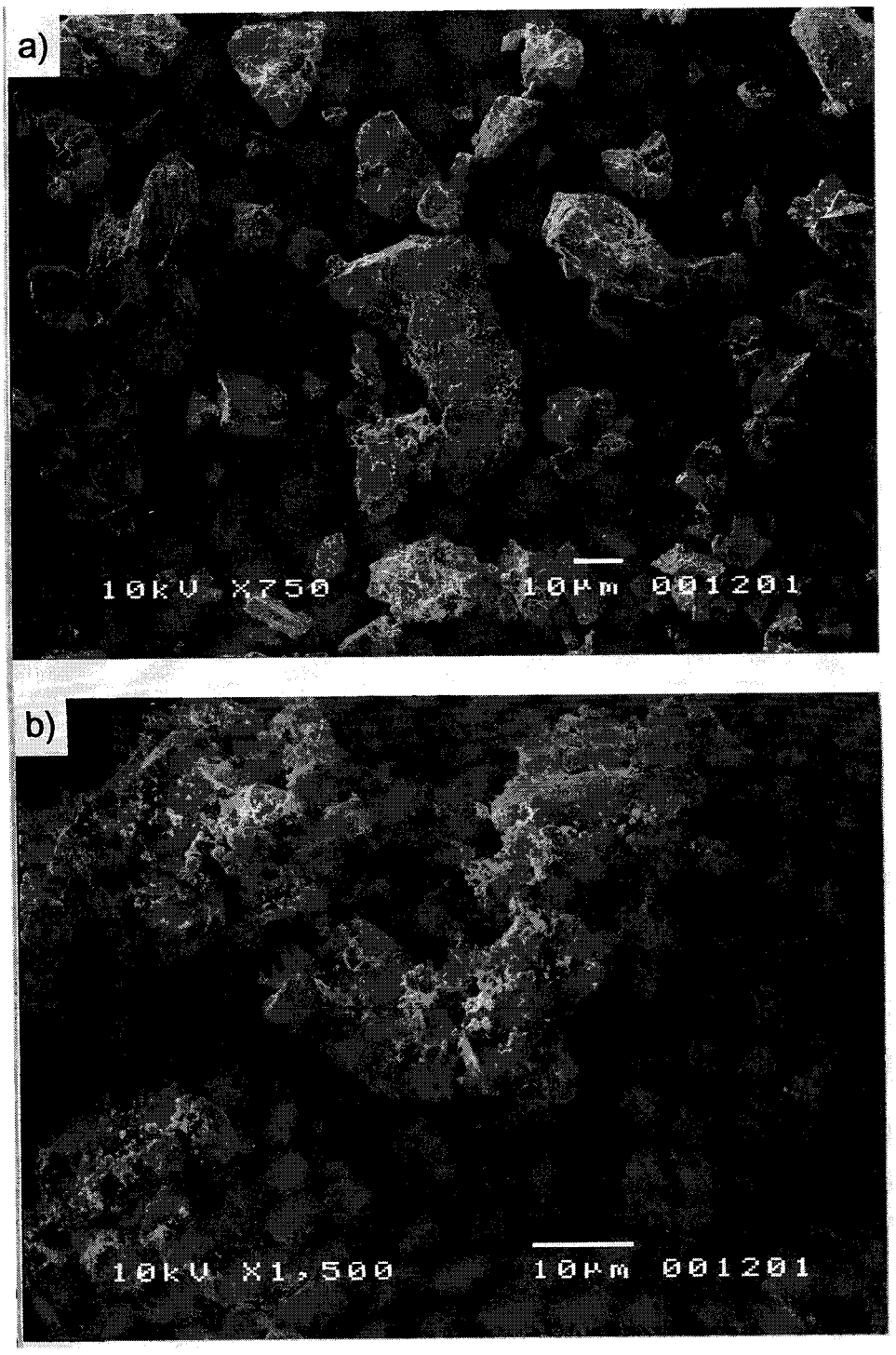

Fig. 4-3 Scanning electron micrographs of the powders used in the present study, a) pure-Nb, and b) Nb_5Si_3 powders.

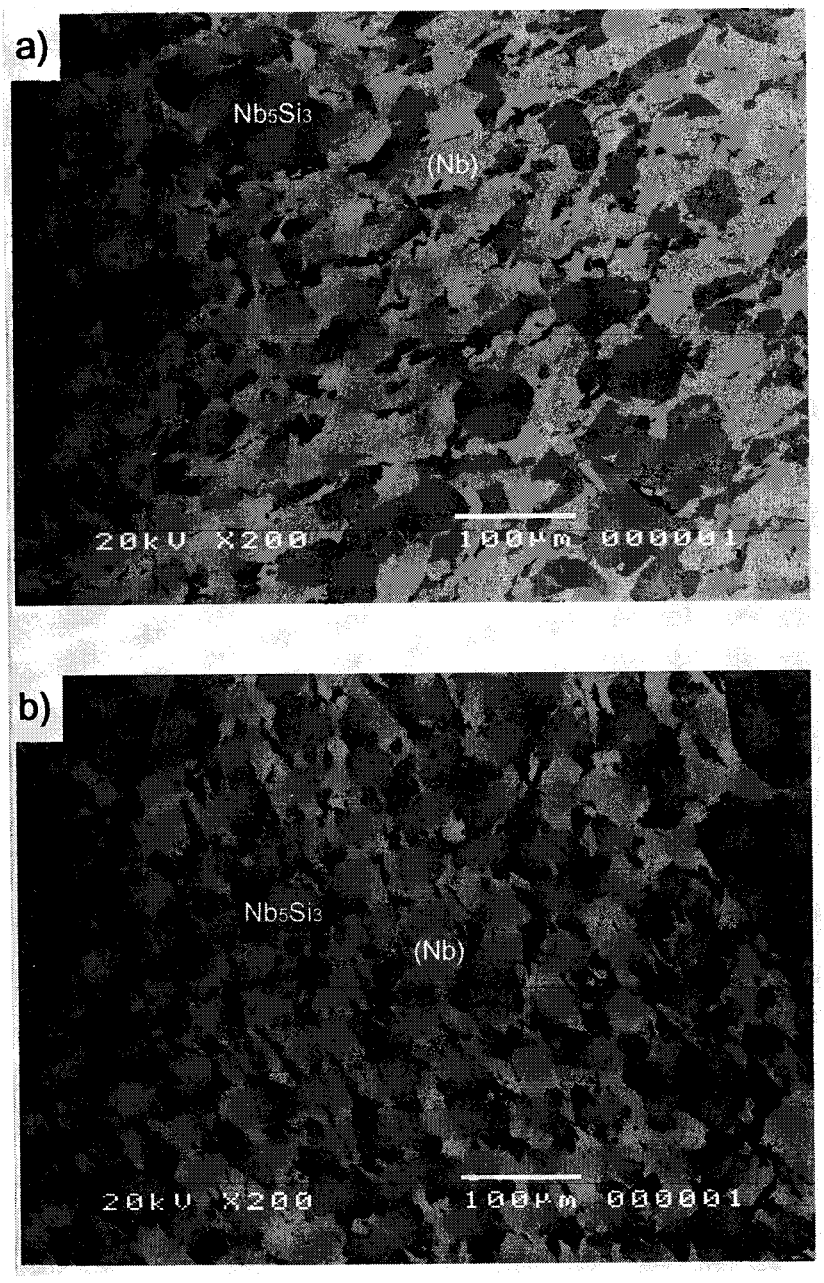

Fig. 4-4 Microstructures of the PM-alloys, a) Nb-18.7Si, and b) Nb-25Si.

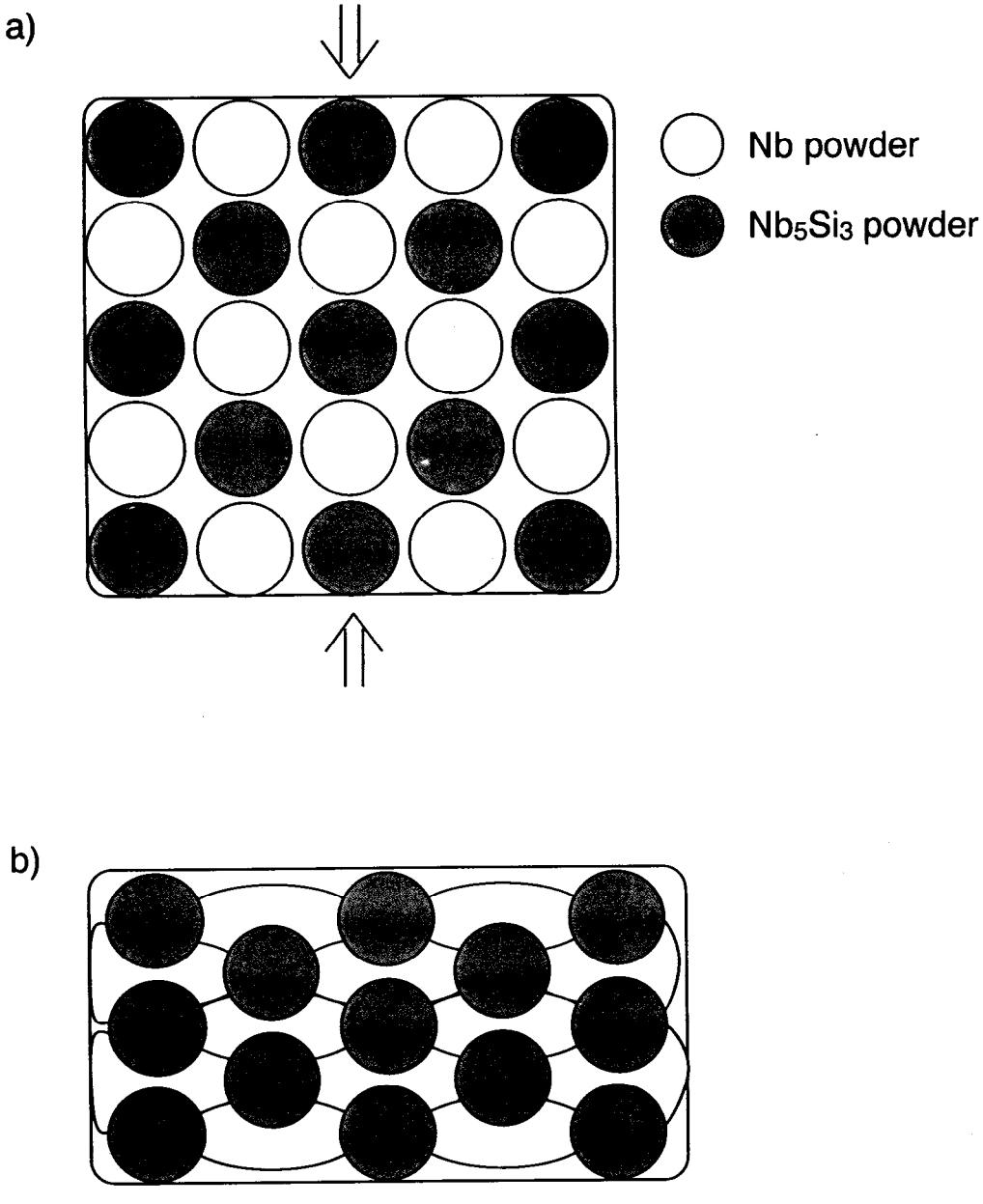

Fig. 4-5 Schematical illustration of consolidation process during hot pressing.

a contamination from the container made of a soft material that easily worn out. It is necessary to use the high-energy type ball milling, at a higher-speed rotation with heavy balls in the hard container, to improve the mixed powders condition preventing the particle adhesion.

3-1-4. Microstructure of AM-Alloys

Typical microstructures of the Nb-18.7Si and Nb-25Si alloys are shown in Fig. 4-6. Bright phase in these micrographs is the (Nb), gray phase the Nb_3Si, and dark phase the Nb_5Si_3, respectively. The as-cast microstructure of the Nb-18.7Si alloy is dominated by the eutectic product consisting of (Nb) particles in the Nb_3Si matrix. In the Nb-25Si alloy, the primary solidification phase is dendritic Nb_5Si_3 phase, and the inter-dendrite region of the primary Nb_5Si_3 is filled by the eutectic product. After the eutectoid decomposition of the Nb_3Si phase during annealing, the eutectoid microstructure, where irregular (Nb) phase particles are dispersed in the Nb_5Si_3 matrix, forms under the influence of the as-cast microstructure. It is difficult to quantitatively evaluate the microstructure because the aspect ratio of (Nb) phase varies widely, but the size of (Nb) phase is roughly estimated to be about 2 to 10 μm.

3-2. Mechanical Properties

3-2-1. Vickers Hardness and the Rule of Mixture

Microstructural observation has revealed that two significant differences exist between the PM- and AM-alloys; the size of ductile (Nb) phase and the matrix phase. The size of ductile phase (Nb) in the PM-alloys is about 50 μm, on the other hand, that in the AM-alloys is about 2-10 μm. The matrix of the PM-alloy is the ductile (Nb) phase and that of the AM-alloys is the brittle Nb_5Si_3 phase. Additionally, it must be noted that the hardness and plastic deformability of (Nb) phase would be totally different between the PM- and AM-alloys due to the solid solution hardening effect regarding the Si content. In the present study, pure-niobium powder was used to fabricate the PM-alloy. It is possible that the Si content is much less than the solubility limit in the (Nb) solid solution phase of the PM-alloy since the atomic diffusion of Si from the Nb_5Si_3 phase into the (Nb) phase would not be sufficient during the consolidation process of the hot pressing. Considering that the solute Si atoms in the solvent (Nb) gives rise to the significant solid solution hardening in the (Nb) phase, as described in the Chapter 2, the difference in the degree of solid solution hardening of (Nb) phase is considerably large to affect the mechanical

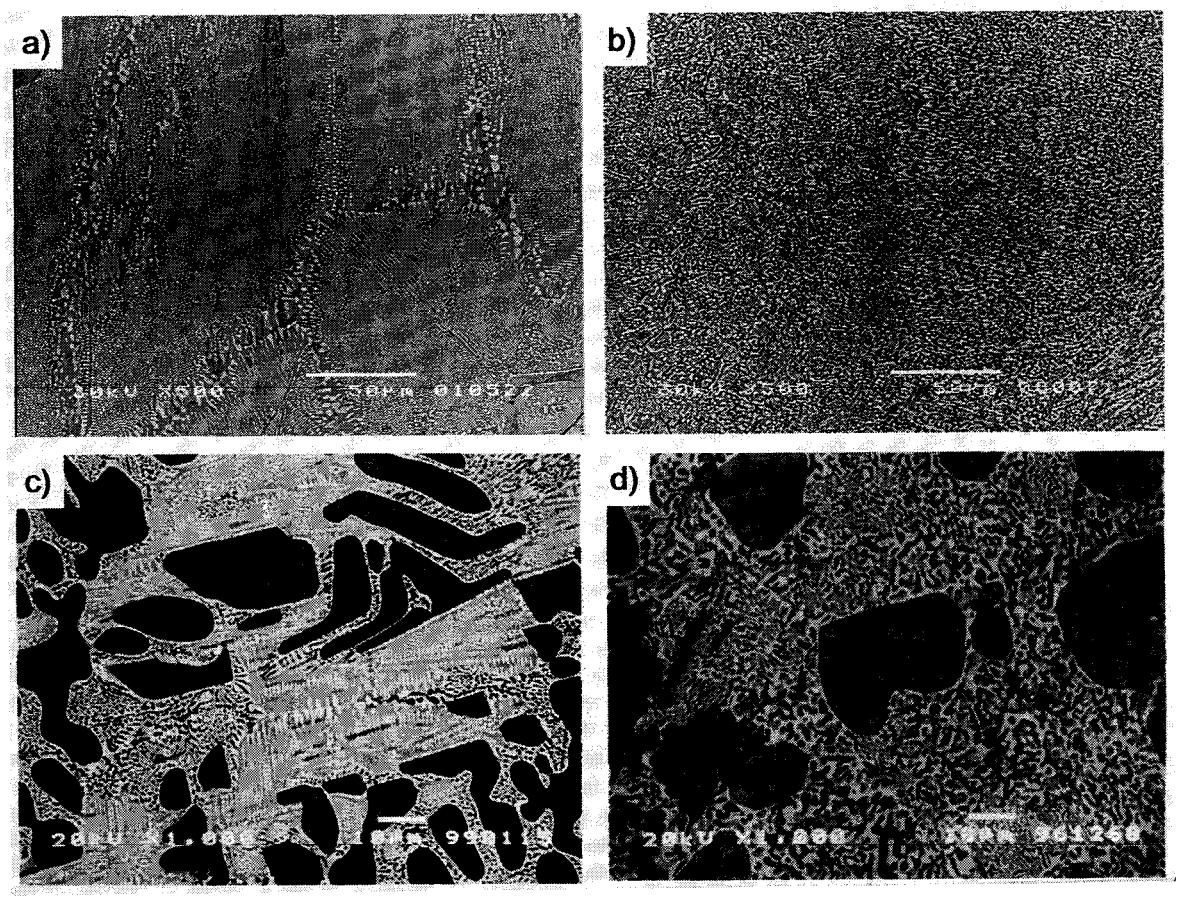

Fig. 4-6 Typical microstructures of the AM-alloys, a) Nb-18.7Si as-cast, b) Nb-18.7Si annealed, c) Nb-25Si as-cast, and d) Nb-25Si annealed.

property of the PM- and AM-alloys.

To investigate effects of the microstructural features originated from the processing methods on the mechanical properties, the Vickers hardness measurement was conducted at room temperature. Measuring the hardness is quite useful and easy way to see the overall propensity of mechanical properties. Table 4-2 is a summary of Vickers hardness measurements of the present alloys. The load for hardness test was chosen as to give a large enough indentation to evaluate the overall hardness of the alloy. Hardness increases with increasing Si content in both the PM- and AM-alloys because the volume fraction of Nb_5Si_3 phase becomes higher. Hardness of the PM-alloys is considerably lower compared to the AM-alloys.

Generally, physical properties and material constants, such as elastic modulus, strength, thermal diffusivity and so forth, can be approximately estimated for composite materials using the rule of mixture (ROM). There are several models proposed to apply to the specific microstructural morphology of composite materials. Based on the most well-known and widely used model, the strength of a composite material is estimated as

$$\sigma_c = \sigma_m V_m + \sigma_f V_f \qquad (1),$$

where σ_c is the average stress of composite, σ_m and σ_f the stress acting in the matrix and strengthener, and V_m and V_f the volume fraction of matrix and strengthener. Moreover, another type of ROM is proposed for the microstructure having spherical particles distributed in the matrix [8]. In this case the relation between the strength and volume fractions of constituent phases is derived from the experimental analysis and given by

$$\log \sigma_c = V_m \log \sigma_m + V_f \log \sigma_f \qquad (2).$$

In respect of the difference in microstructural features, it is interesting to use these two models for explaining the hardness in the present alloys. It must be noted that the estimation based on the ROM is usually available for stress in the elastic region or at most yield stress. An amount of plastic deformation locally induced by the Vickers indentation is thought to be equivalent to about 8 to 10% compressive flow stress [9]. However, the Vickers hardness is used for the ROM analyses instead of the 0.2% flow stress with the reason that it is impossible to measure the 0.2% flow stress of the Nb_5Si_3 single phase alloy, as the reference strength, because

Table 4-2 Summary of the Vickers hadness measurement.

Alloy	Vickers Hardness (Hv)
PM Nb-18.7Si	585
PM Nb-25Si	722
Cast Nb-18.7Si	738
Cast Nb-20Si	820
Cast Nb-25Si	987
pure-Nb	162
Nb-0.5Si	195
Nb-37.5Si (Nb_5Si_3)	1213

of its extreme brittleness. The hardness of pure-niobium is used as the reference hardness for the PM alloys because it is anticipated that Si atom had not diffused sufficiently into (Nb) phase during hot-pressing. In the case of AM-alloy, the hardness of Nb-0.5Si alloy, prepared in the present work for this purpose, is selected as the reference because the solubility of Si in (Nb) phase is reported to be about 0.5at% at temperatures below 1773 K [10,11].

The result of the ROM analyses is shown in Fig. 4-7, the Vickers hardness as a function of the volume fraction of Nb_5Si_3 phase. Note that the value for V_f is estimated form the binary Nb-Si phase diagram. Measured hardness numbers are plotted for the PM- and AM-alloys, and the changes in hardness numbers theoretically calculated from the models, Eq. (1) and (2), are also shown by solid line for the PM-alloy and dashed line for the AM-alloy. The calculation based on the Eq. (1) seems to describe the measured hardness for both the PM- and AM-alloys. However a close examination reveals that the measured hardness of the PM-alloy is located between the predictions by Eq. (1) and (2), which is reasonable because the microstructure of the PM-alloys is that the Nb_5Si_3 phase is dispersed in the (Nb) matrix, but the measured hardness of the AM-alloy is higher than the value evaluated by Eq. (1) and much higher than that by Eq. (2). It means that the extra microstructural factor should be attributed to the strengthening mechanisms other than the particle dispersion considered in the models of Eqs. (1) and (2). It should include the size effect of microstructure and/or the contribution of interfaces. However, the most probable factor must be the matrix phase which causes a difference in propensity between the hardness measurement and ROM analysis in the PM- and AM-alloys. The matrix of the PM-alloys is (Nb) phase and major strengthening mechanism operating in the PM-alloys is the dispersion strengthening by the Nb_5Si_3 phase, so that hardness is properly measured in the PM-alloys. On the other hand, the matrix of the AM-alloys is Nb_5Si_3 phase, therefore, the AM-alloys exhibit higher hardness than that predicted by ROM. Note that the application of the ROM to brittle materials should be carefully deliberated. As will be shown in the section 3-2-3, the present alloys exhibit only a few percent of compressive deformation before the fracture. Deducing from this brittleness of the present alloys, micro- or macro-cracking must be introduced by Vickers indentation. In addition, the effect of work hardening is not considered in the ROM analyses. In this sense, the ROM analyses based on the Vickers hardness measurement would only provide a measure to foresee the mechanism of strengthening for extremely brittle materials like the present alloys.

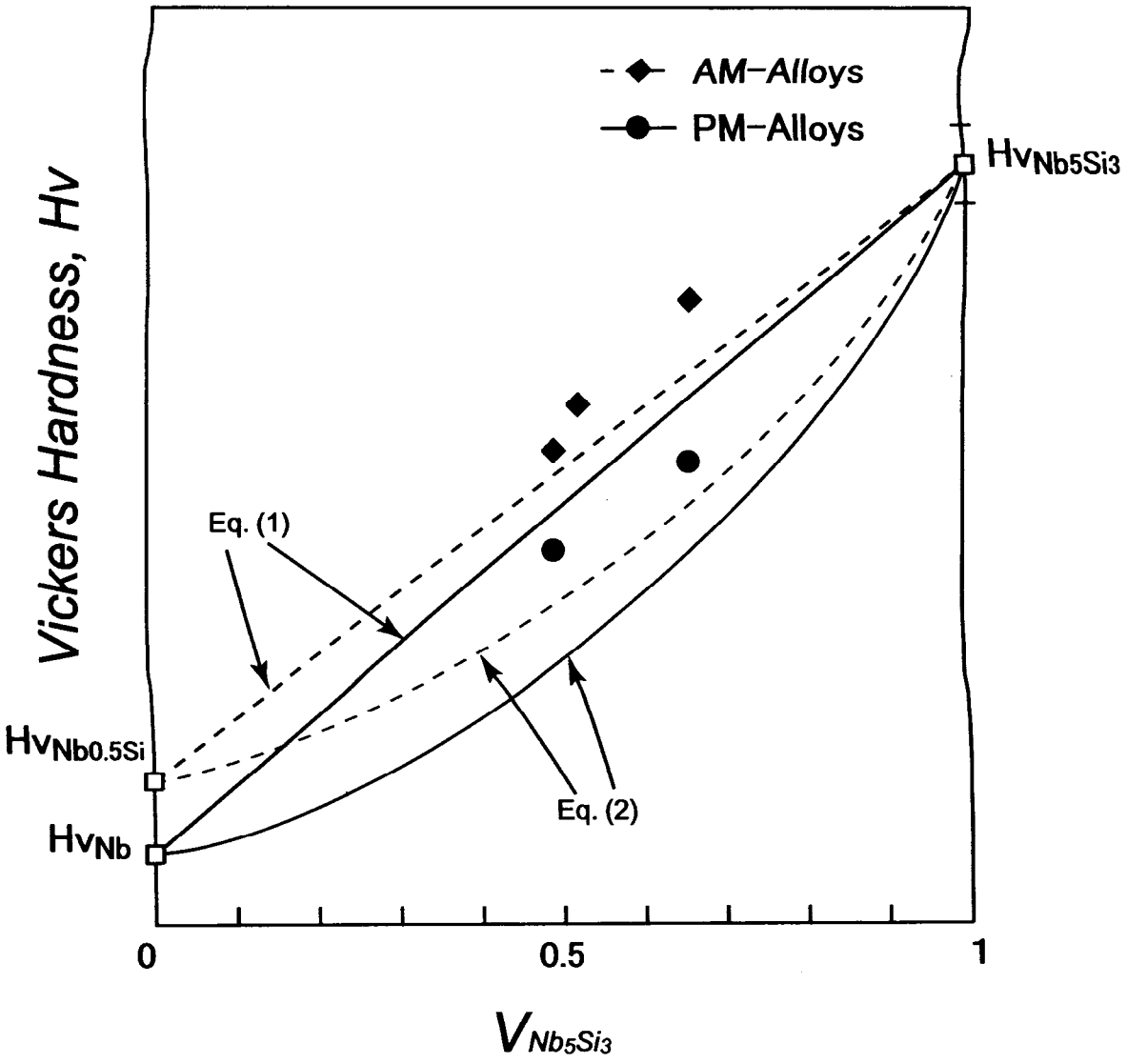

Fig. 4-7 Variation of Vickers hardness as a function of volume fraction of Nb_5Si_3 phase.

3-2-2. Fracture Toughness

Chevron-notch fracture toughness measurement was conducted to evaluate room temperature toughness of the alloys. Figure 4-8 shows a typical load-deflection curve obtained from the PM-Nb18.7Si alloy. Fracture toughness K_Q calculated from the maximum load, P_{max}, using the Bluhm's slice model [12] is summarized in Table 4-3. Measured fracture toughness of the PM-alloys is much higher than that of the AM-alloys. Crack propagation behavior observed in the PM-Nb18.7Si is shown in Fig. 4-9. As the method was described in detail in Chapter 2, the observation was performed on the straight-notched specimen rather than on the chevron-notch specimen because the crack propagating path is restricted in a very small area in the vicinity of the notch and is hard to observe in the chevron-notched specimen. It is clearly seen in Fig. 4-9 that the cracks propagating from the notch root is effectively bridged and blunted by the ductile phase, (Nb). Therefore, the grain size of the ductile phase being about 50 μm is large enough to expect the crack-bridging mechanism to effectively work in the present alloys. Ashby et al. have reported that the stress relief due to the phase decohesion at the interface between ductile and brittle phase plays an important role to enhance the fracture toughness [13]. Such phase decohesion at the (Nb)/Nb_5Si_3 interface is sometimes observed in the present work, indicating that toughness must be increased by the additional effect in the PM-alloys.

The higher fracture toughness in the PM-alloys than in the AM-alloys is mainly due to the size of (Nb) being much larger in the PM-alloys than in the AM-alloys. The difference in ductility of (Nb) phase between the PM- and AM-alloys must be taken into account as well. The plastic deformability of (Nb) phase would be different between the PM- and AM-alloys because the Si content is much less than the solubility limit in the (Nb) solid solution phase of the PM-alloy, as described in the previous section. The difference in the solid solution hardening of (Nb) phase may affect the toughness, while its effect is relatively smaller than the size effect.

3-2-3. Compressive Mechanical Behavior

Compression tests were conducted at the temperature range between room temperature and 1673 K on both the PM- and AM-alloys. Figure 4-10 shows compressive stress-strain curves obtained at all test temperatures. As discussed in the previous chapter, a degree of the fracture resistance can roughly be estimated from the compressive plastic strain to failure. The AM-alloys fracture in an extremely brittle manner without showing any plastic deformation at

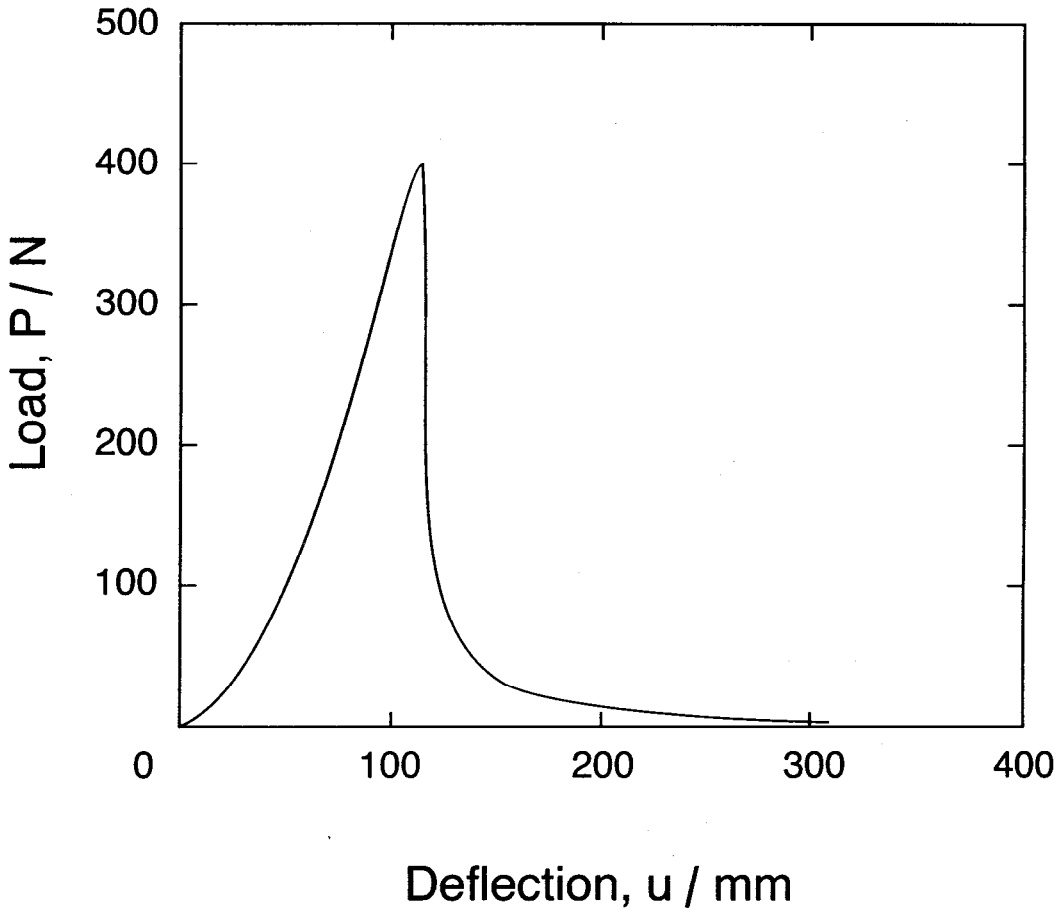

Fig. 4-8 A load-deflection curve of four-point bending test conducted on the PM-Nb18.7Si alloy.

Table 4-3 Summary of the chevron-notch fracture toughness, K_Q, for the PM- and AM-alloys.

Alloy	Process / annealing	K_Q (MPa$\sqrt{m}$)
AM-Nb18.7Si	1673 K / 100 h	3.4
PM-Nb18.7Si	As Hot Pressed	15.1
PM-Nb-25Si	As Hot-Pressed	10.6

Fig. 4-9 Back scattered electron images of the PM-Nb18.7Si alloy showing the crack propagating path from a straight notch observed on the side view of four-point bending test specimen deformed at room temperature.

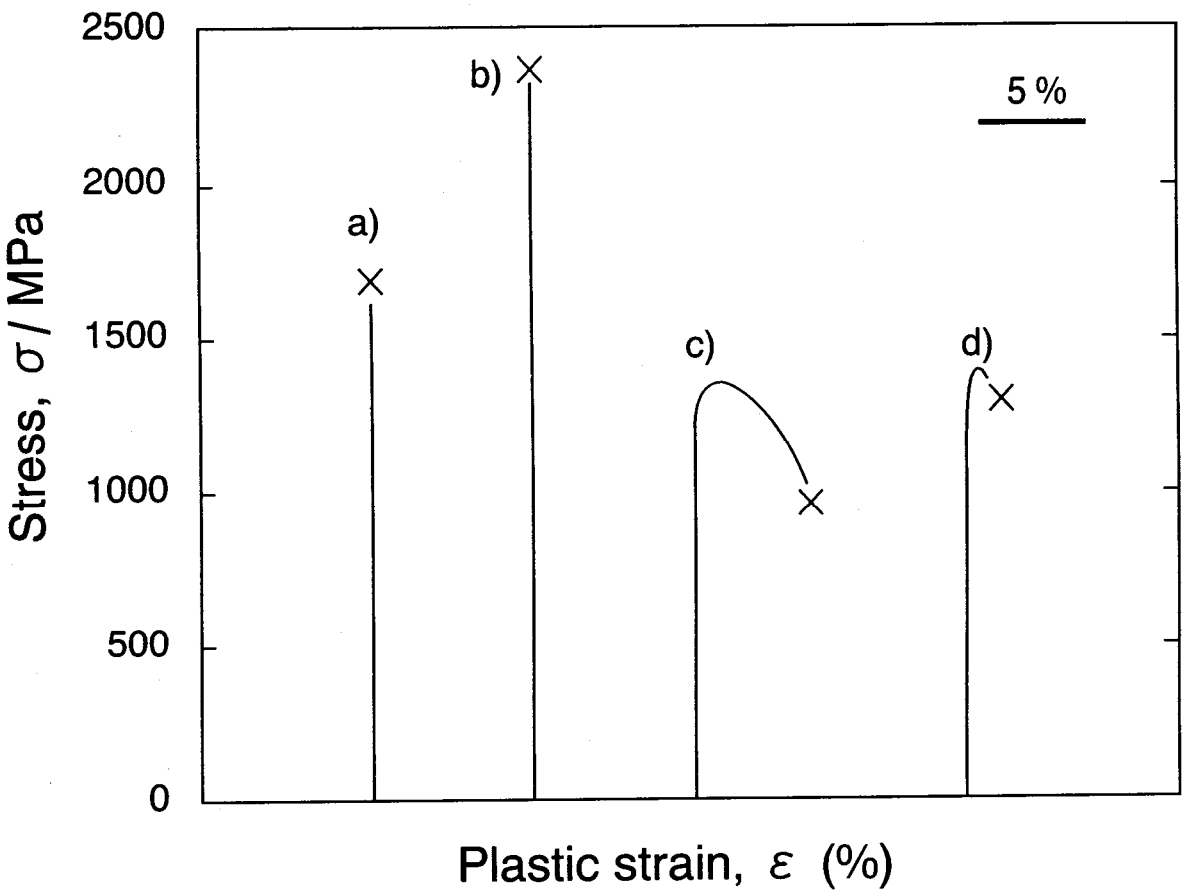

Fig. 4-10 Compressive stress-strain curves of PM- and AM-alloys tested at room-temperature; a) AM-Nb18.7Si, b) AM-Nb25Si, c) PM-Nb18.7Si, and d) PM-Nb25Si.

room temperature, while the PM-alloys show a few percent plastic strain before the fracture. One of the reasons of relatively higher compressive deformability of the PM-alloys than that of the AM-alloys is attributed to that the large size of the (Nb) phase matrix effectively prevent the micro-crack propagation during compression tests. As described in Chapter 2, the present Nb-Si(-Ti) alloys are so brittle that considerable amount of cracks are induced by thermal stress during cooling after the arc-malting in some cast alloys, especially in the Nb-25Si. In fact the preparation of mechanical test specimens was carefully conducted from cast ingots to avoid any micro-cracks. It is confirmed that the powder metallurgy is advantageous to fabricate the crack free sample with less effort.

Figure 4-11 shows the compressive stress-strain curves obtained at elevated temperatures for the PM-alloys. They show a fairly good compressive deformability at 1673 K exceeding over 20% plastic deformation without any cracking. On the other hand, though the results are not shown, the AM-alloy shows the brittle fracture even at 1473 K, and a few cracks are observed after 10 % plastic deformation even at 1673 K. Then the temperature dependence of the 0.2 % flow stress is summarized for the PM- and AM-alloys in Fig. 4-12. The AM-alloy shows excellent strength of about 300 MPa at 1673 K, while the PM-alloys show much lower elevated temperature strength comparable to that of pure-niobium [14].

In general, the finer microstructure causes lower strength at higher temperature region where the interfacial slip assisted by atomic diffusion operates as a deformation mechanism because the total area of interfaces is larger. It is interesting that the present PM-alloys with coarse microstructure exhibit much lower strength at 1673 K than the AM-alloys with fine microstructure. In the many of the eutectoid reactions, the colony or cell structure is formed. In the present AM-alloy, the size of colony formed by the eutectoid reaction should be equivalent or smaller than the size of parent Nb_3Si phase. Provided that the interfacial slip operates chiefly at the original Nb_3Si grain and colony boundaries, and that the (Nb)/Nb_5Si_3 interface produced by eutectoid decomposition is rather stable, there seems to be a small difference in the effective total area of boundary and interfaces in each alloy. From this point of view, it would not be a contradiction that the AM-alloy with a fine microstructure shows higher strength than the PM-alloy with a coarse microstructure. Another point to be considered is the effect of the difference in solid solution hardening of the (Nb) phase between PM- and AM-alloys as already discussed, however, it should be small at high temperature. It has been reported that the strength *of the Nb-1.5Si alloy at 1673 K is comparable to that of pure-niobium [14].* Therefore, the

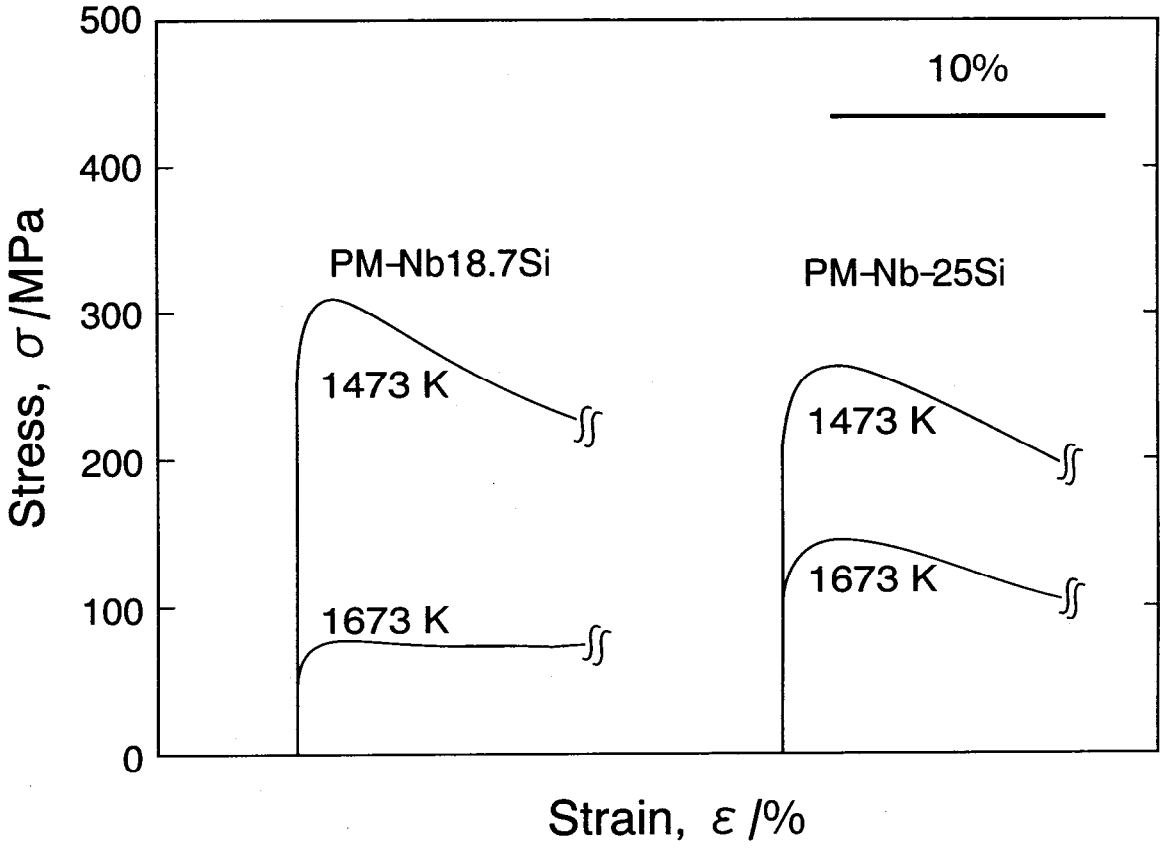

Fig. 4-11 Compressive stress-strain curves of the PM alloys tested at 1473 and 1673 K.

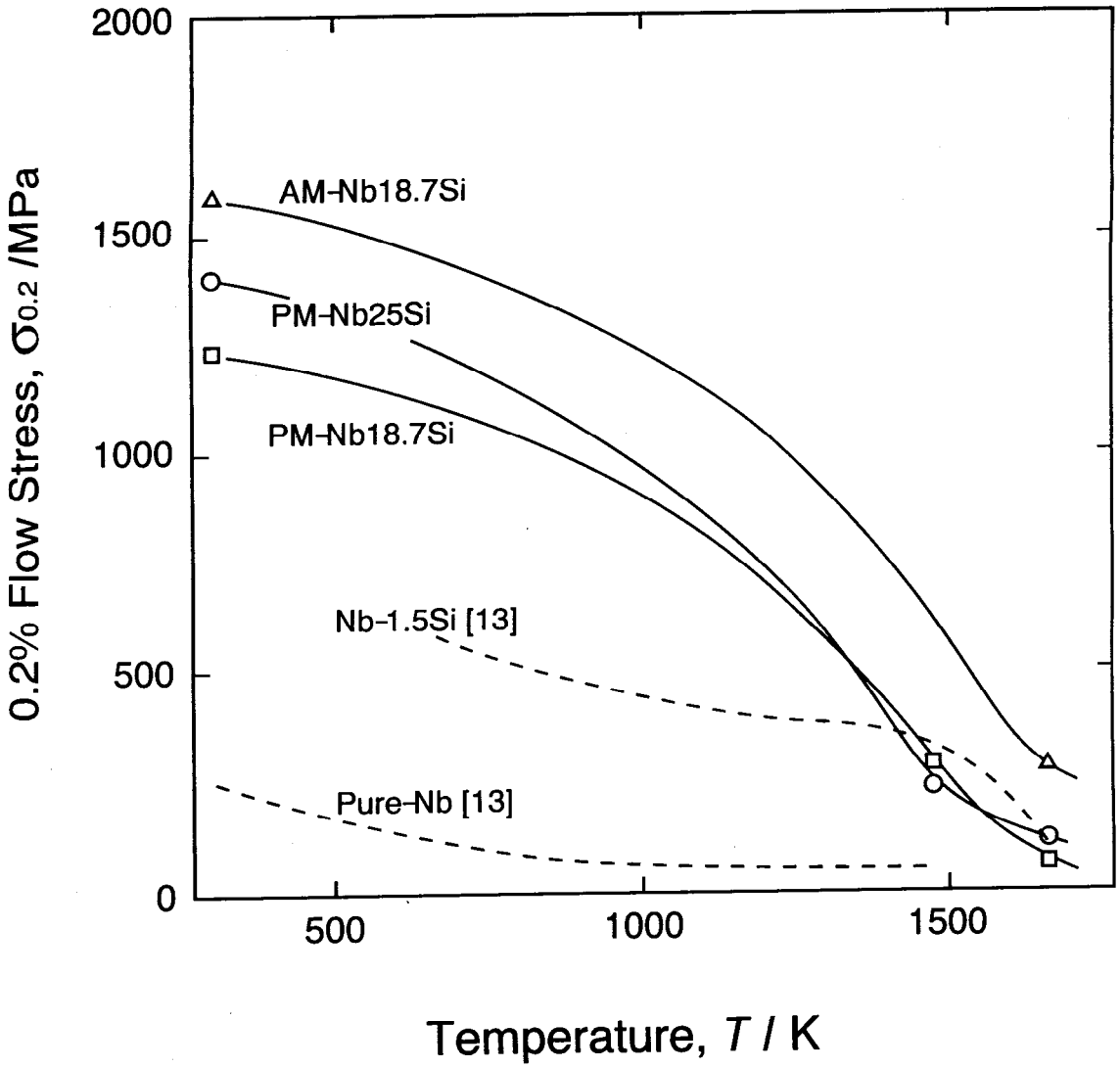

Fig. 4-12 Temperature dependence of 0.2 % compressive flow stress of the present alloys. Bending strength of pure niobium and Nb-1.5Si alloy reported by Mendiratta et al. [13] are also shown for comparison.

difference in strength of (Nb) phase between PM- and AM-alloys at 1673 K should be negligible. It is then concluded that the strength of the PM- and AM-alloys strongly depends on the matrix phase; the ductile (Nb) phase and the hard brittle Nb_5Si_3. The matrix of the PM-alloys is (Nb) phase having low strength at high temperature, therefore, the PM-alloys should exhibit low strength at high temperature. This explanation qualitatively supports a comprehension of the result which the PM-Nb18.7Si and PM-Nb25Si alloys show comparable strength at 1673 K, in spite of that the volume fraction of strengthening phase Nb_5Si_3 is different between them.

3-3. Heat Treatment for the Formation of Lamellar Microstructure

The PM-alloys show moderate fracture toughness at room temperature and extremely low strength at elevated temperatures. On the other hand, the AM-alloys show excellent high temperature strength but low ambient temperature toughness. It means that mechanical properties are much influenced by their microstructural features: the PM-alloys have coarse microstructure with the ductile (Nb) matrix while the AM-alloys have fine microstructure with the brittle Nb_5Si_3 matrix. In this section, the lamellar microstructure control was performed for improving strength of the alloys. Fukui et al. have reported that the elevated temperature strength of the reaction-sintered alloy can be improved by controlling its microstructure from equiaxed two-phase to the lamellar [5]. Figure 4-13 shows microstructures of the Nb-25Si alloy reported by them. The alloy was fabricated by the reaction-sintering using the pure elemental powders of Nb and Si mixed by ball-milling. The hot pressing was conducted at 1653 K for reaction sintering. Fine microstructure consisting of equiaxed (Nb) and Nb_5Si_3 grains is observed in the as hot pressed alloy (see in Fig. 4-13a. As shown in Fig. 4-13b, the reaction-sintered Nb-25Si alloy exhibits the fully lamellar after the following heat treatment. The alloy was solution treated in the Nb_3Si single phase region at 2073 K for 24 h, and subsequently annealed at 1673 K for 72 h for the decomposition of the Nb_3Si phase into the (Nb) and Nb_5Si_3 two-phase lamellar. The fully lamellar alloy shows excellent strength at 1673 K, the 0.2% compressive flow stress being 331 MPa, while the equiaxed alloy exhibits very low strength, 49 MPa. Remarkable improvement of strength at elevated temperature is achieved by the formation of lamellar microstructure.

The high temperature strength of the present PM-alloys can be improved by the microstructural control to form the (Nb)/Nb_5Si_3 lamellar. Figure 4-14 shows microstructures of the PM-Nb18.7Si alloy after the solution treatment in the (Nb)/Nb_3Si two-phase region at 2103

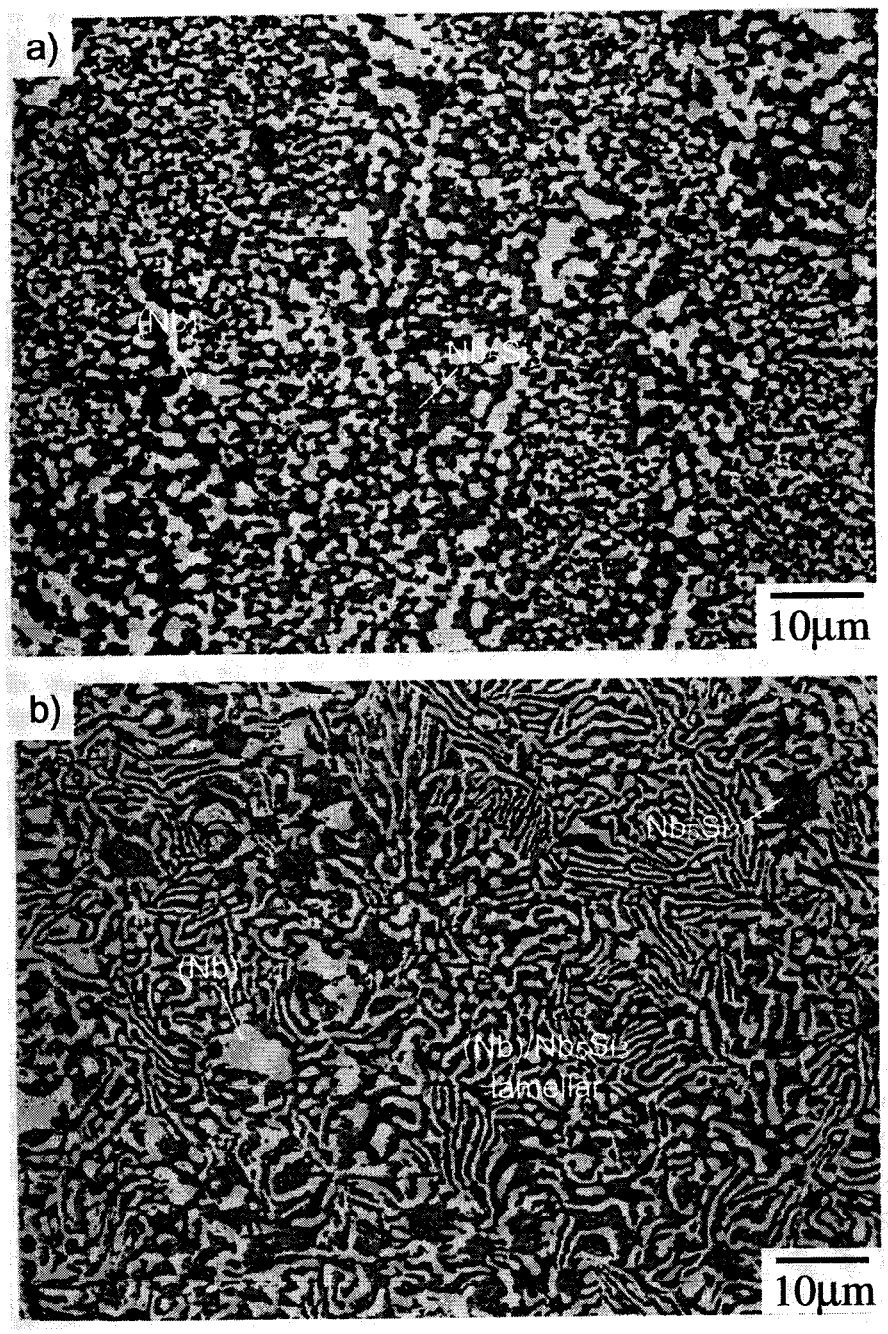

Fig. 4-13 Microstructure of the reaction sintered Nb-25Si alloy reported by Fukui et al. [5], a) homogenized at 1673 K for 72 h after sintering, and b) solution-treated at 2073 K for 24 h, and susequently annealed at 1673 K for 72 h in order to decompose Nb_3Si phase formed by solution treatment.

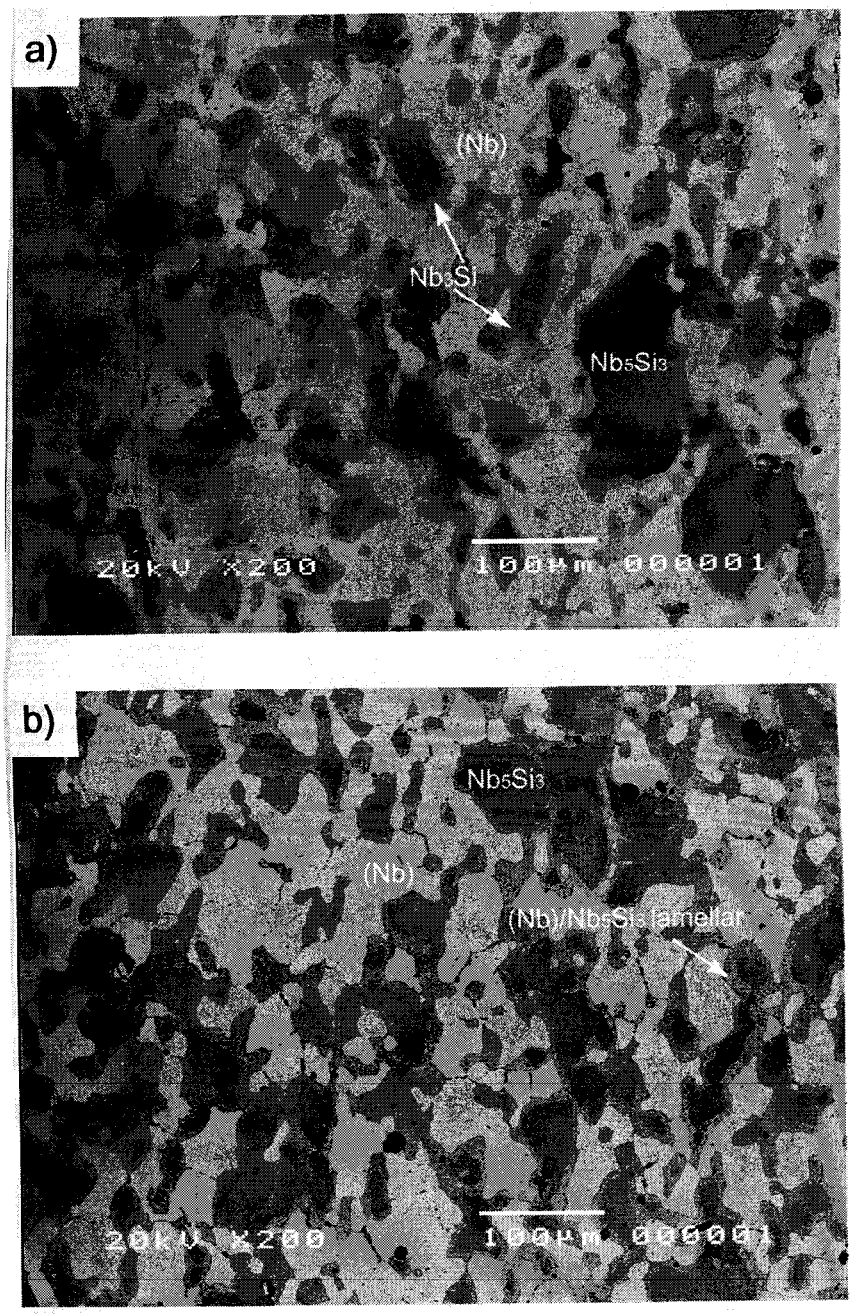

Fig. 4-14 Microstructures of the PM-Nb18.7Si alloy, a) solution treated at 2103 K for 72 h, and b) subsequently annealed at 1673 K for 100 h.

K for 72 h (a), and subsequently annealed at 1673 K for 100 h (b). Bright phase is the (Nb) phase, dark phase the Nb_5Si_3, and gray phase the Nb_3Si, respectively. The existence of Nb_3Si in a region between the (Nb) and Nb_5Si_3 phases in Fig. 4-14a indicates that the Nb_3Si phase is produced by the reverse transformation (Nb)+Nb_5Si_3→Nb_3Si during the solution treatment. The volume fraction of the Nb_3Si phase is very small, less than 5%, as revealed by the quantitative microstructural analysis. During subsequent annealing, the Nb_3Si phase transforms to the (Nb)/Nb_5Si_3 lamellar microstructure. However, compression test revealed that the high temperature strength is not improved since the volume fraction of lamellar region is obviously too small. Generally, the atomic diffusion in an intermetallic phase is slower than that in a metallic phase. Moreover, the diffusion path is long in the coarse and irregular (Nb)/Nb_5Si_3 two-phase microstructure. It requires much longer time than the present solution treatment condition, *for 72 h at 2103 K, to complete the reverse transformation to the Nb_3Si. A desirable* microstructure for the heat treatment of the lamellar microstructure control is that the Nb_5Si_3 phase is finely and homogeneously distributed in the (Nb) phase matrix. It must be achieved in the powder mixing stage by optimizing the ball-milling condition.

4. CONCLUSIONS

A new alloy processing method is proposed in this chapter based on the powder metallurgy to avoid micro-cracking problem caused from thermal stress in casting. To evaluate the effect of this alloy processing, microstructural characterization, compressive mechanical properties and ambient temperature fracture toughness were investigated for the alloys prepared by the proposed powder metallurgy and conventional ingot metallurgy with arc melting. These results were discussed from a view point of the difference in microstructure being resulted from each alloy processing method in order to understand the strengthening and toughening mechanisms.

1. The proposed alloy processing is successful to prepare the PM-alloys having the very high density of 99.8% in the PM-Nb18.7Si alloy. The high dense PM-alloys were obtained through the process in which the ductile niobium particles plastically deform to fill up the spaces among the Nb_5Si_3 particles.

2. The distinctive microstructural feature of the PM-alloys is that the Nb_5Si_3 phase particles are

dispersed in the ductile (Nb) phase matrix, while the matrix of the AM-alloy is the brittle Nb_5Si_3 phase having the dispersion of relatively irregular (Nb) phase particles. The microstructure of the PM alloy is much coarser than that of the AM-alloy.

3. The difference in mechanical properties between AM-and PM-alloys mainly depends on their matrix phases; brittle hard Nb_5Si_3 in the AM- and ductile (Nb) in the PM-alloys. The PM-alloys exhibit higher fracture toughness but lower elevated temperature strength than the AM-alloys.

4. The lamellar microstructure control was unsuccessful in the PM-alloys because of the Nb_3Si phase was not formed sufficiently by the solution treatment. It is necessary to obtain a microstructure where fine Nb_5Si_3 phase is homogeneously distributed in the (Nb) phase matrix in order to increase the volume fraction of Nb_3Si by the solution treatment.

REFERENCES

[1] M.G. Mendiratta, J.J. Lewandowski and D.M. Dimiduk, Metall. Trans. A vol.22A (1991), pp. 1573-1583.

[2] K. S. Kumar and S. K. Mannan, MRS Symp. proc., vol. 133 (1989), pp. 415-420.

[3] M. Nazareth R. V. Perdigao, Jose A.R. Jordao, Claudi S. Kiminami, and Walter J. Botta F., Journal of Non-Crystalline Solid, vol. 219 (1997), pp. 170-175.

[4] J. Kajuch, J.D. Rigney, and J.J. Lewandowski, Mater. Sci. Eng. A, vol. 155 (1992), p. 59.

[5] Fukui et al., "Summary of R&D Report for FY1999 Proposal-Based R&D Program of NEDO" (in Japanese), No.98Ec07-004-3, New Energy and Industrial Technology Development Organization, 1999.

[6] "Handbook of Ternary Alloy Phase Diagrams", Ed. P. Villars et al., ASM Intnl., 1997.

[7] P.C. Tortorici and M.A. Dayananda, Mater. Sci. Eng. A, vol. 261 (1999), pp 64–77.

[8] Y. Kagawa, The university of Tokyo, private communication.

[9] "Frontier in Strengthening of Steels" (in Japanese), Ed. T. Maki, The Iron and Steel Institute of Japan, 1995.

[10] P.R. Subramanian, M.G. Mendiratta, and D.M. Dimiduk, MRS Symp. Proc., vol. 322 (1994), pp. 491-502.

[11] B.P. Bewlay, M.R. Jackson, and R.R. Bishop, Journal of Phase Equilibria, vol. 19 (1998), No. 6, pp. 577-586.

[12] Dietrich G. Munz, Int. Journal of Fracture 16 (1980), p.p. 137-140.

[13] M. F. Ashby, F. J. Blunt and M. Bannister, Acta Metall. Mater., 37 (1989), pp. 1847-1857.

[14] M.G. Mendiratta and D.M. Dimiduk, MRS Symp. Proc., Vol. 133 (1989), pp. 441-446.

CHAPTER 5

MICROSTRUCTURAL CONTROL BY DIRECTIONAL SOLIDIFICATION

1. INTRODUCTION

The unidirectional solidification technique provides a wide variety of possible applications for various metallic and ceramic materials. Microstructural control through the directional solidification is very effective to improve the toughness of composite materials in which the ductile phase plays an important role to impart the toughness for the brittle phase. Generally, the toughness of composite materials is greatly influenced by the morphology, size, and volume fraction of ductile phase. Provided that quite regular eutectic microstructures with the well-aligned ductile phase arrangement in the brittle phase matrix is produced by directional solidification, the toughness of composite alloys should be effectively enhanced due to the extrinsic toughening mechanisms such as crack trapping, crack deflection, crack bridging.

A lot of efforts have been put into the in-situ composite based on the Nb-Si binary and Nb-Ti-Si ternary systems [1-7]. These results indicate that directional solidification effectively enhances not only room temperature fracture toughness but also high temperature strength. In the present alloy, the contribution to toughening by the coarse (Nb) phase is higher than that by the fine (Nb) lamellae when the crack-bridging is expected to operate effectively as a toughening mechanism. If relatively large (Nb) phase plates are well-aligned by the eutectic solidification, the toughness and high temperature strength of the alloy is expected to be greatly improved. Therefore, the special interest of the present chapter is to control microstructure using the directional solidification technique on the (Nb)/Nb_3Si eutectic alloy in the Nb-Si binary and Nb-Si-Ti ternary systems. In addition, taking an advantage of these alloy systems, in which the lamellar microstructural control is possible by utilizing the eutectoid decomposition of Nb_3Si, further improvement is expected for mechanical properties. The microstructure consisting of

fine (Nb)/Nb_5Si_3 lamellar formed by the eutectoid decomposition of Nb_3Si with relatively thick well-aligned (Nb) phase is favorable for excellent fracture toughness and strength. It is well-known that the regularity and morphology of microstructure strongly depend on the conditions of the solidification process. The relationship between microstructures and directional solidification conditions was investigated in this work. The room temperature fracture toughness and strength of directionally solidified alloys were evaluated by chevron-notch fracture toughness measurement and compression test. The toughening mechanisms of the directionally solidified alloys are discussed focusing on the distinctive microstructural features comparing with alloys prepared by arc-melting.

2. EXPERIMENTAL

Nominal compositions of the alloys investigated in this chapter are listed in Table 5-1. To further control the microstructure of the alloys, a directional solidification was performed by means of the floating zone melting. Directionally solidified alloys, here after the DS alloys, were grown from the feed rods, using the optical floating zone (OFZ) furnace at a growth rate ranging from 5 to 200 mm/h under an Ar gas flow. Feed rods, having a dimension of 11 mm in diameter and 70 mm in length, were prepared by arc-melting under an Ar atmosphere using high purity raw materials readily available. Annealing was conducted at 1673 and 1773 K for 100 and 500 h in a vacuum after the directional solidification. The DS-alloy was wrapped with Nb foils to minimize the oxidation during heat treatments. Microstructural observation was performed by means of scanning electron microscope (SEM) using back-scattered electron image (BEI). Constituent phases of the alloys were identified by X-ray diffractometry (XRD), energy dispersive X-ray spectroscopy (EDS), and electron probe X-ray micro analysis (EPMA). Quantitative microstructural evaluation was conducted by two methods; the image analysis by the digital image recording and processing system combined with SEM, and the linear intercept method.

Four-point bending tests were carried out to evaluate the fracture toughness using chevron-notched specimens. Test specimens were prepared by electro-discharge machining (EDM), and were mechanically polished to remove the damaged surface layer prior to testing. The length of each specimen was oriented parallel to the growth direction and the notch was introduced by EDM perpendicular to the growth direction. The geometry of the bending test specimen is shown in a Chapter 2. Tests were carried out using an Instron type testing machine

Table 5-1 Nominal alloy compositions prepared in this chapter.

Nb	Si	Ti *(at%)*
82.5	17.5	0
80.5	17.5	2
77.5	17.5	5
72.5	17.5	10
81.3	18.7	0

at a cross-head speed of 5×10^{-2} mm/min. The bending test specimen was supported by free rollers with the outer and inner spans being 21 mm and 7 mm, respectively. The chevron-notch fracture toughness, K_Q, is calculated using the Bluhm's slice model [8] as described in detail in Chapter 2. The test was done only once on each DS-alloy because there was a limit in a specimen preparation due to the size of DS-alloy ingot, about 10 mm in diameter and 30~40 mm in length. Compression tests were conducted at a nominal strain rate of 1.0×10^{-4} s^{-1} in air at room temperature, and in a vacuum ($1\sim3\times10^{-4}$ Torr) at elevated temperatures. Test specimens, $2\times2\times5$ mm^3 rectangular pillar, were prepared by EDM and were mechanically polished to remove the damaged surface layer prior to testing. Loading direction of each specimen was oriented parallel to the growth direction.

3. RESULTS AND DISCUSSION

3-1. Microstructures

3-1-1. As-Grown Microstructures of the Nb-Si Binary Alloys

To achieve a good alignment of the eutectic (Nb)/Nb_3Si by directional solidification, it is very important to know the true eutectic composition. However, there are several reports on the (Nb)/Nb_3Si eutectic composition in the Nb-Si binary system, 17.5 at%Si [9,10], 18.2 at%Si [1] and 18.7 at%Si [11,12]. Figure 5-1 shows the as-cast microstructures of the Nb-17.5Si and Nb-18.7Si alloys prepared by arc melting. Both alloys exhibit the (Nb)/Nb_3Si eutectic microstructure consisting of the fine (Nb) particles in the Nb_3Si matrix. It is difficult to judge from these micrographs which is the closest composition to the true eutectic. Figure 5-2 shows microstructures of the Nb-18.7Si alloys at the growth rates of 30 and 100 mm/h. These microstructures are characterized by a cellular structure. The primary solidification phase is the faceted Nb_3Si, and the eutectic products is formed surrounding the primary Nb_3Si. A sort of the collapsed eutectic microstructure can be observed in the inter-cellular region. Figure 5-3 shows the microstructures of the as-DS Nb-17.5Si alloy at the growth rates of 10, 30, 100, and 200 mm/h. Cell formation is the feature of microstructures of the alloys grown at the rates over 30 mm/h, but the faceted primary solidification phase of Nb_3Si is not observed. The center of the cellular structure is characterized by the fine (Nb)/Nb_3Si eutectic microstructure consisting of the small and discontinuous (Nb) particles dispersed within the Nb_3Si matrix. The outer portion of the cellular structure is composed with the coarse (Nb)/Nb_3Si eutectic microstructure, and the

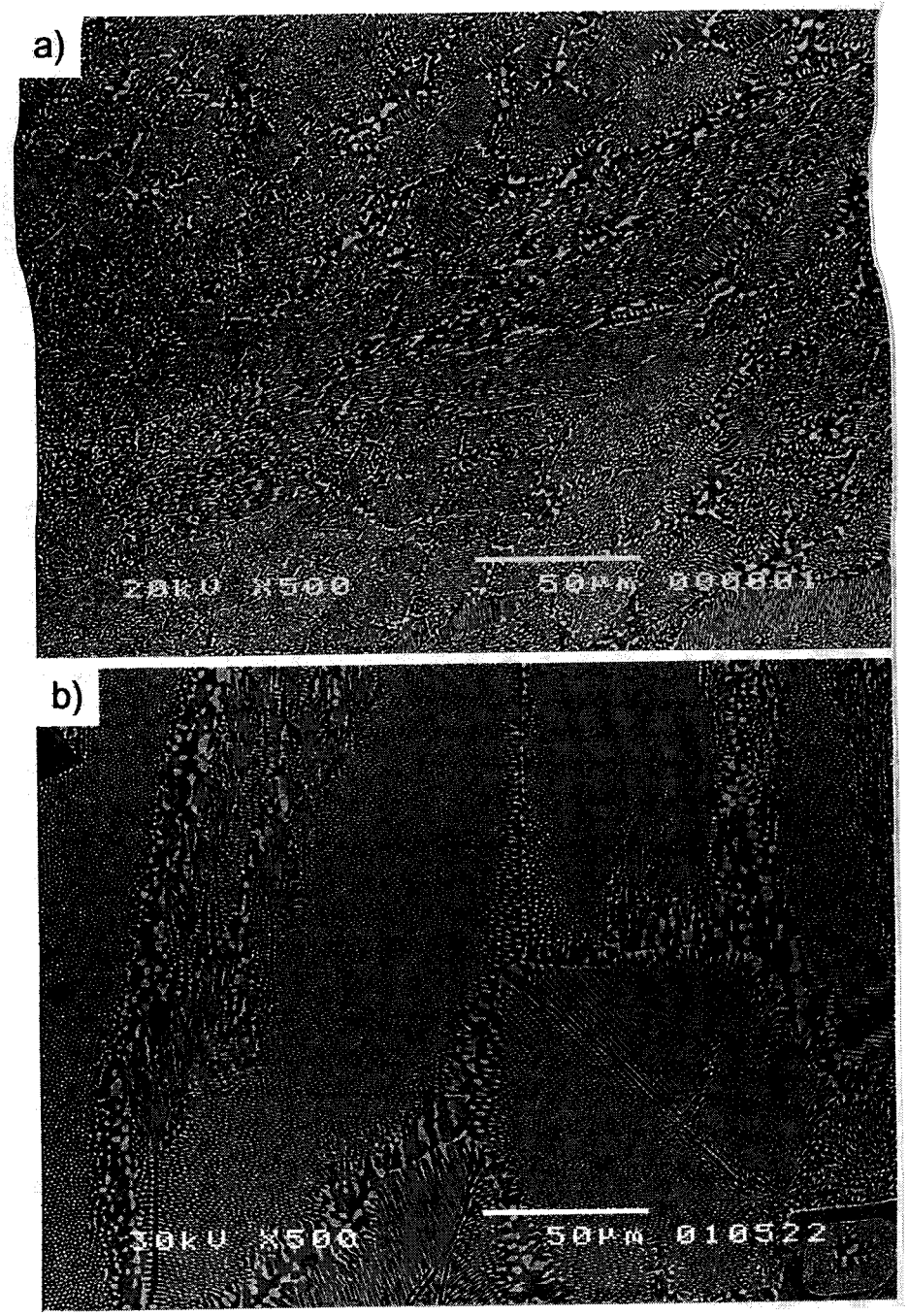

Fig. 5-1 Microstructures of as-cast alloys prepared by arc melting, a) Nb-17.5Si, and b) Nb-18.7Si.

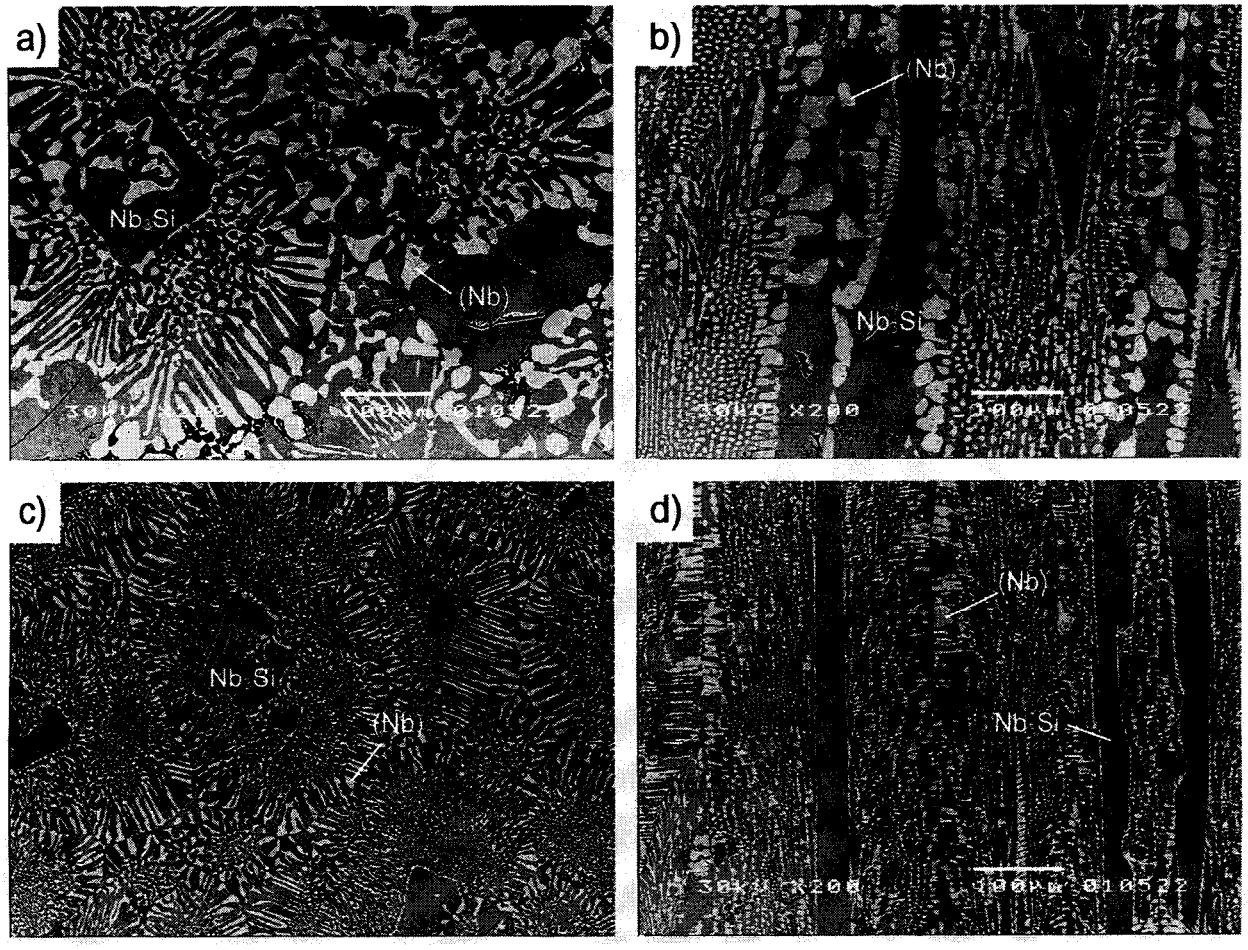

Fig. 5-2 Microstructures of Nb-18.7Si alloys, a) transverse section and b) longitudinal section at the growth rate of 30mm/h, c) transverse section and d) longitudinal section at the growth rate of 100mm/h.

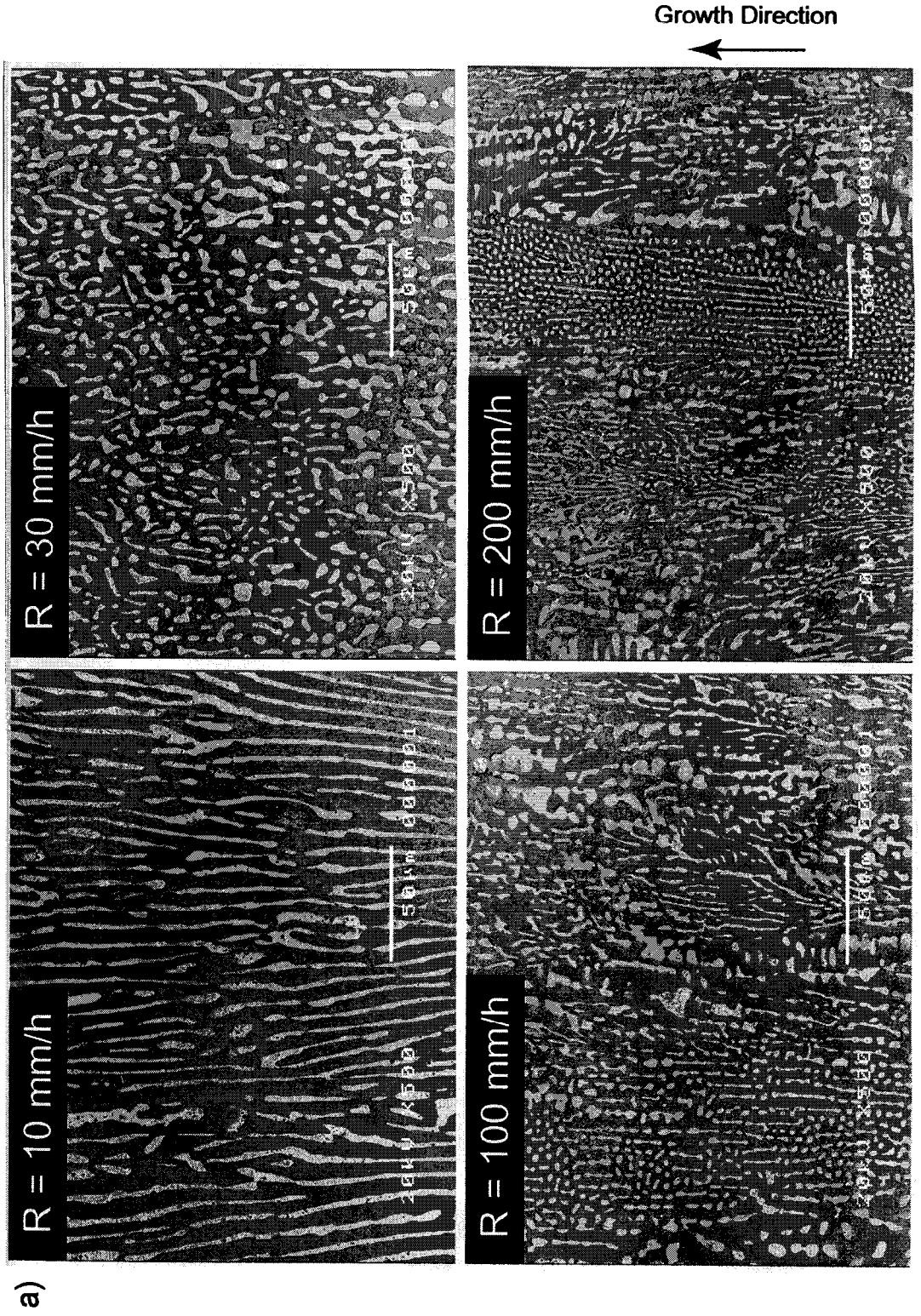

Fig. 5-3 Microstructures of as-directionally solidified Nb-17.5Si alloy grown at the rate of 10, 30, 100, and 200mm/h; a) longitudinal sections and b) transverse sections.

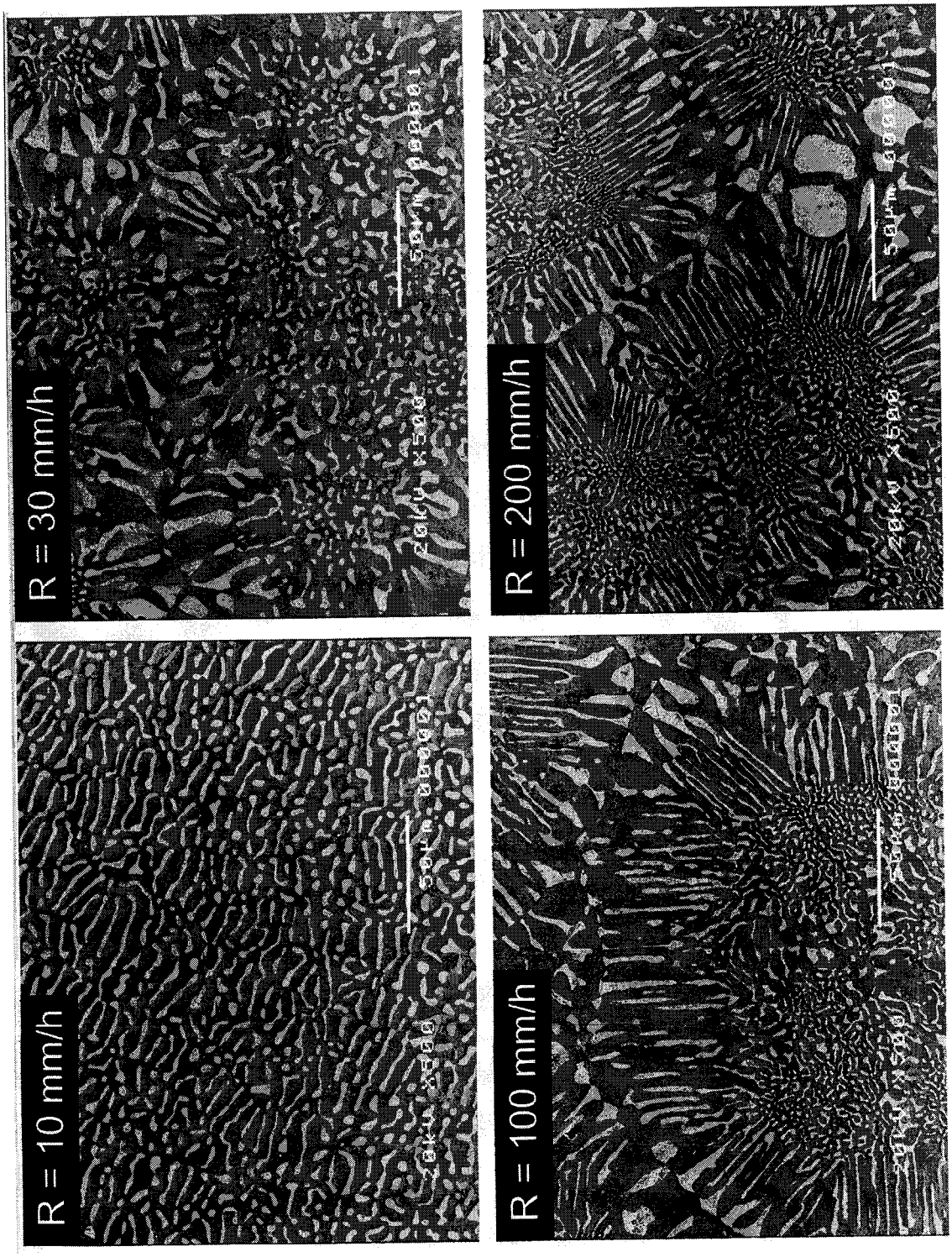

Fig. 5-3 Continued.

inter-cellular region is filled with the (Nb) phase. On the other hand, the microstructural feature of the DS Nb-17.5Si alloy grown at the rate of 10 mm/h is described as the continuous (Nb) plates aligned parallel to the growth direction in the Nb_3Si matrix, and the coarse (Nb) phase is hardly observed. Consequently, the effect of growth rates on microstructures of the Nb-17.5Si alloy is summarized as follows: the volume fraction of irregular and coarse (Nb) phase formed in the inter-cellular region decreases with decreasing growth rates. This propensity implies that the planar front is formed at the liquid/solid interface at the growth rate of 10 mm/h, and the breakdown of the planar front takes place at the growth rate exceeding 30 mm/h. The planar front is formed at a very slow growth rate and the regularly aligned two-phase microstructure, the planar eutectic microstructure, is produced with the homogeneous distribution of constituent phases. There exists the explicit dependency of the condition of planar front formation, i.e. the morphology of produced microstructures, on the growth rate in the DS-alloys. As the growth rate decreases, the morphology changes in this order; dendrite, cellular, and the planar eutectic microstructure. Judging from these aspects, it is suggested that the coupled-zone of the (Nb)/Nb_3Si eutectic is shifted to the Si-rich side as temperature decreases from the eutectic. Generally, it is well known that the coupled-zone tends to shift to the facet phase side in the facet/non-facet eutectic system [13]. Figure 5-4 shows a schematic illustration of the coupled-zone in the Nb-Si binary system predicted in this work. A solidification requires a certain degree of supercooling in any alloy systems. It is reported that the degree of supercooling for a solidification is proportional to the square root of the growth rate [14]. Increasing the growth rate enlarges the supercooling for the solidification. In the alloy having the exact eutectic composition, solidification starts well below the eutectic temperature that is obviously out of the coupled-zone, as predicted from Fig. 5-4. Therefore, the composition of Nb-17.5Si is much closer to the true eutectic composition than that of Nb-18.7Si. Considering that the coupled-zone shifts to the Nb_3Si side, the alloy composition slightly Si-rich from the Nb-17.5Si is favorable to obtain the plane front and thereby the completely aligned eutectic microstructure in a wide range of growth rates.

3-1-2. As-Grown Microstructures of the Ternary Alloys

Directional solidification was also conducted on the Nb-Si-Ti ternary alloys at various growth rates ranging from 5 to 200 mm/h. Figures 5-5, -6, and -7 show the microstructures of

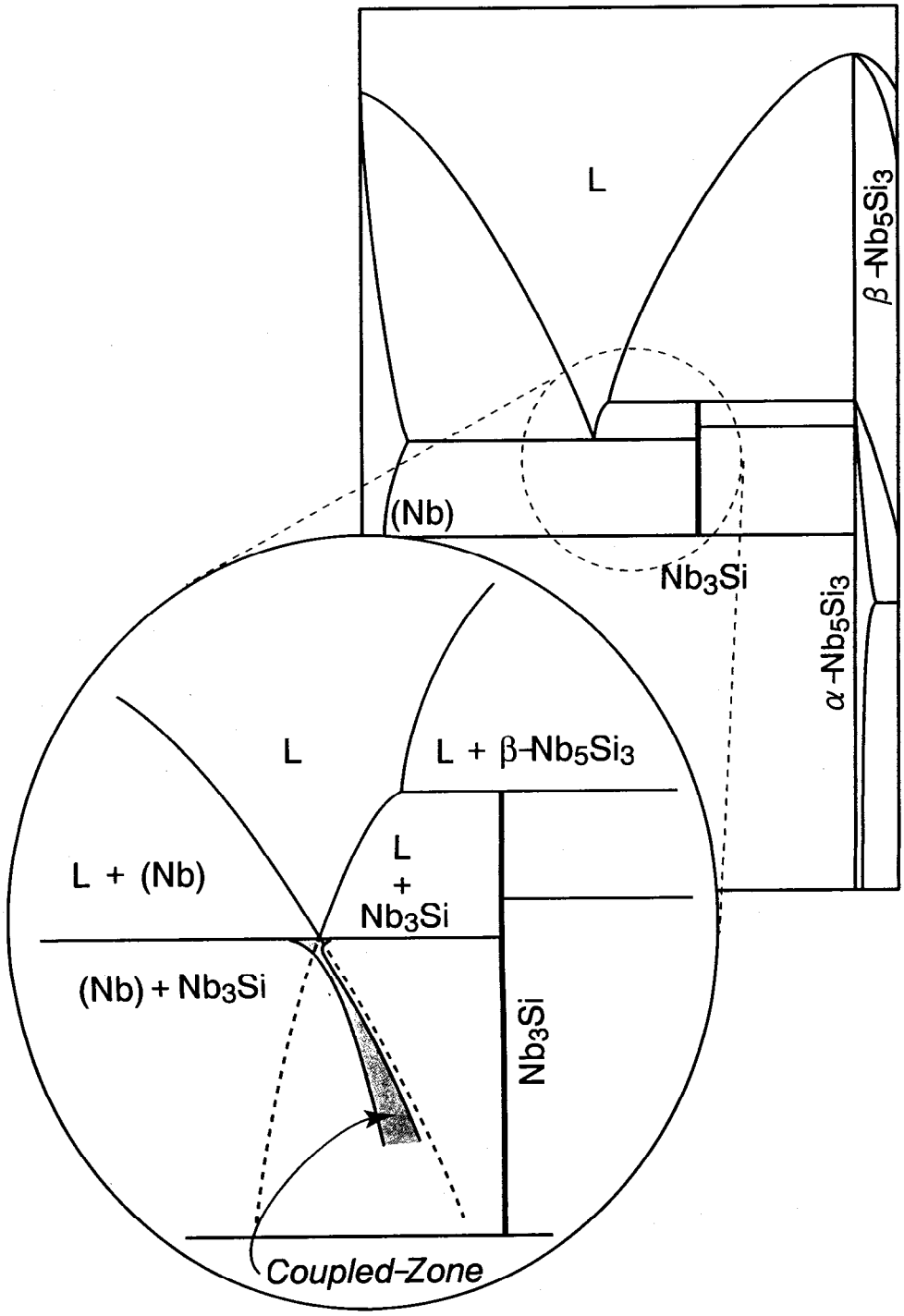

Fig. 5-4 A schematic illustration of the coupled-zone in the Nb-Si binary system.

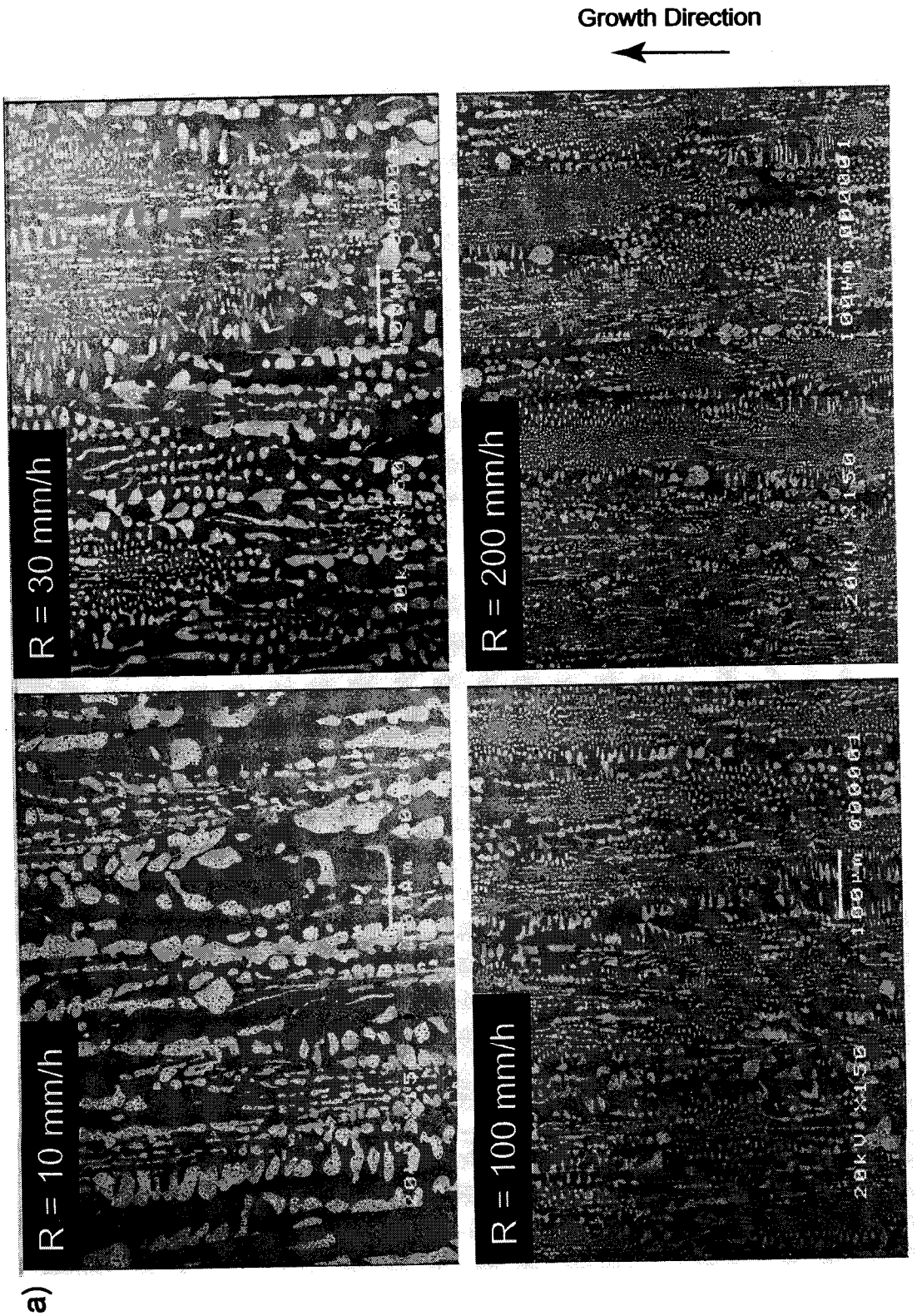

Fig. 5-5 Microstructures of as-directionally solidified Nb-17.5Si-2Ti alloy grown at the rate of 10, 30, 100, and 200mm/h; a) longitudinal sections and b) transverse sections.

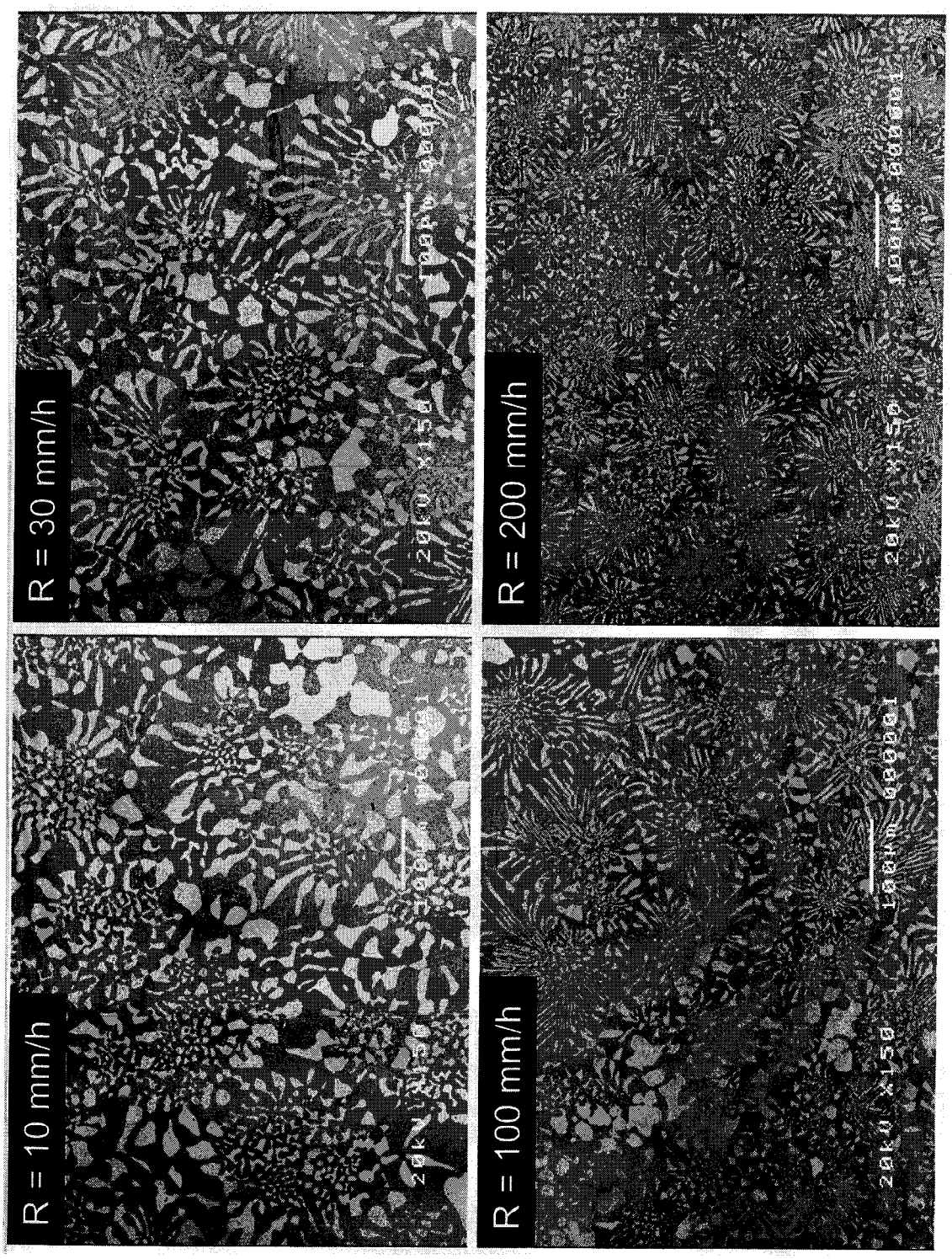

Fig.5-5 Continued.

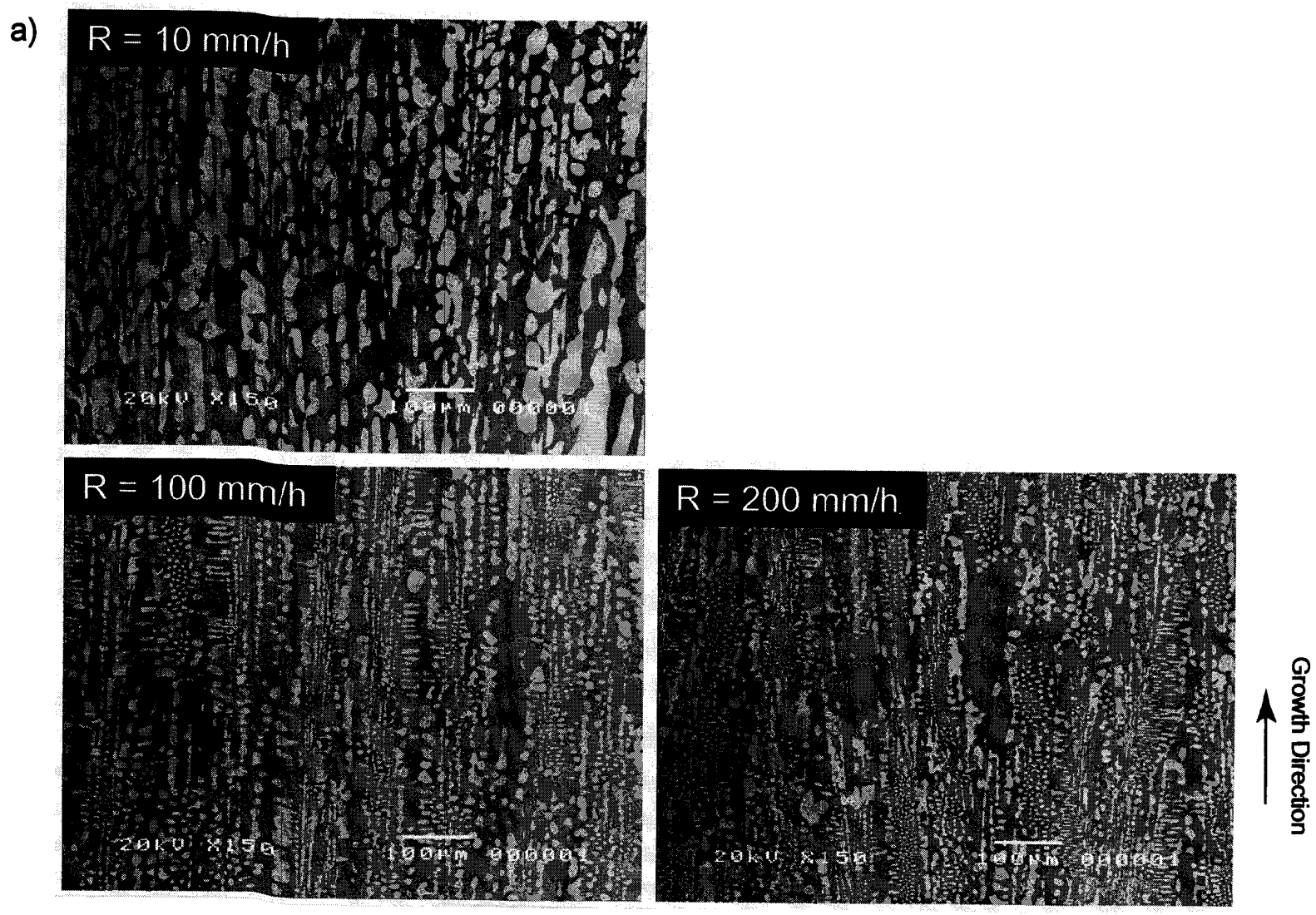

Fig. 5-6 Microstructures of as-directionally solidified Nb-17.5Si-5Ti alloy grown at the rate of 10, 100, and 200 mm/h: a) longitudinal sections and b) transverse sections.

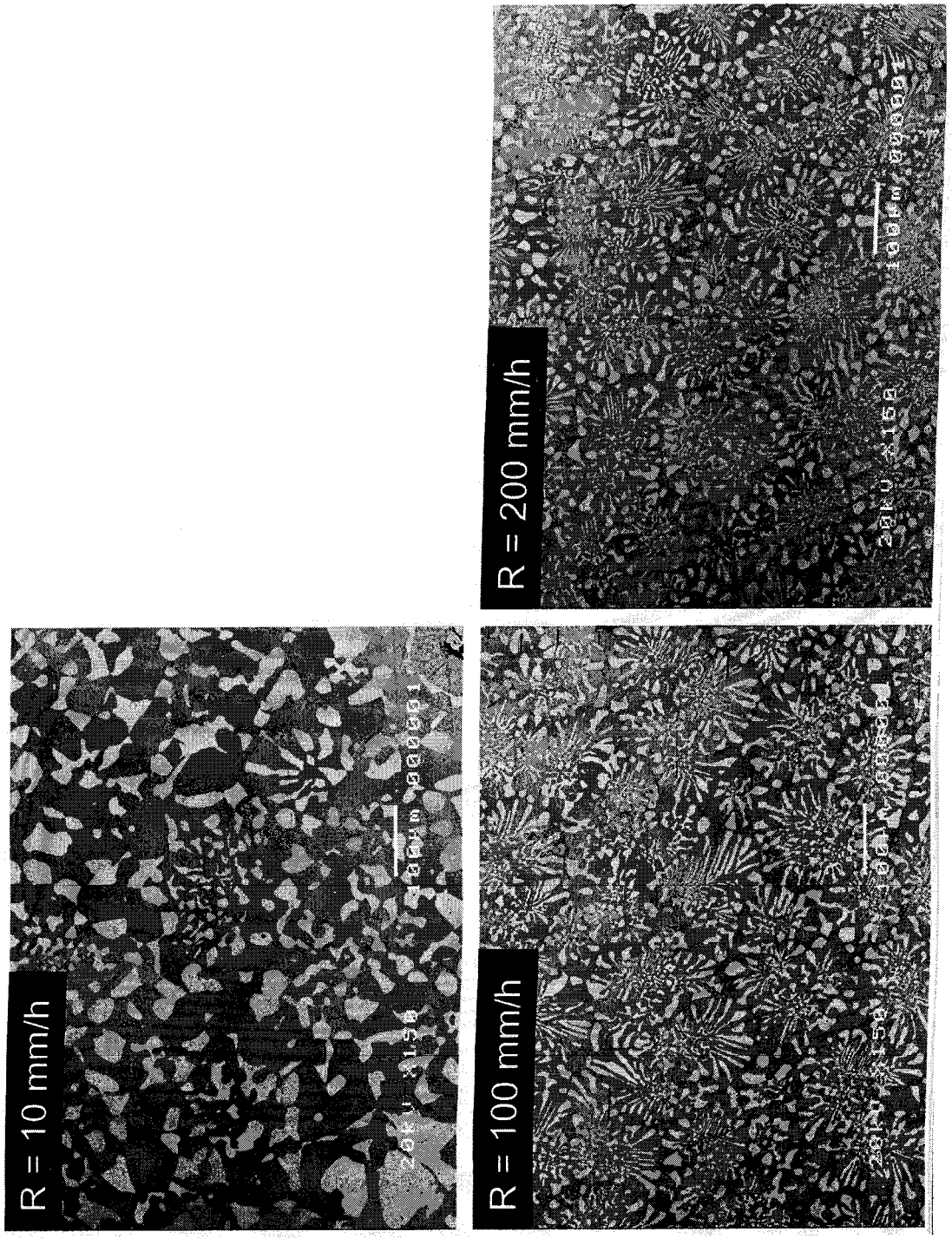

Fig. 5-6 Continued.

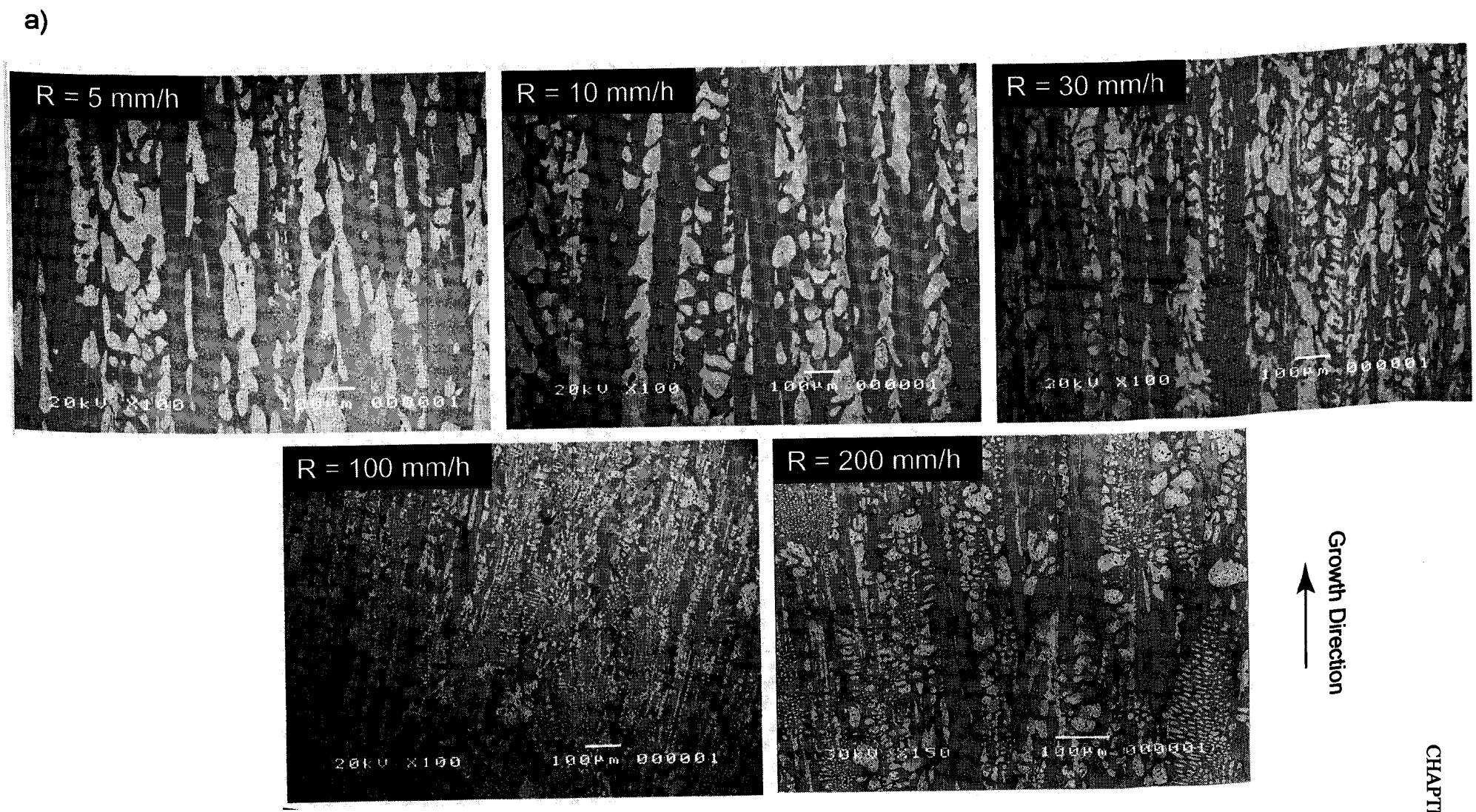

Fig. 5-7 Microstructures of as-directionally solidified Nb-10Ti-17.5Si alloy grown at the rate of 5, 10, 30, 100, and 200mm/h. a) longitudinal sections and b) transverse sections.

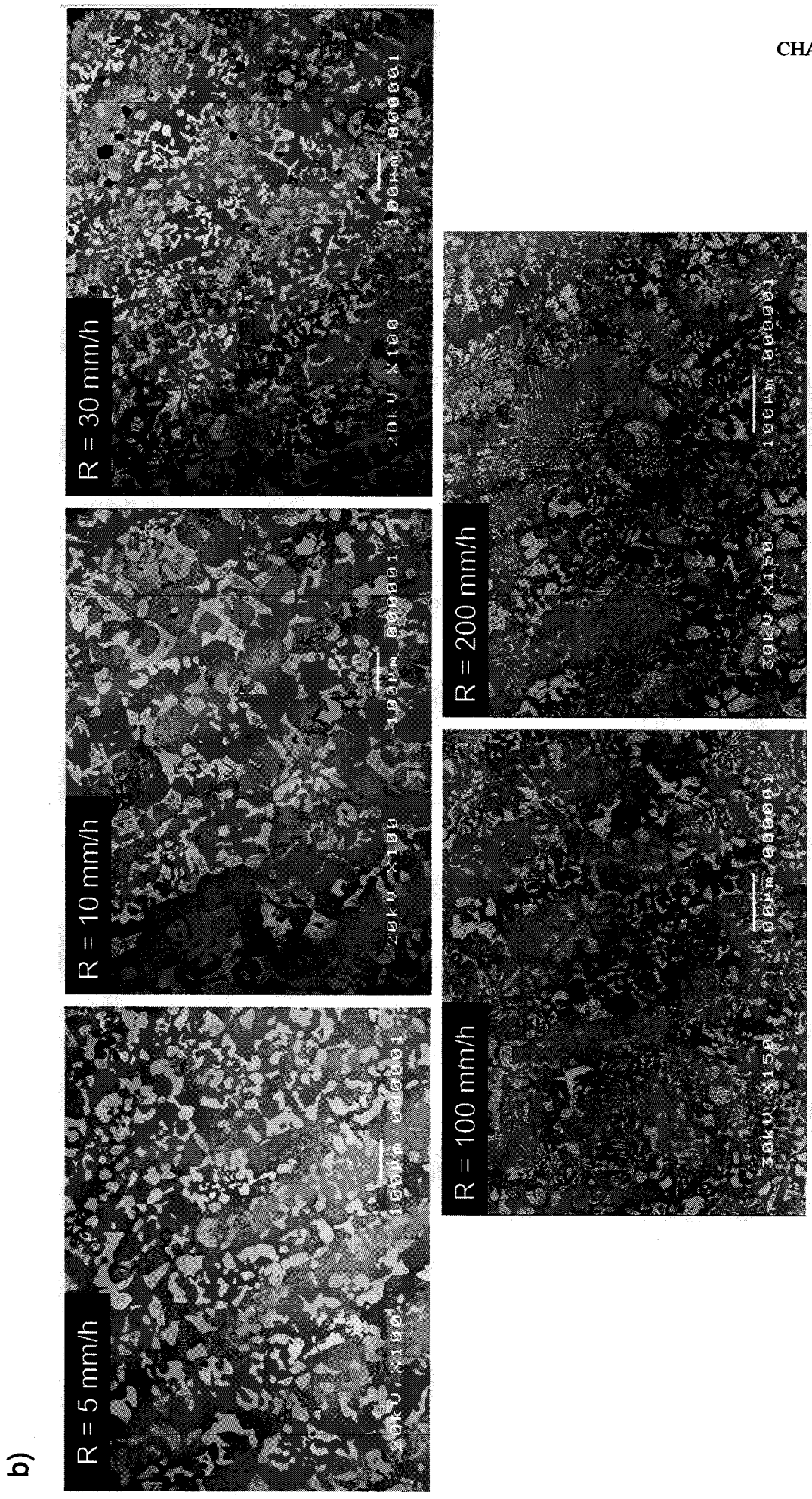

Fig. 5-7 Continued.

the ternary alloys based on the Nb-17.5Si with the Ti content of 2, 5, and 10Ti, respectively. Microstructures of the DS-alloys with 2Ti and 5Ti are characterized by the cellular structure at all the growth rates, where each cell is aligned parallel to the growth direction. The (Nb) phase is discontinuously aligned inside the cell even at the slowest growth rate of 10 mm/h. Microstructures of the DS Nb-17.5Si-10Ti alloy grown at the rates between 5 and 30mm/h are described by the array of discontinuous (Nb) phase aligned parallel to the growth direction. This alloy should have the cellular structure characterized by the discontinuous (Nb) phase dispersed in the Nb_3Si matrix, though the cell boundaries are not clearly identified. The slower the growth rate becomes, the better the microstructure is aligned, though the alignment is not as good as the binary alloys because of the discontinuous (Nb) phase. Moreover, some cells are grown off from the growing direction at the growth rates of 100 and 200 mm/h.

One of the reasons for the poor alignment of microstructures in the ternary alloys is that the solidification involving the "$L \rightarrow (Nb) + Nb_3Si$" is no longer the invariant reaction in the ternary system. The existence of the freezing range may yield a formation of a mushy zone, which makes it difficult to form the planar front at the solid/liquid interface. In addition, a large amount of Ti atoms must be built-up on the solid/liquid interface for the steady state solidification, as schematically illustrated in Fig. 5-8, especially in the alloy with higher Ti contents. In the Nb-Si-Ti ternary system, since the eutectic temperature decreases as the Ti content increases from the Nb-Si binary edge, the Ti content in the liquid phase should be the highest in the constituents of the liquid/(Nb)/Nb_5Si_3 three-phase equilibrium tie-triangle. Atomic diffusion of solutes in the liquid phase becomes more complicated in the ternary than in the binary alloys. The build-up of Ti content necessary for the steady state solidification is hardly achieved, which leads to the local fluctuation of the Ti concentration in the liquid phase especially at higher growth rate. This may explains the fact that the volume of liquid phase periodically repeats increasing and decreasing, depending on the Ti content in liquid phase during directional solidification. Therefore, it becomes difficult to maintain the diameter of the DS-ingot at constant. This phenomenon hardly takes place in the binary eutectic alloy. Another rational reason would be that the (Nb)/Nb_5Si_3 eutectic is the facet/non-facet type eutectic reaction so that the kinetics of growth is very much different in each phase. Figure 5-9 shows the quenched microstructures corresponding to the solid/liquid interface in the DS Nb-17.5Si-2Ti ternary alloy and DS Nb-17.5Si binary alloy. Quenching was conducted during directional solidification by turning off the power supply for the lamps of the OFZ furnace. The boundary corresponding to

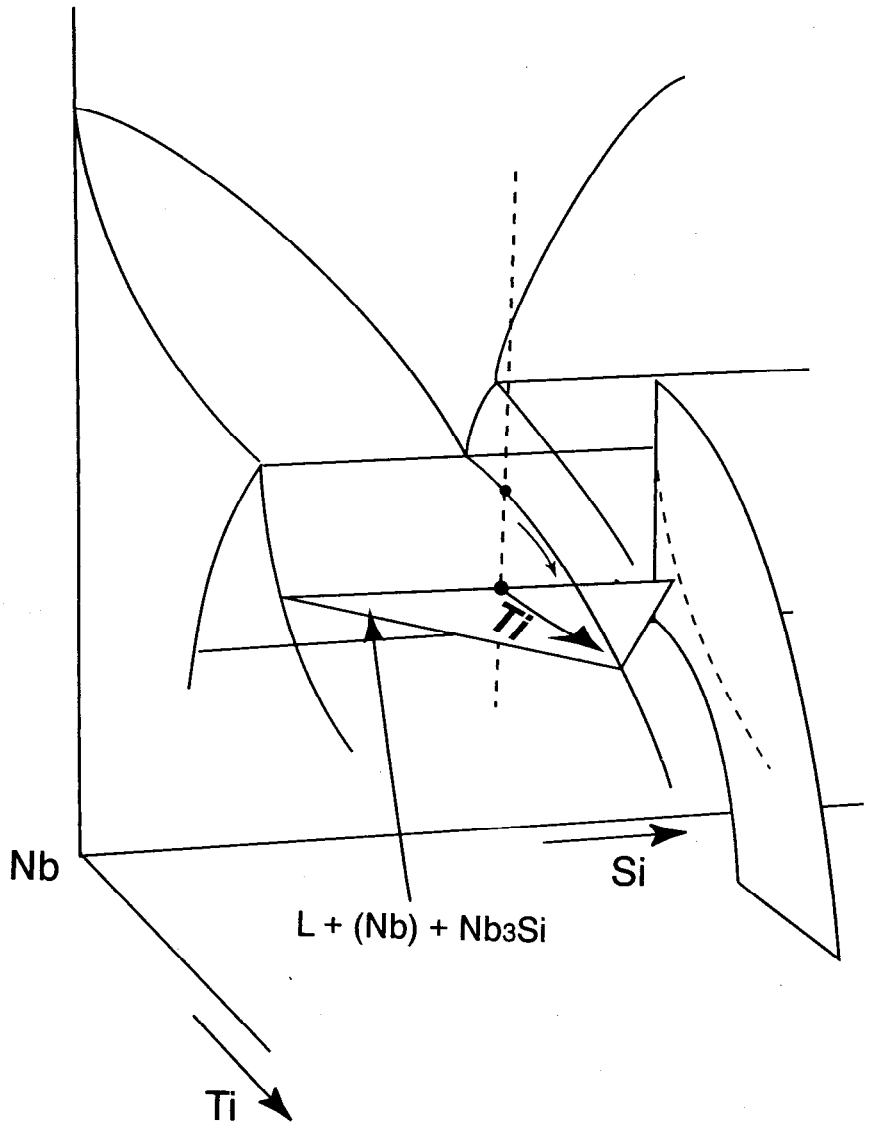

Fig. 5-8 A schematic illustration of the three-phase triangle, (L+Nb_3Si+(Nb)) in the Nb-Si-Ti ternary system.

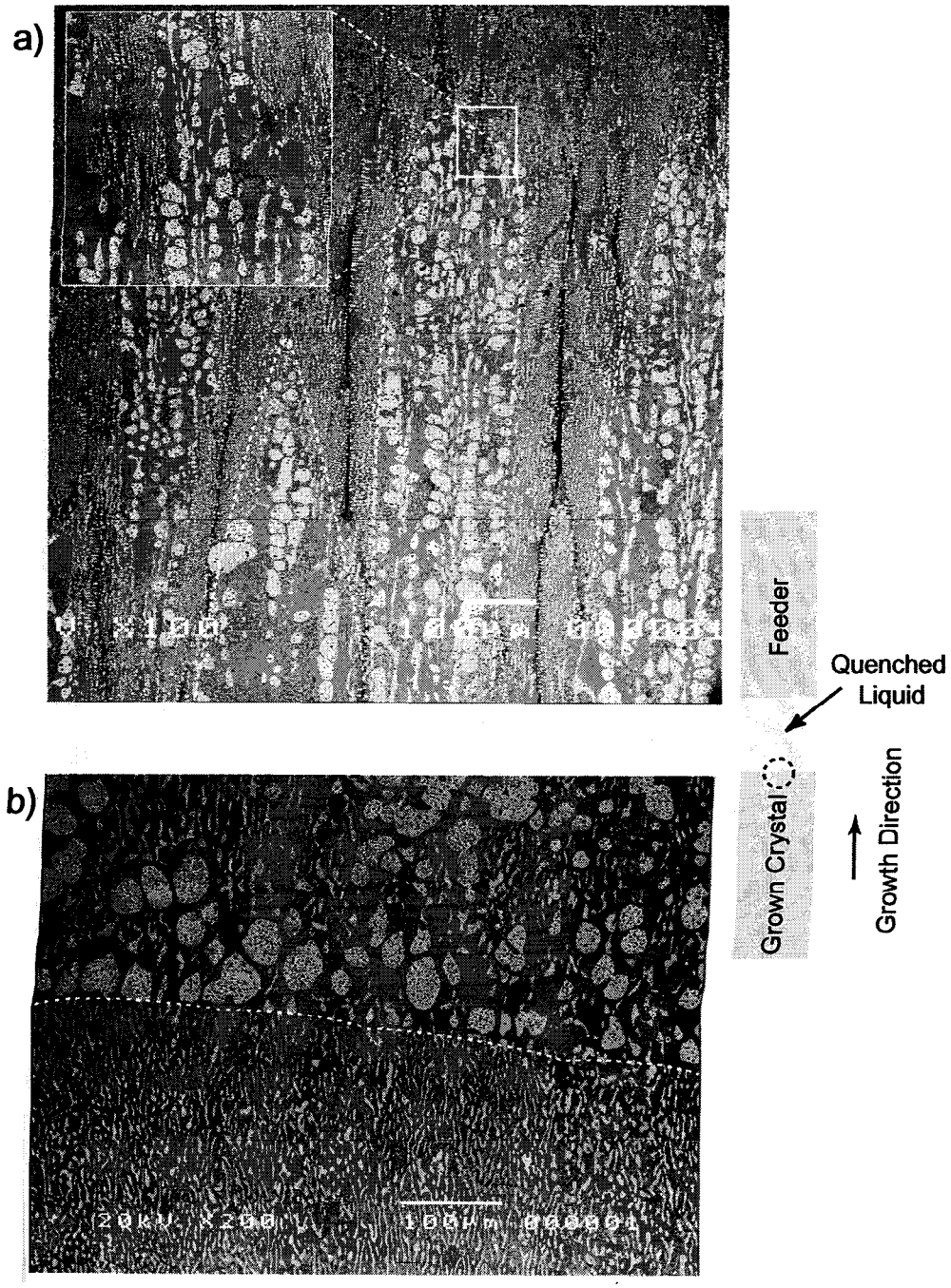

Fig. 5-9 Quenched microstructures showing the moving solid/liquid interface, a) DS Nb-17.5Si-2Ti ternary alloy, and b) DS Nb-17.5Si binary alloy.

the quenched solid/liquid interface is clearly seen in the binary alloy but not in the ternary alloy. The solid/liquid interface is clearly formed in the binary alloy by the fact that the solid and liquid phases are separated since the binary eutectic is an invariant reaction. While the solid and liquid phases coexist thermodynamically stable in the ternary alloy because the "L → (Nb) + Nb_3Si" reaction is a monovariant type. In Fig. 5-9a and b, the fine eutectic-like microstructure region is supposed to correspond to the quenched liquid phase. It is found that the growth of faceted Nb_3Si phase grows leaving the steps on the interface and its growth rate is much faster than the non-faceted (Nb) phase. A large difference in the growth rate of each phase makes it difficult to form the planar front at the solid/liquid interface.

It is reported that a combination of a steep thermal gradient in the liquid phase and the slow growth rate is favorable for the formation of planar front [15,16]. In the (Nb)/Nb_3Si eutectic system, the growth rate of (Nb) phase is much slower than that of Nb_3Si phase. Hence the applied growth rate, i.e. the feeding rate, must be lowered sufficiently slow so that it allows the competitive growth of the (Nb) phase with the Nb_3Si phase to form the planar front. On the other hand, it is reported that the lamellar spacing, λ, formed by the eutectic solidification increases with decreasing the growth rate, R, following the relationship, "$\lambda \propto R^{-0.5}$". Since the formation of coarse lamellar requires the long range diffusion of solute atoms, the feeding rate must be lowered as slow as the growth rate of (Nb) phase which could be the controlling factor of the competitive growth of (Nb) and Nb_3Si phases. Therefore, it is speculated that the feeding rate must be much lower than the lowest employed in the present work, 10 mm/h. Another strategy to successfully form the planar front is to increase the thermal gradient in liquid phase. However, there is an upper limit in the thermal gradient because the liquid phase increases its volume and finally drips off if the local temperature is raised too much as the thermal gradient is only increased by heating. Judging from these aspects, as a consequent, it is much more difficult to obtain well-aligned microstructure in the ternary alloys than in the binary alloys.

3-1-3. Microstructure of the Annealed Alloy

According to the TTT-diagrams shown in Chapter 3 for the (Nb)/Nb_3Si eutectic determined by Bewlay et al. in the Nb-Si binary system and by the present work for the Nb-25Si-10Ti alloy, a sufficient annealing time to complete the decomposition reaction of the Nb_3Si is for 100 h at 1773 K in the binary alloy, and for about 50 h at 1673 K in the ternary

alloy. Figure 5-10 shows microstructures of the DS Nb-17.5Si grown at the rate of 10 mm/h and annealed at 1773 K for 100 and 500 h. Contrary to the prediction from the TTT-diagram, the decomposition is not completed at all even after the annealing for 500 h. It is found that the (Nb)/Nb_5Si_3 lamellar microstructure formed by the eutectoid reaction of Nb_3Si is rarely observed at the center of the alloy, and the decomposition progresses faster in the outer portion than in the center of the ingot. Though it is not clarified why the eutectoid decomposition is much slower in the DS-alloy than in the AM-alloy so far, it is rational that impurities should be greatly reduced by the zone refining effect in directional solidification, and that the eutectoid decomposition rate is somehow enhanced by the inward diffusion of oxygen and/or other impurities during annealing as discussed in Chapter 2. Another possible explanation would be that the stability of the (Nb)/Nb_3Si interface formed in directional solidification should be very high.

Figure 5-11 shows the microstructure of the DS Nb-17.5Si-10Ti alloy annealed at 1773 K for 100 and 500 h. The decomposition of Nb_3Si is kinetically slower in the ternary DS-alloy than that in the alloy prepared by arc-melting. In addition, the decomposition progresses faster in the outer portion than in the center of the ingot in the ternary DS-alloy as well as the binary DS-alloy. The Ti content is speculated to be higher in the center than in the outer portion of the ingot since the Ti addition is known to stabilize the Nb_3Si phase and hence to lower the eutectoid temperature. However the segregation of Ti atoms is not observed by the EPMA in the center of the ingot. It should be noted that the impurity contamination has an effect on the kinetics of decomposition reaction of Nb_3Si. On the other hand, the high temperature phase Nb_3Si completely decomposes by the annealing for 500 h in DS Nb-17.5Si-10Ti alloy. The average lamellar spacing of the alloy is measured as about 0.7~0.8 μm, which shows a good agreement with that of the Nb-20Si-10Ti alloy annealed at the same temperature as described in Chapter 3.

3-2. Quantitative Microstructural Analyses

3-2-1. Variation in the Cell Size

The planar eutectic microstructure is produced at the growth rate of 10 mm/h in the DS Nb-17.5Si alloy, though most of the alloys show cellular microstructures at the growth rates over 30 mm/h. The formation of cells and dendrites occurs due to the perturbations at the liquid-solid interface during solidification, thereby resulting in a non-planar interface [17].

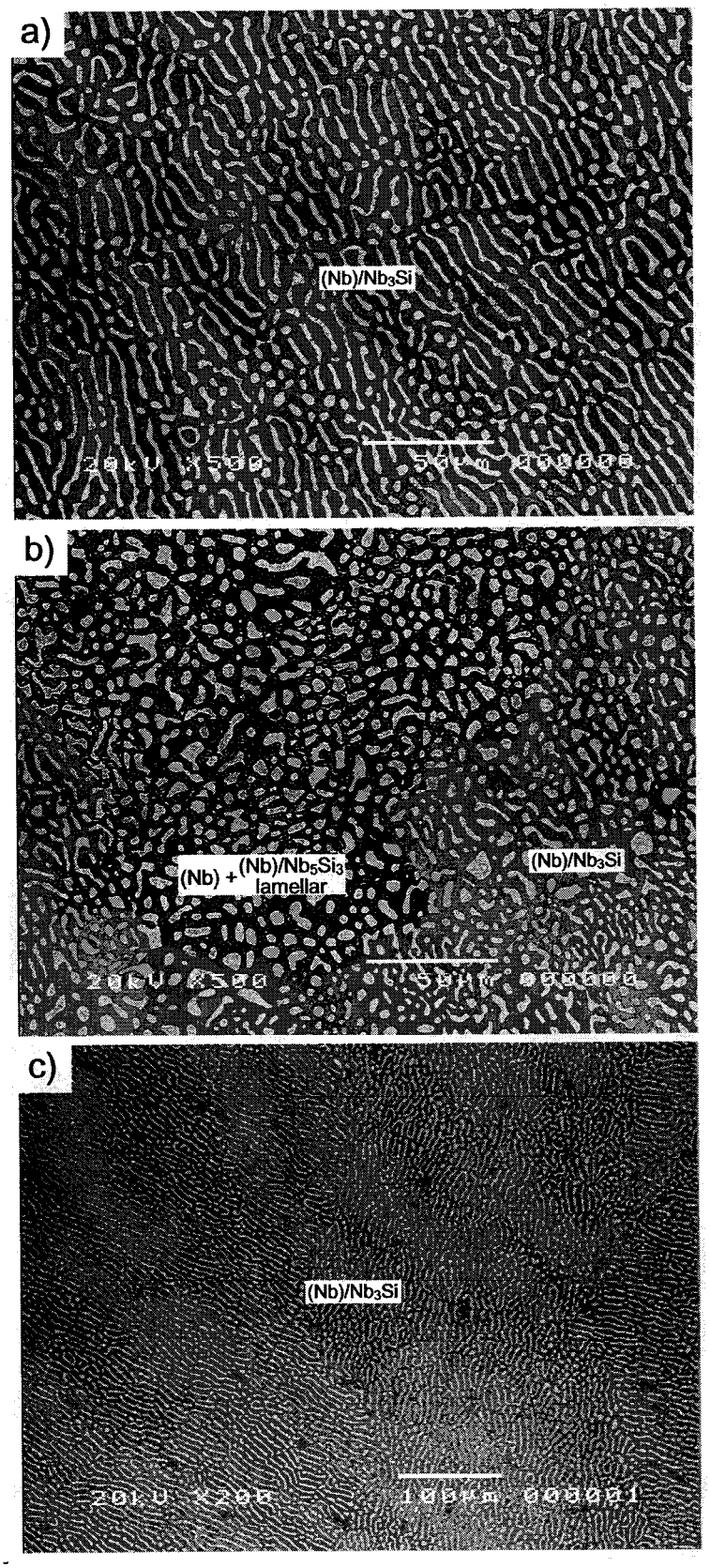

Fig. 5-10 Microstructures of the DS-Nb17.5Si alloy grown at the rate of 10 mm/h followed by annealing at 1773 K for a) 100 h (center portion of DS ingot), b) 100 h (outer portion), and c) 500h (center portion).

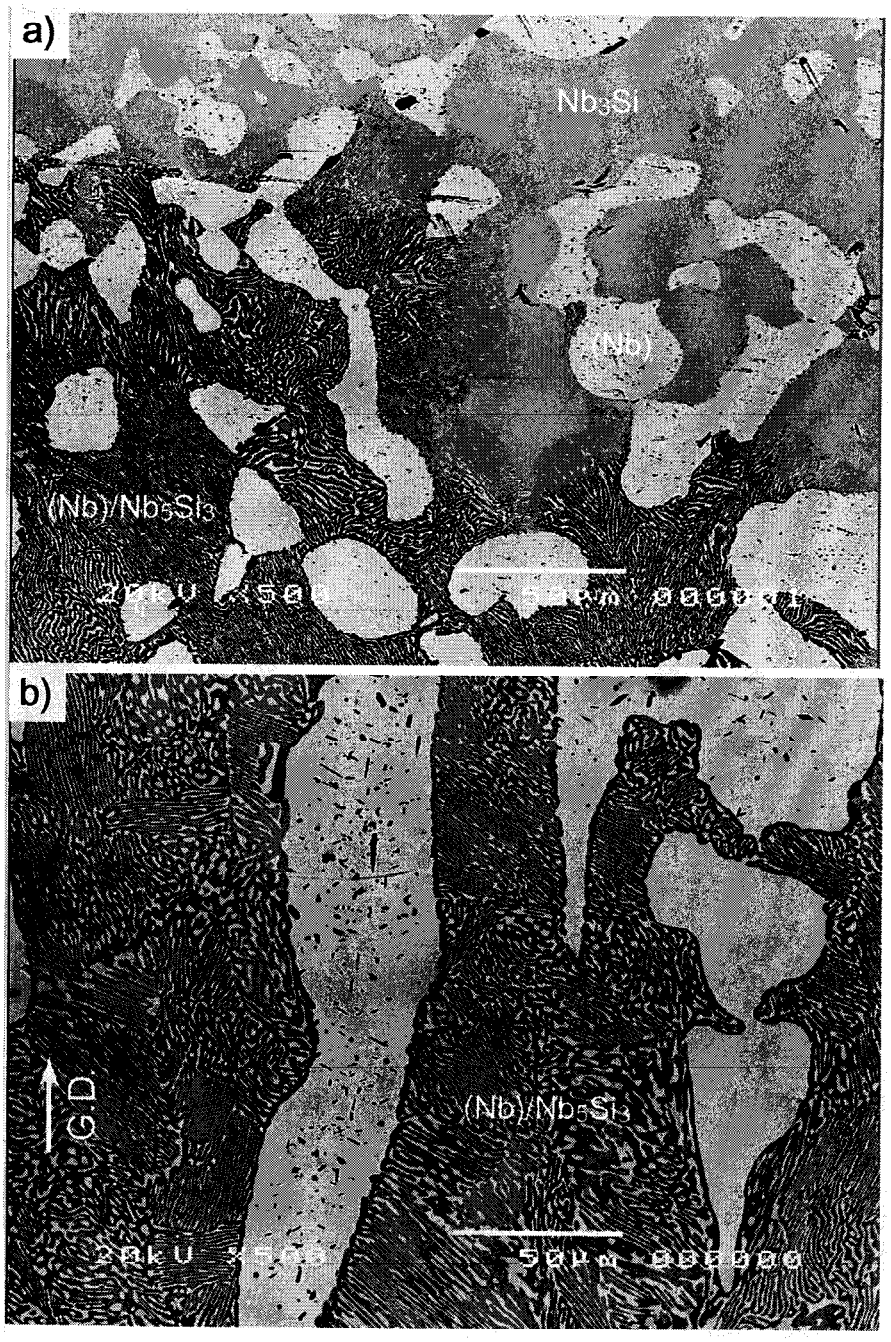

Fig. 5-11 Microstructure of the DS-Nb17.5Si-10Ti alloy grown at the rate of 10 mm/h followed by annealing at 1673 K for a) 100 h (transverse section), and b) 500 h (longitudinal section).

Figure 5-12 shows a schematic illustration of the cellular front formed at the solid/liquid interface. As the growth rate, i.e. the feeding rate of the directional solidification, increases, a planar front gradually becomes unstable and it gently changes to a undulatory front. Finally, a non-planar front is formed by the development of protrusions. The intercellular region solidifies later than the cell body, and the coarse eutectic microstructure forms inclined (or perpendicular) to the feeding axis in the intercellular region. As a result, the breakdown of the aligned eutectic microstructure is observed at the cell boundaries in the cross sectional area perpendicular to the feeding axis.

Microstructural observation also revealed that a cell size varies with the growth rate. Figure 5-13 shows a typical distribution of the cell size measured in the Nb-17.5Si binary alloy comparing the growth rate; R = 10, 30, 100, and 200 mm/h, where population size is between 120 and 180. It is evident that the cell size follows the near-Gaussian distribution for each growth rate, although it exhibits a tendency slightly narrow in the side of smaller cell size. The measurements of the cell size for the Nb-17.5Si-2Ti and Nb-17.5Si-5Ti ternary alloys show the similar tendency in the distribution of the cell size. Figure 5-14 shows a full logarithmic plot of the average cell size against the growth rate. The cell size increases with decreasing in the growth rate. It has been reported that the primary dendrite arm or the cell spacing is proportional to the $R^{-0.25}\ G^{-0.5}$, where R is the growth rate and G is the thermal gradient in the liquid phase [18]. However, it seems difficult to figured out any correlations among the cell size, growth rate, and alloy composition in Fig. 5-14. One of the reasons is that the thermal gradient in the liquid phase can not be controlled in the OFZ melting method. The diameter of the directionally solidified sample and the volume of melting zone determined by the width and height are kept constant at each growth rate during the directional solidification, but the thermal gradient is uncontrollable condition depending on halogen lamp power at each growth rate. It is very much complicated business to find the concrete correlations among a diameter of grown sample, a size of melting zone, and other physical properties such as a thermal diffusivity and melting point. In addition, the complexity of atomic diffusion in a multi-component system makes it more complicated to analyze the relationship among DS conditions and other factors. In this sense, the relation for the cell spacing to be proportional to the $R^{-0.25}\ G^{-0.5}$ is not necessarily applied to the present ternary alloys [14,19,20]. Further experimental data are required to achieve the basis of the microstructural control in the floating zone melting method.

Figure 5-14 shows interesting results that the cell size seems to become constant at slower

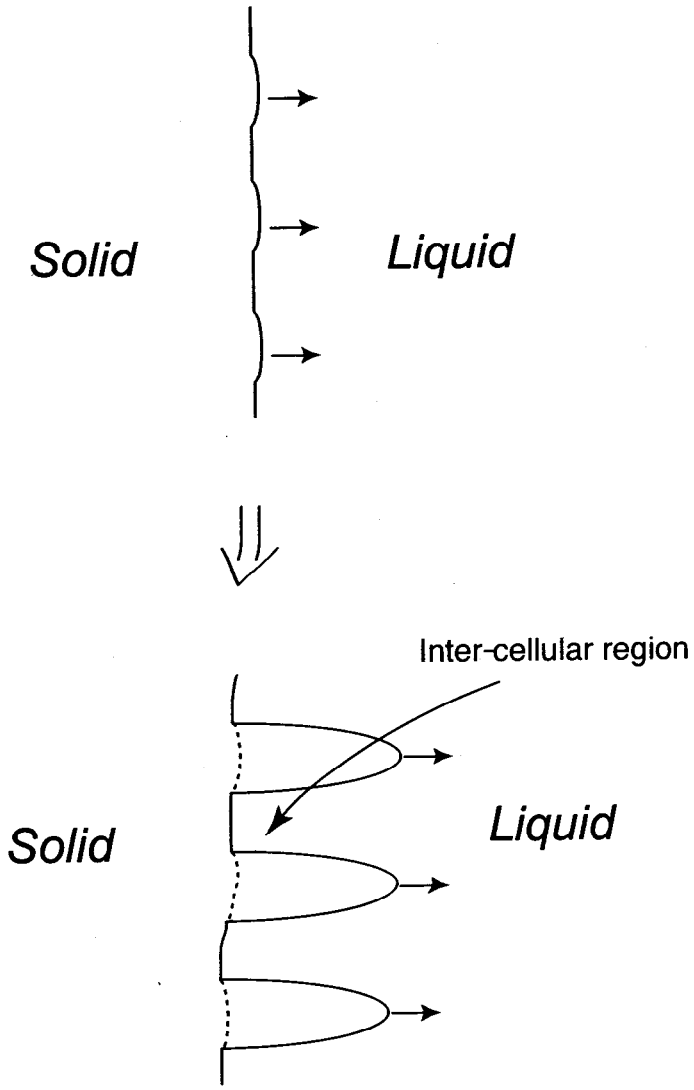

Fig. 5-12 A schematic illustration of the cellular front formation at the solid/liquid interface.

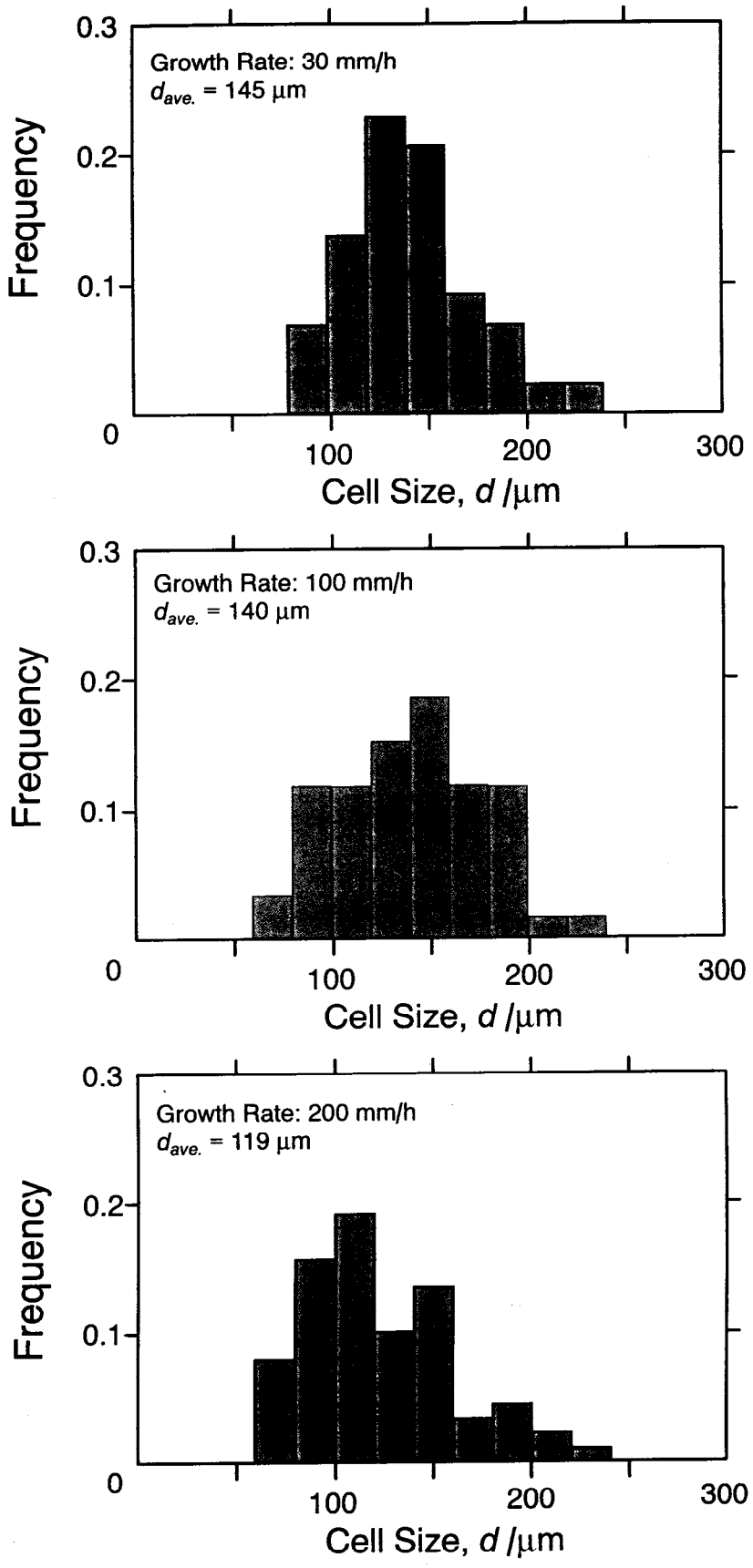

Fig. 5-13 Distribution of cell size measured in the Nb-17.5Si binary alloy comparing the growth rate; R = 30, 100, and 200 mm/h.

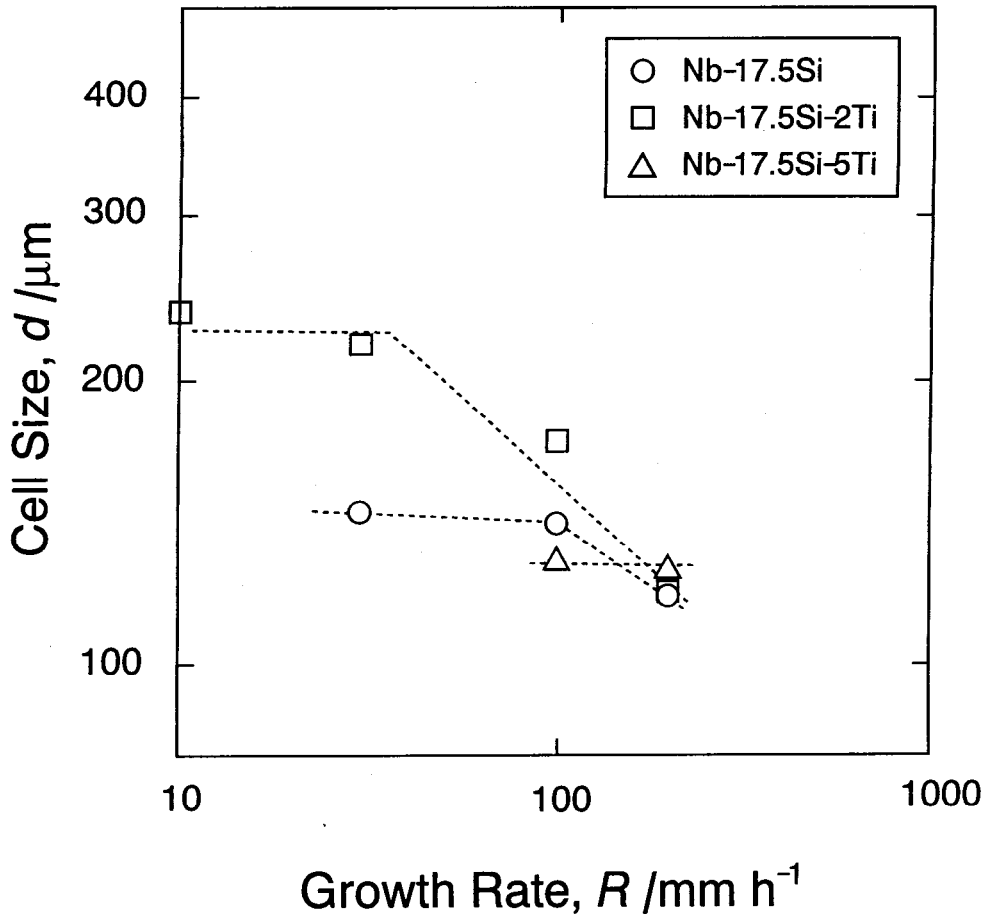

Fig. 5-14 *A full logarithmic plot of the average cell size against the growth rate.*

growth rate than the threshold rate; about 100 mm/h in the Nb-17.5Si alloy, 30 mm/h in the Nb-17.5Si-2Ti, and 200 mm/h in the Nb-17.5Si-5Ti. Under the assumption that there exists the threshold growth rate giving the constant cell size [20], and using the data at the growth rate of 100 and 200 mm/h in the Nb-17.5Si alloy, and those at the growth rate of 30 , 100, and 200 mm/h in the Nb-17.5Si-2Ti alloy, the slopes of the regression lines are close to the value of -0.25($d \propto R^{-0.25} G^{-0.5}$).

3-2-2. Variation in the Size of (Nb) Phase

Microstructural observation also reveals that the size of (Nb) phase increases with decreasing the growth rate. It is well-known that the average lamellar spacing is proportional to the reciprocal of the square root of growth rate in the eutectic lamellar growth [14]. In the present work, however, the planar front is formed only in the Nb-17.5Si alloy at the growth rate of 10 mm/h, and the cellular front is formed in other alloys resulting a discontinuous morphology of the (Nb) phase in a cellular structure. In these alloys, the size of (Nb) phase is widely distributed because of the breakdown in the morphology of eutectic microstructure at the cell boundaries. The dependence of growth rate on interlamellar spacing is strongly affected by the morphology of the solid/liquid interface, whether it is a planar or cellular type. Therefore, measurements of the size of (Nb) phase were conducted only on the DS Nb-17.5Si and DS Nb-17.5Si-10Ti alloys with the growth rate of 10 mm/h. The objective of this measurement is mainly to estimate the fracture toughness increment by calculation using the model based on the crack bridging of ductile (Nb) phase, which is discussed in the later section.

It is found from microstructural observations in the Nb-17.5Si alloy that the (Nb) phase is characterized to have a rod and/or plate type morphology. In the present work it is assumed that the (Nb) phase rod/plate has an ellipse morphology in the cross section perpendicular to the growth axis, as shown in Fig. 5-15a, and the major axis and minor axis were measured for a statistic consideration. In addition, the inter-phase distance, which is defined by the distance between the center of the adjacent ellipses, was also measured for sampling. Figures 5-15b, c, and d show the distribution of each measured value, where the sampling size is between 120 and 200. It is evident that the length of minor axis and inter-particle distance follow the near Gaussian distribution, exhibiting a relatively sharp peak. However the length of the major axis shows a broad distribution having a bimodal or trimodal type. It indicates that the occurrence of branching or coalescence of growing (Nb) plates provides a certain multi-modal distribution.

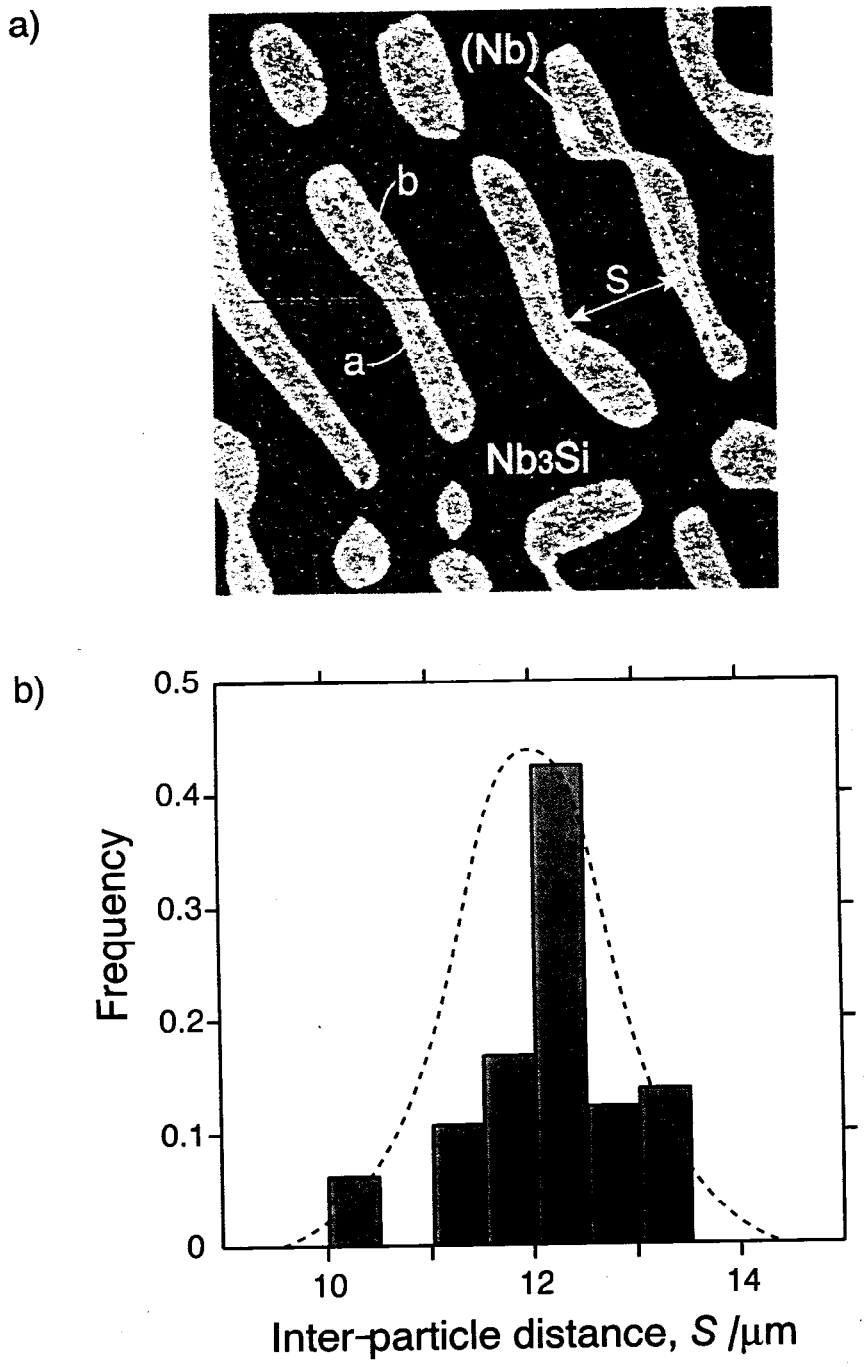

Fig. 5-15 a) A representive microstructure of the DS-Nb17.5Si alloy grown at 10 mm/h in the cross section perpendicular to the growth axis, and the results of image analysis on the distribution of b) inter-particle distance, c) major axis, and d) minor axis.

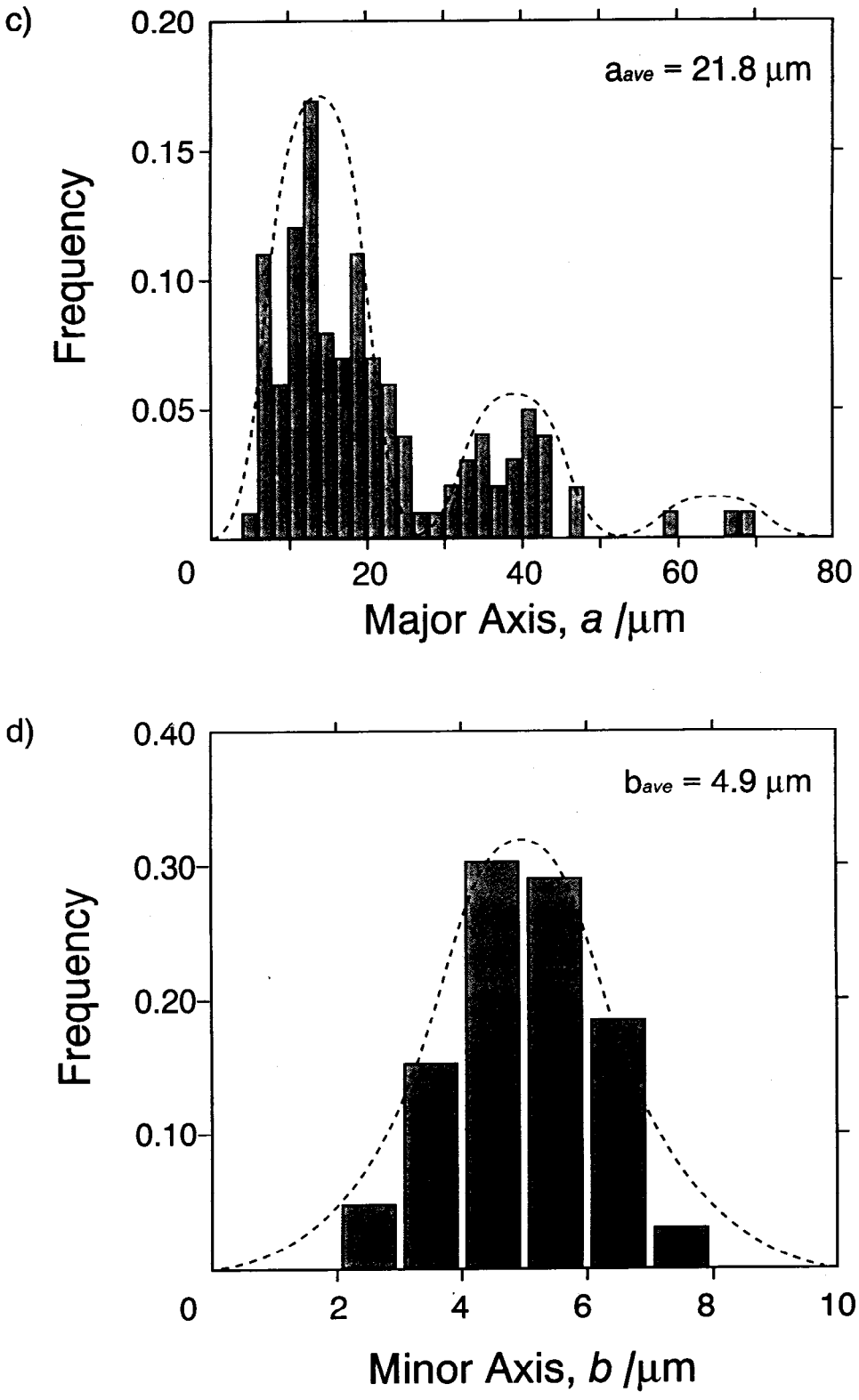

Fig. 5-15 Continued.

Figure 5-16 shows the distribution of the size of (Nb) phase sampled in the DS Nb-17.5Si-10Ti alloy grown at 10 mm/h. A rough approximation was conducted for measuring the average size of (Nb) phase in the microstructure of this alloy shown in Fig. 5-7. The intersected area of (Nb) phase is measured using an image analyzer. The size of the (Nb) phase is defined as the calculated diameter of a circle having the same area of the measured (Nb) phase by an image analyzer. It is difficult to judge from Fig.5-16 whether the type of distribution is asymmetric or bimodal. The average size of (Nb) phase in the Nb-17.5Si-10Ti alloy is 25 μm, which is much larger than that in the Nb-17.5Si binary alloy.

3-3. Mechanical Properties

3-3-1. Fracture Toughness and Crack Propagation Behavior

The chevron-notch fracture toughness measurement was conducted to evaluate the room temperature toughness of the DS alloys. The loading axis of the bending test is perpendicular to the aligned direction of the discontinuous (Nb) phase. The chevron notch fracture toughness, K_Q, calculated from the maximum load, P_{max}, using the Bluhm's slice model [21] is summarized in Table 5-2. The fracture toughness of the Nb-Si binary alloys reported by Bewlay et al. [1] is also shown for a comparison. Hereafter, the alloys are represented by using a simple threefold notation including alloy composition, growth rate and heat treatment condition, as listed in Table 5-2. The fracture toughness is greatly improved in the DS alloys as compared with the cast alloys prepared by arc melting. The (Nb)/Nb_3Si two-phase B10AG and B100AG alloys show the excellent K_Q values of 14.5 and 9.9 MPa $m^{1/2}$ respectively, while the K_Q of the (Nb)/Nb_5Si_3 two-phase Nb-18.7Si alloy is 3.4 MPa $m^{1/2}$ (as shown in Chapter 2), in spite of the fact that the volume fraction of (Nb) phase is twice as higher in the Nb-18.7Si alloy as in the other two. Annealing for the decomposition of the Nb_3Si phase is conducted on the Nb-18.7Si alloy. It is noteworthy that the fracture toughness of 14.5 MPa $m^{1/2}$ obtained in the B10AG alloy is comparable to that of the Nb-10Si alloy [1], though the volume fraction of the ductile (Nb) phase in the former alloy is only a half of that in the latter alloy.

It has been revealed that the directional solidification is effective to improve the room temperature fracture toughness of the Nb-Si-Ti ternary alloys as well as the Nb-Si binary alloys. It is found in both the binary and ternary alloys that the fracture toughness value increases with decreasing the growth rate of directional solidification. Moreover, annealing for the

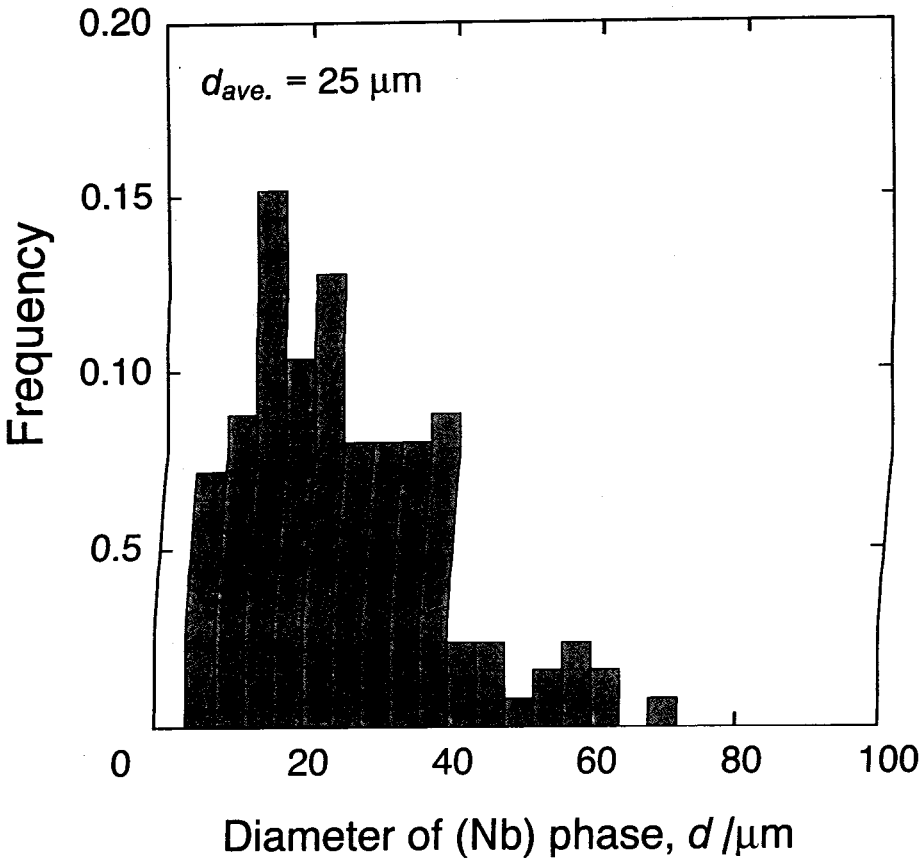

Fig. 5-16 A distribution of the size of (Nb) phase in the DS-Nb17.5Si10Ti alloy grown at 10 mm/h.

Table 5-2 Summary of the chevron-notch fracture toughness, K_Q.

Alloy	Composition	Process / annealing	Constituent Phases	K_Q (MPa$\sqrt{m}$)
	* Nb-10Si	DS (300mm/h ?)	(Nb) Nb_3Si	*14.2 ± 0.5
B10AG	Nb-17.5Si	DS-10mm/h	(Nb) Nb_3Si	14.5
B100AG	Nb-17.5Si	DS-100mm/h	(Nb) Nb_3Si	9.9
	* Nb-18Si	DS (300mm/h ?)	(Nb) Nb_3Si	*5.8 ± 0.5
	Nb-18.7Si	AM 1673 K / 100 h	(Nb) Nb_5Si_3	3.4
T10AG	Nb-17.5Si-10Ti	DS-10mm/h	(Nb) Nb_3Si	15.4
T10H	Nb-17.5Si-10Ti	DS-10mm/h 1673 K / 500 h	(Nb) Nb_5Si_3	18.7
T100AG	Nb-17.5Si-10Ti	DS-100mm/h	(Nb) Nb_3Si	9.8
T100H	Nb-17.5Si-10Ti	DS-100mm/h 1673 K / 500 h	(Nb) Nb_5Si_3	16.0
	Nb-18.7Si-10Ti	AM 2023 K /100 h 1673 K / 100 h	(Nb) Nb_5Si_3	11.8

*: Bewlay et al., 1995 [1]

B ··· Binary alloy (Nb-17.5Si)
T ··· Ternary alloy (Nb-17.5Si-10Ti)
AG ··· As-Grown
H ··· Heat treated to decompose Nb_3Si

decomposition of the Nb_3Si phase into the (Nb)/Nb_5Si_3 lamellar structure is effective to enhance the toughness of the alloy, especially in the T100H alloy. It must be emphasized that the T10H alloy exhibits the highest fracture toughness value of 18.7 MPa $m^{1/2}$ among all the alloys tested in the present work. Microstructure of the T10H alloy is characterized by the discontinuous coarse (Nb) phase aligned parallel to the growth direction and the rest of microstructure is covered with the randomly oriented (Nb)/Nb_5Si_3 lamellar.

Figure 5-17 shows fractographs of the B10AG and T10H alloys. The (Nb) phase exhibits plastic stretching and necking to a chisel point in the B10AG alloy and a small amount of interface debonding is observed. These results indicate that the crack bridging by ductile (Nb) phase is the main contribution to toughening mechanism in this alloy. Nevertheless, the effect of crack bridging is rather small because the thickness of (Nb) phase is very thin. The flat fracture surface corresponds to the straight crack propagation path, and the morphology is dominated by cleavage fracture of the brittle Nb_3Si and/or Nb_5Si_3 phase, as seen in the fractograph. In the T10H alloy, the fractograph is distinguished by the brittle cleavage fracture of the Nb_5Si_3 phase and the ductile fracture relief of (Nb) phase showing the micro-void coalescence and the occasional interface decohesion. The fracture surface is intensively waved corresponding to the crack deflection. Fine (Nb) phase of the lamellar microstructure exhibits plastic stretching and necking to a chisel point. These observations suggest that the work of fracture is derived from the sum of ductile fracture in the (Nb) phase and microcracking and cleavage fracture in the Nb_3Si and/or Nb_5Si_3 phases.

Figure 5-18 shows the crack propagation behavior of the B10AG, T10AG and T10H alloys in bending test using straight notched specimens. As mentioned in the previous chapter, straight notched specimen is more suitable for the observation of the crack propagation path. It is quite difficult to observe the crack propagation path, restricted to the area vicinity of the notch, in chevron notched specimen. It is found in the B10AG alloy that cracks generated from notch root propagate straightly, and the (Nb) phase is sometimes pulled out from the matrix due to the occasional interface decohesion. In the T10AG and T10H alloys, cracks generated from notch root are deflected by the coarse (Nb) phase, and mainly propagate in the brittle Nb_3Si phase or the (Nb)/Nb_5Si_3 lamellar region.

Ashby et al. have proposed the theory based on crack bridging mechanism by a ductile phase, that describes the fracture of composites consisting of brittle and ductile phases in a model system comprised of lead wires constrained by glass [22]. According to their theory, the

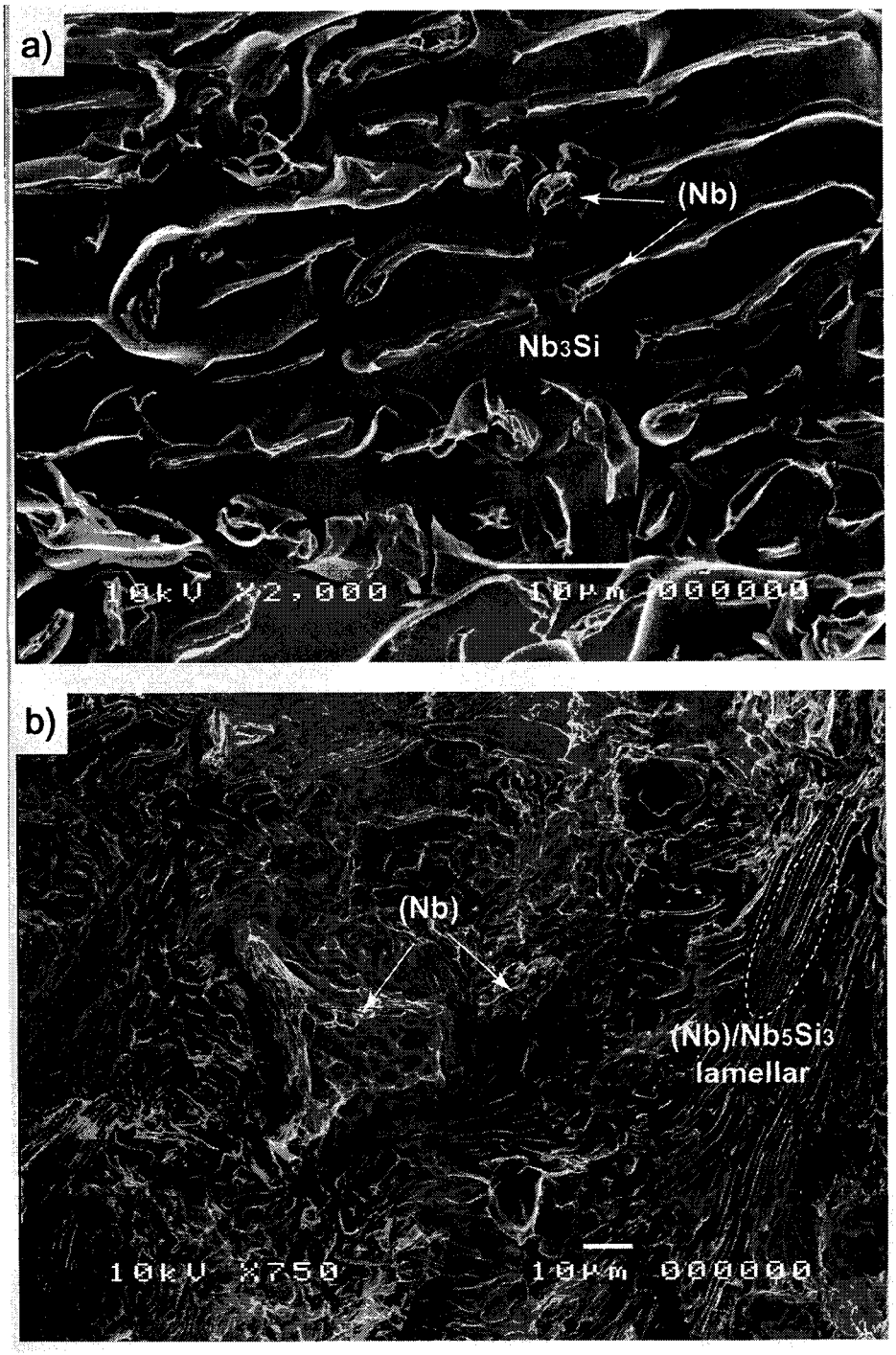

Fig. 5-17 Fractographs of alloys at directionally solidified at the growth rate of 10 mm/h, a) as-grown Nb17.5Si (B10AG), and b) Nb-17.5Si-10Ti annealed at 1673K for 500h (T10H) after DS.

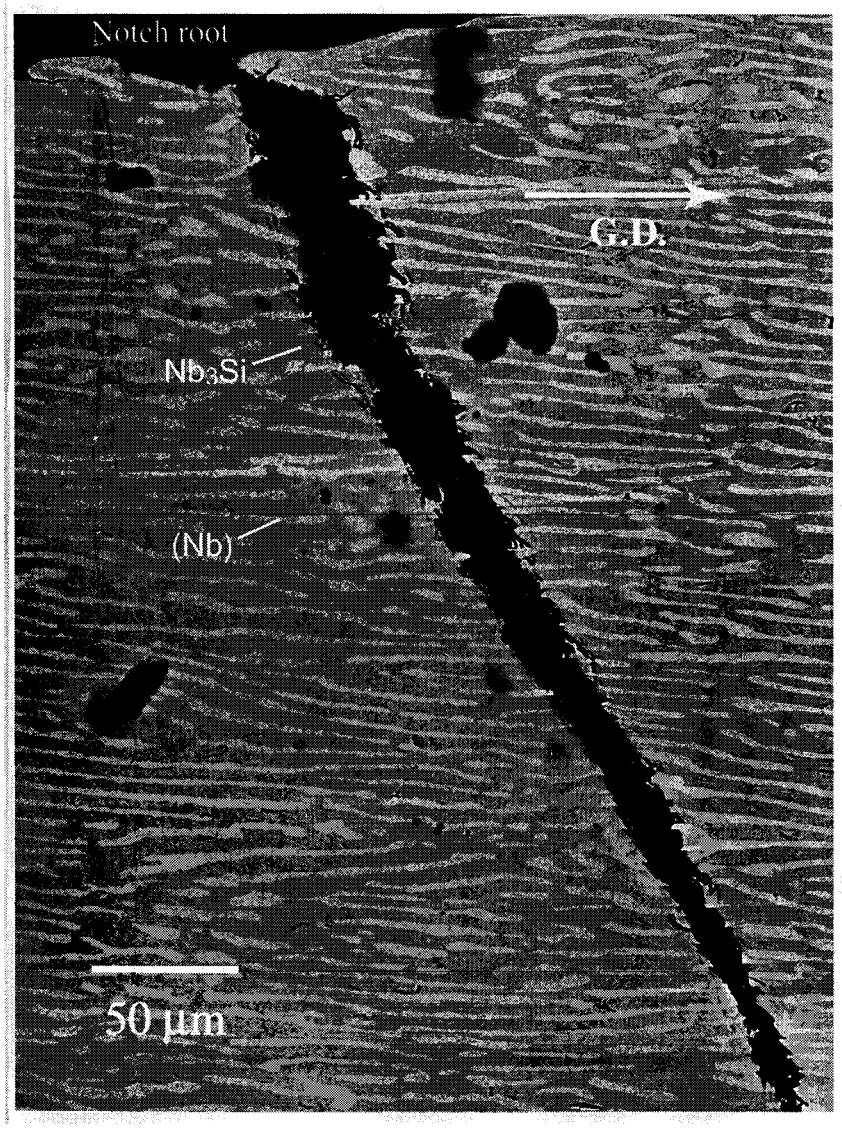

Fig.5-18 Crack path after the straight notch bend test of alloys directionally solidified at a growth rate of 10mm/h, a) B10AG, b) T10AG, and c) T10H.

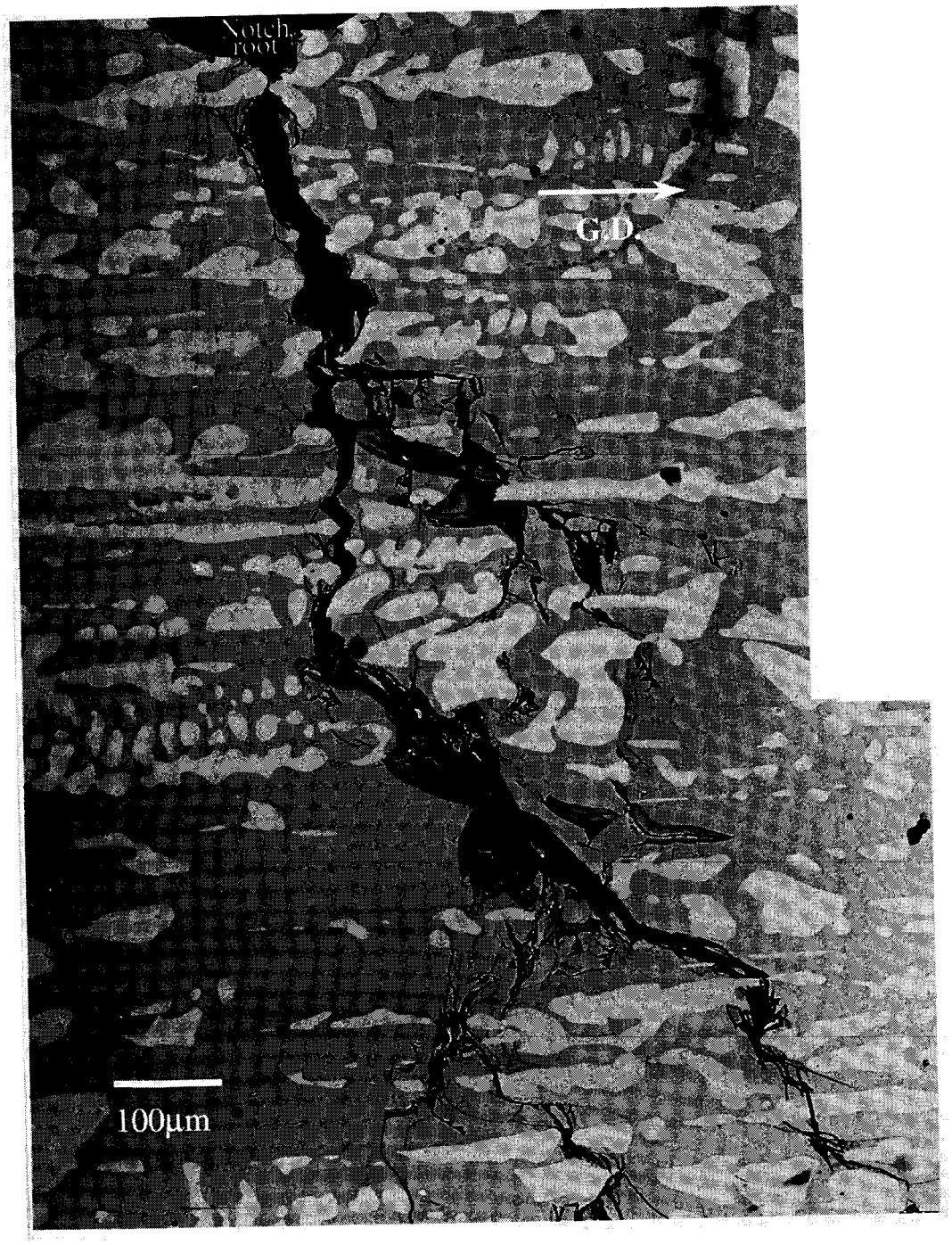

Fig. 5-18 Continued.

Fig. 5-18 Continued.

work of fracture, contributed by crack bridging of ductile particles in the composite, depends on the square root of the size and the volume fraction of the ductile particles, V_f, and depends inversely on the degree of constraint. The toughness increment over that of the matrix, ΔK, can be described by

$$\Delta K = E\sqrt{\frac{CV_f\sigma_0 a_0}{E}} \qquad (1)$$

where E, σ_0, and a_0 are Young's modulus, uniaxial tensile yield strength and the radius of ductile particles, respectively. The parameter C denotes the reciprocal of the degree of constraint imposed on the ductile particle by the surrounding elastic matrix. Here, C is taken as 1.6 according to the analysis by Ashby et al. [22] for the case where interface decohesion is not involved. This equation can be used to estimate the fracture toughness increment in the case of B10AG and T10AG alloy. For this calculation, the physical data used are summarized in Table 5-3, where the value of E is taken from the published data [23], V_f and a_0 are from the present results shown in the previous section, and σ_0 is estimated from measured hardness value of Nb-1Si and Nb-1Si-10Ti shown in Chapter 2 using the relation: $\sigma_0 = 2.4 \times Hv$ (MPa) [24]. The calculated value of fracture toughness increment, 13.8 MPa $m^{1/2}$, in the B10AG alloy shows a good agreement with measured value, considering that fracture toughness of the silicide is reported as 1~3 MPa $m^{1/2}$ [25,26]. However the calculated value for the T10AG alloy, 19.3 MPa $m^{1/2}$, is higher than that of the measured value, 15.4 MPa $m^{1/2}$. Together with the observation of crack propagation behavior, it is concluded that the crack deflection, not bridging, dominates in the T10AG alloy. In general, the crack bridging would be more effective on toughening than the crack deflection.

The reason that the fracture toughness increases with decreasing the growth rate, the feeding rate of directional solidification, is explained from a viewpoint of the alignment of ductile (Nb) phase. The slower the growth rate becomes, the more homogeneous alignment is achieved for the (Nb) phase. Accordingly, the crack propagation is much more frequently prohibited by bridging of the (Nb) phase. Further improvement in the fracture toughness of the ternary alloys can be achieved by the microstructural control, especially the morphology of (Nb) phase in respect of thickness and distribution. For this purpose, it is necessary to lower the feeding rate of the DS down to a level that allows the continuous growth of the (Nb) phase. In

Table 5-3 Parameters used for the calculation of toughness increment based on the equation (1).

Parameter	B10AG	T10AG
Volume Fraction, *f*	0.34	0.34
Size of Ductile Phase, $2a_0$	10 μm [i)]	25 μm
Yield Stress, σ_0	670 MPa [ii)]	520 MPa [ii)]
Elastic Moduli *E*	105 GPa [23]	105 GPa [23]
Calculated Kc	13.8 MPa$\sqrt{m}$	19.3 MPa$\sqrt{m}$
Experimental K_Q	14.5 MPa$\sqrt{m}$	15.4 MPa$\sqrt{m}$

i) $a_0 = (a \times b)^{0.5}$ *(see in Fig. 5-15)*

ii) $\sigma_0 = 2.4 \times Hv$ *(MPa) [24]*

addition, the size of ductile phase increases as the growth rate becomes slower, which results in the enhancement of fracture toughness of the alloy.

3-3-2. Compressive Mechanical Behavior

To investigate the compressive mechanical behavior of the DS-alloys, compression tests were conducted at room temperature and at elevated temperatures ranging from 1273 K to 1673 K. The stress-strain curves obtained from compression tests at room temperature are shown in Fig. 5-19. The as-DS-alloys fails in the elastic region showing no compressive plastic deformation at room temperature. A few percent of compressive plastic strain before fracture can be seen in the T10H and T100H alloys. Microstructure of both alloys consists of (Nb)/Nb_5Si_3 lamellar and are the only ones which have the compressive plastic deformability. It would indicate that the (Nb) lamellar plates are effective to prevent micro-crack propagation during a compression test.

Figure 5-20 shows the compressive stress-plastic strain curves obtained from the tests at 1273 K, 1473 K, and 1673 K. All the alloys show excellent compressive deformability of more than 10% plastic strain at temperatures over 1473 K. The plastic deformability of B10AG alloy seems to be rather low in which relatively large cracks are generated during the test even at 1673 K. The T10H and T100H alloys exhibit good compressive ductility at 1673 K, at least over 10 % plastic strain, without any visible cracks on the surface of specimens. Temperature dependence of the compressive 0.2% flow stress of the present alloys is summarized in Fig. 5-21. The hatched area shows the range of strength of the Nb-20Si-10Ti alloys with different heat treatment conditions, which has been shown in Chapter 3. The B10AG alloy shows excellent high strength at elevated temperatures, 580 MPa at 1673 K. There are three reasons of the excellent elevated temperature strength of the B10AG alloy. The first is that the volume fraction of silicide phases, Nb_5Si_3 and Nb_3Si, is much higher than the other alloys because annealing for the decomposition of Nb_3Si is not conducted on the alloy. The second is that the strength of (Nb) phase in the binary alloy is much higher than that in the ternary alloy, which has been discussed in Chapter 2. Finally, continuous (Nb) plates are aligned parallel to the growth direction in the Nb_3Si matrix. Considering that the B10AG alloy shows the moderate fracture toughness of 14.5 MPa $m^{1/2}$ at room temperature, this alloy would be very promising for high temperature structural application.

The T10H and T100H alloys show superior strength to the Nb-20Si-10Ti alloys fabricated

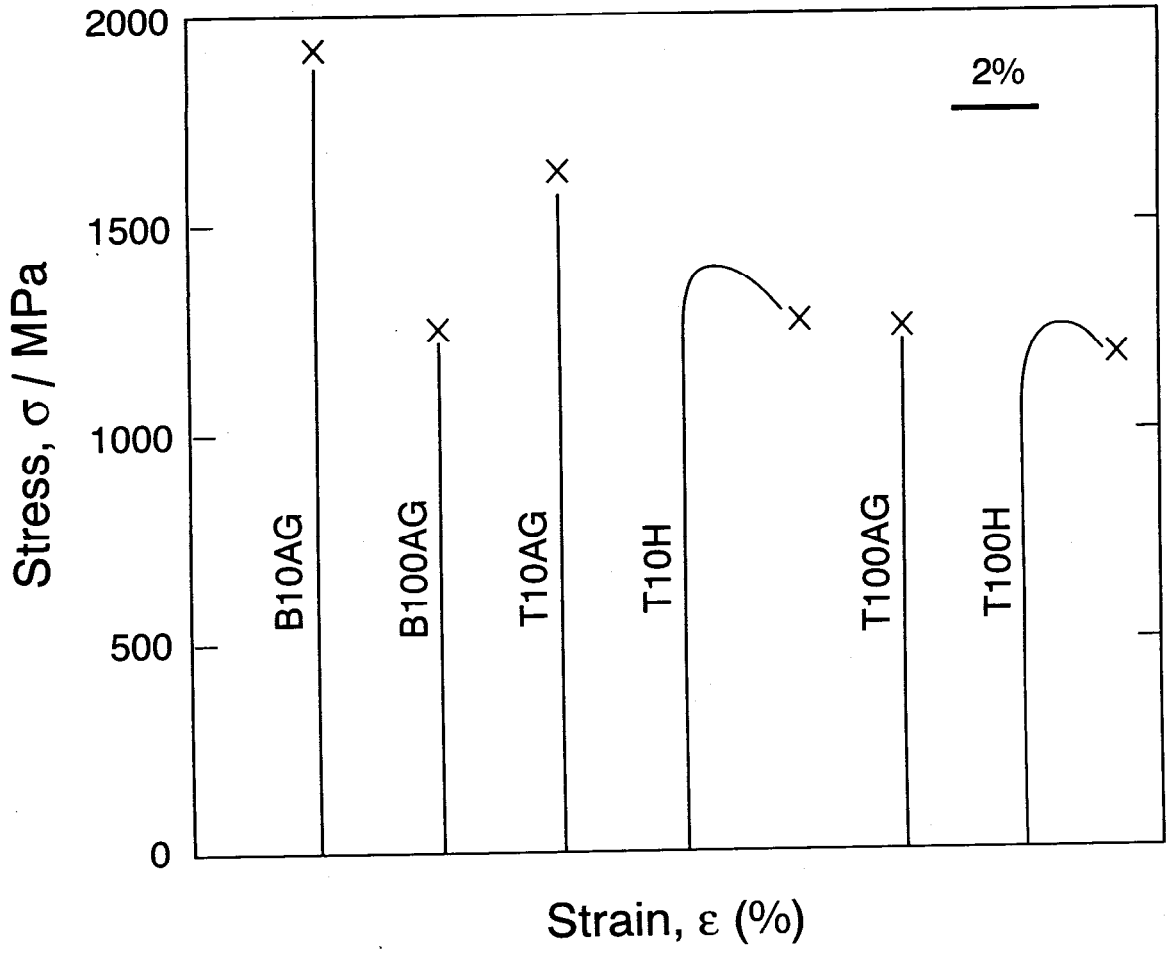

Fig. 5-19 Compressive stress-strain curves of DS-alloys tested at room temperature.

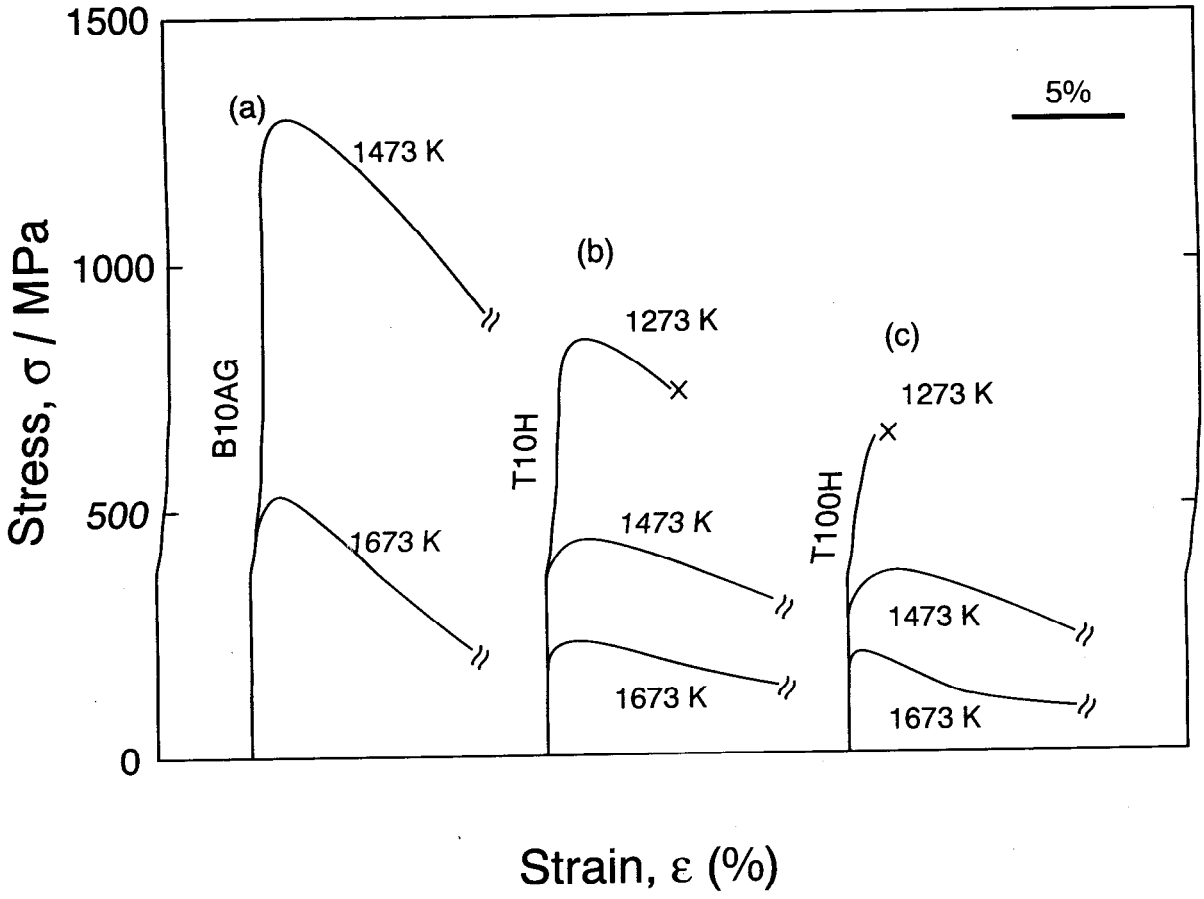

Fig. 5-20 Compressive stress-strain curves of the DS alloys tested at 1273, 1473 and 1673 K; a) B10AG, b) T10H, and c) T100H.

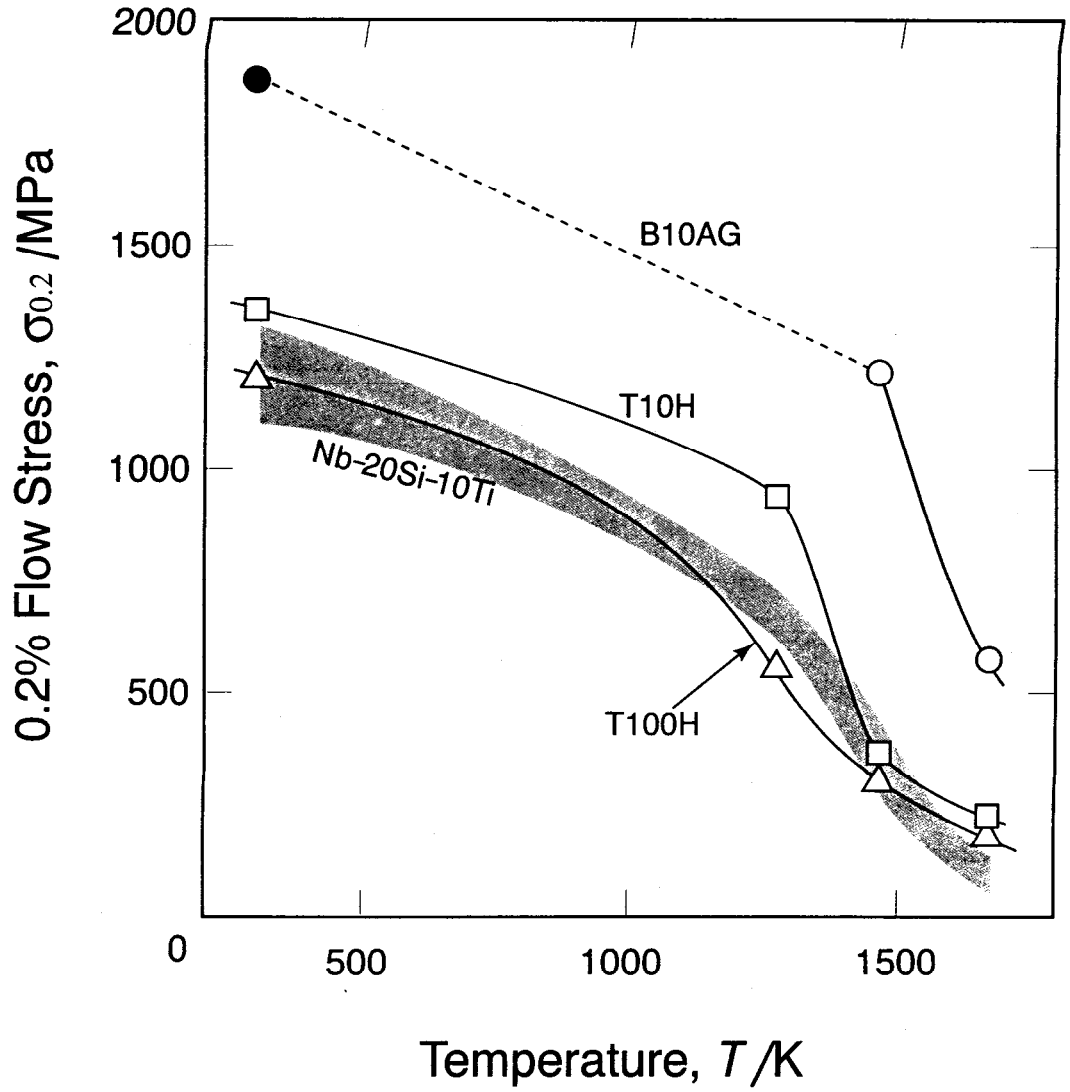

Fig. 5-21 Temperature dependence of compressive 0.2% flow stress of DS alloys. The hatched area shows the range in strength of the Nb-20Si-10Ti alloys with different heat treatment conditions.

by arc-melting AM-alloys. However, strength of the ternary alloy drops drastically at temperatures over 1427 K, and the strength at 1673 K of the alloys are comparable to that of the AM-alloys. As mentioned in Chapter 3, the major deformation mechanism of the AM-alloys is interfacial slip at the (Nb)/Nb_5Si_3 lamellar colony boundaries. Lamellar microstructure is effective to improve the room temperature toughness and compression deformability, however a large amount of interfaces, at which interfacial slips operate at elevated temperature, is introduced by the eutectic reaction.

4. CONCLUSIONS

Directional solidification technique was applied to the (Nb)/Nb_3Si eutectic alloys in the Nb-Si binary and Nb-Si-Ti ternary systems. The basis of microstructural control by directional solidification is established regarding the effect of growth rate on microstructures. It is found that the degree of alignment in microstructure provides a significant effect on mechanical properties and fracture toughness of the DS-alloys. A good alignment, especially of the ductile (Nb) phase, enhances not only the room temperature toughness but also high temperature strength. The effect of the lamellar microstructural control, by the Nb_3Si decomposition, on the compressive mechanical properties and fracture toughness is much more clearly observed in the DS-alloys than the AM-alloys because of a good degree of alignment in microstructure and continuity of (Nb) phase. The following conclusions are drawn in this chapter.

1. It is found by observation of the directionally solidified microstructure that the Nb-17.5Si is the closest to the true eutectic composition among the three compositions previously reported. Since it is predicted that the coupled-zone is shifted toward Si-rich side, the alloy composition slightly Si-rich from the Nb-17.5Si is suitable to obtain the planar front in a wide range of growth rates.

2. Microstructure with continuous (Nb) plates aligned parallel to the growth direction in the Nb_3Si matrix is formed at the growth rate of 10 mm/h in the Nb-17.5Si alloy. Other DS-alloys, including ternary alloys, show the cellular microstructure. The size of cells and (Nb) phase are increased by decreasing the growth rate.

3. Decomposition of the Nb_3Si phase is kinetically slower in the DS-alloy than that in the

AM-alloys. The reason is not fully clarified in the present study but it is suggested that impurity atoms such as oxygen would play a major role.

4. Measured fracture toughness in the B10AG alloy shows a good agreement with the calculated value based on the crack bridging model. It indicates that crack bridging mechanism works effectively in the B10AG alloy.

5. The (Nb)/Nb_5Si_3 lamellar microstructural control by the eutectoid decomposition of Nb_3Si effectively enhances the room temperature toughness, but lowers the high temperature strength of the DS-alloys. It suggests that the lamellar colony boundaries, at which viscous interfacial slip operates, are increased by the eutectoid decomposition.

REFERENCES

[1] B.P. Bewlay, H.A. Lipsitt, M.R. Jackson, W.J. Reeder and J.A. Sutliff, Materials Science and Engineering A, vol. 192/193 (1995), pp. 534-543.

[2] M.G. Mendiratta, J.J. Lewandowski and D.M. Dimiduk, Metall. Trans. A, vol. 24A (1993), pp. 501-504.

[3] B.P. Bewlay, M.R. Jackson, W.J. Reeder and H.A. Lipsitt, MRS Symp. Proc., Vol. 364 (1995), pp. 943-948.

[4] D.M. Dimiduk, P.R. Subramanian and M.G. Mendiratta, Acta Metall. Sinica, 8 (1995), p. 519.

[5] B.P. Bewlay, M.R. Jackson, and H.A. Lipsitt, Metall. Trans. A, vol.27A (1996), pp. 3801-3808.

[6] B.P. Bewlay, M.R. Jackson, and H.A. Lipsitt, MRS Symp. Proc., vol.460 (1997), pp. 715-725.

[7] P.R. Subramanian, M.G. Mendiratta, D.M. Dimiduk, and M.A. Stucke, Materials Science and Engineering A, vol. 239-240 (1997),, pp. 1-13.

[8] Dietrich G. Munz; Int. Journal of Fracture 16 (1980), p. 137.

[9] Yu. A. Kocherzhinskiy, L. M. Yupko, and E. A. Shishkin, Russ. Metall., No. 1 (1980), pp. 184-188.

[10] M.E. Schlesinger, H. Okamoto, A. B. Gokhale and R. Abbaschian, Journal of Phase Equilibria, Vol. 14, No. 4 (1993), pp. 502-509

[11] M.G. Mendiratta and D.M. Dimiduk, Scripta Met. Mat., vol. 25 (1991), p. 237.

[12] H. Okamoto, A.B. Gokhale and G.J. Abbaschian, in "Binary Alloy Phase Diagrams Second Edition", Ed T.B. Massalski et al., ASM Intnl., 1990.

[13] John H. Perepezko, University of Wisconsin, private communication.

[14] K. A. Jackson, and J. D. Hunt, Trans. AIME, 236 (1966), p. 1129.

[15] W. A. Tiller, K. A. Jackson, J. W. Rutter, and B. Chalmers, Acta Met., 1 (1953), p. 428.

[16] J. W. Rutter, and B. Chalmers, Can. J. Phys., 31 (1953), p. 15.

[17] Merton C. Flemings, "Solidification processing", McGraw-Hill, 1974.

[18] McLean M., Directionally Solidified materials for high temperature service, London, UK, The Metal Society.

[19] R. Trivedi, Metall. Trans. A, vol. 25A (1994), p. 977.

[20] S.V. Raj and I.E. Locci, Intermetallics 9 (2001), pp. 217-227.

[21] Dietrich G. Munz, Int. Journal of Fracture 16 (1980), p.p. 137-140.

[22] M. F. Ashby, F. J. Blunt and M. Bannister, Acta Metall. Mater., 37 (1989), pp. 1847-1857.

[23] M.G. Mendiratta, J.J. Lewandowski and D.M. Dimiduk, Metall. Trans. A, vol. 22A (1991), pp. 1573-1583.

[24] D. Tabor, Hardness in Metals, Clarenden Press, London, 1951.

[25] R. Nekkanti and D.M. Dimiduk, MRS Symp. Proc., vol. 194 (1990), p.175.

[26] P.R. Subramanian, M.G. Mendiratta, and D.M. Dimiduk, MRS Symp. Proc., vol. 322 (1994), pp. 491-502.

CHAPTER 6

SUMMARY AND CONCLUSIONS

In the present work, in order to design a new class of heat resistant alloy based on niobium silicides targeting for structural applications at ultra-high temperatures, a systematic investigation was conducted on the Nb-Si binary and Nb-Si-Ti ternary alloys. Investigations for establishing the basis of the alloy design include the microstructural characterization, phase identification, phase diagram evaluation based on the phase equilibria, and microstructure control by heat treatment. The relationship between microstructures and mechanical properties were examined by Vickers hardness measurements, compression tests at wide temperature range from room temperature to 1673 K, and bending tests for ambient temperature fracture toughness measurements using chevron-notched specimens. To optimize the microstructure and mechanical properties, two alloy processing methods were proposed; the powder metallurgy method based on hot pressing using the pulverized Nb_5Si_3 powder and the unidirectional solidification technique using optical floating zone melting furnace. Theoretical prospects and analyses were provided from discussion for microstructural characteristics and the strengthening as well as toughening mechanisms, based on several theoretical and empirical models.

In Chapter 2, phase equilibria and microstructures were investigated for the two-phase (Nb)/Nb_5Si_3 alloys in the Nb-Si binary and Nb-Ti-Si ternary system. Special interest in microstructure control was placed on the lamellar formation by the eutectoid decomposition of the Nb_3Si into (Nb) and Nb_5Si_3. Toughness measurements using chevron-notched specimen and compression tests at wide temperature range were conducted to understand the relationship between microstructures and mechanical properties of the alloys. Conclusions drawn in this chapter are the following.

1. Phase equilibria involving major reactions were experimentally confirmed with the microstructure formation for the related phases, (Nb), Nb_3Si and Nb_5Si_3, in the Nb-Si binary and Nb-Ti-Si ternary systems. Annealing conditions were determined for the eutectoid decomposition of Nb_3Si phase into the (Nb) and Nb_5Si_3 two-phase. The vertical section of the Nb-Si-Ti ternary system was evaluated at a constant 25 at%Si, along the line from Nb_3Si to Ti_3Si.

2. The solution treatment, as defined in the present work, is effective to improve the room temperature fracture toughness through the microstructure modification with two-fold purpose; to eliminate the coarse primary solidification Nb_5Si_3 phase and to form the lamellar microstructure in a subsequent annealing.

3. The crystallographic orientation relationship between (Nb) and Nb_5Si_3 phases was determined in lamellar microstructure formed by the eutectoid decomposition as follows;

$$[331]_{Nb} // [111]_{Nb5Si3}, \quad (\bar{1}10)_{Nb} // (12\bar{3})_{Nb5Si3}.$$

4. The uniform lamellar microstructure with large (Nb) phase is advantageous for pursuing a good balance of ambient temperature fracture toughness and high temperature strength. The Ti addition is effective to improve the fracture toughness by the effects of coarsening microstructure and solid solution softening of the (Nb) phase.

In Chapter 3, to establish the lamellar microstructure control, heat treatment conditions are determined for the eutectoid decomposition of the Nb_3Si phase. The corresponding TTT-diagram was evaluated for the Nb-Si-Ti ternary system. The correlations of inter-lamellar spacing and colony size with annealing temperatures are theoretically discussed considering the degree of super-cooling. The following conclusions are drawn in this chapter.

1. The TTT-diagram was evaluated for the eutectoid decomposition of Nb_3Si in the Nb-Si-Ti ternary system. The C-curve shifts towards lower in temperature and shorter in time from those of the Nb-Si binary alloys. The shift toward lower temperature is in association with lowering the eutectoid temperature while toward shorter time is presumably due to

decomposition rate and/or atomic diffusivity being enhanced by the Ti addition.

2. Lamellar microstructure is successfully controlled for the (Nb)/Nb_5Si_3 two-phase alloys by utilizing the eutectoid decomposition of Nb_3Si phase. The average inter-lamellar spacing is evaluated ranging from 0.2 to 2 μm in the Nb-20Si-10Ti alloy. It is confirmed that the average inter-lamellar spacing, λ, is proportional to reciprocal of the degree of super-cooling, $1/\Delta T$, where ΔT is defined as the difference between annealing temperature and the eutectoid temperature.

3. Compression tests revealed that the alloys with (Nb)/Nb_5Si_3 lamellar microstructure are brittle showing only a few percent of plastic strain at room temperature. Compressive deformability can be improved by increasing inter-lamellar spacing.

4. The dependence on compressive strength for inter-lamellar spacing at room temperature and 1673 K shows inversed tendency. This is due to that the deformation mechanism at elevated temperatures is the interfacial slip mainly at the lamellar colony boundaries. Strength decreases with increase in total area of interfaces as the lamellar colony size is reduced with the inter-lamellar spacing.

In Chapter 4, a new alloy processing based on the powder metallurgy is proposed to avoid micro-cracking due to thermal stress in arc-casting. Microstructures, compressive mechanical properties and ambient temperature fracture toughness were investigated for the alloys prepared by the proposed powder metallurgy comparing with those fabricated by conventional ingot metallurgy of arc-casting. Each alloy processing method resulted in substantially different microstructure though the composition is the same. The strengthening and toughening mechanisms were discussed focusing on the distinctive microstructural features.

1. The proposed alloy processing is successful to prepare the PM-alloys having the very high density of 99.8% in the PM-Nb-18.7Si alloy. The high dense PM-alloys were obtained through the process in which the ductile niobium particles plastically deform to fill up the spaces among the Nb_5Si_3 particles.

2. The distinctive microstructural feature of the PM-alloys is that the Nb_5Si_3 phase particles are dispersed in the ductile (Nb) phase matrix, while the matrix of the AM-alloy is the brittle Nb_5Si_3 phase having the dispersion of relatively irregular (Nb) phase particles. The microstructure of the PM alloy is much coarser than that of the AM alloy.

3. The difference in mechanical properties between AM-and PM-alloys mainly depends on their matrix phases; brittle hard Nb_5Si_3 in the AM- and ductile (Nb) in the PM-alloys. The PM-alloys exhibit higher fracture toughness but lower elevated temperature strength than the AM-alloys.

4. The lamellar microstructure control was unsuccessful in the PM-alloys because of the Nb_3Si phase was not formed sufficiently by the solution treatment. It is necessary to obtain a microstructure where fine Nb_5Si_3 phase is homogeneously distributed in the (Nb) phase matrix in order to increase the volume fraction of Nb_3Si by the solution treatment.

In Chapter 5, the unidirectional solidification technique was applied to the (Nb)/Nb_3Si eutectic alloys. The effect of growth rate on microstructures was determined for the Nb-Si binary and Nb-Si-Ti ternary alloys. Directionally solidified microstructure changes from the planar eutectic to the cellular microstructure as the growth rate increases. Alignment of microstructure, especially of the ductile (Nb) phase, strongly affects not only the room temperature toughness but also high temperature strength. The following conclusions are drawn in this chapter.

1. It is found by observation of the directionally solidified microstructure that the Nb-17.5Si is the closest to the true eutectic composition among the three compositions previously reported. Since it is predicted that the coupled-zone is shifted toward Si-rich side, the alloy composition slightly Si-rich from the Nb-17.5Si is suitable to obtain the planar front in a wide range of growth rates.

2. Microstructure with continuous (Nb) plates aligned parallel to the growth direction in the Nb_3Si matrix is formed at the growth rate of 10 mm/h in the Nb-17.5Si alloy. Other DS-alloys, including ternary alloys, show the cellular microstructure. The size of cells and

(Nb) phase are increased by decreasing the growth rate.

3. Decomposition of the Nb_3Si phase is kinetically slower in the DS-alloy than that in the AM-alloys. The reason is not fully clarified in the present study but it is suggested that impurity atoms such as oxygen would play a major role.

4. Measured fracture toughness in the B10AG alloy shows a good agreement with the calculated value based on the crack bridging model. It indicates that crack bridging mechanism works effectively in the B10AG alloy.

5. The (Nb)/Nb_5Si_3 lamellar microstructural control by the eutectoid decomposition of Nb_3Si effectively enhances the room temperature toughness, but lowers the high temperature strength of the DS-alloys. It suggests that the lamellar colony boundaries, at which viscous interfacial slip operates, are increased by the eutectoid decomposition.

Acknowledgement

I would like to express my gratitude to all those who have supported me in my research work. Many people have contributed to complete this thesis directly or indirectly.

First of all, I would like to thank my advisor, Prof. Yoshinao MISHIMA, for his constant help, encouragement, and advices. His enthusiasm for the work (and baseball) provide me with an enjoyable environment for study. I can hardly express my gratitude to him enough.

I am deeply indebted to Prof. Seiji MIURA (Hokkaido University), Dr. Yoshisato KIMURA, and Dr. Fu-Gao WEI for their stimulating discussions, good advices, and hearty encouragement. Without their help, I couldn't complete this thesis.

I would like to acknowledge the fruitful comments and suggestions of Professors Akikazu SATO, Masaharu KATO, Yakichi HIGO, and Sinji KUMAI. I also want to thank to Professors Kenji WAKASHIMA, Masanori KAJIHARA, Kazuki TAKASHIMA, Susumu ONAKA, Toshiyuki FUJII, and Hideki HOSODA for their valuable advices.

I would like to thank to Prof. Takashi MATSUO, Prof. Masao TAKEYAMA, and Dr. Yukinori Yamamoto for directional solidification and helpful discussions. Many thanks are due to Dr. Ryohei TANAKA (Japan Ultra-high Temperature Materials Research Institute), Mr. Hisao TANAKA (Japan Ultra-high Temperature Materials Research Institute), and Mr. Toshihiko FUKUI (NKK Co.) for their technical supports and fruitful comments. I am greatly obliged to Prof. Takayoshi NAKANO (Osaka University) for his valuable hints and comments for my research work.

The hearty welcome and helpful comments of Dr. Joachim H. SCHNEIBEL (Oak Ridge National Laboratory), Dr. C.T. LIU (Oak Ridge National Laboratory), Prof. John J. LEWANDOWSKI (Case Western Reserve University), and Prof. David P. POPE (University of Pennsylvania) are greatly acknowledged. Especially, I would like to express my gratitude to Prof. John H. PEREPEZKO (University of Wisconsin-Madison). His advices and suggestions about directional solidification were to the point and helpful to write this thesis. It is my great pleasure to work in his group in the near future.

I am appreciative of helpful advices, instructive talks and encouragements from Prof. Tetsuo MOHRI (Hokkaido University), Mr. Okubo (Hokkaido University), Prof. Shuji HANADA (Tohoku University), Dr. Kyosuke YOSHIMI (Tohoku University), Dr. Naoyuki NOMURA (Tohoku University), Prof. Masaharu YAMAGUCHI (Kyoto University), Prof. Haruyuki INUI (Kyoto University), Dr. Kazuhiro ITO (Kyoto University), Dr. Hisatoshi HIRAI (Kyushu National Industrial Research Institute), and Dr. Tatsuo TABARU (Kyushu National Industrial Research Institute).

Thanks to Ms. Kumiko KUYAMA, Ms. Yasuko YOKONO, Mr. Sinji MURAISI, Mr. Natsuki YONEYAMA, Mr. Chihiro WATANABE, Mr. Satoru KOBAYASHI, Mr. Kentaro SHINDO, Mr. Takayuki KIMURA, Mr. Keisuke YAMAMOTO, Mr. Tomoya INAMURA, Mr. Ryuichi TARUMI, Mr. Sung Wng KIM, Ms. Kaoru IIDA, Mr. Kunio HAYASHI, Mr. Kohei NOMURA, Mr. Takahiro KATAYAMA, Mr. Sachiyori SHIINA, Mr. Toshio TAKENAKA, Mr. Hiroshi USUBA, and Mr. Hiroaki YAMAOKA.

Finally, I would like to give my special thanks to my parents for their countless supports.

March, 2002

Nobuaki Sekido

Nobuaki Sekido